



## **Terms and Conditions of Use of Digitised Theses from Trinity College Library Dublin**

### **Copyright statement**

All material supplied by Trinity College Library is protected by copyright (under the Copyright and Related Rights Act, 2000 as amended) and other relevant Intellectual Property Rights. By accessing and using a Digitised Thesis from Trinity College Library you acknowledge that all Intellectual Property Rights in any Works supplied are the sole and exclusive property of the copyright and/or other IPR holder. Specific copyright holders may not be explicitly identified. Use of materials from other sources within a thesis should not be construed as a claim over them.

A non-exclusive, non-transferable licence is hereby granted to those using or reproducing, in whole or in part, the material for valid purposes, providing the copyright owners are acknowledged using the normal conventions. Where specific permission to use material is required, this is identified and such permission must be sought from the copyright holder or agency cited.

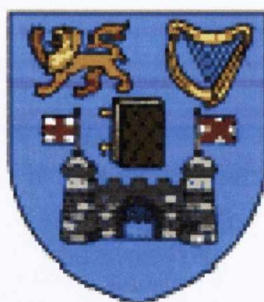
### **Liability statement**

By using a Digitised Thesis, I accept that Trinity College Dublin bears no legal responsibility for the accuracy, legality or comprehensiveness of materials contained within the thesis, and that Trinity College Dublin accepts no liability for indirect, consequential, or incidental, damages or losses arising from use of the thesis for whatever reason. Information located in a thesis may be subject to specific use constraints, details of which may not be explicitly described. It is the responsibility of potential and actual users to be aware of such constraints and to abide by them. By making use of material from a digitised thesis, you accept these copyright and disclaimer provisions. Where it is brought to the attention of Trinity College Library that there may be a breach of copyright or other restraint, it is the policy to withdraw or take down access to a thesis while the issue is being resolved.

### **Access Agreement**

By using a Digitised Thesis from Trinity College Library you are bound by the following Terms & Conditions. Please read them carefully.

I have read and I understand the following statement: All material supplied via a Digitised Thesis from Trinity College Library is protected by copyright and other intellectual property rights, and duplication or sale of all or part of any of a thesis is not permitted, except that material may be duplicated by you for your research use or for educational purposes in electronic or print form providing the copyright owners are acknowledged using the normal conventions. You must obtain permission for any other use. Electronic or print copies may not be offered, whether for sale or otherwise to anyone. This copy has been supplied on the understanding that it is copyright material and that no quotation from the thesis may be published without proper acknowledgement.



# **Fabrication, Characterisation and Applications of some Organic, Inorganic and Organic-Inorganic Hybrid Nanostructures**

By

Anna Drury

A thesis submitted for the degree of

Doctor of Philosophy



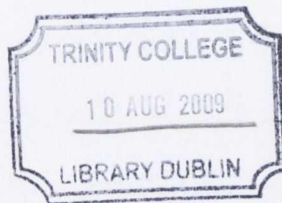
School of Physics  
Trinity College  
University of Dublin

2009



I love science and it pains me to think that so many are terrified of the subject or feel that choosing science means you cannot also choose compassion, or the arts, or be awed by nature. Science is not meant to cure us of mystery, but to reinvent it and reinvigorate it.

- Robert Sapolsky, *Why Zebras Don't Get Ulcers*, p. xii



From science to beauty because you're worth it.

*L'Oreal. Paris*

-She Magazine, August 2008

## **Declaration**

I declare that the work in this thesis has not been previously submitted as an exercise for a degree to this or any other university.

The work described herein is entirely my own, except for the assistance mentioned in the acknowledgements and the collaborative work mentioned in the list of publications.

I agree that Trinity College Library may lend or copy this thesis on request.



February 2009

## Summary

This thesis describes the fabrication, characterisation and applications of some interesting one-dimensional and two-dimensional nanostructures. The bulk of the thesis is concerned with the deposition of metals, polymers, semi-conductors and composite materials into nanoporous alumina templates (PAMs).

Metal nanowires are fabricated by alternating current (AC) and by pulsed electrodeposition (PED) into freshly prepared PAMs. The surface morphology of the PAM is observed by SEM and AFM to be ridged as in an egg box. EDX confirms that the PAMs are filled with metals and that more metal is obtained when plating is done by PED. There are large variations in the diameters of the individual nanowires but their average diameter is in agreement with the pore size of the template and with results obtained by other authors.

CdS nanowires are deposited into PAMS by AC electrodeposition from a non aqueous electrolyte. The nanowires are characterized by SEM, TEM, and Raman, UV-vis and PL spectroscopy. They are found to have a similar morphology to metallic nanowires but are less homogeneous. PL spectroscopy shows that the nanowires exhibit a band gap emission and that the emission intensity depends on the type of PAM in which the nanowires are deposited.

Polyaniline (PANI) nanowires are made by oxidative electropolymerisation of aniline into the nanopores of a PAM by potentiostatic deposition. The nanowires are characterized by SEM, TEM, and Raman and UV-vis spectroscopy. They are found to have a similar morphology to metallic nanowires but are less rigid and more homogeneous in diameter. Raman and UV-vis spectroscopy suggests that the nanowires are in the doped half-oxidised emeraldine base form of PANI. The synthesis of Ag / PANI and Cu / PANI nanocables into PAMs is achieved by simultaneous oxidative electropolymerisation of aniline and reduction of Ag or Cu from an ionic precursor. SEM shows the fibrous nature of the composite nanowires and TEM shows they resemble Ag nanowires. HRTEM indicates that they consist of a metal core surrounded by polymer coating i.e. a nanocable.

Ag / PANI and Cu / PANI thin films are prepared by electropolymerisation of PANI onto ITO from an acidic electrolyte containing silver metal ions and aniline. Ag / PANI composite films are successfully deposited on top of multi-walled carbon nanotube (MWCNT) and single walled carbon nanotube (SWCNT) electrodes. Deposition is



facilitated by using a PAM as it adds stability to the system and the Bucky paper peels off easily after deposition.

The nanostructures are investigated for use in several applications:

a) Electrodes made from copper (Cu) and nickel (Ni) nanowire arrays are incorporated into single layer organic light emitting diodes which use the light emitting polymer Poly[(4-methylphenyl) imino-4,4'-diphenylene-(4-methylphenyl)imino-1,4-phenylene-ethenylene-2-methoxy-5-(2-ethylhexyloxy)-1,4-phenylene-ethenylene-1,4-phenylene)] (TPD-MEH-PPV) as the emissive material. The DC current-voltage characteristics of both devices are measured and compared to equivalent devices with a planar metal electrode. The current density in the nanowire array anode device exceeds that in the planar anode device by a factor of eight. The Ni array devices have better rectification than the Cu ones and achieve a higher maximum current density. A relative increase in the electroluminescence intensity is observed for the nanowire electrode devices.

b) Three types of MWCNTs are grown on iron-filled porous alumina membranes, long tubes and X and Y junction tubes. Current-Voltage (I-V) plots on single MWCNT Y-junctions show ohmic behaviour with resistances considerably lower than those quoted in the literature.

c) Solar cells are made with poly [2-methoxy-5-(2'-ethylhexyloxy)-*p*-phenylene vinylene] (MEH-PPV) as the electron donor and CdS as the electron acceptor. Two types of devices are fabricated with either a blend of CdS and MEH-PPV or MEH-PPV deposited on top of a CdS nanowire array. Significant quenching is observed for both nanostructure devices which indicates that efficient exciton splitting and charge separation takes place. An open circuit voltage of 0.07V is obtained for the blend which showed strongest quenching.

d) The antibacterial properties of the Ag / PANI films and nanowires are investigated by monitoring their response to exposure to bacteria. They are found to inhibit the growth of *Pseudomonas aeruginosa* bacteria and show some activity against *E. Coli* (Gram negative) microbes but not to *S. Aureus* (Gram positive) bacteria.

## Acknowledgements

Firstly, I would like to thank Professor Blau for his continued support, inspiration and patience especially during the course of this thesis. I would also like to thank Dr Michael Kröll, who taught me almost everything I know about porous alumina and Dr Kornelius Nielsch who taught me the rest! I would like to take this opportunity to gratefully acknowledge the others in Kornelius's group who each in their turn helped me during my stay in Halle; Dr Woo Lee, Dr Mato Knez, Dr Manuela Daub, Ran and Jana. I would also like to thank Dr Stephen Lipson (affectionately known as Slipper) who arranged the visit.

I have received help from a wide variety of people during the course of thesis. I am grateful to Dr Shweta Chaure for her help with the PANI nanowires and useful discussions about solar cells. I am also indebted to her for her friendship during her stay in TCD. Many thanks also to Dr Ramesh Babu for help with the thin film and nanotube work and to Dr Ed Moore for all his help with the anti-bacterial tests. Dr Ronnie Russell kindly supplied us with bacteria and instructions on how to deal with them which was essential. A great big thanks goes to Darren Lee for his help with Raman spectroscopy, voltage reduction graphs, proof reading and general gossip. Another big thanks goes to Ed for his many offers of assistance, his good humor, his uncomplaining nature and for proof reading under pressure. Lots of thanks also to Trevor who is always willing to explain the equipment; I appreciate the XRDs you did for me and help with the FTIR. Niall McEvoy is another one of those guys who is always willing to lend a hand, thanks for all the forests you are making for me (even though I haven't used them yet and they have nothing to do with this thesis) and for proof reading. The lovely HRTEM and AFM images of Ag nanowires were taken by Dr Valeria Nicolosi and Denise Charles respectively, many thanks! I would also like to thank Dr Fiona Blighe and Dr Shane Bergin for their advice on how to make good Bucky papers, and to Shane for proof reading. Thanks to Dr Rory Leahy, Dr Adam Strevens and Alex Rakovich for their collaboration on the nanotube, OLED and CdS work which was a team effort; they did most of the work. I would like to thank Adam for help with the pulsed electrodeposition program, for the other AFM image, some PL and some SEMs.



I am indebted to the academic staff for their support and to all the administrative and technical staff for their help, especially Mick Reilly (whom I am still missing), Pat Murphy and Gordon O'Brien from the workshop (who are always making me new cells or copper heating/cooling plates or gas lines), Joe McCauley (for trying to automate our voltage reduction), Ken Concannon (for all the computer stuff), Nigel Carroll (for fixing all my multimeters, heating mantels etc), Pat Flanagan, Gillian Gunnibg, John Kelly and Jemmer Kavanagh for just being there when I need them. Thanks to Marie Callanan for help with project management (again nothing to do with this thesis) and computer skills and for your friendship. Thanks also to Jeanette Cummins, Rebecca Owens and Una Dowling for all their help and nice friendly greeting whenever I go into the office and to Marie Kinsella, Robbie Gallaghe and Suzanne Williams in the other office for all the accounting, orders and their patience with me. The people from the CMA are also always very helpful especially Dave John and Neal Leady, who assisted with some of the images in this thesis. Special thanks also to Peig Brehon and Manuel R  ther from the chemistry department who have helped me out with equipment and advice on numerous occasions. Many thanks also for your very valued friendship Peig and our essential coffee breaks.

Many thanks to the girls (Helen, Paula, Yenny, Denise, Evelyn, Karen, Margarite) for all the girlie cinema trips etc, we miss you Valeria! And to the boys (Phil, Umar, Sekanta, Zhenyu, Martin, Ronan and David R) for messing the labs (although to be honest things aren't the same without David B), to the other boys (Jun, Trevor, Ed, Niall, Darren and Mustafa) for keeping them klean and to Chris for turning off his music when I enter the lab (please.....). Thanks to those who visited me when I broke my ankle (Steffie, Georg, Yenny, Fiona and Shane) and especially for your visits Evelyn, you kept me sane and the painters happy!

Last, but certainly not least, thanks a million Luke, for all your support, shopping, cooking, patience and care during the last few months and for proof-reading this thesis!



# Table of Contents

<i>Declaration</i> .....	<i>iii</i>
<i>Summary</i> .....	<i>iv</i>
<i>Acknowledgements</i> .....	<i>vi</i>
<i>Table of Contents</i> .....	<i>viii</i>
<i>List of Figures and Illustrations</i> .....	<i>xii</i>
<i>List of Tables</i> .....	<i>xviii</i>
<b>Chapter 1 Introduction</b> .....	<b>1</b>
<b>1.1 Nanotechnology and Nanomaterials</b> .....	<b>1</b>
<b>1.2 Uses/Applications of Nanomaterials</b> .....	<b>2</b>
1.2.1 Biomedical Applications.....	3
1.2.2 Electronic Applications.....	3
1.2.3 Optical Applications .....	4
1.2.4 Structural, Functional and Smart Materials .....	4
<b>1.3 Synthesis of One-Dimensional Nanostructures</b> .....	<b>5</b>
1.3.1 VLS (Vapour – Liquid - Solid).....	5
1.3.2 MOVPE (Metal - Organic - Vapour - Phase - Epitaxy).....	6
1.3.3 CVD (Chemical - Vapour - Deposition) .....	6
1.3.4 Laser Ablation and Condensation .....	6
1.3.5 Solvothermal Methods .....	7
1.3.6 Solution Phase Methods.....	7
1.3.7 Size Reduction Methods .....	7
1.3.7.1 Isotropic Deformation.....	8
1.3.7.2 Anisotropic Etching .....	8
1.3.7.3 Lithography .....	8
1.3.8 Self-Assembly.....	9
1.3.9 Template Directed Synthesis .....	10
<b>1.4 Thesis Aims</b> .....	<b>11</b>
<b>Chapter 2 Experimental Background</b> .....	<b>12</b>
<b>2.1 Materials</b> .....	<b>12</b>
2.1.1 Porous Alumina Membranes (PAMs).....	12
2.1.1.1 Advantages of PAMs .....	12
2.1.1.2 Properties of PAMs.....	13
2.1.1.3 Fabrication of PAMs.....	14

2.1.1.3.1 Electropolishing .....	15
2.1.1.3.2 Anodisation .....	15
2.1.1.3.3 Barrier Layer Reduction .....	19
2.1.1.4 Filling of PAMs by Electrodeposition .....	20
2.1.1.4.1 Direct Current (DC) Electrodeposition .....	20
2.1.1.4.2 Alternating current (AC) Electrodeposition.....	22
2.1.1.4.3 Pulsed Electrodeposition (PED) .....	23
2.1.2 One-Dimensional Nanostructures .....	25
2.1.2.1 Metal Nanowires .....	25
2.1.2.1.1 Iron (Fe) .....	25
2.1.2.1.2 Cobalt (Co) .....	26
2.1.2.1.3 Nickel (Ni) .....	26
2.1.2.1.4 Copper (Cu) .....	27
2.1.2.1.5 Silver (Ag) .....	29
2.1.2.2 Conducting Polymer Nanowires .....	29
2.1.2.2.1 Polyaniline (PANI) .....	30
2.1.2.3 Metal / Polymer Composite Nanowires.....	33
2.1.2.4 Semiconductor Nanowires .....	34
2.1.2.4.1 Cadmium sulphide (CdS).....	36
<b>2.2 Characterisation Techniques .....</b>	<b>38</b>
2.2.1. Electron Microscopy .....	38
2.2.1.1 Scanning Electron Microscopy (SEM) and High Resolution Scanning Electron Microscopy (HRSEM) .....	38
2.2.1.2 Transmission electron microscopy (TEM) and High Resolution Transmission Electron Microscopy (HRTEM).....	40
2.2.1.3 Atomic Force Microscopy (AFM) .....	42
2.2.2 X-Ray Analysis .....	43
2.2.2.1 Energy Dispersive X-Ray Analysis (EDX) .....	43
2.2.2.2 X-ray Diffraction (XRD) .....	44
2.2.3 Spectroscopy .....	46
2.2.3.1 Fourier Transform Infra-Red Spectroscopy (FTIR) .....	46
2.2.3.2 Raman Spectroscopy.....	48
2.2.3.3 Ultraviolet, Visible and near Infra-red (UV-Vis-NIR) Absorption Spectroscopy .....	49
2.2.3.4 Fluorescent or Photoluminescent (PL) Spectroscopy .....	51
2.2.4 Electrical Characterisation.....	53
 <b>Chapter 3 Results: One-Dimensional Nanostructures in Porous Alumina Membranes.....</b>	 <b>55</b>
<b>3.1 Porous Alumina Membranes (PAMs).....</b>	<b>55</b>
3.1.1 Preparation of Aluminium Foils .....	55
3.1.2 Fabrication of PAMs.....	58
3.1.3 Reduction of the Barrier Layer .....	63
<b>3.2 One-Dimensional Nanostructures .....</b>	<b>64</b>
3.2.1 Metal nanowires.....	64
3.2.1.1 Fabrication by Chemical Electrodeposition.....	64
3.2.1.2 Characterisation .....	66
3.2.1.2.1 Preparation of Samples for Characterisation .....	66
3.2.1.2.2 SEM and HRSEM.....	68
3.2.1.2.3 TEM and HRTEM .....	70



3.2.1.2.4 AFM .....	72
3.2.1.2.5 EDX .....	74
3.2.1.2.6 Summary .....	77
3.2.2 Polymer Nanowires .....	77
3.2.2.1 Preparation of PANI Nanowires .....	77
3.2.2.2 Characterisation of PANI nanowires .....	78
3.2.2.3 Summary .....	81
3.2.3 Metal / Polymer Nanowires .....	81
3.2.3.1 Preparation of Composite Nanowires .....	81
3.2.3.2 Characterisation of Composite nanowires .....	82
3.2.3.2.1 SEM, TEM and HRTEM .....	82
3.2.3.2.2 EDX and XRD .....	85
3.2.3.2.3 Raman Spectroscopy .....	88
3.2.3.2.4 FTIR Spectroscopy .....	92
3.2.3.2.5 UV-Vis Absorption Spectroscopy .....	95
3.2.3.3 Summary and Proposed Formation Mechanism of Composite Nanowire Synthesis.....	96
3.2.4 Semiconductor Nanowires .....	98
3.2.4.1 Preparation of CdS nanowires.....	98
3.2.4.2 Characterisation of CdS nanowires.....	98
3.2.4.3 Summary .....	105
<b>Chapter 4 Results: 2-Dimensional Nanostructures .....</b>	<b>106</b>
<b>4.1 Silver / Polyaniline (Ag/PANI) Thin Films .....</b>	<b>106</b>
4.1.1 Electrochemical Preparation of Thin Films .....	107
4.1.2 Characterisation of Thin Films .....	108
4.1.2.1 Raman Spectroscopy .....	108
4.1.2.2 XRD .....	110
4.1.2.3 UV-Vis Absorption Spectroscopy .....	111
4.1.2.4 Electrical Measurements .....	112
<b>4.2 Polyaniline films containing Ag nanowires.....</b>	<b>116</b>
4.2.1 Film Preparation.....	116
4.2.2 Film Characterisation.....	117
4.2.2.1 Raman Spectroscopy.....	117
4.2.2.2 XRD .....	118
<b>4.3 PANI and Ag / PANI Films on Carbon Nanotube Electrodes .....</b>	<b>119</b>
4.3.1. PANI on Multi Wall Carbon Nanotube Electrodes (MWCNT) .....	119
4.3.2. Ag / PANI on MWCNT .....	120
4.3.3 Ag / PANI on Single Wall Carbon Nanotube Electrodes (SWCNT) ....	122
4.3.4 PANI on SWCNT Electrode by Filtration through a Commercial PAM	124
4.3.5 PANI on Commercial PAM by Filtration .....	124
4.3.6 PANI on Gold Electrode by Electrodeposition through a Commercial PAM.....	126
4.3.7 Summary .....	126
<b>4.4 Conclusions and Potential Applications.....</b>	<b>127</b>
<b>Chapter 5: Device Applications .....</b>	<b>128</b>
<b>5.1 Nanowire array electrodes for light emitting diodes .....</b>	<b>128</b>



5.1.1 Background .....	128
5.1.2 Device Fabrication .....	128
5.1.3 Device Characterisation .....	131
5.1.3.1 Current voltage characteristics .....	131
5.1.3.2 Electroluminescence (EL) .....	133
5.1.4 Summary .....	134
<b>5.2 Metallic nanowires as catalysts for carbon nanotubes (CNT) growth....</b>	<b>135</b>
5.2.1 Background .....	135
5.2.2 Growth of MWCNTs on PAMs .....	136
5.2.2.1 Preparation of PAMs .....	136
5.2.2.2 Chemical vapour deposition procedure .....	137
5.2.2.3 Characterisation of Carbon nanotubes grown in the custom-built CVD system .....	137
5.2.3 Summary .....	141
<b>5.3 CdS Nanowire arrays in photovoltaic – organic solar cells .....</b>	<b>142</b>
5.3.1 Background .....	142
5.3.2 Device Fabrication .....	143
5.3.2.1 Blend Devices .....	144
5.3.2.2 Nanorod Devices .....	145
5.3.3 Device characterisation .....	146
5.3.3.1 PL Studies .....	146
5.3.3.2 Current Voltage characteristics .....	149
5.3.4 Summary .....	150
<b>5.4 Antibacterial studies of Polyaniline Composites .....</b>	<b>151</b>
5.4.1 Background .....	151
5.4.2 Antimicrobial testing using Agar plates .....	152
<b>Chapter 6 Conclusions .....</b>	<b>155</b>
6.1 Conclusions .....	155
6.2 Future Work .....	158
<b>References .....</b>	<b>162</b>
Appendix A 1 Analysis of a typical 40 V PAM .....	206
Appendix A 2 Analysis of single Ag nanowires made in a 20 V PAM .....	207
Appendix B Publication List .....	209

# List of Figures and Illustrations

<b>Figure 2.1: Cross section of an anodized aluminium foil showing pores of diameter <math>d</math>, height <math>h_2</math> and a barrier layer of height <math>h_1</math> .....</b>	<b>13</b>
<b>Figure 2.2: Top view of an anodised aluminium foil showing pores of diameter <math>d</math> .....</b>	<b>14</b>
<b>Figure 2.3: Plot of inter-pore distance versus anodisation potential for disordered pore arrays (line). Self ordered pore arrays (symbols) fit on the same curve (taken from reference 223). .....</b>	<b>17</b>
<b>Figure 2.4: Schematic of the 2-step anodisation process .....</b>	<b>18</b>
<b>Figure 2.5: Schematic of the scheme used for DC electrodeposition in an AAO template .....</b>	<b>21</b>
<b>Figure 2.6: Schematic of the filling of a PAM with Nickel by PED taken from Nielsch et al. [169]. .....</b>	<b>24</b>
<b>Figure 2.7: Base forms of PANI (a) Leucomeraldine base (LEB), (b) Emeraldine base (EB) and (c) Pernigraniline base (PNB) .....</b>	<b>30</b>
<b>Figure 2.8: Oxidised bi-polaronic Emeraldine salt (ES) .....</b>	<b>31</b>
<b>Scheme 1: Chemical Oxidative Polymerisation of Aniline .....</b>	<b>32</b>
<b>Scheme 2: Electrochemical Polymerisation of Aniline .....</b>	<b>32</b>
<b>Figure 2.9: Energy level diagram for a p-doped (a) and n-doped (b) semiconductor, where <math>E_e = -q.\phi</math> is the potential energy of a free unmoved electron (the elementary charge <math>q = 1.6 \times 10^{-19}</math> C and <math>\phi =</math> macro potential), <math>E_{ea} =</math> electron affinity, <math>E_{wf} =</math> work function, <math>E_c =</math> energy of a stationary free conduction electron, <math>E_f =</math> energy of an electron in the Fermi level, <math>E_v =</math> energy of a stationary valence electron in a bond and <math>E_g =</math> energy gap [433]. .....</b>	<b>35</b>
<b>Figure 2.10: Energy band structure for CdS (a) shows the valence band for the rocksalt form of CdS with a lattice constant of <math>a_0 = 5.818\text{\AA}</math>, (b) and (c) show the conduction bands for zincblend and rock salt CdS with a lattice constant of <math>a_0 = 5.818\text{\AA}</math> adapted from [438]. .....</b>	<b>36</b>
<b>Figure 2.11: Schematic of how an SEM works [472] .....</b>	<b>39</b>
<b>Figure 2.12: Schematic of how TEM works [474] .....</b>	<b>41</b>
<b>Figure 2.13: Schematic of an Atomic Force Microscope [477]. .....</b>	<b>42</b>
<b>Figure 2.14: A typical EDX spectrum [480] .....</b>	<b>44</b>
<b>Figure 2.15: Schematic of crystal planes to illustrate Braggs Law [482] .....</b>	<b>45</b>
<b>Figure 2.16: The general regions of the infrared spectrum [485]. .....</b>	<b>48</b>
<b>Figure 2.17: Energy level diagram .....</b>	<b>50</b>
<b>Figure 2.18: Schematic of the typical components of a fluorimeter [490]. .....</b>	<b>52</b>
<b>Figure 2.19: Energy level diagram showing rotational and vibrational levels in the ground and first excited state of a chemical species [491] .....</b>	<b>53</b>
<b>Figure 3.1: Schematic drawing of the electropolishing process .....</b>	<b>56</b>



<b>Figure 3.2: Typical SEM images of a 99.999% Al foil (a) untreated, ( b) after chromic acid treatment, (c) after electropolishing at 15 V, (d) after electropolishing at 15 V taken at a higher magnification.....</b>	<b>57</b>
<b>Figure 3.3: Typical SEM images of a 99 % Al foil (a) after electropolishing at 15 V, (b) after electropolishing at 15 V taken at a higher magnification .....</b>	<b>57</b>
<b>Figure 3.4: Schematic of anodisation set-up .....</b>	<b>58</b>
<b>Figure 3.5: SEM images of PAMs made with (a) sulphuric acid, (b) oxalic acid and (c) phosphoric acid.....</b>	<b>59</b>
<b>Figure 3.6: SEM images of PAMs made with sulphuric acid at 20 V (a) from the top surface and (b) from the bottom after removal of the barrier layer.....</b>	<b>60</b>
<b>Figure 3.7: SEM image of membranes made with (a) oxalic acid at 40 V overnight, (b) after removal of oxide and (c) after second anodisation at 40 V .....</b>	<b>61</b>
<b>Figure 3.8: SEM images of PAMs doubly anodised with oxalic acid at 40 V shown at different magnifications .....</b>	<b>61</b>
<b>Figure 3.9: SEM images of oxalic acid PAMs taken at (a) 35K and (b) 50K magnification....</b>	<b>62</b>
<b>Figure 3.10: SEM images of oxalic acid PAMs at a 52.0° tilt angle .....</b>	<b>62</b>
<b>Figure 3.11: (a) AFM image of an oxalic acid PAM with (b) corresponding surface plot and (c) surface roughness measurement .....</b>	<b>62</b>
<b>Figure 3.12: Plot of voltage reduction of a PAM made at 40 V in oxalic acid and the response in current.....</b>	<b>63</b>
<b>Figure 3.13: HRSEMs of PAMs made at 40 V which have been voltage reduced to (a) 10.2 V and (b) 14.1 V .....</b>	<b>64</b>
<b>Figure 3.14: Schematic of apparatus used for AC electrodeposition in a PAM .....</b>	<b>66</b>
<b>Figure 3.15: SEM of a PAM made at 40 V which was over- plated with Ni (a) top view (b) top view after polishing (c) side view after polishing .....</b>	<b>67</b>
<b>Figure 3.16: HRSEMs of PAMs made by anodisation at 40V filled with Cu by AC electrodeposition for (a) 4 min and (b) 8 min.....</b>	<b>69</b>
<b>Figure 3.17: SEM images of Ag filled PAMs taken from (a) the side and (b) the top.....</b>	<b>69</b>
<b>Figure 3.18: Cross sectional SEM images of PAMs filled with Ni by PED (a) for 60 min, (b) for 30 min, (c) for 20 min and (d) top SEM view of PAM filled for 60 mins then polished.....</b>	<b>70</b>
<b>Figure 3.19: TEM images of (a) and (b) Ni nanowires from a PAM made at 40 V and filled by PED, (c) Ag nanowires from a PAM made at 20 V and filled by AC deposition and (d) HRTEM of similar Ag nanowires.....</b>	<b>71</b>
<b>Figure 3.20: AFM images (a) normal and (b) filtered of Ag nanowires extracted from a PAM made at 60 V with height profiles A and B from the filtered image shown below {(c) and (d)} .....</b>	<b>73</b>



<b>Figure 3.21: AFM images (a) normal and (b) filtered of Ag nanowires extracted from a PAM made at 30 V with height profiles A and B from the filtered image shown below {(c) and (d)} .....</b>	<b>73</b>
<b>Figure 3.22 Schematic of AFM probe tip scanning over a flat surface which has a nanowire adsorbed on it adapted from: <a href="http://chemistry.jcu.edu/mwaner/research/AFM/tipconv.htm">http://chemistry.jcu.edu/mwaner/research/AFM/tipconv.htm</a>.....</b>	<b>74</b>
<b>Figure 3.23: EDX Spectrum of PAM made at 40 V and filled with Sn by AC deposition .....</b>	<b>75</b>
<b>Figure 3.24: EDX Spectrum of PAM made at 20 V and filled with Cu by AC deposition.....</b>	<b>75</b>
<b>Figure 3.25: EDX Spectrum of PAM made at 40 V and filled with Ni by PED .....</b>	<b>75</b>
<b>Figure 3.26: EDX Spectrum of a PAM made at 40 V and filled with Ag by AC deposition with analysis table in inset.....</b>	<b>76</b>
<b>Figure 3.27: EDX Spectrum of a PAM made at 40 V and filled with Ag by PED with analysis table in inset.....</b>	<b>76</b>
<b>Figure 3.28: (a) SEM image of PANI nanowires in a PAM made at 10 V and etched with NaOH, (b) TEM image of PANI nanowires extracted from PAM.....</b>	<b>78</b>
<b>Figure 3.29: Raman spectrum of a PANI nanowire array in a PAM (excitation <math>\lambda = 633</math> nm) .....</b>	<b>79</b>
<b>Figure 3.30 UV-vis spectrum of a PANI nanowires array in a PAM made at 10 V. ....</b>	<b>80</b>
<b>Figure 3.31 UV-vis spectrum of a dispersion of PANI / DBSA salts diluted by deionized water taken from [500].....</b>	<b>80</b>
<b>Figure 3.32 UV-vis spectrum of EB prepared PANI in THF taken from [502]. ....</b>	<b>81</b>
<b>Figure 3.33: SEM images of Ag / PANI nanowires in a PAM made at 60 V (etched with NaOH).....</b>	<b>82</b>
<b>Figure 3.34: TEM images of Ag / PANI nanowires extracted from a PAM which was made at 30 V.....</b>	<b>83</b>
<b>Figure 3.35: HRTEM images of Ag nanowires from a PAM made at 20 V .....</b>	<b>84</b>
<b>Figure 3.36: HRTEM image of Ag / PANI nanowires from a PAM made at 20 V, with corresponding diffraction pattern in inset and (b) .....</b>	<b>85</b>
<b>Figure 3.37: HRTEM image of Ag / PANI nanowires from a PAM made at 40 V, with corresponding diffraction pattern (b).....</b>	<b>85</b>
<b>Figure 3.38: EDX of composite sample (PAM made at 40V with Ag / PANI deposited at 9V for 20 min) .....</b>	<b>86</b>
<b>Figure 3.39: XRD of the Ag / PANI composite array (a) compared to Ag nanowire array (b) .....</b>	<b>87</b>
<b>Figure 3.40: XRD of the Cu / PANI composite array (a) compared to a Cu nanowire array (b).....</b>	<b>87</b>

<b>Figure 3.41: Raman spectra of a composite nanowire array in a PAM made at 15 V, a PANI array in a PAM made at 10 V, a silver nanowire array in a PAM made at 20 V and an empty PAM (excitation <math>\lambda = 633</math> nm).....</b>	<b>89</b>
<b>Figure 3.42: Raman spectra of Ag/PANI composite nanowire arrays in PAMs made at 10 V, 15 V, 30 V, 40 V, 60 V and 80 V (excitation <math>\lambda = 633</math> nm).....</b>	<b>91</b>
<b>Figure 3.43: Raman spectra of Cu / PANI composite nanowire arrays in PAMs made at 7 V, 20 V, 80 V , 100 V and 140 V (excitation <math>\lambda = 633</math> nm).....</b>	<b>92</b>
<b>Figure 3.44: FTIR of composite wires extracted from PAM made at 40 V (a) and PANI film (b).....</b>	<b>93</b>
<b>Figure 3.45: UV vis of a composite nanowire array in a PAM made at 20 V compared to an Ag nanowire array in a PAM made at 20 V and a PANI nanowire array in a 10 V PAM.....</b>	<b>95</b>
<b>Figure 3.46: UV-vis of composite samples in PAMs made at 20 V, 80 V and 140 V.....</b>	<b>96</b>
<b>Figure 3.47: TEM images of CdS nanowires liberated from a PAM made at 40 V.....</b>	<b>99</b>
<b>Figure 3.48: SEM image of a CdS filled PAM (made at 40 V), which was etched with NaOH to expose the nanowires.....</b>	<b>99</b>
<b>Figure 3.49: Raman spectrum of CdS deposited into a 60 V PAM (excitation <math>\lambda = 633</math> nm). 100</b>	
<b>Figure 3.50: UV/vis of CdS samples in PAMs made at 20 V, 40 V, 60 V, 80 V, 100 V and 140 V compared to an empty PAM made at 20 V.....</b>	<b>101</b>
<b>Figure 3.51: PL spectrum of CdS samples in PAMs made at 20 V, 40 V, 60 V, 80 V and 100 V.....</b>	<b>102</b>
<b>Figure 3.52: Normalized emission spectra of CdS nanowires in a PAM made at 80 V.....</b>	<b>103</b>
<b>Figure 3.53: Emission spectrum of a sample in a PAM made at 20 V compared to an empty.....</b>	<b>103</b>
<b>20 V PAM.....</b>	<b>103</b>
<b>Figure 3.54: PL spectra of CdS nanowire arrays which were deposited into PAMs made at 10 V, 20 V, 40 V, 60 V, 80 V and 100 V.....</b>	<b>104</b>
<b>Fig 3.55: PL of CdS samples in PAMs made at 20 V, 40 V, 60 V, 80 V and 100 V corrected for PL contribution due to the empty PAMs.....</b>	<b>105</b>
<b>Figure 4.1: Schematic of apparatus used for potentiostatic electrodeposition onto ITO.....</b>	<b>107</b>
<b>Figure 4.2: Raman spectrum of a film of Ag / PANI on ITO prepared at 1.0 V for 1000 s (excitation <math>\lambda = 633</math> nm).....</b>	<b>109</b>
<b>Figure 4.3: Raman spectrum of a film of PANI on ITO prepared at 1.0 V for 1000 s compared to a film of Ag / PANI (1.4 V, 500 s) {excitation <math>\lambda = 633</math> nm}.....</b>	<b>109</b>
<b>Figure 4.4: Normalised Raman spectrum of a film of Ag / PANI on ITO prepared at 1.4 V for 500 s compared to a film of PANI (1.0 V, 1000 s) {excitation <math>\lambda = 633</math>nm}.....</b>	<b>110</b>
<b>Figure 4.5: XRD pattern of the Ag/PANI film made at 0.8 V for 500 s.....</b>	<b>111</b>



<b>Figure 4.6: UV-Vis of an Ag / PANI film on ITO prepared at 1.0 V for 1000 s compared to a film of PANI on ITO prepared under the same conditions .....</b>	<b>111</b>
<b>Figure 4.7: Voltage-Current characteristics for a film of Ag / PANI on ITO (1 V, 2000 s)...</b>	<b>112</b>
<b>Figure 4.8: Plot of sheet conductivity against anodising voltage for composite and PANI films .....</b>	<b>114</b>
<b>Figure 4.9: Plot of sheet conductivity against anodising time for composite and PANI films .....</b>	<b>114</b>
<b>Scheme 4.1: Polymerisation of aniline with ammonium peroxydisulfate in water .....</b>	<b>116</b>
<b>Figure 4.10: A PANIES film containing Ag nanowires drop-cast on glass compared to PANIEB, PANIES and doped PANIEB films on glass (excitation <math>\lambda = 633</math> nm).....</b>	<b>117</b>
<b>Figure 4.11: Raman spectrum for PANIES (baseline corrected, excitation <math>\lambda = 633</math> nm).....</b>	<b>118</b>
<b>Figure 4.12: XRD Diffraction pattern of a film of PANI ES containing Ag nanowires cast onto a glass slide.....</b>	<b>118</b>
<b>Figure 4.13: Schematic of the different steps involved in the production of a “Bucky” paper (adapted from Fraunhofer Institute for Interfacial Engineering and Biotechnology IGB web-site [552]).....</b>	<b>119</b>
<b>Figure 4.14: Raman spectrum of underside of MWCNT electrode (excitation <math>\lambda = 633</math> nm) .</b>	<b>120</b>
<b>Figure 4.15: Raman spectrum of underside of MWCNT electrode (excitation <math>\lambda = 633</math> nm) .</b>	<b>120</b>
<b>Figure 4.16: Raman spectrum of top of MWCNT electrode (excitation <math>\lambda = 633</math> nm).....</b>	<b>121</b>
<b>Figure 4.17: XRD Diffraction pattern of Ag / PANI electrodeposited onto a MWCNT electrode through a commercial PAM.....</b>	<b>121</b>
<b>Figure 4.18: Raman spectrum of bottom of SWCNT electrode (excitation <math>\lambda = 633</math> nm) .....</b>	<b>122</b>
<b>Figure 4.19: Raman spectrum of top of SWCNT electrode (excitation <math>\lambda = 633</math> nm) .....</b>	<b>123</b>
<b>Figure 4.20: XRD Diffraction pattern of Ag / PANI ES electrodeposited onto a SWCNT electrode through a commercial PAM.....</b>	<b>123</b>
<b>Figure 4.21: Raman spectra of top and bottom of commercial PAM and top and bottom of Bucky paper after filtration of ES (excitation <math>\lambda = 633</math> nm).....</b>	<b>124</b>
<b>Figure 4.22: Raman spectrum of bottom of commercial PAM after filtration of ES (excitation <math>\lambda = 633</math> nm) .....</b>	<b>125</b>
<b>Figure 4.23: Raman spectrum of top of commercial PAM after filtration of ES (excitation <math>\lambda = 633</math> nm) .....</b>	<b>125</b>
<b>Figure 4.24: Raman spectra of top of commercial PAM after deposition of PANI.....</b>	<b>126</b>
<b>(excitation <math>\lambda = 633</math> nm) .....</b>	<b>126</b>
<b>Figure 5.1: (a) Profile of the nanowire array device structure showing the multiple layers of the structure and (b) a top view showing the build up of layers on top of the sheet of aluminium foil [324].....</b>	<b>128</b>
<b>Figure 5.2: Chemical structure of TPD-MEH-PPV, the emissive polymer used in the OLED devices.....</b>	<b>130</b>



<b>Figure 5.3: Chemical structure of TPD-MEH-PPV, the emissive polymer used in the OLED devices [325].</b> .....	130
<b>Figure 5.4: Current Density vs. Voltage for the device made with an unfilled PAM, Cu filled PAMs and a planar electrode. The inset shows the positive and negative bias characteristic for the 7 min Cu-filled PAM device [325].</b> .....	131
<b>Figure 5.5: EL spectra for the 7 minute Cu-filled PAM (open circle and dotted line) and the Cu planar electrode device (open square and dash dot line) compared to the PL spectrum for the emissive material (open triangle and solid line). The inset shows the chemical structure of the emissive polymer [296].</b> .....	133
<b>Figure 5.6: EL spectra of Ni nanowire array device compared to the Ni planar electrode device and an ITO electrode device [296].</b> .....	134
<b>Figure 5.7: SEM images showing long tubes grown on porous alumina membranes (A-C) and silicon dioxide substrate (D) [297]</b> .....	138
<b>Figure 5.8: SEM images of CNT junctions grown on PAM substrates [297]</b> .....	139
<b>Figure 5.9: SEM images showing two separate Y-junctions grown from raised areas of PAM surface [297].</b> .....	140
<b>Figure 5.10: Typical Raman spectrum for MWCNTs grown on Fe-filled PAMs. The spectrum was taken using 632 nm laser light [297].</b> .....	140
<b>Figure 5.11: Schematic of device structures for (a) blend and (b) nanorod / conducting polymer composites [612].</b> .....	144
<b>Figure 5.12: Chemical structure of MEH-PPV, the emissive polymer used in the solar cell devices</b> .....	144
<b>Figure 5.13: Blend solar cells on ITO, (a) shows the actual devices with Al electrodes on top, (b) is a schematic which shows the device architecture [612].</b> .....	145
<b>Figure 5.14: Processes used in fabrication of CdS nanorod solar cell device</b> .....	146
<b>Figure 5.15: PL of a film made with a blend of 91% w/w CdS nanocrystals and MEH-PPV, a CdS nanorod array coated with MEH-PPV and MEH-PPV on its own [612]</b> .....	147
<b>Figure 5.16: Photoluminescence (PL) of blends of bulk CdS and MEH-PPV [605].</b> .....	148
<b>Figure 5.17: PL of CdS nanocrystals and nanorods compared to bulk CdS [612].</b> .....	149
<b>Figure 5.18: I-V curve for a blend of 93.8% w/w bulk CdS and MEH-PPV [605].</b> .....	150
<b>Figure 5.19: (a) Biofilm growth of pseudomonas aeruginosa bacteria, (b) individual pseudomonas aeruginosa.</b> .....	152
<b>Figure 5.20: Ag / PANI thin film, which was prepared by electrodeposition onto ITO at 1 V for 1000 s, after exposure to pseudomonas aeruginosa bacteria for 11 days</b> .....	153
<b>Figure 5.21: Ag / PANI thin film, which was prepared by electrodeposition onto ITO at 1 V for 2000 s, after exposure to pseudomonas aeruginosa bacteria for 11 days</b> .....	153
<b>Figure 5.22: Ag / PANI nanowires, which was prepared by electropolymerisation into a PAM, after exposure to pseudomonas aeruginosa bacteria for 11 days</b> .....	154



## List of Tables

<b>Table 3.1 Conditions used for anodisation of aluminium foils .....</b>	<b>60</b>
<b>Table 3.2 Deposition conditions employed for metallic nanowires .....</b>	<b>65</b>
<b>Table 3.3 Nanowire Dimensions .....</b>	<b>72</b>
<b>Table 3.4 Ag Nanowire Dimensions from AFM Measurements .....</b>	<b>74</b>
<b>Table 3.5 Assignments for Raman bands in a PANI sample deposited in a PAM which was made at 10 V. ....</b>	<b>79</b>
<b>Table 3.6 Assignments for Raman bands in a Ag / PANI composite sample in a PAM made at 20 V .....</b>	<b>89</b>
<b>Table 3.7 Assignments for Raman bands in a Cu/PANI composite in a 7V PAM.....</b>	<b>91</b>
<b>Table 3.8 Assignments for FTIR bands in a composite sample extracted from a PAM made at 40 V .....</b>	<b>93</b>
<b>Table 4.1 Assignments for Raman bands in films on ITO samples.....</b>	<b>108</b>
<b>Table 4.2: Conductivities of Ag / PANI composite and PANI films on ITO.....</b>	<b>113</b>

# Chapter 1 Introduction

## ***1.1 Nanotechnology and Nanomaterials***

There are many definitions of nanotechnology; in fact nanotechnology is a very broad term which encompasses different nanotechnologies in several areas of science and engineering. The unifying factor is that it involves phenomena on the nanoscale (normally 1 to 100 nanometers {1-100 nm}) i.e. below the wavelength of visible light. This means we are dealing with processes almost at the atomic and molecular scale (e.g. typical carbon-carbon bond lengths are in the range 120-154 pm or 0.12 -0.15 nm).

The applications of these different nanotechnologies are enormous and nanodevices are now used in the fields of medicine, ecology, biology, chemistry, informatics as well as many industries such as the auto industry (see detailed discussion and references in section 1.2 below). This has led to much interdisciplinary research collaboration and the establishment of many nanotechnology research centres in recent years.

Such collaborations and co-research lead to the possibility of fabricating devices with novel properties and new capabilities, plus the added advantages that miniaturization brings such as reduction in material needed, power expenditure and life cycle costs.

However, recent studies on the toxicology of nanoparticles have shown that these materials may also cause problems because of their size; for example nanostructures such as long thin carbon nanotubes have high aspect ratios which can cause them to behave like asbestos particles. The health and environmental impacts were reported in 2004 in a study conducted by the Royal Society and Royal Academy of Engineering [1]. It is thus important to follow current guidelines in the manufacture and characterisation of nanomaterials [2, 3].

In general materials are considered to be “nano” if they have at least one dimension smaller than 0.1  $\mu\text{m}$  or 100 nm [4, 5]. The concept is credited to Feynman who predicted in 1959 that the field of manipulating and controlling things on a small scale (i.e. nanotechnology) would have an enormous number of technical applications, that the elements of computers would have to be miniaturised and that electron microscopes would have to be more powerful [6]. It is thus possible to have different shaped



nanomaterials depending on which dimension is restricted e.g. 2D layers, 1D nanotubes and nanowires, and 0D nanodots or nanoclusters [7]. Because the size of the material is changed in one or more dimensions we would expect a change in the physical properties of the material due to quantum size effects, e.g. the melting point of nano gold is at least 300 °C less than that of bulk gold [8], the hardness of some transition metals such as gold and nickel is increased when the crystallite size is reduced [9, 10] and the band gap of semiconductors such as cadmium sulfide varies between 4.5 and 2.5 eV as the size goes from the molecular range to the macroscopic crystal [11]. Many nanomaterials display new interesting properties e.g. nanomaterials of gold, platinum and palladium have been shown to have magnetic moments [8]. Many display higher chemical reactivity because of the increased number of surface atoms in the nanomaterials compared to the bulk materials [12].

In fact nanomaterials usually have improved optical, electrical and mechanical properties compared to the bulk material and present objectives involve tailoring such materials to obtain properties suitable for a given application. The goal of this thesis is to fabricate structures of conducting polymers and nanowires which can be used in the fields of nanotechnology. This will open the possibility to make devices with unique optical, electrical, magnetic or mechanical properties.

## ***1.2 Uses/Applications of Nanomaterials***

As a result of their unique and often enhanced properties compared to the bulk materials nanomaterials can be used for a wide variety of applications and are responsible for many new technologies. Their use is already well established in many industries, for example titanium dioxide nanoparticles are used as additives in sunscreen and cosmetics; silver nanoparticles are used in food packaging; disinfectants and photography; nanoclays are used in the manufacture of tennis balls and car bumpers; carbon black nanoparticles are mixed with the rubber to improve the wear and strength of tyres; nanoparticles of organic pigments and metal oxides are used in ink and ink-jet printers and many coatings and adhesives contain polymer nanoparticles [5, 13]. They are also used as catalysts, ultra fine polishing compounds and optical fibre cladding. Two of the most important applications are the use of nanomaterials in medicine and the fabrication of nanodevices.

### 1.2.1 Biomedical Applications

Many nanomaterials possess antibacterial properties, for example silver nanoparticles have been used for purification throughout the ages. Nowadays nanoparticles of both silver and titanium dioxide are used as coatings for surgical masks [14]. Nanoporous membranes are also used in renal dialysis and for water purification. Polymeric membranes that contain a collection of monodisperse gold nanotubules can be used as ultra filters for selective transport of molecules (such as proteins) and ions [15].

The detection and separation of DNA has been done using nanoporous alumina filters [16] and DNA has also been translocated through synthetic nanopores [17, 18, 19]. It is relatively easy to functionalise nanomaterials with biological materials as they are of similar size, thus nanomaterials can be used to deliver drugs. Timed drug release can be achieved by encapsulating the drugs into a biodegradable polymer [20]. There is also potential for delivery of anticancer drugs and localised destruction of cancerous cells [21]. The use of polymer nanospheres for nasal vaccination is presently being researched [22]. Some nanomaterials are used to make nanoscaffolds, for example central nervous system cells are regenerated by nanofibre scaffolds [23]. The use of miniaturised detection systems is predicted to be the future trend for biomedical and biotechnical applications. This will involve the use of microchip technology in molecular biology and using a micro array for sequencing and analysing protein complexes [24, 25].

### 1.2.2 Electronic Applications

Electronics is one of the fastest growing areas in nanotechnology. Faster microprocessors can be achieved by the incorporation of more circuit elements such as transistors and logic gates, thus reducing their size is important. According to Moore's Law the number of transistors that can be inexpensively placed on an integrated circuit is doubling approximately every two years [5, 26]. Displays of televisions and computers can be improved by using nanomaterials such as nanocrystalline zinc selenide, zinc sulphide, cadmium sulphide, and lead telluride [27]. A large amount of information can be stored on discs or tapes which are composed of arrays of magnetic nanoparticles as well as thin films [28, 29]. This area of research has been well patented but is still on going, there is even a centre for magnetic recording research [28].

Carbon nanotubes, in particular, because of their unique dimensions and unusual current conduction mechanism, may be ideal components of electrical circuits, transistors, Micro-Electro-Mechanical Systems (MEMS), interconnects, and other circuit elements



[30, 31]. Many nanomaterials are already used to make field effect transistors [32, 33], detectors and sensors ranging from radiation detectors to biological and chemical sensors [24, 25, 34, 35, 36, 37, 38, 39, 40, 41], high energy density batteries [42, 43] and nanoelectrode arrays [44, 45].

### 1.2.3 Optical Applications

The number of nanomaterials with optical applications is also vast and ranges from their use in the manufacture of “self cleaning windows” to more conventional applications of photonics such as the fabrication of photonic crystals, tuneable optical filters, microcavities, waveguides, solar cells, photovoltaic cells, light emitting diodes, optical sensors, optical switches, optoelectronic memory devices and their use in display technology [46, 47, 48, 49, 50, 51, 52, 53, 54, 55, 56, 57]. Because of the present quest for new and renewable energy sources much present research is concentrated on solar cells and photovoltaic cells.

It is well known that the addition of carbon nanotubes greatly improves the efficiency of photovoltaic devices [58, 59]. Research in this area is on-going using other nanoparticles as well as carbon nanotubes [60, 61]. Organic solar cells have been made using porphyrins and fullerene units deposited on nanostructured tin oxide electrodes [62]. Lead sulphide nanoparticles have also been used to make photovoltaic devices [63] and cadmium selenide quantum dot-single wall carbon nanotube complexes have been used in the manufacture of polymeric solar cells [64]. Solar cells can also be made from other nanomaterials e.g. highly-ordered titanium dioxide nanotube-arrays [65].

### 1.2.4 Structural, Functional and Smart Materials

A large area of research focuses on the creation and development of new nanostructured materials with controlled size, morphology and architecture which have functional properties. Such materials have physical or chemical properties which are sensitive to changes in the environment such as pressure, temperature, humidity, acidic or basic conditions; presence of gas molecules; application of an electric or magnetic field and optical wavelength. They respond to these changes with an intelligent action [66]. Some examples are responsive or electroactive polymers which can be used to make smart bioactive materials for medical applications such as synthetic polymer muscles [67], nanostructured polymer thin films to make artificial skin and shape memory

polymers to make stain resistant and wrinkle free fabrics; and clothes which respond to changes in heat and moisture [68, 69].

Nanomaterials can also be used to make nano tools such as nano tweezers and novel probe microscopy tips [7,70,71].

Nanotechnology offers us the opportunity to understand how nature works at the atomic scale; operating at the nanoscale means that the classical laws of physics may no longer be applicable and quantum effects take over. The properties of nanomaterials differ not only from those of their corresponding bulk materials but also from those of their corresponding molecular compounds. This is of fundamental interest to scientists.

### **1.3 Synthesis of One-Dimensional Nanostructures**

Two main approaches are used to produce nanomaterials. In the "top-down" approach, nano-objects are constructed from the bulk material by physical means such as lithography, where the material is cut and shaped for the specified requirement. In the "bottom-up" approach, materials and devices are built from molecular components by self assembly or chemical reactions. Although the top-down approach is widely used, and the miniaturisation of tools used in nanotechnology have improved dramatically in the last decade which facilitates this, the bottom-up approach has the advantage that new materials can be made and reproduced whereas the top down method often leads to non-reproducible results [72]. Materials which exhibit desired novel properties can also be especially designed using this method.

One-dimensional nanostructures are of particular interest because of their potential applications in the electronic and optoelectronic industry [73].

#### **1.3.1 VLS (Vapour – Liquid - Solid)**

One of the earliest methods used to produce one-dimensional nanostructures is VLS. This was proposed by Wagner and Ellis in 1964 [74] who made single crystal whiskers via a gas phase reaction involving a vapour-liquid-solid process. This involves the condensation of a species from the vapour phase onto a miscible liquid, followed by supersaturation of the species to form a solid phase [75]. The big drawback at the time was that most of the structures produced had diameters greater than 1  $\mu\text{m}$  which were



determined by the liquid metal catalysts used [7]. Since then growth conditions have improved and this method is still used today [76]. The main advantage is that single crystal wire structures can be fabricated.

### 1.3.2 MOVPE (Metal - Organic - Vapour - Phase - Epitaxy)

Metal Organic Vapour Phase Epitaxy (MOVPE) is a method of creating controllable epitaxial layered structures by atomic deposition on a suitable substrate. A substrate wafer is heated in a reaction vessel. The reaction products are grown in a hydrogen atmosphere and then form epitaxial layers on the substrate as they decompose. MOVPE was first used by Hiruma et al. in the early 1990s [77, 78, 79, 80] to produce single crystal gallium arsenide nanowires with diameters between 15-40  $\mu\text{m}$  on  $\text{SiO}_2$  pre-patterned substrates using trimethylgallium and arsine as source materials and gold as a growth catalyst. This method is still used today [81].

### 1.3.3 CVD (Chemical - Vapour - Deposition)

The method used in Chemical Vapour Deposition (CVD) is similar to that of MOVPE. The desired solid product is deposited from the reaction of a vapour or gas or mixture of vapours / gases onto the surface of the substrate. This method can be used to make thin films as well as nanowires and nanotubes. The materials can be crystalline or amorphous, conducting, semiconducting or insulating. It is one of the most common methods used to produce carbon nanotubes. In that case a carbon-containing gas molecule, such as methane, acetylene or carbon dioxide at sub-atmospheric pressure is used and the substrate contains a layer of metal catalyst particles, most commonly nickel, cobalt or iron. There are several different types of CVD which are named after the conditions used, e.g. plasma enhanced CVD involves processes that use a plasma to speed up the chemical reactions of starting materials, thus allowing deposition at a lower temperature [82].

### 1.3.4 Laser Ablation and Condensation

This was first used to generate nanoclusters [83] and later adapted by Morales and Lieber [84] to prepare bulk quantities of single crystal silicon and germanium nanowires with diameters in the 10 nm regime.

Many of the methods used are a combination or adaptation of VLS, CVD and laser ablation, for example Lee and co-workers used an oxide-assisted method to synthesise several semiconductor nanowires, including silicon, germanium, gallium arsenide and gallium phosphide by laser ablating a suitable target [85]; and Pan et al. synthesized nanobelts of semiconducting oxides of zinc, tin, indium, cadmium, and gallium by simply evaporating the desired commercial metal oxide powders at high temperatures [86].

### 1.3.5 Solvothermal Methods

This method was pioneered by Heath et al. for generating semiconductor nanowires [87] and used by many authors to produce nanotubes [88] and nanowires [89]. Basically the precursor and reagents are added to a solvent in appropriate ratios; the mixture is then placed in an autoclave where a reaction leading to nanowire growth takes place at elevated temperatures and pressures [90].

### 1.3.6 Solution Phase Methods

Semiconductor nanorods and metal nanowires have been synthesised by using capping reagents to control the shape of colloidal particles which are produced by solution phase methods [90 and references therein]. For example cadmium selenide quantum rods were obtained by adding hexylphosphonic acid (HPA) to a cadmium selenide precursor in trioctylphosphine oxide [91]; and silver nanowires with controllable lateral dimensions and lengths were produced by reduction of silver nitrate in ethylene glycol in the presence of poly(vinylpyrrolidone) [92].

### 1.3.7 Size Reduction Methods

Many of the above methods are not suitable for the production of 1-D nanostructures with diameters less than 10 nm. In this case it is sometimes better to use the “top-down” approach of miniaturization or size reduction. Manufacturers tend to favour this approach and there have been many recent advances in the technology used. The most common methods are lithography and chemical etching.



### **1.3.7.1 Isotropic Deformation**

This is a very simple method which was used by Taylor in the 1920s to produce metal filaments [90, 93]. A metal wire is enclosed in a glass capillary and enough heat is applied to melt the metal and soften the glass tube so that it can be drawn out. Filaments of lead, antimony, bismuth, gold, silver, copper, iron, tin, thallium, cadmium, cobalt, gallium, and indium have been made by this method. The glass capillary can be left for protection or removed with hydrofluoric acid. Metal filaments as thin as 10 nm have been made by this method [90, 94].

### **1.3.7.2 Anisotropic Etching**

Parallel arrays of nanowires can be formed by etching a substrate which has been pre-patterned with trenches [90, 95]

### **1.3.7.3 Lithography**

Lithography is the process of removing parts of a thin film and transferring patterns from one material to another. Optical lithography uses light to form patterns or arrays on thin layers of photoresist materials which have been deposited on a suitable substrate. This can then be used as a mask or removed to make nanowire arrays. It is an inexpensive and rapid method for fabricating large arrays, but may leave a large number of defects and is restrictive in the shapes and sizes that it can produce plus it can require extremely clean operating conditions. Colloidal nanosphere lithography (NSL) can also be used to produce highly ordered nanostructures at low cost. It involves the self assembly of nanodisperse colloidal spheres of equal size on silicon substrates which then serve as templates for novel nanostructures such as nanodots and nanowires [96]. However this method may also cause damage to the crystal structure. Direct write methods such as “E-beam lithography” (EBL) and “Focused Ion Beam” (FIB) are often used instead of conventional photolithographic techniques as the resolution is greater [97]. Here a focused beam of electrons is used to form patterns on the resist. As the e-beam has to be scanned over the whole surface this method is much slower than photolithography, where the whole system is patterned in one go, but it offers better control of size, shape and lattice spacing and fewer defects are made; however it is usually much more expensive. Electron beam direct write lithography (EBDW) is more flexible since there is no need to use a mask which leads to savings in cost and time and each sample can also be personalised [98].

The first e-beam lithography machines were developed in the 1960s [99] using SEM technology. The first potential useful structures were made in 1964 by Boers [100]. This method is now widely used to make metal nanostructures. Nanoparticles of gold, silver, palladium, cobalt, nickel and molybdenum have been fabricated by using thin film resists made from organic complexes, inorganic salts and solutions of nanoparticles [99]; and silver, silicon and palladium nanowires have been made by EBDW or FIB [101, 102, 103].

Nanoimprint lithography can also be used to imprint patterns on a resist using a nanostamp or mould with nanostructures on its surface. The compressed areas of the residual resist are then removed by etching. This method is low cost as it doesn't use expensive e-beam or light sources and there are no associated problems of low resolution due to backscattering and interference [104].

Dip-Pen-Nanolithography (DPN) uses an AFM tip to deposit molecules by direct write techniques. It is also cheaper than e-beam or photolithography. It was first used by Mirkin and co-workers in 1999 [105] and has been traditionally used to make templates, create biological patterns and deposit metals. It is now used in microfluidic ink delivery systems, independently actuated cantilevers, and as a tool in the medical industry e.g. DNA arrays or conductive metal traces using nanoparticle based inks [106].

Kim et al. have recently shown that optical lithography followed by a metal deposition / lift off process can be used to make metal nanoelectrodes with a 20 nm size gap [107].

### 1.3.8 Self-Assembly

Top-down patterning methods are also used to pre-pattern catalysts on a substrate which is then used to produce nanowires by self assembly [97]. Nanoparticles can also self assemble through chemical lithography [108]. In 1998 Korgel and Fitzmaurice showed that silver nanocrystals made by self assembly from solutions containing silver ions could be fused into 2-D nanowire arrays [109]. In 2002 Hassenkam et al. produced 2-D gold nanowires using assembly in the presence of surfactants [110] and Tang et al. discovered that cadmium telluride nanoparticles reorganised themselves into crystalline nanowires when the organic stabiliser used in their production was removed [111].

Self assembly can also be guided by templates. In 1997 Schmid and co-workers made gold nanowires by filling alumina templates with gold nanoparticles or clusters



[112, 113]. Biopolymers, peptides and DNA have also been used to guide the assembly of gold nanoparticles into chains or lattices [114, 115, 116].

### 1.3.9 Template Directed Synthesis

Since the properties of nanomaterials are very dependant on the size and shape of the nanoparticle it would be useful to use a synthetic method which could control this. One such method is templated synthesis. The template serves as a solid support and usually consists of a porous membrane into which nanomaterials are directly synthesised. The most common membranes used are track etched polymeric membranes made from polycarbonate and polyester; porous alumina membranes made by anodisation of aluminium; and mesoporous zeolites. However, many other structures such as step edges on the surface of a solid substrate, protein cages and even viruses have been used for nanowire growth.

The Martin group developed the template method. In 1990 they made polymer microtubules in a polycarbonate membrane filter by both heterogeneous synthesis and electrochemistry [117, 118]. They adapted this method to synthesize nanomaterials in the early 1990s [119, 120, 121]. They used track etched polymeric membranes and porous alumina membranes (PAMs) and deposited the materials by metal ion reduction. Track etched membranes are made by bombarding the material, usually polycarbonate or polyester, with nuclear fission fragments. This creates tracks in the material which can then be chemically etched to make pores. The pores will all be of uniform diameter (which can be as small as 10 nm) but they are randomly distributed throughout the membrane. PAMs, on the other hand, contain cylindrical pores of uniform diameter which are arranged in a uniform hexagonal array [122]. They are usually made by the anodisation of aluminium in an acidic medium as described by Masuda and Fukuda in 1995 [123] and are thus also known as anodic aluminum oxide (AAO).

Other templates made around the same time include nanochannel array glass with pore diameters down to 33 nm and pore densities as high as  $3 \times 10^{10}$  pores  $\text{cm}^{-2}$  made by Tonucci et al. [124]; thin metallic membranes containing uniform pores with diameters around 40 nm have also been replicated from these [125]. Zeolites and molecular sieves are popular templates for both conjugated polymers and inorganic materials [72] and mesoporous zeolites with diameters as small as 3 nm have been prepared from MCM-41, a honeycomb-like structure of amorphous silica [126, 127]. As well as polymeric ion-track membranes other organic polymer hosts and block co-polymers have been used as templates [128, 129]. Recently a new generation of track-etched templates made from

nanoporous thin polycarbonate which can be used to make nanostructures of diameters between 15-10 nm and lengths between 200 nm to several  $\mu\text{m}$ s have been developed [130]. Templates made from biological molecules include polypeptide cages [131], peptide fibrils, tubules and assemblies [132, 133], cell membrane proteins [134], DNA [115, 116, 135, 136, 137] and viruses [138, 139, 140]. Templating against features on a solid surface such as V-grooves and step edges is also a popular method to make 1-D nanostructures. Examples include: shadow sputtering against an array of V-grooves which have been etched onto silicon wafers or faceted sodium chloride [141], electrodeposition at step edges [142, 143] and cleavage overgrowth (CEO) on the cross section of a semiconductor multilayer structure [144]. In 1994 Ramanathan et al. [145] used electrodeposition between electrodes in channels created on semiconducting and insulating surfaces to fabricate conducting polymer nanowire arrays of controlled dimensions. Nanotubes themselves can also be used as templates; for example, carbon nanotubes have been filled with molten metals or salts by capillary action [90, 146], with metal oxides by wet chemical techniques [147] and with metals and/or their compounds using the arc-discharge method [148].

## **1.4 Thesis Aims**

The goal of my research is to fabricate new hybrid inorganic/organic nanostructures with a view to enabling new applications. This thesis describes the synthesis of metallic and semiconducting nanowires and metal / polymer composite nanocables from the “bottom up” by electrodeposition into a pre-formed porous alumina membrane and the synthesis of metal / polymer thin films by electroplating. Possible applications of these structures are discussed.

One motivation behind this is the work done in this research group on carbon nanotubes / polymer composites which showed improved mechanical and opto-electrical properties [149, 150, 151, 152, 153, 154, 155, 156]. This suggests that new composites using non-carbon nanoparticles should also have interesting and novel properties.



# Chapter 2 Experimental Background

## 2.1 Materials

### 2.1.1 Porous Alumina Membranes (PAMs)

#### 2.1.1.1 Advantages of PAMs

Even with the large variety of templates available today templating with PAMs remains one of the most popular methods to produce 1-D nanostructures. There are several reasons for this: they consist of a highly ordered arrangement of uniform and parallel pores organized in an almost perfect hexagonal structure, the pores are nanometre sized (average pore diameters range from 10 nm to 200 nm) and have a high aspect ratio (lengths from 100 nm to 200  $\mu\text{m}$ ). The pore sizes are controllable on a larger scale by simply changing the anodisation parameters and pore densities vary between  $10^9$  and  $10^{11}$  pores  $\text{cm}^{-2}$ .

In addition their synthesis is cheap, versatile and simple and there have been vast improvements in production techniques in the last ten years [157, 158, 159, 160] resulting in membranes of high quality in terms of pore size uniformity and high pore size distribution with good thermal and mechanical properties [160, 161, 162, 163, 164]. The membranes themselves have good chemical and physical stability and good insulation properties. They are transparent in the ultraviolet, visible and infrared spectral range, which may be useful for characterisation and integration into devices or chips. The alumina template also protects the nanowires from oxidation and avoids the problem of aggregation which many nanowires and nanotubes suffer from. It is very easy to dissolve the membrane to leave free-standing nanowires. They are also commercially available.

The main advantage of using PAMs as templates for nanowire synthesis is their versatility; they can be used to prepare nanowires, nanorods and nanotubes of metals [112, 113, 119, 120, 122, 123, 165, 166, 167, 168, 169, 170, 171, 172, 173, 174, 175, 176, 177, 178] conducting polymers [118, 119, 122, 179, 180, 181, 182, 183, 184], semiconductors [118, 122, 185, 186, 187, 188, 189, 190, 191, 192, 193, 194], carbon [119, 122, 195, 196, 197, 198], composite nanostructures [199] and segmented composite or striped nanowires [200, 201, 202, 203, 204, 205]. They can be filled by several

different techniques [140] which can also be used to tailor the properties of the nanomaterials; for example filling by electrodeposition is known to produce nanomaterials with higher electronic conductivities [118] and gold nanorods made by this method exhibit higher order surface plasmon resonances [148]. They are thus used in a wide variety of applications, some of which are described in section 1.2. There is also the possibility of observing quantum effects as it is possible to get pore sizes down to the order of the Bohr radius of some bulk semiconductor excitons [63].

### 2.1.1.2 Properties of PAMs

It is well known that when high purity aluminum is anodized in polyprotic acids a porous oxide film develops [157, 158, 206, 207, 208, 209, 210, 211, 212, 213, 214, 215, 216]. The pores form in a long, narrow, parallel geometry orientated perpendicular to the substrate. A schematic of this is shown below (Figure 2.1).

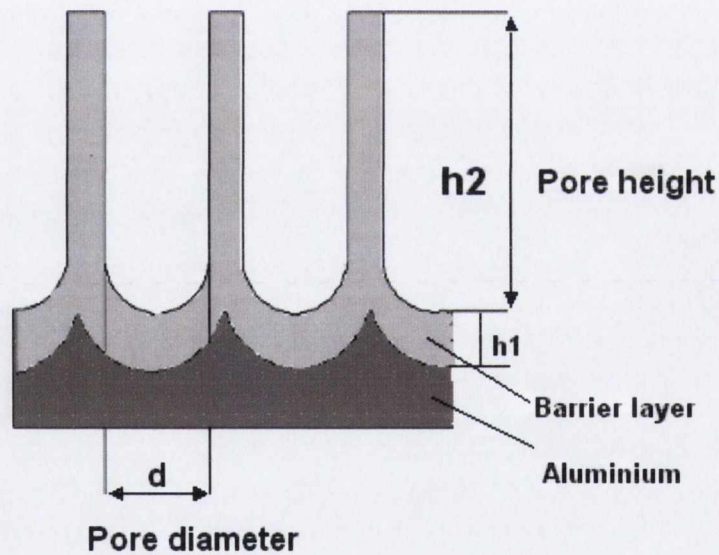


**Figure 2.1:** Cross section of an anodized aluminium foil showing pores of diameter  $d$ , height  $h_2$  and a barrier layer of height  $h_1$

They consist of a thin non-porous barrier layer next to the metal and a porous layer on top of this. The thickness of the barrier layer depends on the anodising voltage (applied cell potential); it is usually 0.8-1.2 nm per applied volt [214, 216]. The structure and chemistry of the barrier layer depends on this acid used for anodisation [223]. The thickness of the porous layer ( $h_2 =$  height of the pores) depends mainly on anodising time, but also on the current density, which is determined by the electrolyte and



anodisation voltage. A layer of thickness of about 5-10  $\mu\text{m}$  is obtained after 2 hours for high and 19 hours for low current densities [217]. The pore diameter ( $d$ ) depends on the pH of the electrolyte used and the anodising potential [209]. Typical diameters are between 1.0 - 1.5 nm / V. The pore density also depends on the applied cell potential  $U$ , and falls off with rising voltage [210, 211, 212, 213]. The interpore distance  $D_{\text{int}}$  is linearly proportional to  $U$

$$D_{\text{int}} = kU \quad (2.1)$$

where  $k$  is the proportionality constant approximately = 2.5 nm / V [174].

The arrangement and shape of the pores can also vary depending on the anodising conditions. Self ordered porous alumina has an almost perfect hexagonal structure across the surface of the substrate as shown in Figure 2.2. To obtain such perfect arrangements a porosity of the alumina of 10% is required [174, 218]

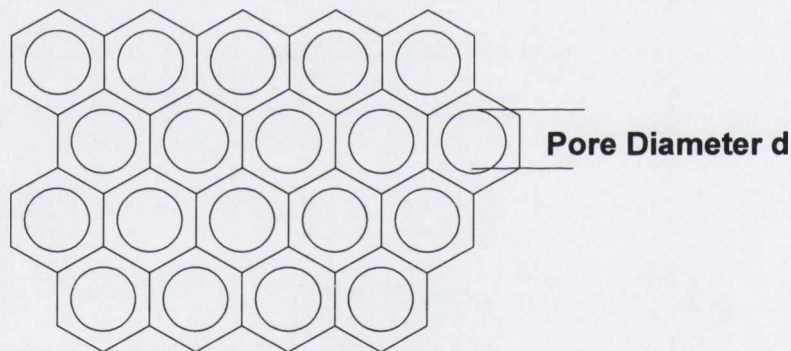


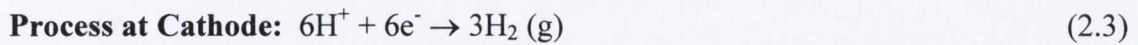
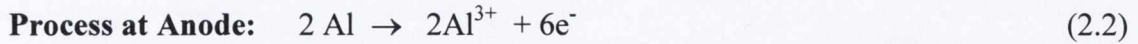
Figure 2.2: Top view of an anodised aluminium foil showing pores of diameter  $d$

### 2.1.1.3 Fabrication of PAMs

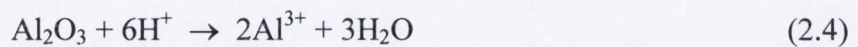
PAMs are made by the anodisation of aluminium foil. Before anodisation it is necessary to pre-treat the surface of the foil as described in section 4.1.1 of this thesis i.e. the foil is first annealed, cleaned and then electropolished.

### 2.1.1.3.1 Electropolishing

During electropolishing the aluminum foil is connected to the positive terminal i.e. used as an anode, while lead (Pb) is used as the cathode. When a potential is applied, the electrolyte acts as a conductor and metal ions are removed from the aluminium.



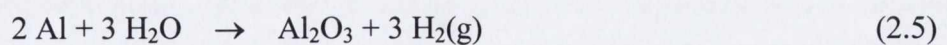
Any alumina formed is re-dissolved in the hot acid.



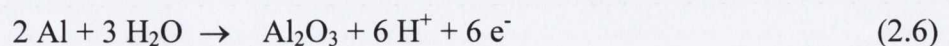
The voltage used for electropolishing depends on the voltage which will be used later for anodisation of the foil. If an anodisation voltage of less than 10 V is used then the electropolishing is carried out at 10 V. If an anodisation voltage greater than 15 V is used then the anodisation is carried out at 15 V. For anodisation between 10-15 V, electropolishing is done at the anodisation voltage. This gives a current density between 0.5 and 1.5 A cm<sup>-2</sup> [219].

### 2.1.1.3.2 Anodisation

The anodisation process is similar to that of the electropolishing, except that the oxide layer is not dissolved by the electrolyte and builds up on the aluminium as described in section 2.1.1.2. The process can be summarised as follows:



Oxidation takes place at the anode (Aluminium foil) leading to the production of alumina as follows:



This takes place in several stages.



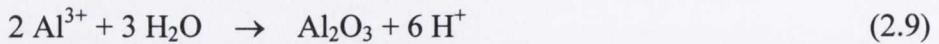
At the metal oxide interface the following reaction takes place:



Aluminium ions are produced by dissolution of aluminium:



Leading to further production of alumina at the oxide/electrolyte interface:



The amount of metal removed (and thus oxide produced) depends on the electrolyte, operating temperature and current density achieved.

Reduction takes place at the cathode whereas hydrogen gas is evolved



The number of electrons transferred increases until the anodisation is halted and therefore determines the total amount of alumina produced. Thus oxidised thickness increases linearly with time. However the growth rate of oxide also depends on the strength of the acid, for example Gerein and Haber found a growth rate of 6.0  $\mu\text{m} / \text{hr}$  in sulphuric acid and 2.4  $\mu\text{m} / \text{hr}$  in oxalic acid [220].

The electrolyte used also affects the size of the pores and determines the applied voltage. Smaller pore diameters are obtained when the pH of the electrolyte is lower as the pore tip is less likely to be dissolved i.e. smaller pores are obtained for stronger acids at lower voltages [221, 222]. In fact there is a relationship between electrolytes used, anodisation potential and inter-pore distance; as shown in the following plot (Figure 2.3) from the Multifunctional Nanowires and Nanotubes group in Max-Planck-Institut für Mikrostrukturphysik, Weinberg 2, D-06120 Halle, Germany [206, 223].

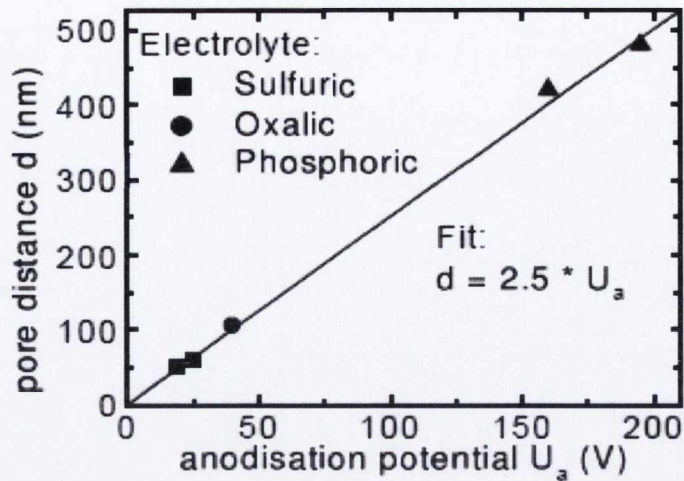


**Figure 2.3:** Plot of inter-pore distance versus anodisation potential for disordered pore arrays (line). Self ordered pore arrays (symbols) fit on the same curve [223].

Recent research has concentrated on improving the ordering and homogeneity of the pore array. This can be done in several ways. It has long been known that a better honeycomb structure is obtained by anodisation over long periods under constant conditions as oxide growth is from the foil interface and pore ordering improves as this growth continues [208]. The arrangement of the pores at the base of the alumina layer is thus more ordered than on the surface. This is confirmed by SEM images of the top and bottom of PAMs [206]. To obtain better ordering Masuda and Fukuda exploited this fact. In 1995 they developed a 2-step anodisation process [123].

The first step involves anodising the aluminium foil overnight or for several days, depending on the thickness of the foil, and then removing the resulting oxide using hot chromic acid (as used in the electropolishing step or reference 157). This leaves a regular hexagonal pattern on the aluminium surface which acts as a template for the second, shorter anodisation process. Lastly a voltage reduction is done to thin the barrier layer [172].

This is illustrated in the following schematic (Figure 2.4):



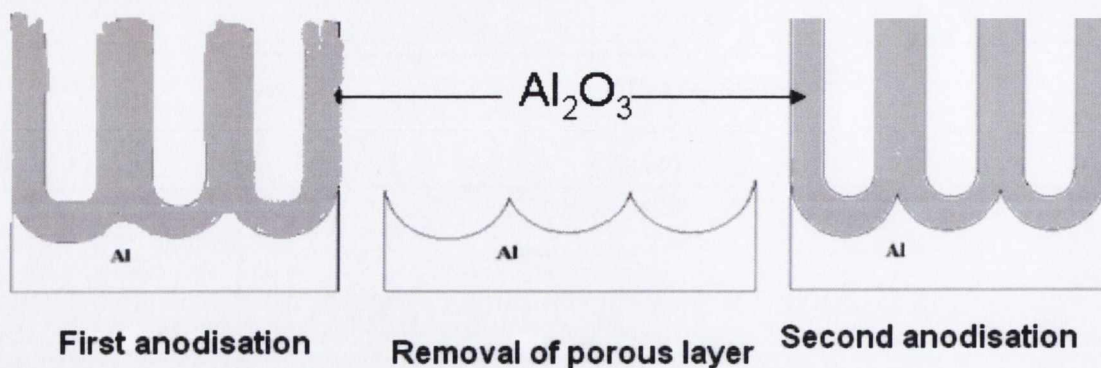


Figure 2.4: Schematic of the 2-step anodisation process

Jessensky also stressed the importance of using constant conditions for regular pore growth [208]. In 2002 Nielsch achieved a highly ordered alumina pore array with interpore distances of 65 and 100 nm [224]. He used a modified Jessensky cell with improved thermal isolation and temperature control so that the temperature difference between the electrolyte, aluminium substrate and cooling plate did not exceed 2 °C.

Pore growth follows the domain structure of the aluminium. However to obtain monodomain porous arrays the aluminium surface can be pre-textured by e-beam lithography or by nanoimprinting methods [157]. Masuda and co-workers obtained defect free PAMs with hexagonal, triangular or rectangular pore arrays by combining nanoimprint lithography and self assembly of porous alumina [225, 226, 227, 228]. In 2003 they showed that an arrangement of initiation sites, which is different from ordinary hexagonal cell arrangement, could significantly control the growth of anodic porous alumina [159]. Around the same time Mikulskas et al. used commercially available optical gratings to pre-structure rhombohedral edges on aluminium which were used to guide pore growth during anodisation [229]. In 2003 Choi et al. made monodomain porous alumina with a high aspect ratio and an interpore distance smaller than the lattice constant of the pre-pattern by using the correct anodising conditions and SiN pyramids as a master stamp [158]. They also extended this method to make PAMs with Moiré patterns [230]. In 2005 a new template directed method was developed by using gold catalyst templates. These were electrochemically replicated from ordered porous alumina [231]. These gold nanotubes which have been deposited inside PAMs have also been used as metal nanotube membranes which can be used as shadow masks for generating nanopatterned substrates and extended 2-D arrays of metal nanorods via sputter deposition [232]. They would be much stronger than the brittle alumina membranes. Similar moulds with nanopillar structures were fabricated by using anodic aluminium

oxide (AAO) for nanoimprint lithography (NIL). This involves sputtering aluminium into the porous alumina walls of the AAO template (or PAM) so that the pillars had skin layers of aluminium/alumina composite which added additional mechanical strength and chemical resistance [233]. In 2006 Woo Lee et al. used large area Ni stamps to pre-pattern the aluminium and produced long range ordered oxide arrays in hexagonal, rectangular and square lattices [234]. The same group developed a new oxalic acid based hard anodisation process [160]. This new process has several advantages over conventional anodisation processes e.g. faster processing time, allowing 2,500–3,500% faster oxide growth and with improved ordering of the nanopores. A new self-ordering regime with interpore distances, ( $D_{int}$ ) = 200 –300 nm, which was not previously achieved by mild anodization processes was obtained. Perfectly ordered alumina membranes with high aspect ratios (>1,000) of uniform nanopores with periodically modulated diameters were made and a better understanding of the mechanism governing the self-ordering of oxide nanopores during the aluminium anodisation was obtained [160]. Recently a new route for the formation of PAMs in neutral electrolytes was done by Tsuchiya et al. [235]. They found that the addition of fluoride ions to the electrolyte increased the ordering of the oxide layer. The concentration of fluoride also influenced the thickness and growth rate of the porous layers.

### **2.1.1.3.3 Barrier Layer Reduction**

Because the barrier layer is highly insulating it inhibits anodic current in the electro-deposition process used for filling the pores and should therefore be reduced if it is greater than about 20 nm thick (thus all foils anodised at voltages greater than 20 V). The barrier layer thickness is reduced by reducing the anodising voltage, however if this is done in one step it has been found that reduction will only happen at the base of a few pores due to uneven chemical dissolution [236]. Uniform barrier layer thinning can be achieved by using current limited anodisation steps. This was done by Furneaux et al. in 1989 [212] and is the method used in this thesis. Other authors have used similar methods, for example Nielsch et al. [169] reduced the voltage by a factor of two after anodisation steps of 10-15 minutes each until the voltage was down to 6-7 V and a barrier layer of 10 nm was achieved. They have also done this by using a Labview computer program linked to the power supply [224]. Gerein and Haber [220] lowered the voltage by 2 V / min until it was reduced by 75%, after which the voltage was lowered by 1 V/min until a final anodisation voltage was reached, depending on the barrier layer thickness



required. The anodisation was then continued for 8-10 min at this final voltage to allow for equilibration of the barrier layer.

The barrier layer can also be removed without removing the Aluminium backing using a chemical etching technique which involves immersing the templates in aqueous phosphoric acid [169, 172]. This method can also be used to widen the pores [173].

#### **2.1.1.4 Filling of PAMs by Electrodeposition**

The porous alumina templates can be filled in several ways. The most commonly used methods to fill the pores with metals are chemical reduction of a metal salt [120, 121, 122, 123, 165] and electrochemical reduction of a suitable electrolyte [122, 169, 172]. Semiconductors are usually filled by electrochemistry [185, 186]; polymers have been deposited into the pores electrochemically [179, 182] and by wet solution [183, 184].

Electrodeposition is the preferred method to produce nanowires as the nanowires created have large aspect ratios and are highly conductive. Structural analysis of metallic nanowires shows they are dense, continuous and highly crystalline compared to CVD deposited wires [237]. This is because the growth starts at the pore tip and builds up successfully [169]. It has also proven to be a low cost and high yield technique [123, 237]. Electrochemically deposited nanopolymers have much higher conductivities than powder or thin film forms and are more stable than those produced by chemical means [118, 181, 238].

In this thesis metals, polymers and metal/polymer composites were filled by electrochemical means. This was done in three different ways.

##### **2.1.1.4.1 Direct Current (DC) Electrodeposition**

Using Electrodeposition to fill the pores of a membrane was patented by Charles P. Bean in 1969 [239]. In 1970 Possin demonstrated the use of nanoporous membranes as templates when he deposited tin inside a track etched mica film [240]. This method was refined in 1984 by Williams and Giordano [241] who deposited gold wires in mica but it was not until the 1990s that this method really took off due to the work of C. R. Martin who used track etch polymeric membranes and porous alumina to prepare polymers,

metals, semi-conductors and other nanoscopic materials [119]. He also showed that alumina membranes are superior to track etched membranes as the pore distribution is regular rather than random. The pores are also deeper and denser than polycarbonate membranes [121].

Electrodeposition by DC is very unstable and uniform filling of the pores cannot be achieved due to the cathodic side reaction which leads to partial removal of the barrier oxide, formation of holes in the barrier layer and local deposition in single pores [69, 242]. To overcome this, the aluminium metal and barrier layer directly underneath the porous layer are removed, and a conductive layer (usually gold or platinum) is sputtered (or thermally evaporated) on top of the exposed pores beneath. This layer will thus have direct contact with the porous oxide, and can thus act directly as a working electrode [243]. This is illustrated in Figure 2.5.

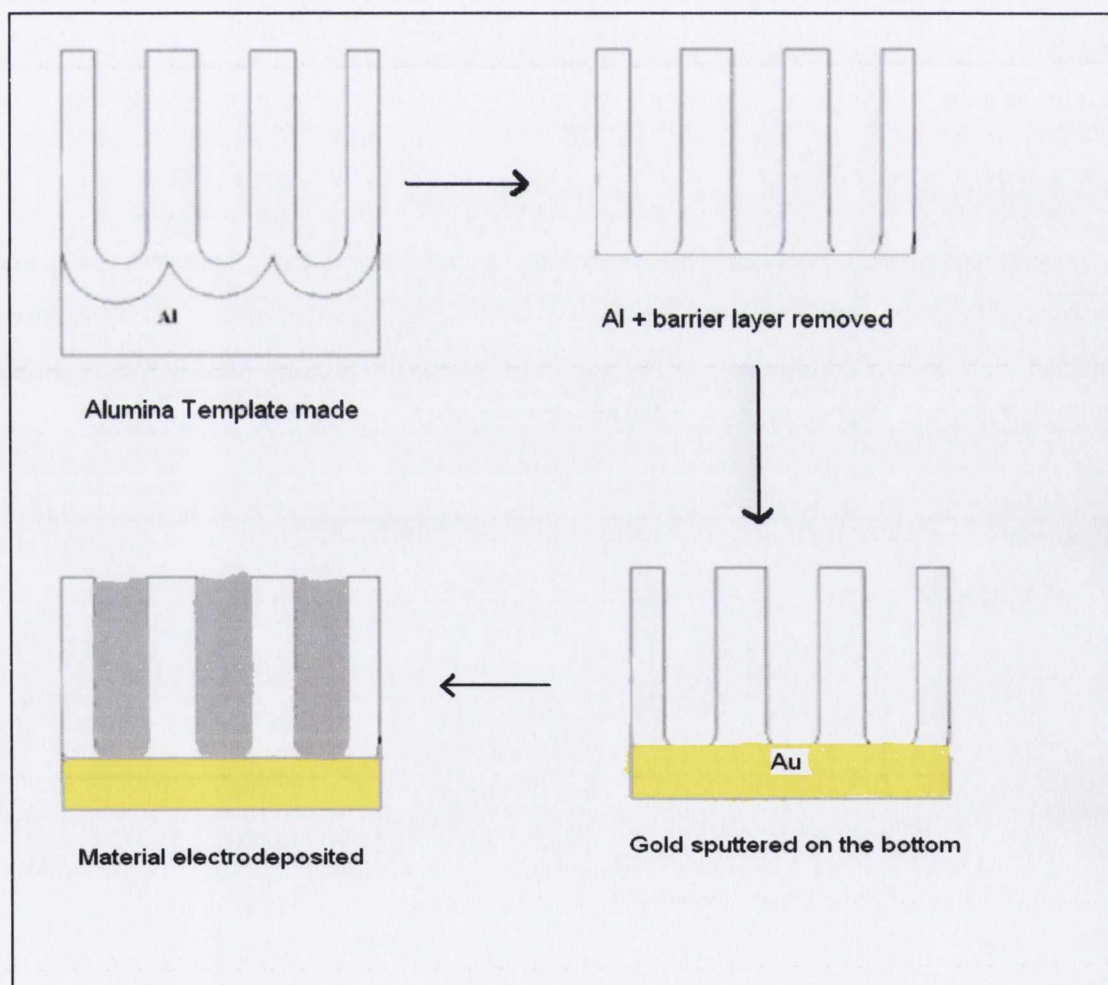


**Figure 2.5 Schematic of the scheme used for DC electrodeposition in an AAO template**



The conductive layer is used as the cathode and another conductor (such as graphite, platinum or gold is used as the anode. Reduction of the conducting material such as a metal salt takes place at the cathode leading to a deposition of metal in the pores:



whereas hydrogen is evolved at the anode:

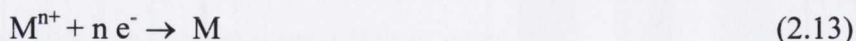


A disadvantage of DC is the fact that it is usually restricted to deposition into large pore diameters as it is difficult for the metal to get down narrow pores. This leads to deposition of metals on the surface of the membrane and the formation of colloids in the pores [244]. It has also been found that some pores are preferentially filled to others leading to a large surface build up of metal [245].

#### 2.1.1.4.2 Alternating current (AC) Electrodeposition

AC deposition was first developed and patented by Caboni in 1936 [246] and Langheim-Pfandehauser GmbH in 1940 [247]. It has been developed and used primarily for colouring anodised aluminium [248] and extensively for making nanowires in porous alumina [171, 187, 249, 250, 251, 252, 253, 254, 255].

The material M is deposited in the pores during the cathodic half cycle



and hydrogen is produced at the other electrode:



Some material is re-dissolved during anodic half cycle





There is however a net deposition of metal because of the valve nature of the barrier layer which acts as a rectifier and preferentially conducts the cathodic current. If the barrier layer is too thick the anodic current is inhibited; for successful deposition by AC it is necessary to do a voltage reduction at the end of the anodisation process as described in section 2.1.1.3 and chapter 3, section 3.1.3.

Although AC deposition is successful for many pore sizes when the barrier layer is effectively reduced; filling by AC is not homogeneous and usually results in only about 10% of the pores being filled. Deposition can be inhibited by the high cathodic potentials due to the evolution of hydrogen [168]. Also many pores are only partially filled [121]. This is because the pores are filled from the base upwards as the electric field is greatest at the base, if however, the pores get narrower or inhomogeneous then the electric field is affected and deposition may stop [256].

Filling can be improved when the homogeneity of the matrix is improved. Better filling is also achieved by using modulated pulse signals or filling by pulsed electrodeposition (PED).

#### **2.1.1.4.3 Pulsed Electrodeposition (PED)**

The concept of “Pulsed Plating” was developed by Puipe and Leaman in 1986 [257] and patented by Erb et al. [258] in 1993. It has been used to fill PAMs by many authors [169, 172, 177, 178, 224, 259, 260].

PED allows for better control over the deposition parameters and results in better deposition by increasing the concentration of metal ions at the pore tips. This is achieved by introducing a time delay between deposition pulses which allows the concentration of metal ions to recover. The concentration of metal ions is also increased by using a Watts bath electrolyte which uses a much higher concentration of metal salts. It contains metal chlorides as well as sulphates. The chloride ions improve the conductivity of the electrolyte and oxide dissolution thus allowing better deposition of the metal [261]. The Watts bath also contains Boric acid which acts as a buffer and maintains the pH of the electrolyte to 4-5 to avoid corrosive attack of the aluminium template (as it is weakened in solutions of high pH).

The pre-treatment of the alumina template is the same as for AC except it is necessary to reduce the barrier layer even further (i.e. reduce the voltage to 5-6 V in small



steps) so that the thickness of the barrier layer is uniform and deposition is homogeneous [178].

The procedure for PED is illustrated in the following graphs:

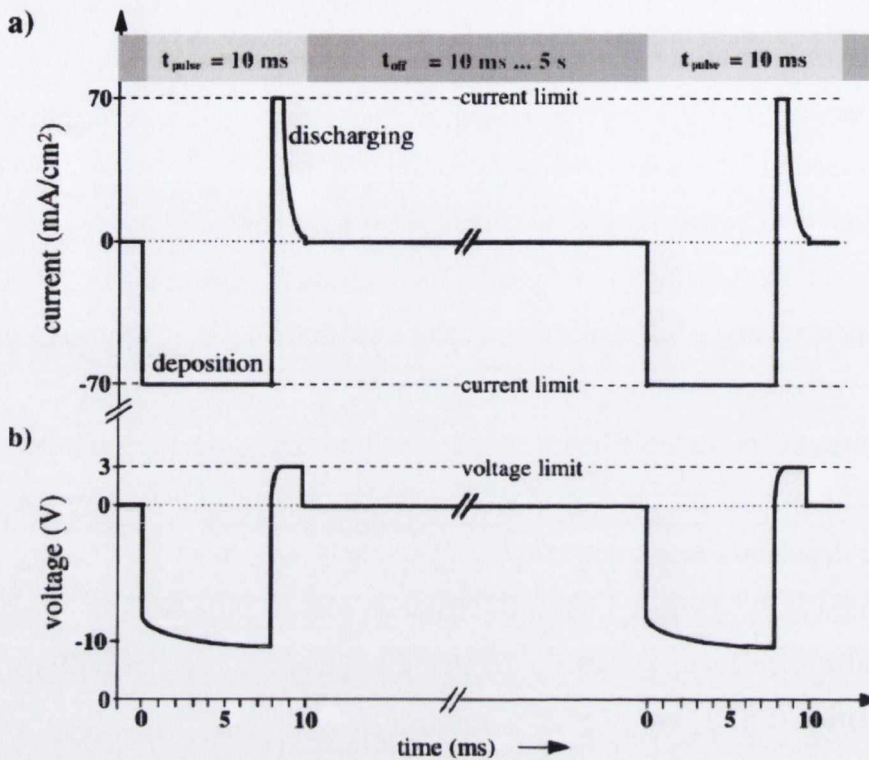


Figure 2.6: Schematic of the filling of a PAM with Nickel by PED taken from Nielsch et al. [169]

First a negative current pulse is applied for 10 ms during which time the material is deposited at the pore base {graph (a) of Figure 2.6}. There is a corresponding short abrupt rise in the negative deposition voltage followed by a further increase which is due to the charging of the capacitance of the barrier layer and the depletion of metal ions near the deposition interface {(graph (b))}. A short pulse of positive polarization is then applied to discharge the capacitance of the barrier layer and interrupt the electric field at the deposition interface. This positive pulse also repairs discontinuities in the barrier layer. A time delay is then introduced to avoid depletion of metal ions at the deposition interface and allows the ionic concentration to recover before the next double pulse is applied. This improves the homogeneity of the deposition and prevents excessive hydrogen evolution. This process is continued until there is a drop in deposition potential as the deposition of metal overflows from the pores and starts on the surface of the template. PED results in almost complete filling of the pores [172, 177, 178, 259, 260].

## 2.1.2 One-Dimensional Nanostructures

The importance of 1-dimensional nanostructures has been described in chapter 1 of this thesis. The synthetic methods used to fabricate metal, polymer and composite nanostructures in alumina templates is described in this section.

### 2.1.2.1 Metal Nanowires

The metals used in this study were the transition metals iron (Fe), cobalt (Co), nickel (Ni), copper (Cu) and silver (Ag). A transition metal is defined as "an element whose atom has an incomplete *d* sub-shell, or which can give rise to cations with an incomplete *d* sub-shell" by the International Union of Pure and Applied Chemistry (IUPAC) [262]. Transition elements have many interesting properties as a result of their partly filled *d* sub-shells and we would thus expect transition metal nanostructures to have novel properties and applications.

#### 2.1.2.1.1 Iron (Fe)

Fe is a transition metal with a body-centred cubic structure (bcc). It belongs to the space group Im-3m (space group number: 229). It has high melting and boiling points (1811 K and 3134 K respectively) and high thermal conductivity ( $80 \text{ Wm}^{-1}\text{K}^{-1}$ ) [263]. It is also highly conducting (electrical resistivity  $\rho = 9.7 \times 10^{-8} \Omega \text{ m}$ ) but very reactive and corrodes in air and at elevated temperatures. It is thus mostly used commercially as an alloy (e.g. in steel) [263].

Fe nanowires are usually fabricated by the template method in PAMs [264, 265, 266, 267] or on mesoporous silica [268, 269]. Other methods include self assembly using CVD [270], electrodeposition on glass [271] and on Cu (III) [272]. Fe nanowires are mostly known for their ferromagnetic properties and have potential application such as high density storage devices (HDSD) because of their magnetism reversal properties [170, 171, 265, 266, 267, 268, 269]. Their potential use as a magnetic force generator has also been studied [273]. Fe nanowire arrays are also used as a catalyst precursor for the growth of carbon nanotubes [274, 275, 276].

The use of Fe nanowires as catalysts for CNT growth is described in chapter 5, section 5.2. MWCNTs were successfully grown on the PAMs which were filled with Fe by electrodeposition.



### 2.1.2.1.2 Cobalt (Co)

Co is a transition metal with a hexagonal close-packed crystal structure (hcp) and space group P63 / mmc. It has similar melting and boiling points to Fe (1768 K and 3200 K respectively) and high thermal conductivity ( $100 \text{ W m}^{-1} \text{ K}^{-1}$ ). It has low electrical resistivity ( $\rho = 6 \times 10^{-8} \text{ } \Omega \text{ m}$ ) so is a good electrical conductor [277].

Minerals of Co have been used since Egyptian times to colour glass deep blue. It is best known for its hardness and its magnetic properties. Co nanowires have potential applications in magnetic storage and field emission devices [203, 278, 279, 280, 281, 282]. Co nanowires with controlled magnetism direction have been made which are particularly useful for applications where self-biasing of magnetism is necessary [283, 284]. They are also used in the synthesis of aligned CNT arrays [275, 285, 286, 287]. An attempt was made to grow CNT by CVD (as described in chapter 5, section 5.2) using PAMs filled with Co (as described in chapter 3, section 3.2.1.1).

Co nanowires are usually fabricated by electrodeposition in PAMs [175, 278, 279, 281, 283, 284, 285] but have also been made by deposition into porous track polycarbonate membranes [203, 280] on biomolecules [288] and by template free methods [282].

### 2.1.2.1.3 Nickel (Ni)

Nickel is a transition metal with ferromagnetic properties. It has a face centred cubic crystal structure and has good thermal conductivity ( $91 \text{ W m}^{-1} \text{ K}^{-1}$  at 300 K) and low electrical resistivity ( $69.3 \text{ n } \Omega \text{ m}$  at  $20 \text{ }^\circ\text{C}$ ), thus it is fairly conductive [289]. It has long been used for coinage because of its stability in air but is now mainly used for preparing alloys of high strength, ductility and chemical resistance e.g. stainless steel. Like copper it can be easily drawn into wires.

The main application of Ni nanowires is in information storage [28, 29], due to the magnetisation-reversal mechanism of nanowires which leads to a high coercive fields. It has been shown that coercivity is mainly dependant on the nanowire shape [290] and magnetic measurements have shown that coercive fields are higher for nanowires with smaller diameters [291]. The coercivity of the nanowire is also affected by the temperature of the electrolyte and is explained by a shift in their crystallographic orientation [291]. High storage density and magnetic memories can be achieved from patterned perpendicular storage media consisting of magnetic nanowire arrays in magnetic insulating material matrices such as PAMs [200].

Ni thin films were shown to be promising materials for optical media as far back as 1996 [292]. Suspensions of magnetic nickel nanowires display magneto-optical properties similar to ferrofluids and could thus act as magneto-optical switches using light instead of electricity to relay information [293]. Ni nanowires have also been used as interconnects on ferromagnetic electrodes [294] and have shown potential in applications for high frequency noise absorbers; power absorption of the Ni nanowire array was estimated to be 50% in the frequency range above 2 GHz [295]. They are also useful when working with nanoscale circuit parts as external magnets can be used to dictate the orientation and position of magnetic Ni nanowires within these electronic systems [293].

None of these applications were studied in this work as they have been thoroughly researched by other authors. Some of the Ni nanowire arrays made here were used to fabricate nanoelectrodes for use in light emitting diodes [296]. This novel application is discussed in detail in chapter 5. Ni nanowire arrays were also used as a catalyst for the growth of ordered carbon nanotubes [297, 298, 299].

Ni nanowire arrays have been fabricated by electrochemical deposition in PAMs since 1998 [169, 170, 171, 259, 291, 300, 301, 302, 303]. Ni nanowires of diameter less than 10 nm have been made inside carbon nanotubes [304]. Recently Ni nanowires were linked by self assembly using soft template methods with ethylene glycol solutions [305]. In this work nanowires were made by AC electrodeposition [219] and by pulsed electrodeposition (PED) into PAMs [169, 259].

#### **2.1.2.1.4 Copper (Cu)**

Copper is a transition metal with a face centred cubic crystal structure. It has high electrical and thermal conductivity ( $59.6 \times 10^6 \text{ S m}^{-1}$  at 20°C and  $401 \text{ W m}^{-1}\text{K}^{-1}$  at 300 K respectively) [306] and thus has many applications as an electrical and heat conductor. Copper plays an important role in the electronics industry because of its low electrical resistivity and its resistance to electron migration [307]. It also has good mechanical strength and high ductility so can be easily drawn into wires. Since 1997 it has replaced aluminium as an interconnecting material for on-chip wiring because it carries electrical signals faster than aluminium [308]. Due to its antibacterial properties, it has many applications in the healthcare industry [309, 310].

By reducing Cu to the nanoscale it is hoped to achieve an increase in electrical conductivity and tensile strength; because of this copper nanowires are of particular interest for potential applications in nanodevices, such as interconnects and field emission



displays [311, 312, 313]. Electronic transport properties and oxidation processes in individual polycrystalline Cu nanowires were investigated by Toimil Molares et al. Their measurements of current-voltage (IV) characteristics indicate that the Cu nanowires showed metallic behaviour, so could be used for metallic or structural elements in nanoscale devices, however their studies at high temperature showed increased resistance of the nanowires which they attribute to the oxidation of Cu to Cu<sub>2</sub>O [314]. Electrical measurements were also done on arrays of Cu nanowires in an alumina template [315]. They observed non-linear IV characteristics which they attributed to impurities near the wire-lead contact region. Other authors have studied the electronic properties and the band structure of Cu nanowires for diameters of 60 and 160 nm and found that the fundamental resistances of these Cu nanowires were larger than those predicted by Ohm's law [316]. The mechanical characteristics of Cu nanowires were investigated by Bansal et al. [317]. They found that their mechanical properties were comparable to those of bulk Cu. The quantum size effects are more noticeable on the optical properties of Cu, for example nanoscale Cu exhibits strong absorption peaks in the visible region due to surface plasmons [141]. Both transverse and longitudinal resonance peaks were observed. The transverse resonance peak was found to be affected by the diameter and aspect ratio of the nanowires and the resonance peak was found to be sensitive to the direction of polarised light [318]. A theoretical study on the polarisation properties of ordered Cu nanowire microarrays embedded in a PAM predicts that the nanostructures could serve as a novel polarising element in the infrared region [319]. Investigations by Pang et al. have found that they could be used as a wire grid type micropolarizer [320].

Cu nanowires have been prepared by electrodeposition in PAMs since 1997 [122, 321]. Recent syntheses include adaptations of this method to achieve Cu nanowires which will be suitable for incorporation into nanoelectronic and nanophotonic devices [141, 308, 315, 318, 320, 321, 322, 323]. Gerein and Haber compared deposition of Cu by AC and PED into PAMs. They found comparable uniformity of pore filling by both methods but less damage to the PAM was done by PED. They also discovered that PED with square waveforms produced better pore filling than sine waveforms, and concluded that this was due to enhanced resonant tunnelling through the barrier layer and re-oxidation of Cu in faster filling pores [220]. The synthesis of a novel Cu nanoelectrode which has been used in the fabrication of an organic light emitting diode is described in this thesis (chapter 5, section 5.1) and references [324, 325].

### 2.1.2.1.5 Silver (Ag)

Ag is a transition metal with a face centred cubic structure. It has the highest electrical and thermal conductivity of all known metals (electrical resistivity of 15.87 nΩm at 20 °C and thermal conductivity of 429 Wm<sup>-1</sup>K<sup>-1</sup> at 300 K) [326]. It has low toxicity and has been used to purify water throughout the ages [14]. It is also a well known catalyst for many chemical reactions and more recently has been known for its ability to promote surface enhanced optical phenomena [327, 328].

Ag nanoparticles in particular, show enhanced catalytic activity, high electrical conductivity and unique optical properties [202, 329] and are used in a variety of applications such as antibacterial agents [90], nanoconnectors and nanoelectrodes [90], optical and electrical nanodevices and nanosensors [330, 331]. Their biomedical applications are described in chapter 1 section 1.2.1 of this thesis. Ag nanoparticles have been fabricated in PAMs by DC, AC and pulsed electrodeposition [172, 332, 333, 334, 335, 336, 337]. In this thesis AC deposition [332] and PED were used [172].

Other methods to fabricate Ag nanowires include an aqueous phase synthesis by reduction of silver nitrate (AgNO<sub>3</sub>) [338], photochemical synthesis by decomposition of AgNO<sub>3</sub> under ultraviolet radiation [339] and sol-gel synthesis [340, 341]. In 2007 Kim et al. synthesised Ag nanowires from Ag nanoparticles which were produced by the reduction of AgNO<sub>3</sub> with hydrazine. This method allowed control over the lengths of the nanowires [342].

### 2.1.2.2 Conducting Polymer Nanowires

Conducting polymers have been studied since 1964 when D. E. Weiss and co-workers noticed high conductivities in doped polymers [343, 344, 345]. A decade later, in 1974, John Mc Guinness et al. demonstrated the first organic-polymer switch [346] and Shirakawa and co-workers developed the first semiconducting polymer polyacetylene [347, 348, 349, 350] during the 1970s. In 1977 Heeger and co-workers showed that polyacetylene doped with iodine achieved conductivities comparable to metals [351, 352]. Extensive research has been done since then resulting in the development of organic devices such as polymeric light emitting diodes [353], photodiodes [354], photovoltaic cells [355], field effect transistors [356] and optically pumped lasers [357]; and in 2000 Alan J. Heeger, Alan G. MacDiarmid and Hideki Shirakawa received the Nobel Prize in chemistry for the discovery and development of conductive polymers. During the past decade research has concentrated on syntheses of nanostructures of conducting polymers



[179, 180, 181, 182, 183, 358, 359]. Polymer nanostructures which have been synthesised by template methods have been shown to have electrical conductivities well above those of powder or thin film forms of the same polymer [181, 354] and have many potential applications in nanodevices [360]. As well as potential applications of nanomaterials for device structures they are also of fundamental interest. Nanowires of conjugated polymers are ideal systems for studying 1D confinement effects on optical, electronic and electron transport properties.

### 2.1.2.2.1 Polyaniline (PANI)

Polyaniline (PANI) was discovered in the 1800s by Letheby who noticed that aniline was oxidised by stomach acids [361]. It has been used in industry as the dye aniline black since the 1800s and was discovered to have high electrical conductivity in the 1980s by MacDiarmid [362]. It is still widely used in industry because of its flexibility, its stability in air and its electrical, electrochemical and optical properties. Many useful devices such as chemical and biological sensors [363, 364], batteries [365, 366], electrochromic devices [367, 368], electromagnetic shielding devices [369, 370], capacitors [368], anticorrosion coatings [371, 372, 373], antistatic coatings, infrared polarizers and light emitting diodes can be made from it [374, 375, 376].

PANI can be synthesised in several insulating forms shown below (Figure 2.7).

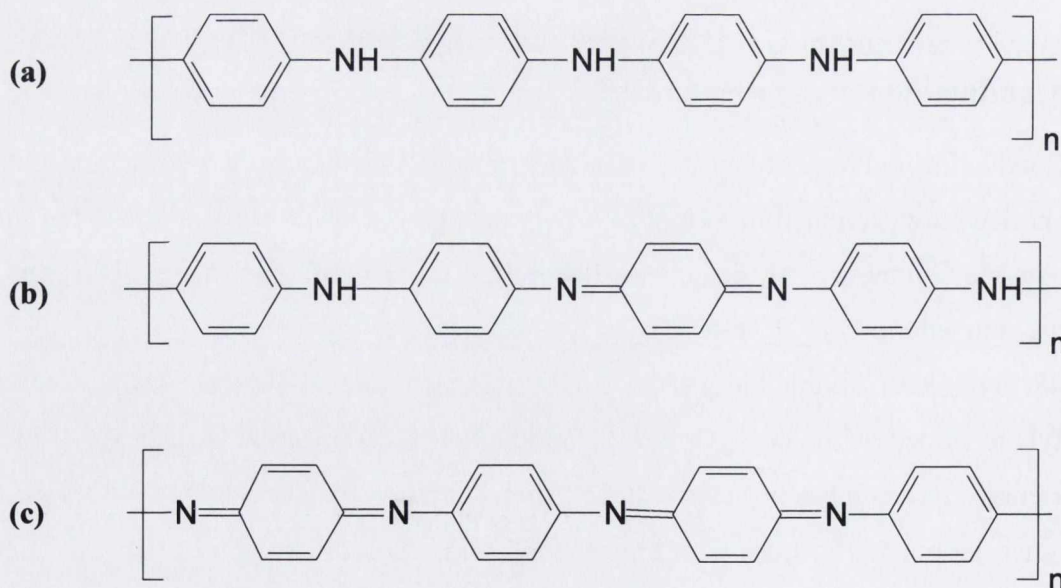


**Figure 2.7: Base forms of PANI (a) Leucoemeraldine base (LEB), (b) Emeraldine base (EB) and (c) Pernigraniline base (PNB)**

Conducting PANI is achieved by doping the EB with a protonic acid to give the structure below (Figure 2.8).

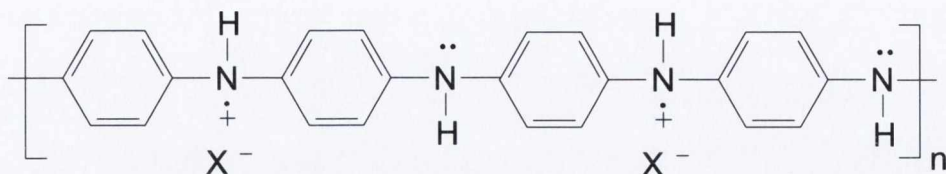
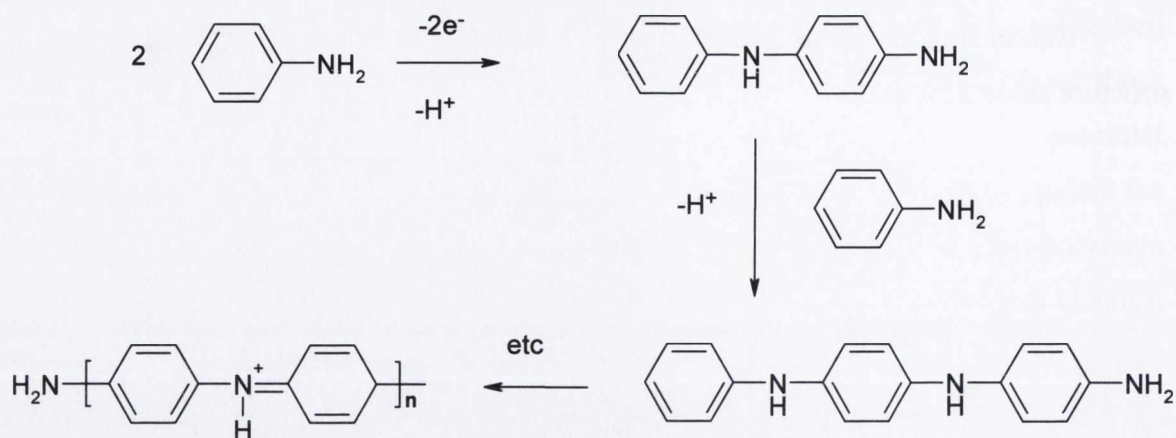


**Figure 2.8: Oxidised bi-polaronic Emeraldine salt (ES)**

It is possible to switch between the four oxidation states of PANI by doping and de-doping thus allowing control over the electronic properties [359, 360, 362, 367, 368, 377, 378, 379, 380, 381]. Thus it can be tailored for specific applications; its uses can range from insulation for the non-conductive form to electrical uses for the highly conductive form. Recent research has concentrated on PANI nanostructures such as nanowires and nanofibers since they combine the properties of organic conductors and nanomaterials and may thus have interesting novel properties and potentially useful applications [382, 383, 384, 385, 386, 387, 388, 389, 390]. Because of the larger surface areas and higher aspect ratio of nanomaterials nanostructured PANI is more responsive than bulk PANI to external stimuli [387]. In many cases there is an increase in processability, responsiveness and performance which may result in the production of much faster and more responsive chemical sensors [388, 389]. In addition the many new nanoscale phenomena that are not possible with current inorganic systems may be achieved [390].

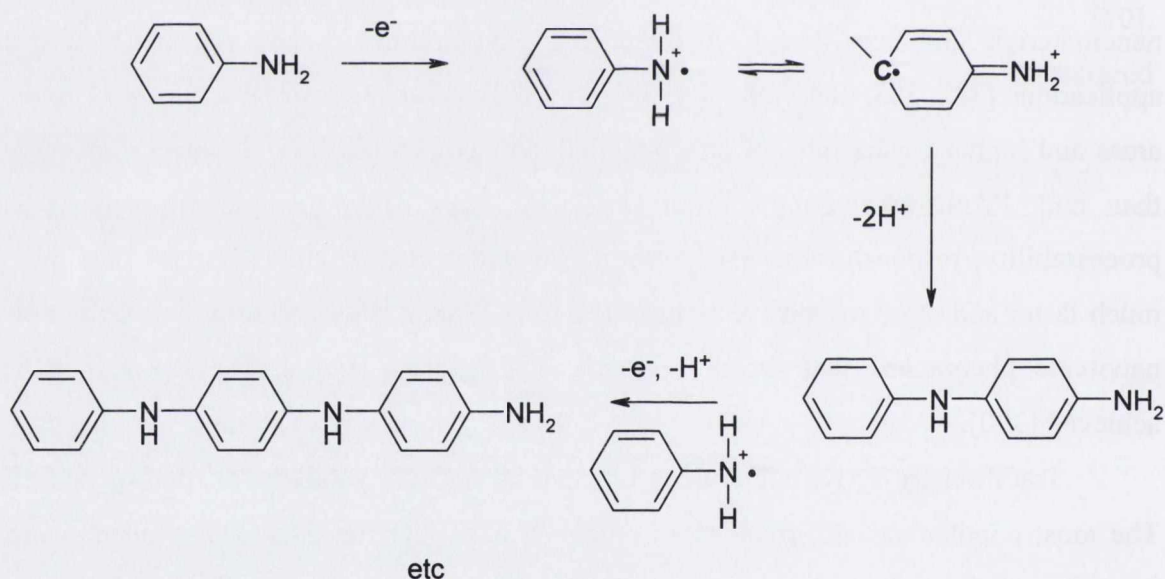
Traditionally PANI is produced by chemical oxidative polymerisation of aniline. The most popular method involves an oxidising agent such as ammonium persulphate, potassium dichromate or hydrogen peroxide in an acidic medium such as hydrochloric acid [391, 392, 393, 394] but many authors use sulphuric acid, sulphanilic acid and camphorsulphonic acid [395, 396, 397]. The mechanism involves a 2-electron chain reaction.





**Scheme 1: Chemical Oxidative Polymerisation of Aniline**

PANI may also be produced electrochemically by anodic oxidative polymerisation; this is a radical recombination reaction.



**Scheme 2: Electrochemical Polymerisation of Aniline**

Chemical polymerisation has the advantage that large batches of polymer can be produced. However, electrochemical polymerization has many more advantages; for example, the electrochemically deposited polymers adhere strongly to the electrode

surface, they are chemically stable, their synthesis is easily reproducible and their conductivity can easily be tuned over a wide range by changing the dopant or the doping level [398, 399].

PANI nanostructures can be made by self assembly using functional molecules such as surfactants, organic dopants, or polyelectrolytes as structural directors [400]. Alternatively templates such as porous membranes or zeolites can be used where the aniline is polymerised inside in the 1-D nanochannels of the template [401, 402]. It is also possible to synthesis PANI nanotubes from aniline by self assembly using a protonic acid as an external dopant [403, 404].

### **2.1.2.3 Metal / Polymer Composite Nanowires**

Since the discovery of the first semi-conducting polymer polyacetylene [348, 349, 350, 351] organic systems have become serious competitors to inorganic systems for electronic applications, mainly because of their easier and cheaper processability. It is also possible to further increase the conductivity of these systems by doping with a suitable material [351, 352, 353, 354, 355, 356, 357]. The incorporation of carbon nanotubes (CNTs) into conducting polymers has lead to the development of new composite materials with increased mechanical and electrical properties which have potential industrial applications, for example lighter stronger materials which contain CNTs as fillers are becoming increasingly important in the aerospace and automotive industries [405, 406, 407, 408]. Recently nanocomposites containing high aspect ratio metal nanoparticles as alternatives to CNTs have been used for electronic applications [409]. The incorporation of metal and metal oxide particles into conducting polymer films has been shown to enhance their electro-catalytic activity and other properties [329]. Many PANI/metal nanoparticles possess enhanced sensing and catalytic capabilities compared to pure PANI [410 and references therein]. Filler dispersion is probably the limiting factor when producing composites as the efficiency of the filler will be reduced by aggregation. How the filler is added also has an effect on its dispersion within the polymer matrix. A stronger interface between filler and polymer matrix can be achieved by in-situ polymerisation as for example in the case of multi-walled carbon nanotubes (MWCNT) and poly(methylmethacrylate) (PMMA) [411, 412, 413, 414].

Various techniques have been used to incorporate metallic nanoparticles (such as gold, copper, platinum and palladium) into polymer matrices [415]. It is possible to



introduce metals into the PANI polymer system via the lone pair of electrons on the nitrogen [410, 416, 417, 418, 419, 420]. Polyaniline and metal nanoparticle composites have been made by a one pot synthesis [421, 422, 423]. There have also been recent advances in fabricating nanorods containing metal cores surrounded by a polymer coat [167, 419, 424, 425]. Many chemical and physical methods have already been used to incorporate Ag nanoparticles into polymer films [426], however homogenous dispersion into the polymer matrix is difficult as suspensions or dispersions of Ag nanoparticles tend to aggregate [427]. Gelves et al. used Cu nanowires which were made and extracted from PAMs to prepare Cu/polystyrene composites. They found these composites had similar electrical properties to fullerene nanotubes-filled polymer composites. They achieved better dispersion by surface functionalisation with alkyl chains but this resulted in reduced electrical conductivity as a result of the insulating nature of the coating [428]. Recently self-doping PANI nanotubes with Ag nanoparticles assembled along them have been made [429]. Khanna et al have also prepared Ag / PANI nanocomposites by a photochemical reaction [430]. Multicomponent one dimensional rod structures with tailorable electronic structures have recently been made by electrodeposition into alumina templates by the Mirkin group [431] and Kinyanjui et al. [420] have made PANI / Pt composites inside the pores of an alumina template. Such syntheses avoid loss of conductivity associated with the reduction of metal ions into a pre-formed polymer.

This thesis describes a method of preparing Ag / PANI and Cu / PANI composite films and Ag / PANI and Cu / PANI nanocables into the pores of an anodic alumina membrane (AAO) by simultaneous oxidative electropolymerisation of aniline and reduction of Ag or Cu from an ionic precursor. One advantage of this method is the strong particle-polymer interaction which should give rise to enhanced properties of the films/nanostructures [432]. The possible applications for Ag / PANI composites will be described in chapter 4, section 4.4 and chapter 5, section 5.4.

#### **2.1.2.4 Semiconductor Nanowires**

Semiconductors are materials whose electrical conductivity lies between that of a conductor and an insulator. They can be pure elements e.g. silicon, or compounds such as gallium arsenide. Their conductivity can be altered by doping, i.e. by adding impurities which either donate electrons to the material (n-type doping) or create holes by taking an electron from the material (p-type doping). An energy band diagram of a typical semiconductor is shown in Figure 2.9.

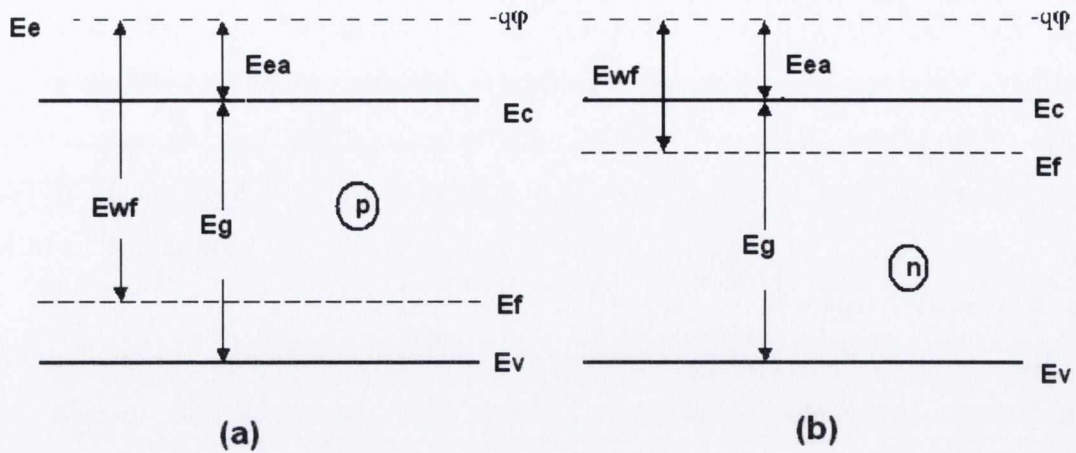


**Figure 2.9:** Energy level diagram for a p-doped (a) and n-doped (b) semiconductor, where  $E_e = -q\phi$  is the potential energy of a free unmoved electron (the elementary charge  $q = 1.6 \times 10^{-19}$  C and  $\phi$  = macro potential),  $E_{ea}$  = electron affinity,  $E_{wf}$  = work function,  $E_c$  = energy of a stationary free conduction electron,  $E_f$  = energy of an electron in the Fermi level,  $E_v$  = energy of a stationary valence electron in a bond and  $E_g$  = energy gap [433].

The energy necessary to free an electron from the conduction band edge is called the electron affinity. The Fermi level for doped semiconductors depends on the amount and type of impurities present. It characterizes the occupation probability of available energy states in the conduction and valence band with electrons or holes [433]. For non-degenerate semiconductors the Fermi level is in the forbidden band, for degenerate semiconductors it can dip into the valence or conduction bands. The work function  $E_{wf}$  is the energy difference between  $E_e$  and  $E_f$  and also depends on the type of material and doping.

Semiconductor nanowires are 1-D semiconductors and thus are subject to confinement in two dimensions. Subsequently they have many novel properties and potential applications as described in chapter 1. Semiconductor nanomaterials are particularly useful for electronic and optical applications such as nanowire microcavity lasing, phonon transport and chemical sensing [434]. Group II-VI semiconductor nanowires such as Cadmium sulphide (CdS) in particular, have novel optoelectronic properties and thus many interesting potential applications [187, 435, 436, 437].

#### 2.1.2.4.1 Cadmium sulphide (CdS)

CdS is a direct band gap semiconductor i.e. the minimum energy of the conduction band and the maximum energy of the valence band are at the same wave



vector in momentum. It is thus possible for an electron at the minimum in the conduction band to combine with a hole at the maximum in the valence band without losing momentum. When this happens energy is emitted in the form of a photon of light whose energy is equal to the band gap energy  $E_g$ . Thus when a direct band gap semiconductor is given energy greater than  $E_g$  spontaneous emission of light (luminescence) occurs. In fact in most semiconductors the band gap is small enough that visible light is sufficient to permit carriage of charge.

CdS can exist in two structures, hexagonal (wurtzite) and a tetrahedrally coordinated cubic (zincblend). This can be transformed into an octahedrally co-ordinated phase with a close packed sodium chloride (rocksalt) structure upon application of pressure. The computed band gap (Hartree-Fock calculations) for the band gap of rock salt CdS was 2.9 eV [438] which is larger than the experimental value of 2.42 eV at 300 K [439], but it is possible to tune the band gap between 2.4 and 4 e V by reducing the size of the crystal. The energy band structure of CdS is shown in Figure 2.10.

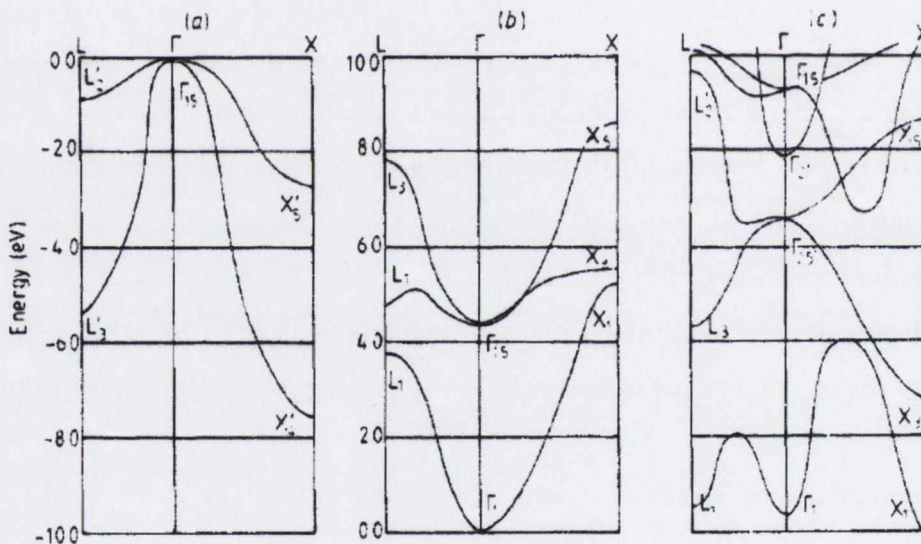


**Figure 2.10:** Energy band structure for CdS (a) shows the valence band for the rocksalt form of CdS with a lattice constant of  $a_0 = 5.818\text{\AA}$ , (b) and (c) show the conduction bands for zincblend and rock salt CdS with a lattice constant of  $a_0 = 5.818\text{\AA}$  adapted from [438].

The Bohr diameter of the 1S exciton of CdS is 4 nm [440] so quantum confinement effects should be visible in nanowires with diameters in the region of 10 nm [441]. We would thus expect CdS nanostructures to have many novel optical properties and applications. For example CdS shows electroluminescence when an electric current is passed through it so could be used as a light emitting diode; CdS insulating nanocrystals have been shown to exhibit green luminescence [442] and blue luminescence can be

obtained from CdS nanowires [443]. Its resistance is lowered when exposed to light so it can be used as a photoresistor [439] and as a light sensing device [444]. In fact CdS sensitivity is comparable to that of the human eye [436]. CdS has been used for solar cells since 1954 [445, 446, 447]. More recently Lieber and co-workers have investigated the possibility of using single crystal CdS nanowires as an electrically driven laser [448].

There are many ways to prepare CdS nanostructures. For example CdS nanocrystallines with different morphologies have been prepared by sonochemical reduction [449]. CdS nanoparticles of various sizes have been prepared by gas evaporation [450]. CdS thin films have been prepared by electrodeposition from a non-aqueous bath [451] and from aqueous solutions [452], by vacuum evaporation [453] and by electrochemical atomic layer epitaxy [454]. CdS nanowires have been prepared by ultraviolet radiation [455], microwave irradiation [456],  $\gamma$ -irradiation [457], by reaction of CS<sub>2</sub> with CdCl<sub>2</sub> [458], by surfactant assisted synthesis [459], by laser assisted catalytic growth [435] and more recently by solvothermal synthesis [460].

However, by far the most popular way to produce CdS nanowires is by electrochemical deposition into PAMs either by DC electrodeposition [435, 459, 461, 462, 463] or AC electrodeposition [187, 321, 436]. Highly crystalline structures in a well-aligned and monodispersed array are achieved by this method, which is important for device applications. The optical transparency of PAMs is an added advantage. Furthermore PAMs which are made in oxalic acid have also been shown to demonstrate blue luminescence [464]. It is generally believed that the luminescence is due to oxalate impurities incorporated into the film during formation [465, 466]. Heat treatment of PAMs formed in oxalic acid has been found to influence the photoluminescent properties [467] and it has recently been shown that CdS nanowires embedded in PAMs increase the light emitting intensity and induce a red shift of the photoluminescent band [468]. Thus it would be possible to produce optoelectronic devices based on these semiconductor structures. The controlled variability of the particle diameter and compositions might also be used to tune in desired optical properties [201].

The fabrication of a solar cell with a light emitting polymer MEH-PPV (poly[2-methoxy-5-(2'-ethylhexyloxy)-*p*-phenylene vinylene]) and CdS is described in chapter 5, section 5.3.



## **2.2 Characterisation Techniques**

### **2.2.1. Electron Microscopy**

The development of microscopic techniques in the early 1980s facilitated the investigation of nanomaterials as it allowed direct observation and analysis on an atomic scale [469]. Microscopic features of samples can now be visually observed; in fact it is largely due to the development of electron and atomic force microscopes that such strides in nanotechnology have been made in recent years.

#### **2.2.1.1 Scanning Electron Microscopy (SEM) and High Resolution Scanning Electron Microscopy (HRSEM)**

The surface morphologies of the samples can be observed by scanning electron microscopy (SEM); this allows investigation of pore structure. Pore filling is investigated by HRSEM which allows deeper penetration into the material.

##### **Equipment:**

In this thesis, SEM was performed on a Hitachi S-4300 SEM at the Centre for Microscopy and Analysis (CMA) at TCD and HRSEM was done using a Philips XL30 SFEG SEM by AlCove Surfaces GmbH, D-45966 Gladbeck, Germany.

The S-4300 is a computer controlled high resolution field emission scanning electron microscope with resolutions between 1.5 nm at 15 kV to 2.5 nm at 5 kV, accelerating voltage from 0.5 to 30 kV in 100 V steps and a specimen stage of 100 mm by 50 mm with two motorised axes [470].

The Philips XL30 SFEG is a high-resolution scanning electron microscope capable of resolutions better than 2 nm, magnifications over 600,000, and operating voltages from 200 V up to 30 kV [471].

##### **Sample Preparation:**

Small pieces of the samples are mounted on aluminium metal stubs with double sided conductive adhesive tape or with silver paint for surface imaging at the CMA. For cross-sectional imaging in AlCove the sample is set in an epoxy resin which is then cut and mounted with the pores parallel to the surface of the metal stub. To view the nanowires out of the pores the surface of the samples is previously etched with 0.2 M NaOH to remove the alumina. Most of the samples are coated with about 5-10 nm of

sputtered gold. This is used to prevent surface charging of non-conducting samples; some metal-filled PAM samples are imaged without gold coating. For coated samples, the beam current is about 11 pA with an accelerating voltage of 20 kV and for uncoated samples it is 20 pA with an accelerating voltage of 5 kV. The working distance (sample-gun distance) is varied between 6 and 14 mm and images are generally taken at various magnifications up to 200 K for each sample.

**Theory:**

The SEM uses a stream of monochromatic electrons which is focused onto the sample surface to form an image. A stream of electrons from the electron gun at the top of the microscope travels through a vacuum and is focused through the microscope column by a series of electromagnetic lenses into a narrow coherent beam.

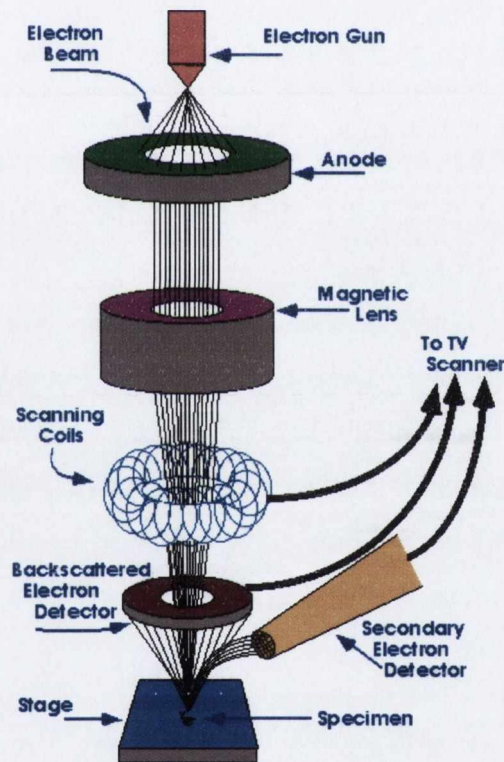


Figure 2.11: Schematic of how an SEM works [472]

It is then swept across the sample by a set of coils and focused onto the desired spot by the objective lens. These bombarding electrons, the primary electrons, dislodge secondary and backscattered electrons from the specimen itself which are collected by a positively biased grid or detector, and then translated into a signal and converted into an image (see Figure 2.11). The low energy secondary electrons form a standard image and the high



energy back-scattered electrons provide an image with good atomic number contrast. The magnification is changed by changing the size of the sample scan.

### **2.2.1.2 Transmission electron microscopy (TEM) and High Resolution**

#### **Transmission Electron Microscopy (HRTEM)**

Although pore structure and filling can be investigated with HRSEM it is not possible to use it to compare the uniformity of the nanowires electrodeposited in the PAMs as many will be cut by the cleavage sectioning. Thus TEM is carried out to check their uniformity and measure their size. HRTEM enables particles of the order of 1 nm to be seen. In addition spot patterns which are created in crystal specimens can be used for identification of crystal structure and orientation.

#### **Equipment:**

In this work TEM was done using HITACHI H-7000, operated at 100 kV, at the Centre for Microscopy and Analysis (CMA) at TCD and HRTEM was done on a FEI TECNAI F20 (HRTEM), operated at 200 kV, at the Centre for Nanostructured Media in Queen's University of Belfast [473]. Measurement of diameters and lengths is achieved using the "UTHSCSA" image tool computer program.

The H7000 is a high resolution transmission electron microscope with an accelerating voltage range of 10 kV to 125 kV and resolution of 0.5 nm. The stage tilt is + or - 60 degrees. Images are digitally recorded with a CCD camera.

The FEI Tecnai F20 field emission high-resolution transmission electron microscope has a 200 kV accelerating voltage enabling resolution at the atomic level for imaging of defects and interfaces in microstructures.

#### **Sample Preparation:**

TEM samples are prepared by placing a few drops of a suspension of the nanowires in Millipore filtered de-ionised water onto a formvar coated copper grid or a holey carbon-coated TEM support grid and drying them overnight in a vacuum oven at 40°C. The nanowires are extracted by shaking the filled alumina membrane in a solution of 0.1 M NaOH and 30 g L<sup>-1</sup> PVP for 12-24 hrs, followed by washing several times in Millipore filtered de-ionised water. The aluminum foil is first removed from the back of the membrane by a solution of 0.2 M CuCl<sub>2</sub> in 3 M HCl as described in chapter 3 section 3.2.4.2. and references 244 and 245.

## Theory:

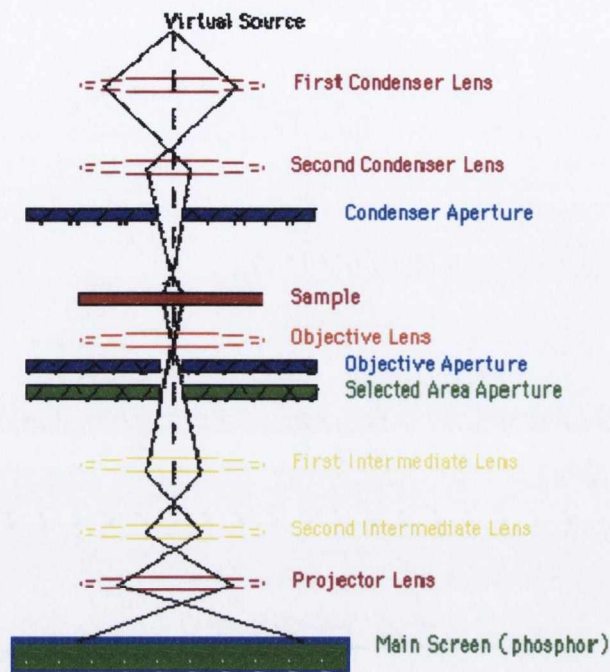


Figure 2.12: Schematic of how TEM works [474]

The TEM works on the same principal as the SEM. A stream of electrons from the electron gun or virtual source at the top of the microscope travels through a vacuum and is focused by various apertures and lenses into a thin monochromatic beam and accelerated towards the sample using an electromagnetic lens as shown in Figure 2.12. If the sample is thin enough, parts of the beam are transmitted through it and focused by an objective lens, passed down the column and enlarged through more lens eventually reaching a fluorescent screen at the bottom of the microscope. This differs from SEM where the samples are thicker and the electrons are backscattered from the sample. In TEM the high angle diffracted electrons are blocked out by an objective aperture so that when the image strikes the screen there are lighter and darker regions depending on how many electrons are transmitted through ( the denser areas where fewer electrons get through will be darker). The crystal structure of the samples can also be determined by the periodic diffraction of electrons which is obtained after the beam goes through a selected area aperture. Thus TEM is complementary to x-ray diffraction. The energy of the electrons in the TEM determines how deep the electrons can penetrate the sample and thus the thickness of sample which can be examined.



### 2.2.1.3 Atomic Force Microscopy (AFM)

Information about the surface roughness of the samples is obtained from AFM as it is quite difficult to get topological information from a regular SEM or TEM instrument.

#### Equipment:

The AFM used was a Nanoscope III A by Digital Instruments plus an E type scanner with a max scan area of  $13\mu\text{m}^2$  [475].

#### Sample Preparation:

The PAMs did not need any special preparation for AFM analysis. The AFM cantilever was aligned using a class 3 laser by maximizing reflection of an image of the cantilever onto a piece of white paper. To image the PAM samples tapping mode AFM was used, slightly off resonance and at a slow scan speed with low gains.

#### Theory:

AFM was developed by Binnig et al in 1986 [476]. It is used to create 3-D micrographs with resolution in the atomic scale.

The basic operation mode of an AFM is shown in Figure 2.13 [477].

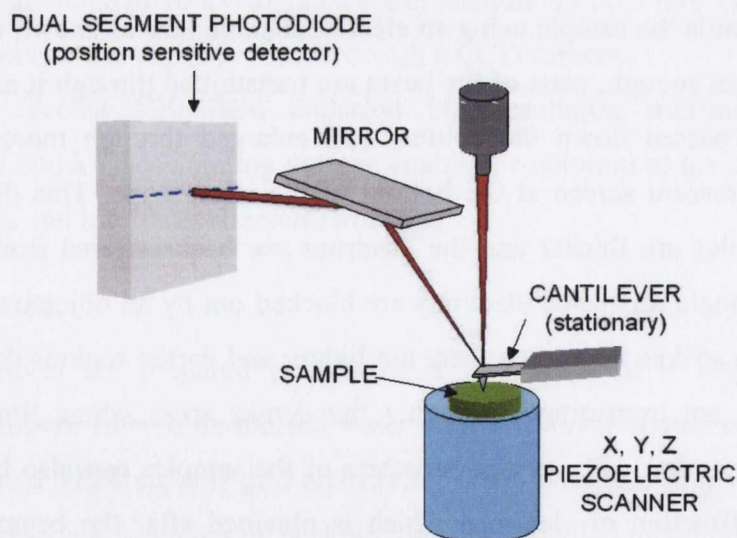


Figure 2.13: Schematic of an Atomic Force Microscope [477].

The sample is mounted on a ceramic piezo-scanner which can be moved in three directions (x, y and z). The morphology of the sample surface is probed with a nanometre sized tip which is usually made of silicon nitride. The tip itself is mounted on the edge of

an elastic cantilever which has a low spring constant so that the probe remains in contact with the surface. The displacement of the tip due to the surface morphology of the sample is measured by an optical laser and a 3-D scan is obtained as the probe is moved in the x and y directions over the sample. The tip can also be used in tapping and non-contact mode to avoid large shear forces on the sample created when the tip is dragged over the surface. Tapping mode is the most commonly used mode in AFM. The surface is lightly tapped with an oscillating probe and as the surface topology changes, the oscillation amplitude of the cantilever changes and the image is recorded [478]. It is also possible to study probe-sample interaction by modifying the chemistry of the tip.

## 2.2.2 X-Ray Analysis

X-rays can be used to determine the crystal structure and elemental composition of materials. X-rays are a form of electromagnetic radiation which results from inner orbital transitions or deceleration of high energy electrons [479]. They have shorter wavelengths and thus higher energies than normal light. They can be used to determine crystal structure from crystalline samples by x-ray diffraction techniques or to give elemental information from sample surfaces, by measuring the energy of emitted x-rays during SEM imaging.

### 2.2.2.1 Energy Dispersive X-Ray Analysis (EDX)

EDX is a qualitative and quantitative elemental analysis technique. It is non-destructive and has resolution in the micrometer region. It is used for the detection of elements.

#### **Equipment:**

EDX was performed using a HITACHI S-3500N variable pressure scanning electron microscope with a Princeton Gamma-Tech Spirit X-Ray microscope system in backscatter mode.

#### **Sample Preparation:**

Because pore filling is better at the base of the PAM and the surface may contain bulk deposits from overfilling, the EDX measurement is either done from the bottom of the PAM after removal of the Al and barrier layer of alumina or a polished sample is



used. The samples are prepared as for SEM. There is no need to gold coat conductive samples and samples containing gold or non-conductive samples are coated with carbon.

### Theory:

When the material is irradiated by the focused ion beam from the SEM some of the electrons from the material are displaced. A displaced electron from an inner electron shell is eventually replaced by one from an outer or higher energy shell accompanied by the release of an x-ray photon to compensate for the difference in energy. The amount of energy released by the x-ray during the process is unique to each element and can thus be used to characterise the sample. An index of x-rays is collected from a particular spot on the specimen surface and plotted against an arbitrary pixel count. The height of the peak in the spectrum corresponds to the amount of that element in the specimen. The peak position identifies the element and the type of x-ray (corresponding to the particular electron relaxation) so that more than one peak can be got from each element. For example in Figure 2.14 there are several Cu peaks.

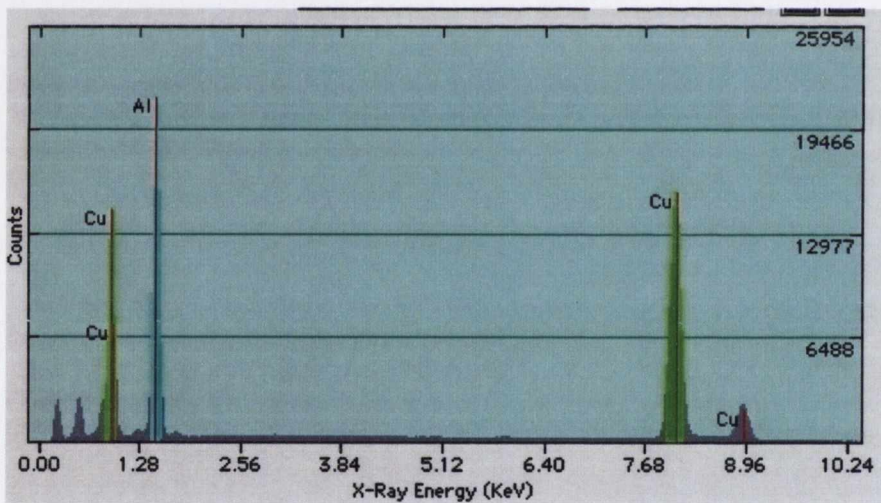


Figure 2.14: A typical EDX spectrum [480]

### 2.2.2.2 X-ray Diffraction (XRD)

X-ray diffraction is the most widely used form of crystal diffraction for bulk structure determination [481]. This is mainly because x-rays can penetrate far into solids and their wavelengths are comparable to the size of atoms ( $\sim 1 \text{ \AA}$  or 0.1 nm).

### Equipment:

Crystal structure measurements were made with a Siemens D500 Kristalloflex XR diffractometer fitted with a monochromatic Cu -K $\alpha_1$  radiation source ( $\lambda=1.5406\text{\AA}$ ) for thin film measurements and small angle measurements were performed on a Philips PW3040160 X'Pert PRO in  $\theta$ -2 $\theta$  coupled mode.

### Sample Preparation:

The samples were mounted on a glass slide which fitted into the sample chamber.

### Theory:

X-ray diffraction analysis can be done on single crystals, powdered solid samples and thin films. The diffraction pattern is obtained by rotating the sample on a goniometer and bombarding it with x-rays. If the sample is crystalline the scattered x-rays will constructively interfere when Bragg's Law is obeyed and a diffracted beam will be produced as shown in Figure 2.15.

Braggs Law states:

$$n \lambda = 2 d \sin \theta \quad (2.17)$$

- where  $n$  = an integer, 1,2,3 etc representing the order of the diffraction peak
- $\lambda$  = wavelength of the incident x-radiation (e.g.  $1.54 \text{\AA}$  for copper)
- $d$  = spacing between diffracting planes
- $\theta$  = the angle of incidence or diffraction (in degrees)

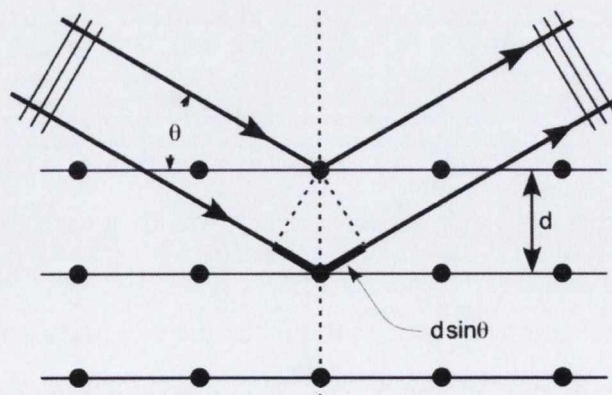


Figure 2.15: Schematic of crystal planes to illustrate Bragg's Law [482]

Each crystalline solid has a unique diffraction pattern so solids can be identified and their crystal structure can be determined from Bragg's law. The positions of the



atoms in the unit cell can also be calculated from the intensity of the diffracted beams [483].

## 2.2.3 Spectroscopy

Spectroscopic methods involve the interaction of electromagnetic radiation with matter. Substances can be identified by examining their emitted or absorbed spectrum as a function of the wavelength or frequency of the electromagnetic source. In this thesis, spectroscopy is used to determine the chemical composition of the nanowires and to give an insight into the molecular bonding.

### 2.2.3.1 Fourier Transform Infra-Red Spectroscopy (FTIR)

Infra-red (IR) spectroscopy is one of the most important analytical techniques in chemistry. It is used to detect and identify the vibrations of molecules. Analysis of an IR spectrum shows what types of bonds are present in the sample.

#### **Equipment:**

Transmission spectra were performed using a Nicolet Nexus FTIR spectrometer with step-scan capability and equipped with a Nicolet Continuum microscope. The microscope has a fully programmable stage which allows samples to be mapped in the x and y directions. It uses a liquid nitrogen-cooled MCT (mercury-cadmium-telluride) detector. Reflectance spectra were performed on a Perkin Elmer Spectrum 1 FTIR with a universal ATR diffuse reflectance sampling accessory. Omnic software was used for analysis. Both machines had a range of  $450\text{ cm}^{-1}$  to  $4000\text{ cm}^{-1}$  and a resolution of  $4\text{ cm}^{-1}$ .

#### **Sample Preparation:**

The nanowires were extracted from the template and rolled flat onto a glass slide so that the sample was transparent; the microscope was then used to position the sample for measurement with the Nexus spectrometer. It is necessary to cool the detector beforehand with liquid nitrogen. The ATR device enables measurement of samples at room temperature and humidity, without any pre-treatment and is used for measurements on the Perkin Elmer spectrometer.

## Theory:

The conventional IR spectrometer consists of a source of infra-red light which is split into two beams of equal intensity. One beam passes through the sample and the other through a reference via a monochromator, so that only light of a particular wavelength or frequency passes through the sample and reference at any one time. When the sample absorbs light of a particular frequency the intensity difference in the two beams is calculated and a spectrum is plotted. In FTIR both of the beams are passed through the sample but one beam has a longer path than the other so that when they recombine interference patterns are produced. The difference in the two paths is systematically changed and an interferogram is obtained which reflects the difference in the optical path. Fourier transform of this interferogram converts it into a familiar IR spectrum of absorption versus wavenumbers [484].

Not all molecules absorb infra-red radiation. They have to have molecular vibrations which result in a change of molecular dipole otherwise there will be no interaction with the oscillating electric vector of the infra-red beam. Thus vibrations which are not centrosymmetric are active in the infra-red. Most molecular vibrations have energies in the same region as infra-red radiation (2 - 25  $\mu\text{m}$  or 400 - 5000  $\text{cm}^{-1}$ ). The different vibrational modes of molecules can be used to identify many functional groups. Some of these modes involve the whole molecule while some are localised i.e. they are associated with the vibrations of the individual bonds or functional groups.

The absorption bands of functional groups are usually found in the region above 1500  $\text{cm}^{-1}$  in the IR spectrum. The region below 1500  $\text{cm}^{-1}$  is called the "fingerprint" region as it contains bands which are unique to each individual compound. The absorption of triple bonds (e.g.  $\text{C}\equiv\text{N}$  and  $\text{C}\equiv\text{C}$ ) usually occur at higher frequencies than double bonds (2500-2000  $\text{cm}^{-1}$ ) and double bonds (e.g.  $\text{C}=\text{O}$  and  $\text{C}=\text{C}$ ) occur higher than single bonds (2000-1500  $\text{cm}^{-1}$ ). Because hydrogen is a low mass atom, the absorption of single bonds to hydrogen (e.g. C-H, O-H, N-H stretching) usually occur at the high frequency region of the spectrum. The fingerprint region also contains bands due to bending vibrations such as rotation and stretching, and combination bands which are of lower frequency. This is summarised in the Figure 2.16.



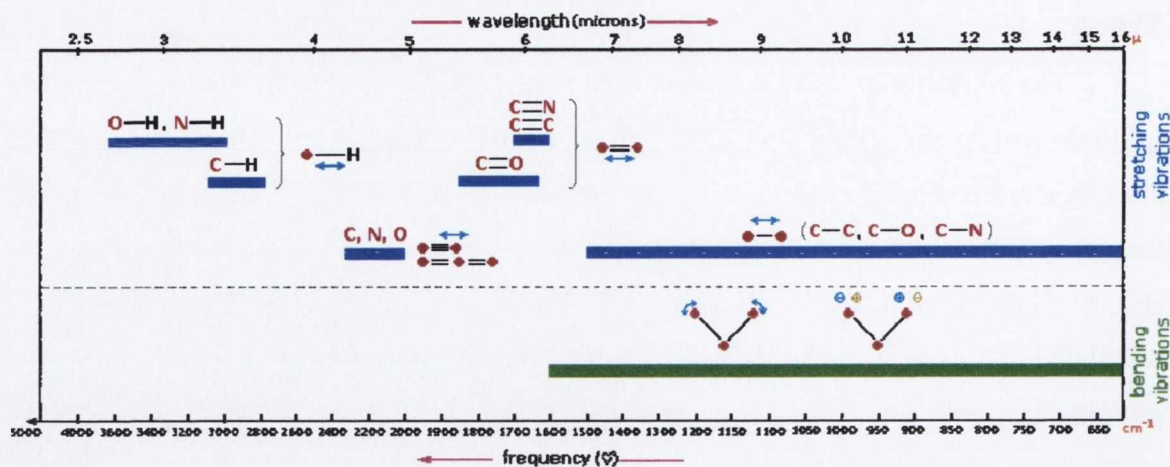


Figure 2.16: The general regions of the infrared spectrum [485]

### 2.2.3.2 Raman Spectroscopy

Raman spectroscopy is usually done with a machine which uses a laser as a light source and the light scattered by the sample is measured. Raman is complementary to IR spectroscopy.

#### Equipment:

Spectra were recorded using a HORIBA Jobin Yvon LabRAM HR fitted with a confocal microscope and digital camera. It has an 800 mm focal length spectrometer giving it a quoted resolution of  $0.3 \text{ cm}^{-1}$  and uses either a green or red laser light source. In this work the 632.8 nm line from a HeNe laser was used for excitation and calibration is that of the  $520.07 \text{ cm}^{-1}$  peak in a spectrum taken of a known Si sample.

#### Sample Preparation:

Very little sample preparation is need for solid samples. They are attached to a glass slide so that the sample is as flat as possible and a good image is obtained with the confocal microscope. Liquid samples and solutions can also be analysed in a glass or quartz cell.

#### Theory:

Molecular vibrations of molecules are also detected by Raman spectroscopy. The scattered light obtained after the sample is irradiated consists of a parent line due to

absorption and re-emission of light (Rayleigh Scatter) which is coupled with the accompanying vibrational excitation and decay (Stokes and anti-Stokes Raman scattering). The frequency of the corresponding vibration is then given by the difference in frequency between the parent and Raman line [484]. The Raman band positions are unique to each sample as they are given by the amount of energy shift for each type of bond and associated vibration present in all molecules. In contrast to IR spectroscopy only vibrations which are symmetrical about a symmetry axis are active in the Raman, so it is usually used in conjunction with IR, however, unlike FTIR, there are a distinct number of advantages when using Raman. It is non-destructive, requires little or no sample preparation and can also be used to analyse aqueous solutions; in addition the intensity of spectral features in solution is directly proportional to the concentration of the absorbing species and when this method is used in conjunction with a Raman microscope the spatial resolution and depth discrimination is superior to FT analysis [486].

### **2.2.3.3 Ultraviolet, Visible and near Infra-red (UV-Vis-NIR) Absorption Spectroscopy**

Electromagnetic radiation is absorbed by molecules in the ultraviolet (200-400 nm), visible (400-800 nm) and near infrared (800-2700 nm) spectral region when transitions occur between different electronic energy levels. UV-Vis-NIR is used to measure how much light of a particular wavelength is absorbed by the sample. It can be used for qualitative, quantitative and structural identification of samples [487]. It may also give us an insight into the intermolecular interactions and optical transitions involved in composite materials.

#### **Equipment:**

UV-Vis spectra were recorded in the wavelength range 300-1000 nm on a Perkin Elmer Lambda 900 UV-Vis/NIR spectrometer.

#### **Sample Preparation:**

The aluminum foil was first removed from the back of the membrane by a solution of 0.2 M  $\text{CuCl}_2$  in 3 M HCl. It is not necessary to remove the alumina template as it is transparent in the region under investigation.



## Theory:

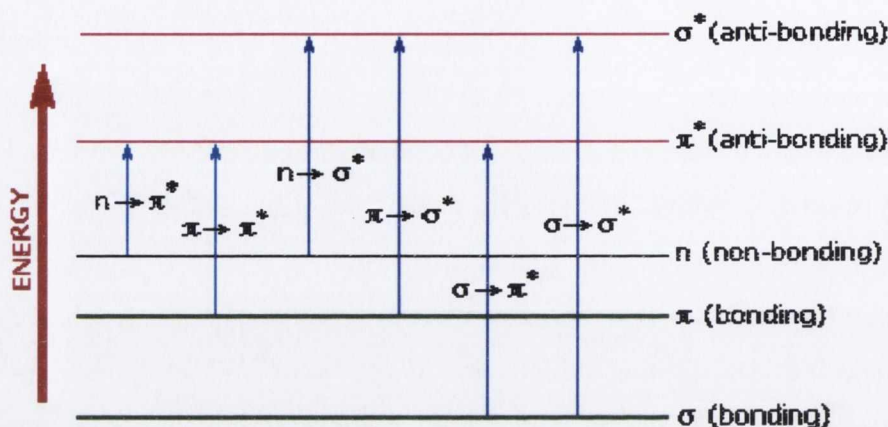


Figure 2.17: Energy Level diagram

As the atom or molecule absorbs energy an electron transition will occur between a bonding and unfilled non-bonding orbital. This results in the creation of an excited species as the electron is promoted from the ground to an excited state as shown in the energy level diagram above (Figure 2.17). The difference between the energy levels is characteristic for each chemical element and gives rise to a peak on the absorption spectrum.  $\pi \rightarrow \pi^*$  transitions require lower energy (and occur at longer wavelengths) than  $\sigma \rightarrow \sigma^*$  transitions and  $n \rightarrow \pi^*$  transitions will be found at longer wavelengths than  $\pi \rightarrow \pi^*$  transitions [488]. However each electronic transition is accompanied by rotational and vibrational transitions which appear as fine structure in the absorption line which thus becomes a broad peak. The molecule thus absorbs at a range of wavelengths surrounding a max wavelength or  $\lambda_{\max}$ . Solvent interaction will sometimes mask the fine structure. The intensity or peak height at  $\lambda_{\max}$  is related to how much energy is absorbed by the molecule.

The concentration of the absorbing species can be measured by applying the Beer-Lambert Law [489]:

$$A = \epsilon d c \quad (2.18)$$

- where  $A$  = measured absorbance
- $\epsilon$  = wavelength dependant molar absorption (or extinction) coefficient in  $M^{-1}cm^{-1}$
- $d$  = path length in cm

- $c$  = molar concentration

The absorbance or optical density is given by:

$$A = \log_{10} I_0/I \quad (2.19)$$

- where  $I_0$  = intensity of incident light
- $I$  = intensity of transmitted light

The spectrometer usually measures the transmittance  $T$  of the light where:

$$T = I/I_0 \quad (2.20)$$

$$\text{Thus absorbance } A = -\log_{10}T \quad (2.21)$$

#### **2.2.3.4 Fluorescent or Photoluminescent (PL) Spectroscopy**

Fluorimetry is used to measure the intensity and wavelength distribution of light emitted when the samples are excited at certain wavelengths, usually the UV maximum of their absorption band.

##### **Equipment:**

Emission (or PL) spectra were recorded in the wavelength range 200-900 nm on a Perkin Elmer LS 50B spectrometer with a pulsed Xenon discharge lamp (7.3 W average power at 50 Hz). Alternatively excitation at 266 nm with a Jag laser was used. Figure 2.18 is a schematic of the components of a typical fluorimeter.



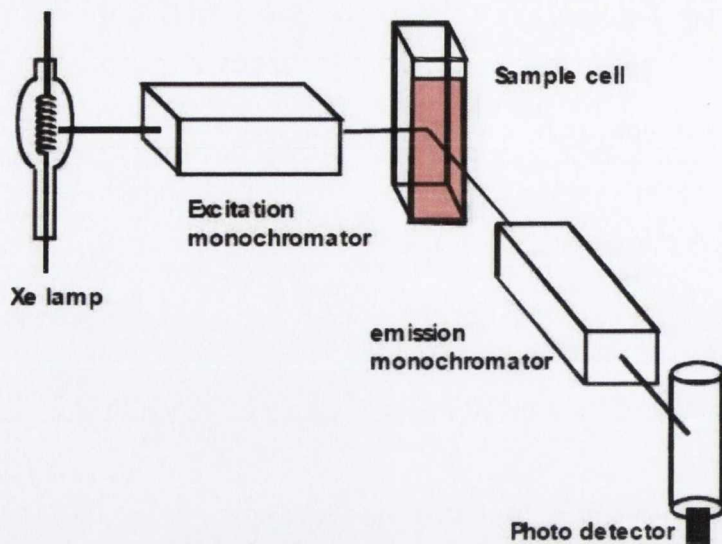


Figure 2.18: Schematic of the typical components of a fluorimeter [490].

A monochromator may be used to select certain wavelengths for transmission. This is not necessary when using a laser as a laser only emits light of high irradiance at a very narrow wavelength interval however the wavelength of a laser cannot be changed by much. A filter is used to catch some of the emitted light and pass it to the detector.

### Sample Preparation:

The aluminum foil was first removed from the back of the membranes by a solution of 0.2 M  $\text{CuCl}_2$  in 3 M HCl. The nanowires were not removed from the PAM as they were measured in the solid state and luminescence measurements of the empty PAMs were also made.

### Theory:

Fluorescence spectroscopy investigates the different frequencies of light emitted when a species in the excited electronic state relaxes back to its ground state.

Each electronic state consists of vibrational and rotational energy levels as shown in Figure 2.19.

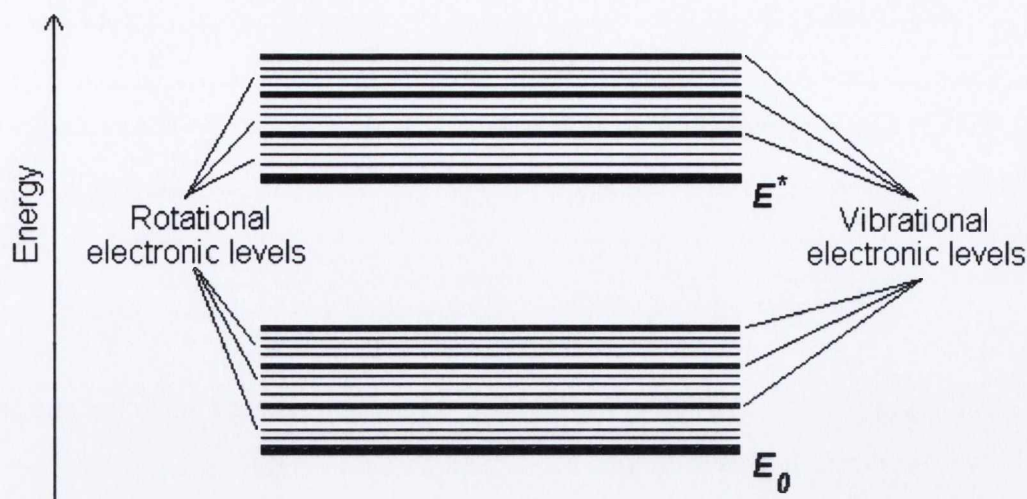


**Figure 2.19: Energy level diagram showing rotational and vibrational levels in the ground and first excited state of a chemical species [491]**

When the species is excited it may be in any one of the vibrational levels; however it loses vibrational energy by internal conversion until it reaches the lowest vibrational level in the excited electronic state. It then drops into one of the vibrational levels in the ground state and loses the rest of its energy by emitting a photon. By examining the frequencies of light emitted for fixed wavelength excitation (usually at the wavelength of maximum absorption) an emission spectrum of the sample is obtained. It is also possible to obtain an excitation spectrum by detecting at the maximum of the emission spectrum. These spectra are then used to analyse the vibrational energy levels in the ground state.

#### 2.2.4 Electrical Characterisation

The electrical characteristics of the samples were obtained at room temperature using a Keithley 2400 sourcemeter. A Keithley IV program was used to measure direct (DC) voltage-current characteristics. Sheet resistivities of the samples were calculated from these measurements.

#### **Sample Preparation:**

Silver wire contacts were attached along each side of perfectly square samples with conducting silver paint; these were placed inside a metal box to reduce interference and then connected to the Keithley source.

#### **Theory:**

The electrical resistance of a conductor of rectangular shape is given by:



$$R = \rho_B L / WT \quad (2.22)$$

- where R = electrical resistance
- $\rho_B$  = bulk resistivity of the material
- L = length of the sample
- W = width of the sample
- T = thickness of the sample

For very thin samples the length and width are much greater than the thickness and sheet resistivity is used [492]. This is defined as:

$$\rho_S = \rho_B / T \quad (2.23)$$

Combining (2.22) and (2.33) gives:

$$R = \rho_S L / W \quad (2.24)$$

So for a square sample of uniform thickness ( $L = W$ )

$$R = \rho_S \quad (2.25)$$

Thus the sheet resistivity for a square sample can be calculated from the measured resistance of the sample [493].

# Chapter 3 Results: One-Dimensional Nanostructures in Porous Alumina Membranes

## 3.1 Porous Alumina Membranes (PAMs)

The alumina templates were made by anodisation of high purity aluminium foil (purity from 99%- 99.999%, depending on the application, and thicknesses between 0.25 -1.0 mm, Goodfellow).

### 3.1.1 Preparation of Aluminium Foils

The surface of the foil is quite rough and is covered with a thermal oxide layer; thus it needs to be pre-treated before anodisation. When possible the foils were pre-annealed at 500 °C under N<sub>2</sub> to remove mechanical stress and enhance grain size. They were then sonicated in acetone for 5 minutes, washed with deionised water, iso-propanol and finally deionised water once again. Then the thermal oxide layer (~1-10 nm thick) and grease on the foil surface were removed by dipping in hot chromic acid (48 g/L potassium dichromate in 10% Phosphoric acid solution) for 5-10 minutes. Finally any surface inhomogenities and scratches were removed by electropolishing the foil in a temperature controlled bath of concentrated sulphuric and phosphoric acids (11:7 (v/v) mixtures at ~ 75 °C for approximately 3 minutes). The Al foil was positively biased i.e. used as the anode and a lead sheet was used as the cathode. The voltage used depended on the voltage which was used for anodisation of the foil, as explained in chapter 2, section 2.1.1.3.1. The apparatus is shown in Figure 3.1.



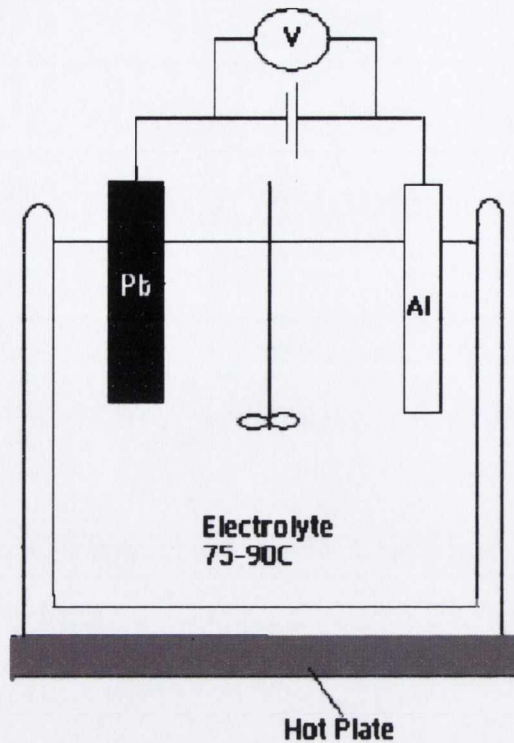


**Figure 3.1: Schematic drawing of the electropolishing process**

After electropolishing the foils were rinsed immediately in hot water, acetone and deionised water. A mirrored, stress and occlusion free surface with unidirectional patterning is produced, thus improving the reflectivity of the aluminium. An alternative electropolishing electrolyte was sometimes used which contained a mixture of perchloric acid and ethanol. 18 V was applied at 10 °C for 4 minutes (see chapter 2, section 2.1.1.3.1).

SEM images were taken at each stage of this process and are shown in Figure 3.2. Figure 3.2(a) shows an untreated 99.999% pure aluminium foil. The grained surface is produced as the foils are rolled during production. After chromic acid treatment the foil has less debris and the grained surface is more defined as the thermal oxide layer is removed {Figure 3.2(b)}. Electropolishing produces a flatter surface {Figure 3.2(c)} which is similar to an anodised surface {as seen at higher magnification in Figure 3.2(d)}, however as the electrolyte used here is hot, any oxide produced during the electropolishing will be dissolved and then washed away in the rinsing process.

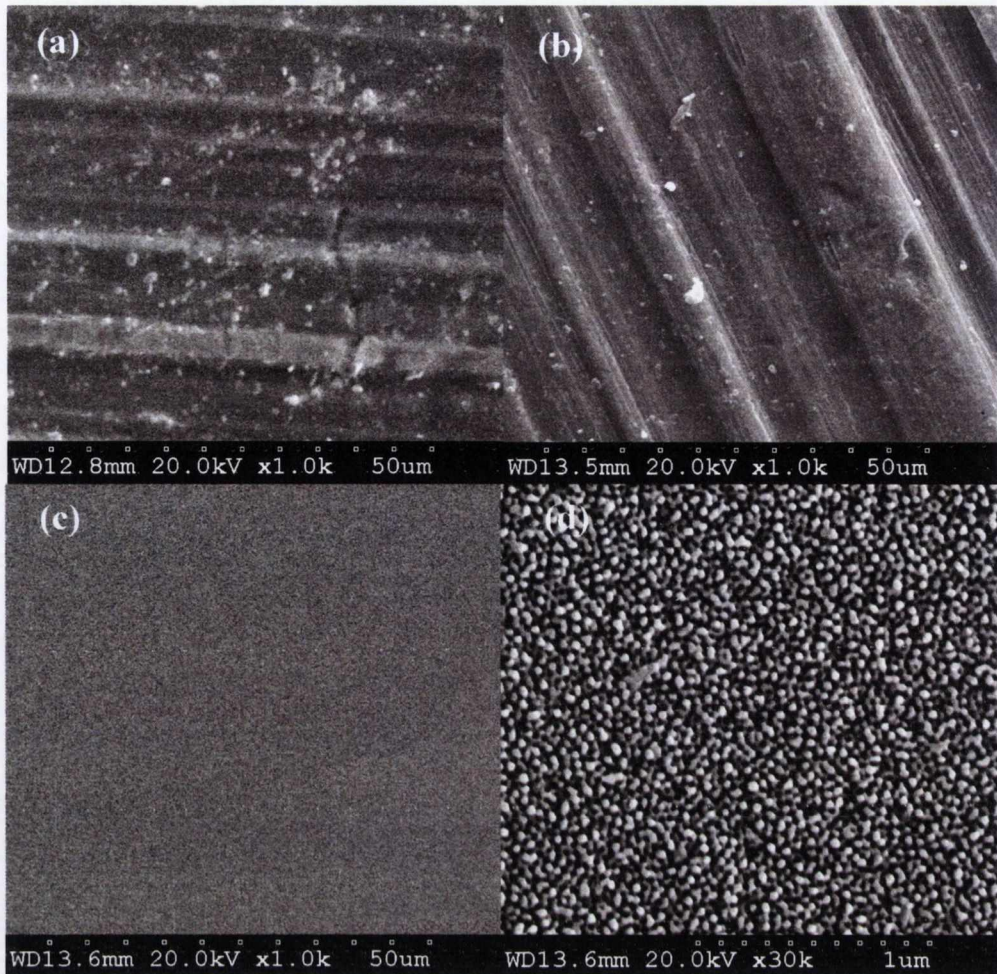


Figure 3.2: Typical SEM images of a 99.999% Al foil (a) untreated, (b) after chromic acid treatment, (c) after electropolishing at 15V, (d) after electropolishing at 15V taken at a higher magnification.

Figure 3.3 shows two foils of lower purity which have been electropolished in the same way. The lower purity foil (99%) shows more defects and debris {Figures 3.3(a) and (b) compared to the higher purity foil Figure 3.2}.

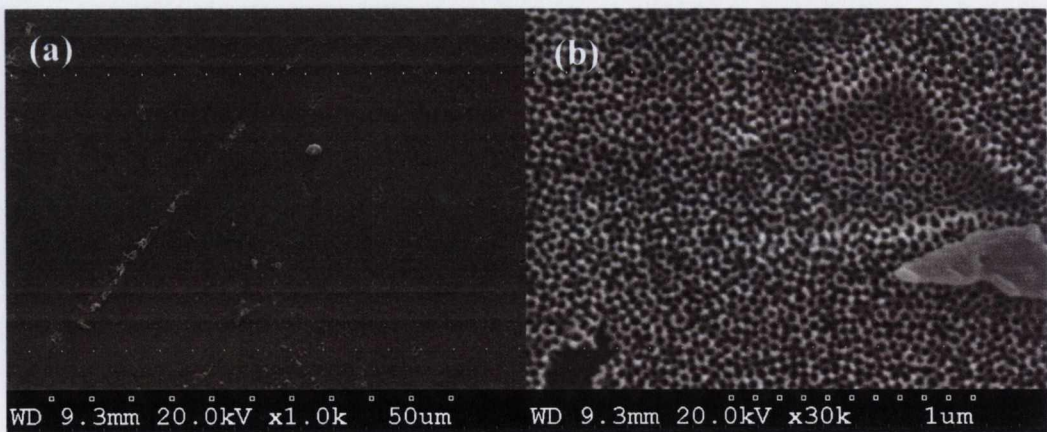


Figure 3.3: Typical SEM images of a 99% Al foil (a) after electropolishing at 15V, (b) after electropolishing at 15V taken at a higher magnification



### 3.1.2 Fabrication of PAMs

Anodisation was carried out using the following set up (Figure 3.4). Again Al was used as the anode and lead as the cathode.

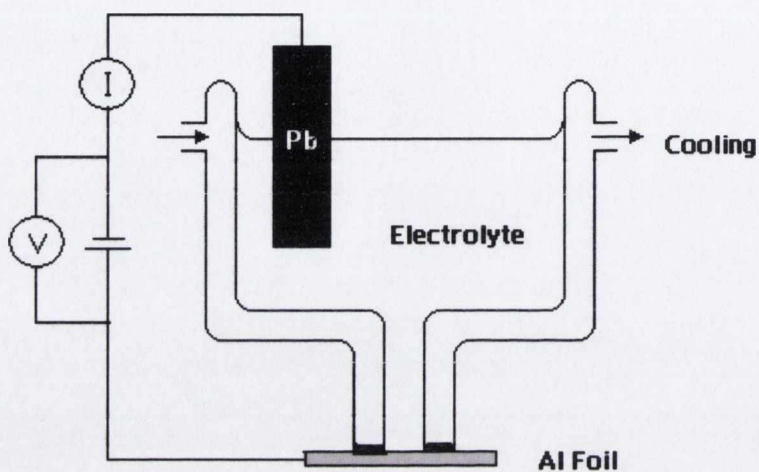
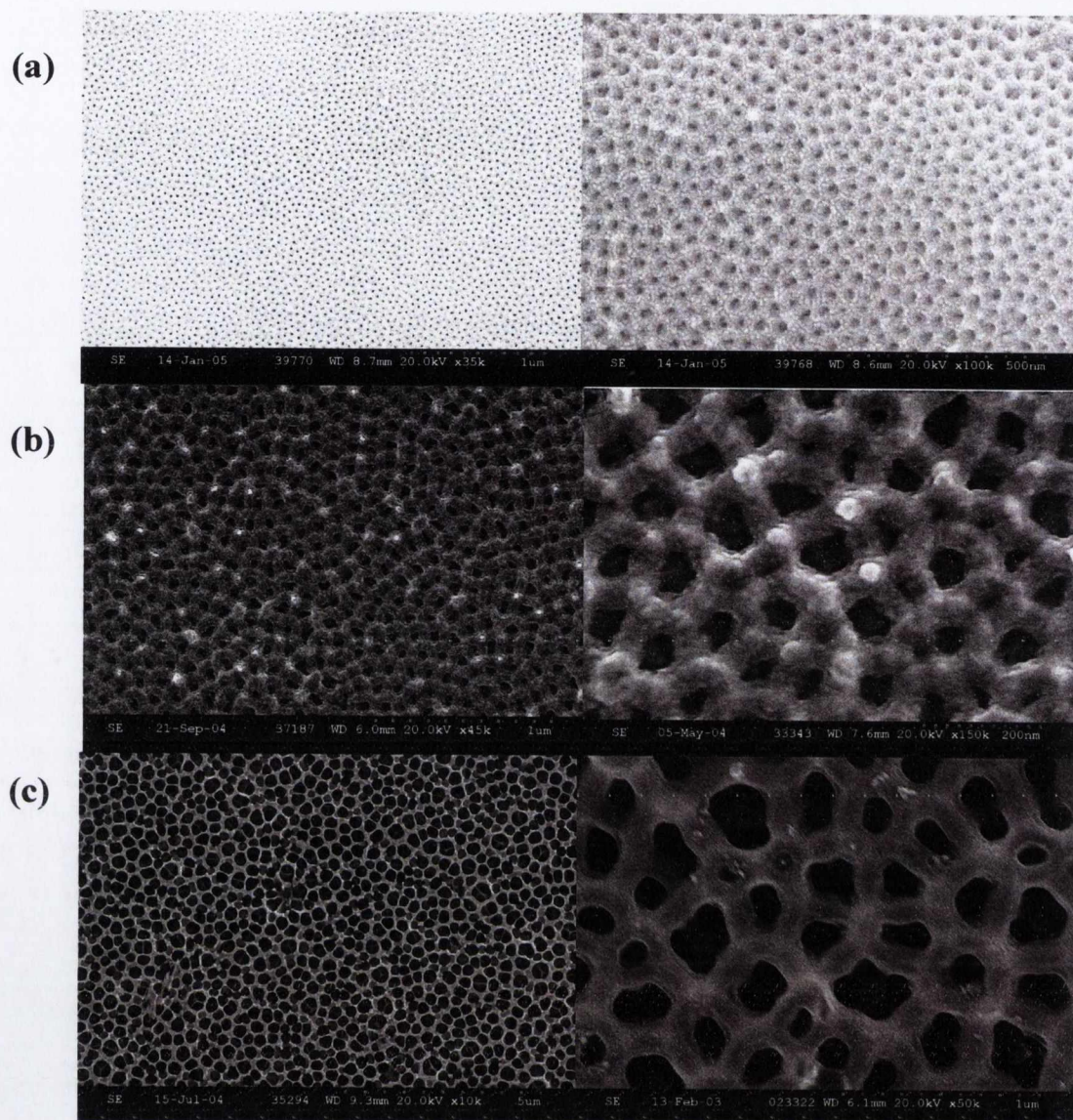


Figure 3.4: Schematic of anodisation set-up

The temperature of the solution was maintained using a Lauda low temperature thermocirculator with automated temperature control; a mixture of water and ethylene glycol was used in the cooling bath. The foil was mounted on a Perspex slide and held in position with a rubber o-ring and clamp. The cell was thermally isolated by a polystyrene cover to avoid temperature fluctuations. The electrolyte and applied voltage used depended on the size of pores required (see chapter 2, section 2.1.1.3.2). In this study 10% sulphuric acid ( $\text{H}_2\text{SO}_4$ ) was used at 0 °C at voltages between 5 and 20 V for the smaller pore diameters. 1% oxalic acid ( $\text{H}_2\text{C}_2\text{O}_4$ ) was used between 40 and 80 V at 0 °C and gave pore diameters between 40 and 120 nm. For larger pores a 2% phosphoric acid ( $\text{H}_3\text{PO}_4$ ) electrolyte was used from 100-140 V at 10 °C. The pore diameter is directly related to the anodisation voltage (1-1.5 V/nm) [210, 211, 213, 219]; thus pore sizes up to 200 nm could be achieved. Figure 3.5 shows a SEM of each type of membrane produced.



**Figure 3.5: SEM images of PAMs made with (a) sulphuric acid, (b) oxalic acid and (c) phosphoric acid**

It can be seen from Figure 3.5 that the smaller pore membranes have thicker walls. There is also a large standard deviation in pore diameter for the larger pores although the oxide wall thickness is less variable {Figure 3.5(c)}. Optimal conditions for ordered growth are obtained when a moderate expansion of the oxide occurs during anodisation. This was found to depend on the anodisation voltage; the best results were obtained for PAMs made at 40 V in oxalic acid [208].

Anodisation was carried out for 30 min to 10 hrs depending on the electrolyte used and pore depth required. To obtain an alumina layer of 8 – 10  $\mu\text{m}$  the conditions in the table below (Table 3.1) were used.



**Table 3.1 Conditions used for anodisation of aluminium foils**

Pore Diameter	Anodisation Voltage	Electrolyte	Temperature	Time
10 -15 nm	10 V	10% H <sub>2</sub> SO <sub>4</sub>	0 °C	6 hr
20 – 30 nm	20 V	10% H <sub>2</sub> SO <sub>4</sub>	0 °C	2 hr
40 – 60 nm	40 V	1% C <sub>2</sub> H <sub>2</sub> O <sub>4</sub>	0 °C	4 hr
60 – 90 nm	60 V	1% C <sub>2</sub> H <sub>2</sub> O <sub>4</sub>	0 °C	2 hr
80 – 120 nm	80 V	1% C <sub>2</sub> H <sub>2</sub> O <sub>4</sub>	0 °C	30 min
100 – 150 nm	100 V	2% H <sub>3</sub> PO <sub>4</sub>	10 °C	3.5 hr
120 – 180 nm	120 V	2% H <sub>3</sub> PO <sub>4</sub>	10 °C	2 hr
140 – 210 nm	140 V	2% H <sub>3</sub> PO <sub>4</sub>	10 °C	30 min

As discussed in chapter 2, section 2.1.1.3.2 better pore ordering at the interface is obtained by anodisation over long periods under constant conditions [206, 208]. This is illustrated in Figure 3.6 which shows the top of an alumina membrane compared to the bottom which has had the barrier layer removed.

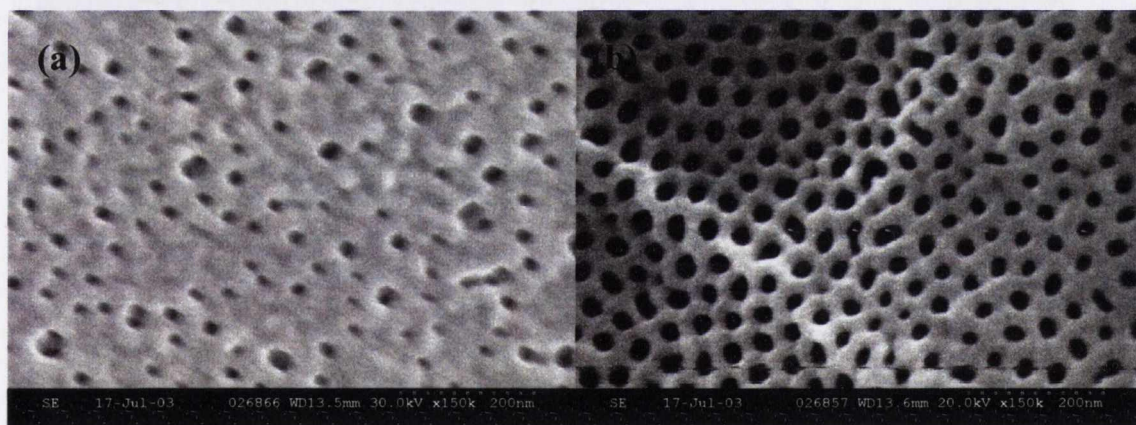


**Figure 3.6: SEM images of PAMs made with sulphuric acid at 20V (a) from the top surface and (b) from the bottom after removal of the barrier layer**

As can be seen from Figures 3.5 and 3.6 ordered domains separated by regions of defects are obtained i.e. pore growth follows the domain structure of the aluminum. Better pore arrays are achieved by pre-patterning the surface by lithography or by using a two-step anodisation as described in section 2. In this work 2-step anodisation was used. An SEM of each step was taken to illustrate this (shown in Figure 3.7).



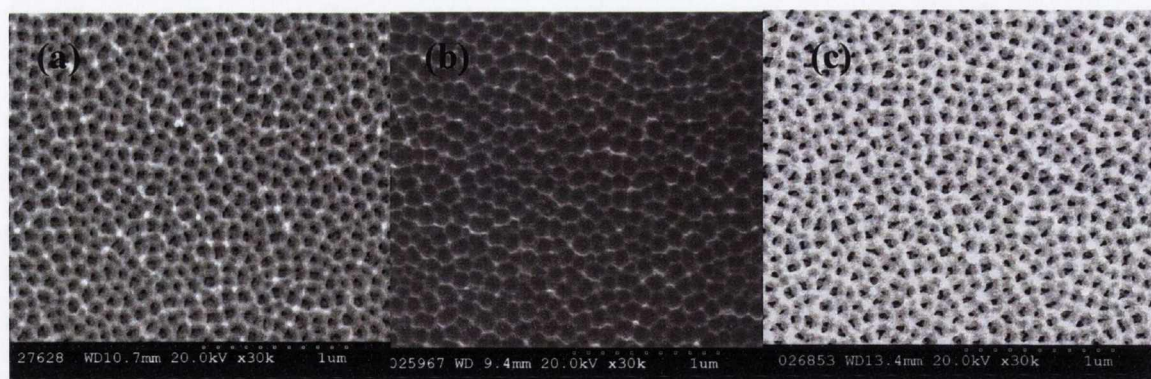


**Figure 3.7:** SEM image of membranes made with (a) oxalic acid at 40 V overnight, (b) after removal of oxide and (c) after second anodisation at 40 V

Even better ordering can be achieved by careful temperature control as is achieved in the Nielsch group in Halle [494]. Figure 3.8 shows an SEM image of a 40 V membrane which was made there. The first anodisation was done at 3 °C for 24 hr after a 60 min delay to make sure the cell had reached equilibrium. The oxide was removed at 35 °C overnight and the second anodisation was done for 3 hrs after the same time delay. A voltage reduction was done at the end of the anodisation to thin the barrier layer.

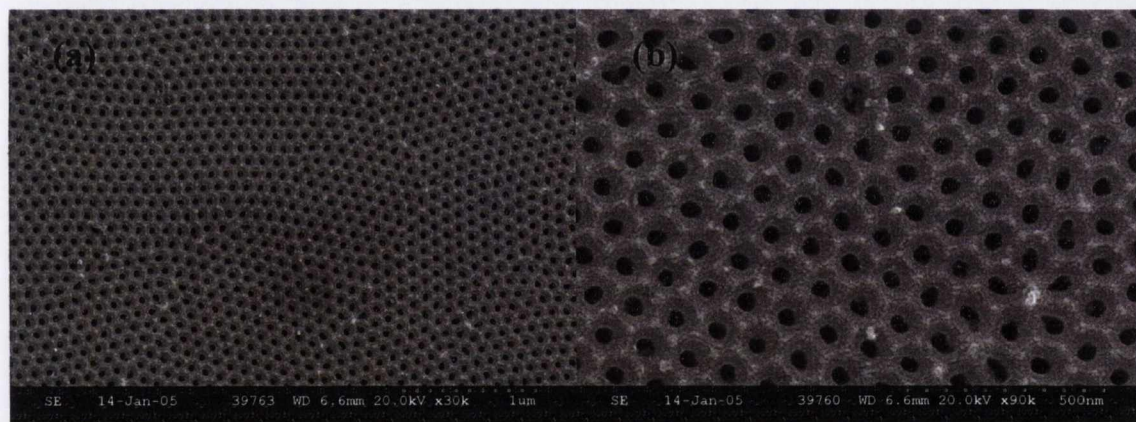


**Figure 3.8:** SEM images of PAMs doubly anodised with oxalic acid at 40V shown at different magnifications

The SEM images show the surface morphology but not the topology of the PAMS {e.g. Figure 3.9(a)}. However, a close up view {Figure 3.9(b)} suggests that the surface is not planar and by tilting the sample as in Figure 3.10 it is clear that the sides of the pores are higher than the pore mouths. This is confirmed by the AFM image (Figure 3.11) which shows that the surface has an egg-box topology. Image (c) shows that a 2  $\mu\text{m}^2$  area of the PAM has a surface roughness of at least 30 nm. However, as shown in image (b), many areas contained features up 140 nm high.



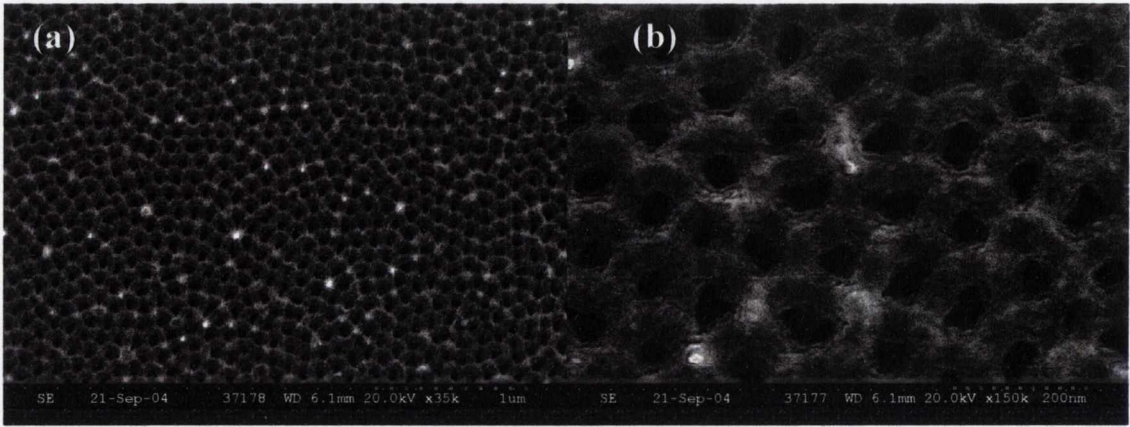


Figure 3.9: SEM images of oxalic acid PAMs taken at (a) 35K and (b) 50k magnification

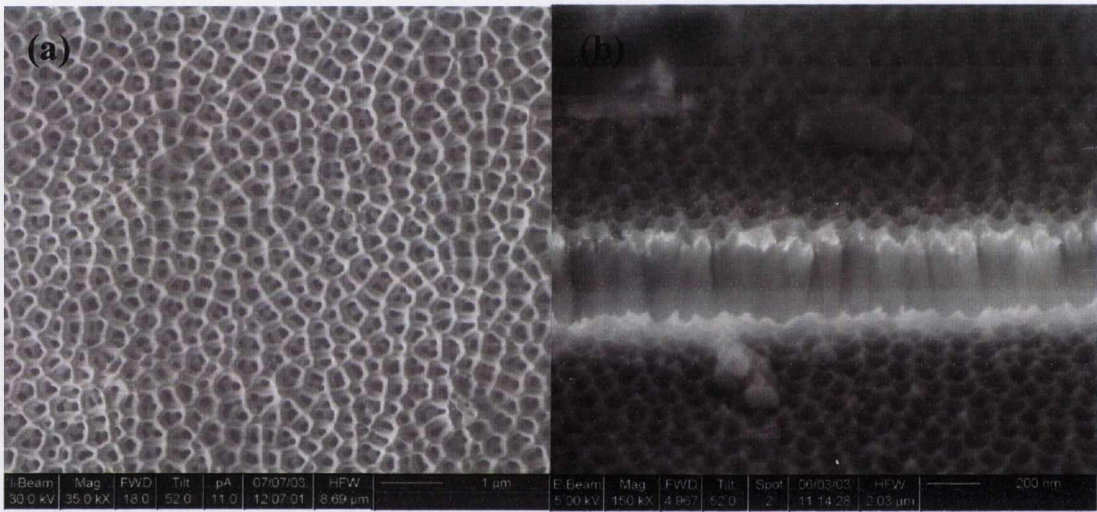


Figure 3.10: SEM images of oxalic acid PAMs at a 52.0° tilt angle

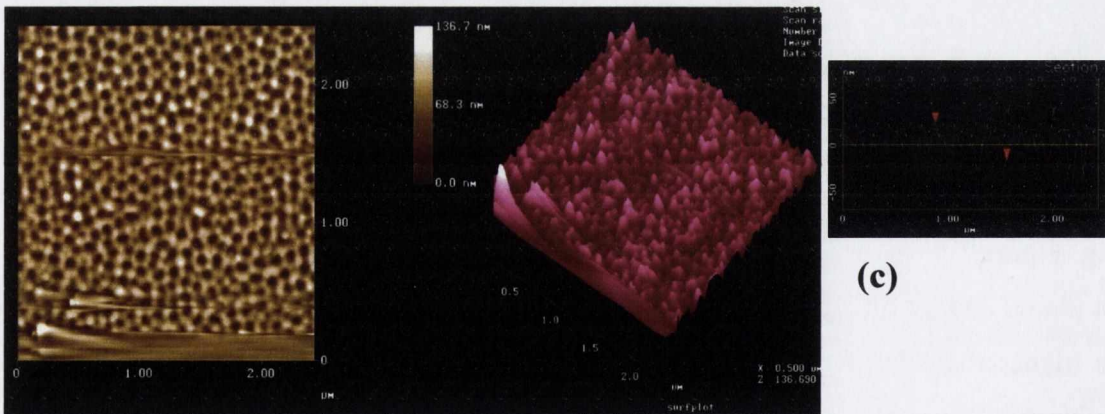
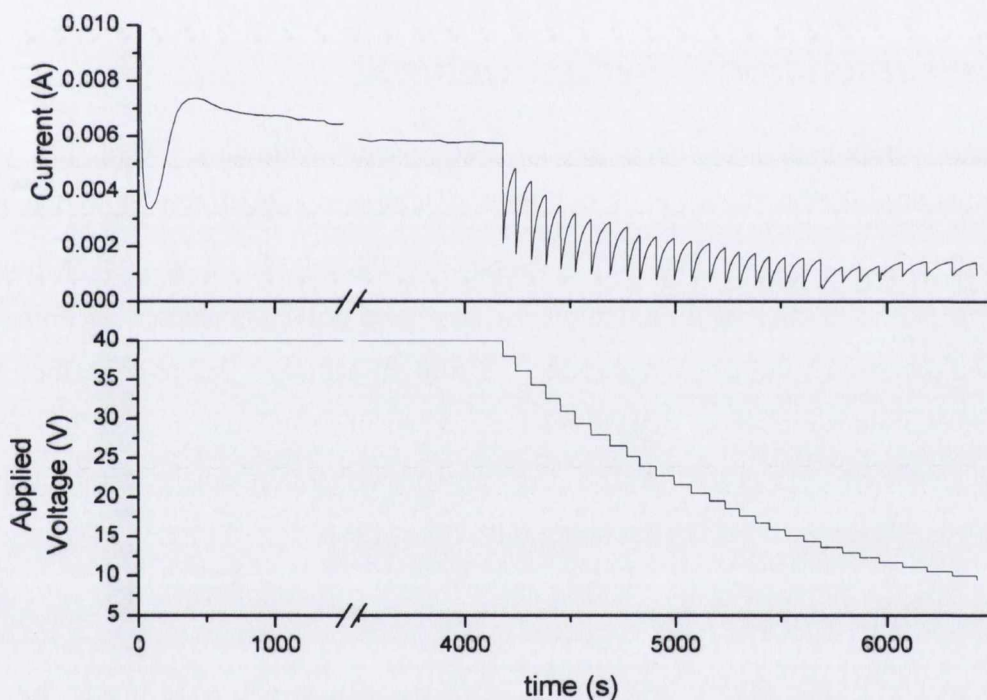


Figure 3.11: (a) AFM image of an oxalic acid PAM with (b) corresponding surface plot and (c) surface roughness measurement

### 3.1.3 Reduction of the Barrier Layer

Before the PAMs can be filled by AC electrodeposition it is necessary to reduce the barrier layer for all foils anodised at voltages greater than 20 V (see section 2.1.1.3). This was done by the method of Furneaux et al. [212] i.e. by decreasing the voltage in small steps of 5% of the original voltage. It is important that each voltage step is done before the current reaches its steady value (as the voltage is dropped the current falls rapidly then rises to a maximum when the barrier layer is formed) thus each step is done when the rate of current rise had fallen to 75% of its maximum value. Figure 3.12 shows the response in current as the voltage is reduced from 40 V to 10 V for barrier layer reduction of a PAM made at 40 V in oxalic acid.



**Figure 3.12: Plot of voltage reduction of a PAM made at 40 V in oxalic acid and the response in current.**

The voltage was reduced to 15 – 20 V for deposition by AC and 4 - 14 V for pulsed electrodeposition (PED). The HRSEMs below Figure 3.13(a) and (b) show how the barrier layer has been reduced as the pores in the barrier layer region have branched into smaller pores during this reduction process.



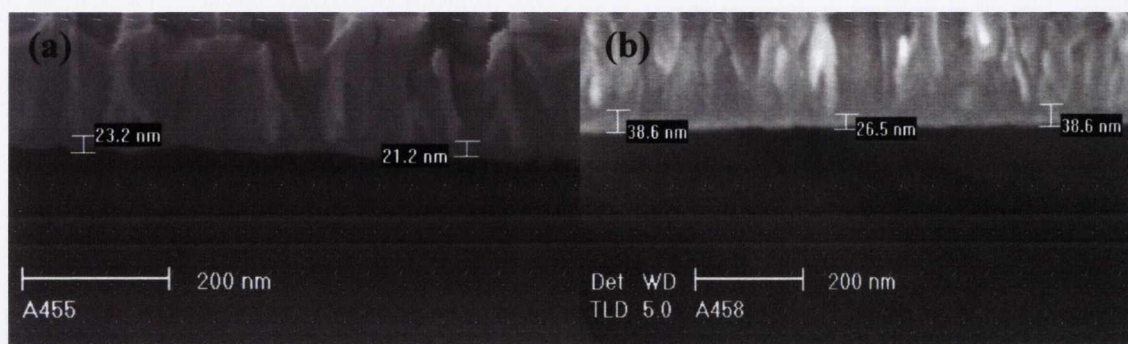


**Figure 3.13: HRSEMs of PAMs made at 40V which have been voltage reduced to (a) 10.2 V and (b) 14.1 V**

## 3.2 One-Dimensional Nanostructures

Metal, polymer, semiconductor and composite nanowires were made by electrodeposition into PAMs. It is important to use a freshly made PAM which has been well rinsed with deionised water for homogeneous deposition in aqueous solutions. Shönerberger et al. found that if the templates (they used polycarbonate) were immersed in deionised water with ultrasonic agitation for 2 min immediately before deposition they obtained growth over the whole deposition area. When this step was omitted they found pore growth started in some pores first, and then proceeded in others resulting in an increasing electrochemical reduction current with time [495].

### 3.2.1 Metal nanowires

Copper, nickel, silver, iron, cobalt and tin nanowires were made by AC electrodeposition; nickel, cobalt and silver nanowires were also made by pulsed electrodeposition (PED). Both methods are described in sections 2.1.1.4.2 and 2.1.1.4.3 in chapter 2.

#### 3.2.1.1 Fabrication by Chemical Electrodeposition

The conditions and electrolytic solutions used for deposition are summarized in Table 3.2.

**Table 3.2 Deposition conditions employed for metallic nanowires**

<b>Metal</b>	<b>Method</b>	<b>Electrolyte Composition</b>	<b>Reference No</b>
Copper (Cu)	AC @13 V (RT)	35 g / L CuSO <sub>4</sub> , 20 g / L MgSO <sub>4</sub> , H <sub>2</sub> SO <sub>4</sub> added till pH = 1.3	Goad and Moskovits [496]
Nickel (Ni)	AC @16 V (RT)	50 g / L NiSO <sub>4</sub> *7 H <sub>2</sub> O, 25 g / L H <sub>3</sub> BO <sub>3</sub> , 20 g / L C <sub>3</sub> H <sub>5</sub> (OH) <sub>3</sub> (glycerol)	Kawai and Ishiguro [497]
Nickel (Ni)	PED @ 6 V or 70 mA / cm <sup>2</sup> (35 °C)	300 g / L NiSO <sub>4</sub> * 6 H <sub>2</sub> O, 45 g / L NiCl <sub>2</sub> *6H <sub>2</sub> O, 45 g / L H <sub>3</sub> BO <sub>3</sub> , pH = 4.5	Niensch et al. [169, 224]
Silver (Ag)	AC @ 9 V (RT)	1 g / L Ag NO <sub>3</sub> , 41 g /L MgSO <sub>4</sub> * 7 H <sub>2</sub> O, H <sub>2</sub> SO <sub>4</sub> added till pH = 2	Kröll [219]
Silver (Ag)	PED @ 6 V or 15 mA / cm <sup>2</sup> (RT)	8.5 g / L Ag <sub>2</sub> SO <sub>4</sub> , 200 g / L C <sub>6</sub> H <sub>14</sub> N <sub>2</sub> O <sub>7</sub> (diammonium hydrogen citrate)	Sauer et al. [172]
Iron (Fe)	AC @16 V (RT)	120 g / L FeSO <sub>4</sub> * 7 H <sub>2</sub> O, 45 g / L H <sub>3</sub> BO <sub>3</sub> , 1 g / L C <sub>6</sub> H <sub>8</sub> O <sub>6</sub> (ascorbic acid)	Al-Mawlawi et al. [290]
Cobalt (Co)	AC @16 V (RT)	50 g / L CoSO <sub>4</sub> * 7 H <sub>2</sub> O, 25 g / L H <sub>3</sub> BO <sub>3</sub> , 20 g / L glycerol	Kawai and Ishiguro [497]
Cobalt Co	PED @ 6 V or 70 mA / cm <sup>2</sup> (25 °C)	240 g / L CoSO <sub>4</sub> * 7 H <sub>2</sub> O, 40 g / L H <sub>3</sub> BO <sub>3</sub> , 1 g / L ascorbic acid	Niensch et al. [169, 224]
Tin (Sn)	AC @ 13 V (RT)	20 g / L SnSO <sub>4</sub> , with enough H <sub>2</sub> SO <sub>4</sub> added until the solution was clear	Kröll [219]

AC deposition was performed in a cell with the PAM and a graphite rod as the working and counter electrodes as shown in Figure 3.14. The aluminium foil was placed onto a glass plate and clamped onto the glass tube by means of an o-ring.



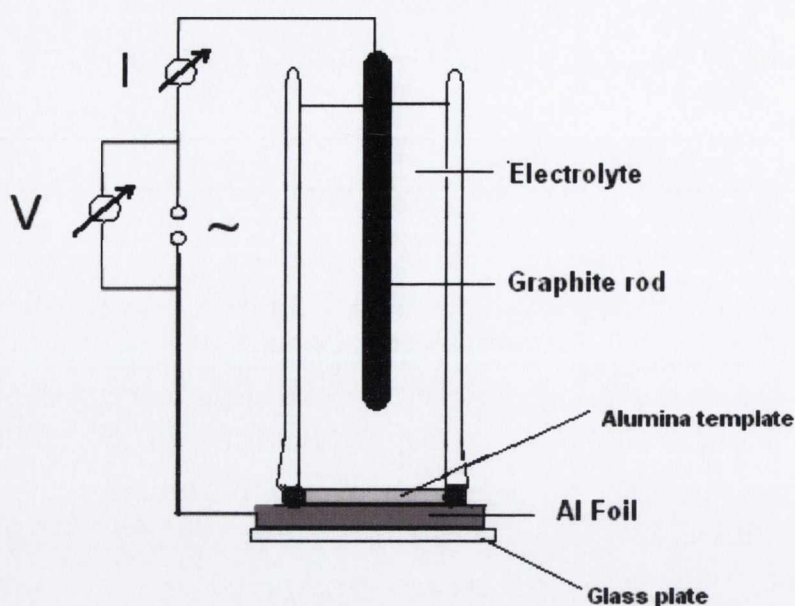


**Figure 3.14: Schematic of apparatus used for AC electrodeposition in a PAM**

PED was done in a similar apparatus except a programmed pulsed voltage source was used. The method used in this thesis is described in chapter 2, section 2.1.1.4.3 and references 169, 172 and 224. A current pulse of  $-70 \text{ mA} / \text{cm}^3$  was applied for 8 ms, followed by a short positive potential pulse of  $+3 \text{ V}$  for 2 ms (during which time  $I_{\text{max}}$  was limited to  $\pm 70 \text{ mA}$ ).  $T_{\text{off}}$  was set to 1s.

### 3.2.1.2 Characterisation

#### 3.2.1.2.1 Preparation of Samples for Characterisation

Many different techniques are used to characterise nanowires made in PAMs. Some of these can be used without altering the finished structure (e.g. Raman spectroscopy) but most require some preparation.

#### Polishing Samples

Samples for electrical characterization should not contain bulk deposition of metal on the surface of the membrane; however it is equally important that the wires reach the surface. It is thus important to fully fill the membrane and then polish the surface to rid it of over plated material and any surface debris. This was done by mechanically polishing for 4 hrs on a Buehler Potropol polishing system at 80 rpm using 300 nm  $\text{Al}_2\text{O}_3$  particles and  $\text{H}_2\text{O}$  as carrying fluid.

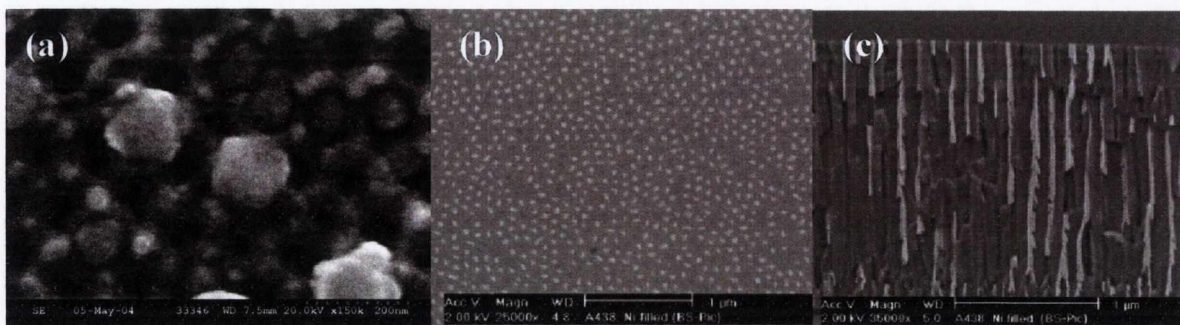


**Figure 3.15: SEM of a PAM made at 40V which was over-plated with Ni (a) top view (b) top view after polishing (c) side view after polishing**

Figure 3.15(a) shows a SEM of an over-plated Ni sample whereas Figures 3.15 (b) and (c) show the surface and side view of a similar over-plated PAM after it has been polished.

### **Extracting Nanowires**

Characterisation techniques such as TEM and FTIR require free standing nanowires. The nanowires were extracted from the template by first taking off the aluminium and barrier layer and then removing the template.

There are several different ways to remove the aluminium. First the foil was clamped in a glass cell as in Figure 3.14 instead this time the non-porous layer was facing upwards. 20% phosphoric acid was added to the cell to a depth of approx 1 cm and the whole arrangement was placed in an ultrasonic bath for 12 min. The phosphoric acid was then removed and the cell rinsed with deionised water. A solution of bromine in methanol (10%) was added and the cell left until the aluminium was dissolved [219]. It was then rinsed with acetone and deionised water. The porous alumina template should now be clearly visible. Alternatively the aluminium can be removed by covering the foil with a solution of copper chloride in hydrochloric acid [244, 245]. In this thesis a solution of 0.2 M  $\text{CuCl}_2$  in 3M HCl was used. It was usually necessary to renew the solution several times before the aluminium was completely removed. During this process copper was formed which can be washed away with deionised water:



To remove the barrier layer which was underneath the aluminium a 20% phosphoric acid solution was used. The time to do this varied for each membrane as the barrier layer



height depends on the voltage used to make the membrane. In general the barrier layer should be 40 nm or less as a voltage reduction is usually done at the end of the anodisation period for membranes made at voltages greater than 20 V. This size barrier layer should be completely dissolved after 15 min. It has been found that 12, 10 and 8 min is sufficient to remove the barrier layer for membranes made at 15 V, 10 V and 5 V respectively [219].

Lastly the porous alumina template was removed by shaking the whole template in a solution of 0.1 M NaOH and 30 g / L poly(vinylpyrrolidone) (PVP) for 12-24 hr, allowing the nanowires to settle out overnight and carefully decanting off the dissolved alumina and NaOH solution. The PVP surrounds the nanowires thus facilitating their separation and dispersion. This procedure can be repeated if the solution is very cloudy and is followed by washing and shaking the nanowires in distilled, Millipore filtered H<sub>2</sub>O.

#### **3.2.1.2.2 SEM and HRSEM**

The pore structure and surface morphologies of the samples were investigated by SEM. Pore filling was investigated by cross sectional HRSEM which allows deeper penetration into the material and thus determination of barrier layer heights, pore heights and diameters and nanowires heights and diameters.

Analysis of several doubly anodized PAMS made at 40 V in oxalic acid and filled with Ni by PED revealed that the nanowire diameter was  $57 \text{ nm} \pm 13 \text{ nm}$  and the barrier layer ranged from  $20 \text{ nm} \pm 3 \text{ nm}$  to  $40 \text{ nm} \pm 5 \text{ nm}$  depending on the voltage reduction ( $40 \text{ V} \rightarrow 10 \text{ V}$  or  $40 \text{ V} \rightarrow 18 \text{ V}$ ). Analysis of a similar empty membrane (see Appendix A1 for details) gave the average diameter as  $50 \text{ nm} \pm 10 \text{ nm}$  and centre to centre pore spacing as  $124 \text{ nm} \pm 21 \text{ nm}$  (1<sup>st</sup> anodisation) and  $126 \text{ nm} \pm 18 \text{ nm}$  (2<sup>nd</sup> anodisation).

Nanowire growth was also monitored by SEM. Total plating time depended on the height of the oxide layer; for example it took 8 min to fill a PAM, which has a  $4.5 \mu\text{m}$  porous layer, with Cu or Ni by AC electrodeposition. Different plating times were used to monitor growth; this is illustrated in Figure 3.16. After 4 min the PAM is approx half full, after 8 min it is slightly overfilled as can be seen from the Cu deposits on top of the foil. This also shows that filling is non-uniform, some pores are only half full and many pores are left empty.

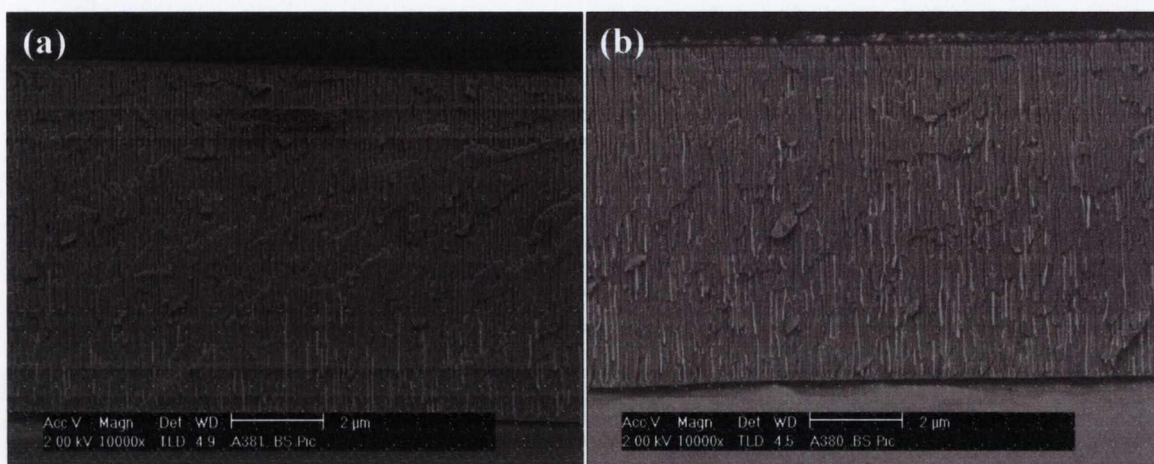


**Figure 3.16: HRSEMs of PAMs made by anodisation at 40V filled with Cu by AC electrodeposition for**

**(a) 4 min and (b) 8 min**

Figure 3.17 shows SEMs of PAMs made at 20 V in  $H_2SO_4$  and filled with Ag at 9 V for 3 min. It illustrates that although there is a large deposition at the pore tips only a few wires reach the top of the membrane.

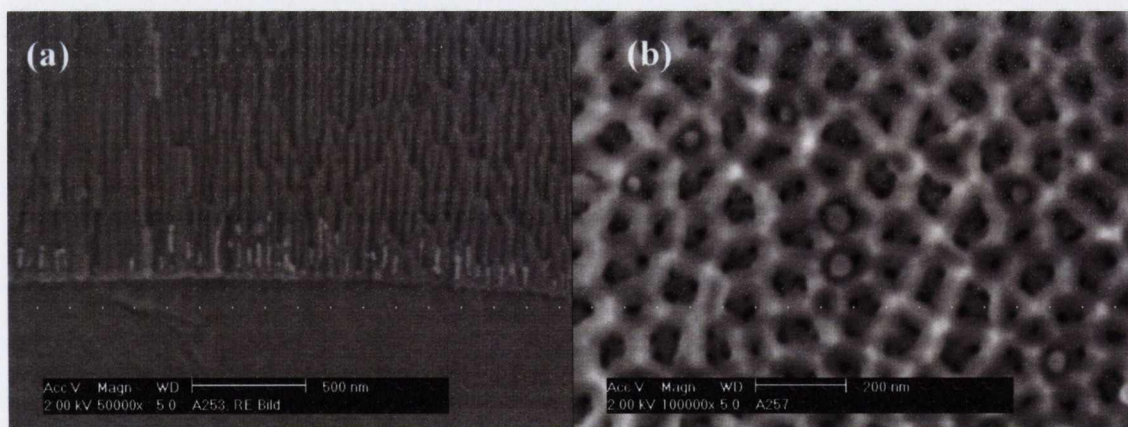


**Figure 3.17: SEM images of Ag filled PAMs taken from (a) the side and (b) the top.**

Better filling was achieved by using pulsed electrodeposition (PED). Plating times were much longer due to the delay introduced between deposition pulse signals, however 80-95% filling was achieved for various metals as illustrated in the SEM images below.



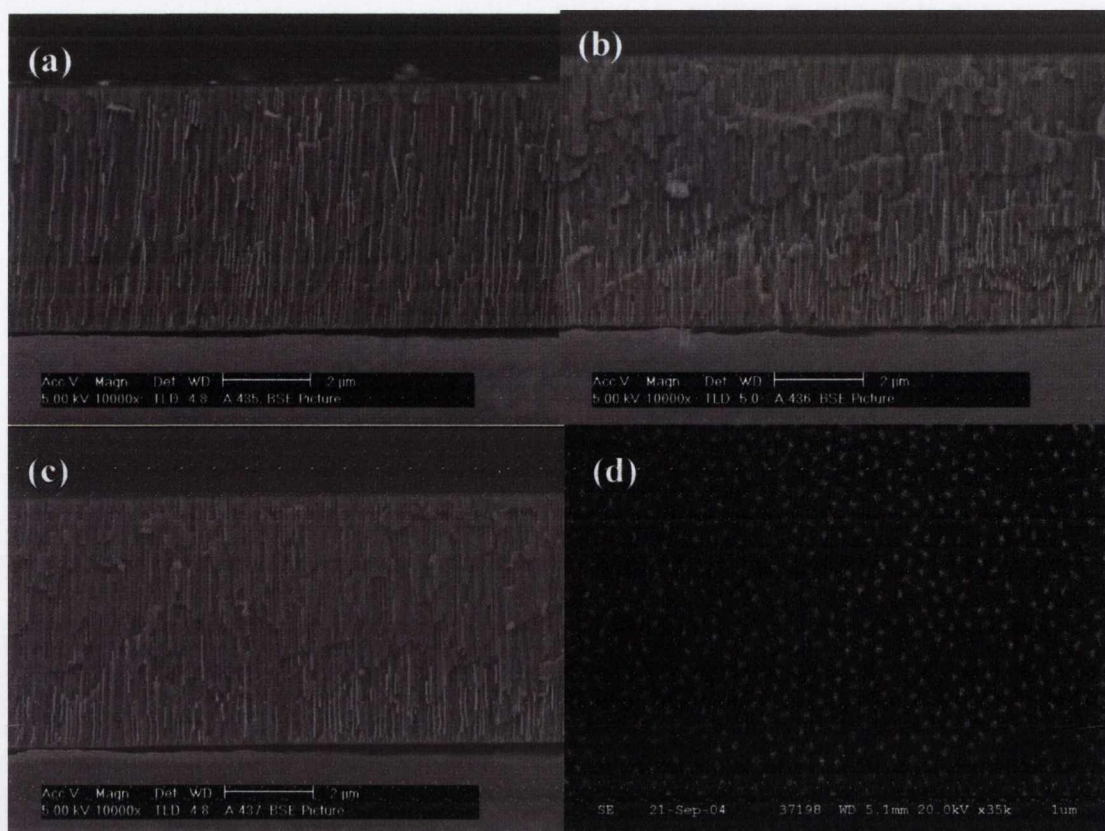


**Figure 3.18: Cross sectional SEM images of PAMs filled with Ni by PED (a) for 60 min, (b) for 30 min, (c) for 20 min and (d) top SEM view of PAM filled for 60 mins then polished.**

Figure 3.18(a) shows a PAM which was anodised twice at 40 V (17 hr, 3.5 hr) and filled with Ni by PED for 1 hr. Most nanowires have reached the surface and there is very little over-plating. Figure 3.18(b) shows a similar PAM which has been filled for 30 min and shows that nanowires growth is about half way up the pores. Figure 3.18(c) shows 20 min filling and 3.18(d) shows the top of a PAM made under the same conditions and filled to the top with Ni nanowires. The top surface has been polished to reveal the nanowires tips and shows that nearly all the pores are filled with Ni.

### 3.2.1.2.3 TEM and HRTEM

TEM was done to test the structural uniformity of the nanowires and to measure their average diameters and lengths (although many of the wires may break when extracted from the PAM). It can also tell us something about the crystallinity of the nanowires which can be further investigated with HRTEM.

Figure 3.19 shows some typical TEM images of metal nanowires. Figure 3.19(a) and (b) show nanowires extracted from a PAM made at 40 V (anodized twice, 4 hr + 3.3 hr) which was filled by PED with Ni for 2 hr. In Figure 3.19 (a) there is a bundle of



nanowires clumped close together which indicated that there was good pore filling of the template and that even after removal they remained parallel to each other. The branched structure at the base of the nanowires (due to branching of the pores as the barrier layer is reduced) is also visible. Although the nanowires are straight they contain some little ridges or branches {Figure 3.19(b)} which suggest that the pore structure was not homogeneous. Their crystalline nature is evident from the different contrasts in the TEM images due to the different crystal domains. This is even more obvious in the single Ag nanowires shown in Figure 3.19(d). Figure 3.19(c) shows Ag nanowires which were electroplated by AC and extracted from the PAM. As filling by AC is much poorer (10-30%) the nanowires do not come out in clumps but they tend to aggregate together and are also attracted to the sides of the sample holder. The Ag nanowires showed wide variations in lengths and diameters. The diameter of individual nanowires was also not homogeneous and varied as much as 5 nm for the smaller nanowires and 20 nm for the larger ones.

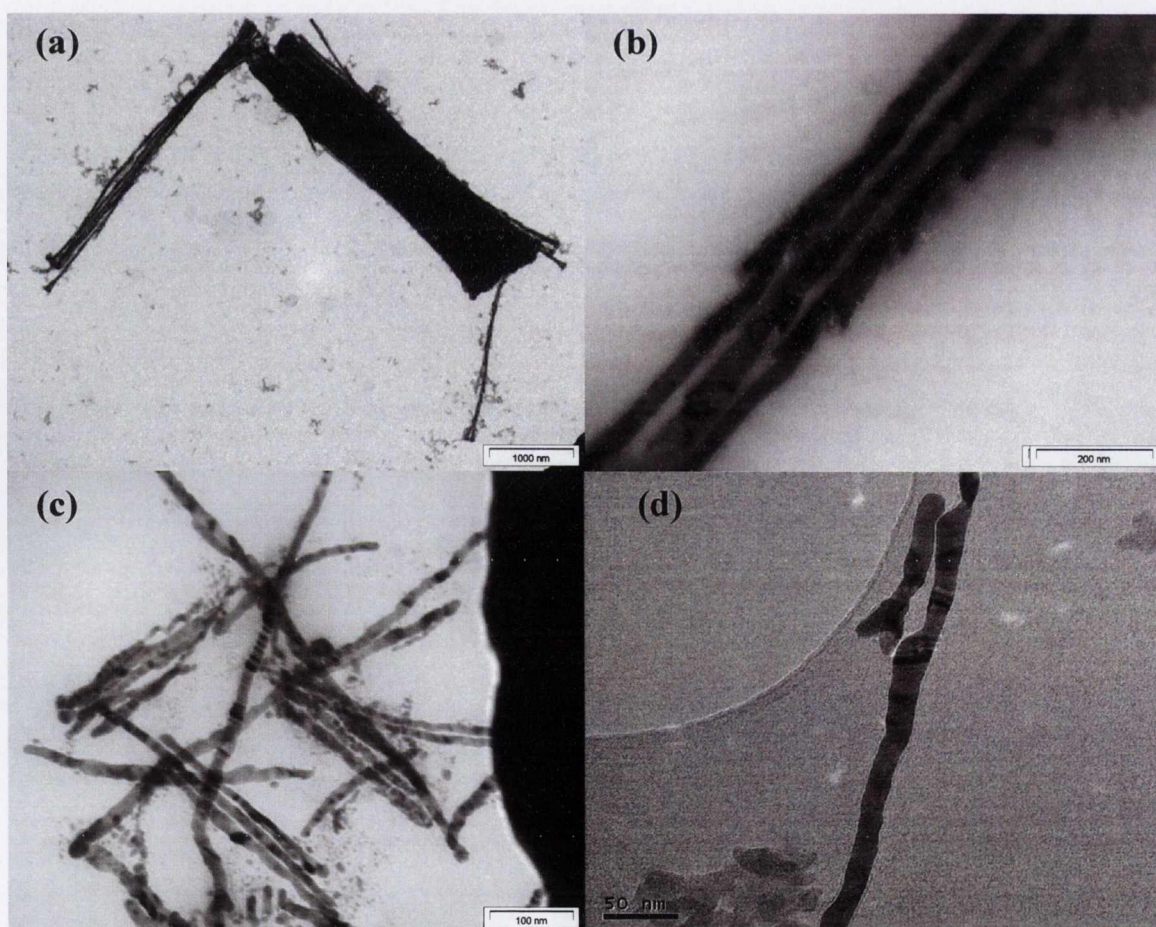


**Figure 3.19: TEM images of (a) and (b) Ni nanowires from a PAM made at 40 V and filled by PED, (c) Ag nanowires from a PAM made at 20 V and filled by AC deposition and (d) HRTEM of similar Ag nanowires.**



Table 3.3 shows some of the diameters and lengths obtained for various nanowires (measured by UTHSCSA computer program).

**Table 3.3 Nanowire Dimensions**

Type of Nanowire	Type of PAM (and filling time)	Length Range (nm)	Average Length (nm)	Diameter Range (nm)	Average Diameter (nm)
Cu (AC)	80 V (10 min)	1298 - 4329	3227 ± 983	55 - 220	102 ± 37
Ni (PED)	40 V (2 x 3.5 hr)	1770 -6622	4094 ± 712	20 - 58	46 ± 11
Ag (AC)	20 V (2 hr)	176 -1229	487 ± 180	2.5 -27	15 ± 3
Fe (AC)	67 V (2 x 1.5 hr)	14482 - 19945	17714 ± 2732	62 - 98	89 ± 11

The variations in length could be due to inhomogeneous filling or to broken nanowires. The diameter dimensions are in accord with those of the pores and in agreement with other authors [206, 209, 220, 221 222]. There was less variation in nanowire diameters for the doubly anodized samples (Ni and Fe), due to better pore ordering. However the diameters' variations were due not only to inhomogeneity in pore diameter but also to variations in the individual wires' diameters. A better picture is got from the analysis of single nanowires (as shown in Appendix A2). It should also be noted that the variation in nanowires' diameters was greater than that of pores' diameters (see section 3.2.1.2.2) which suggests that the plating of the PAM also has an effect on the homogeneity of the nanowires. Gerin and Haber have reported that continuous AC deposition causes damage to the PAM [220]. This is supported in this work which shows less variation in pore diameters for the PED plated PAMs.

#### 3.2.1.2.4 AFM

AFM was performed on some of the Ag nanowires to check their topology and dimensions. The images (Figure 3.20 and Figure 3.21) show that the nanowires diameters are reasonably homogeneous and that the nanowires have a ridged topology.

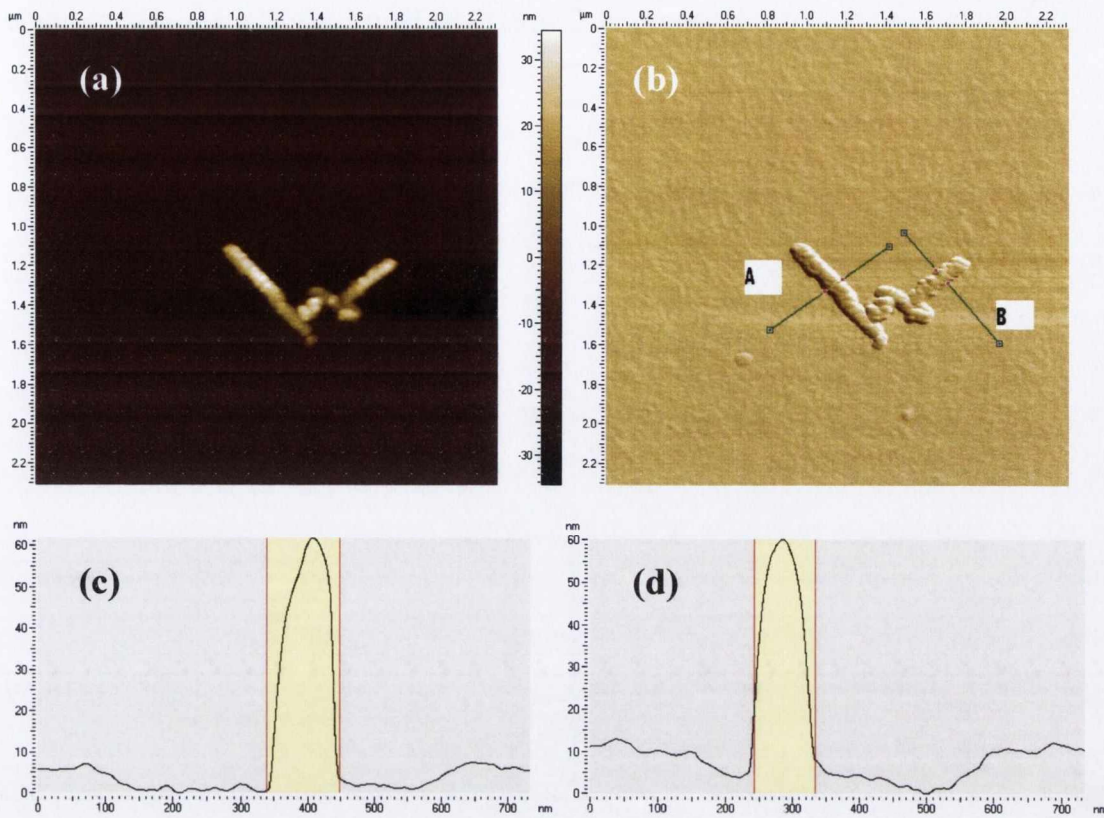


**Figure 3.20: AFM images (a) normal and (b) filtered of Ag nanowires extracted from a PAM made at 60 V with height profiles A and B from the filtered image shown below {(c) and (d)}**

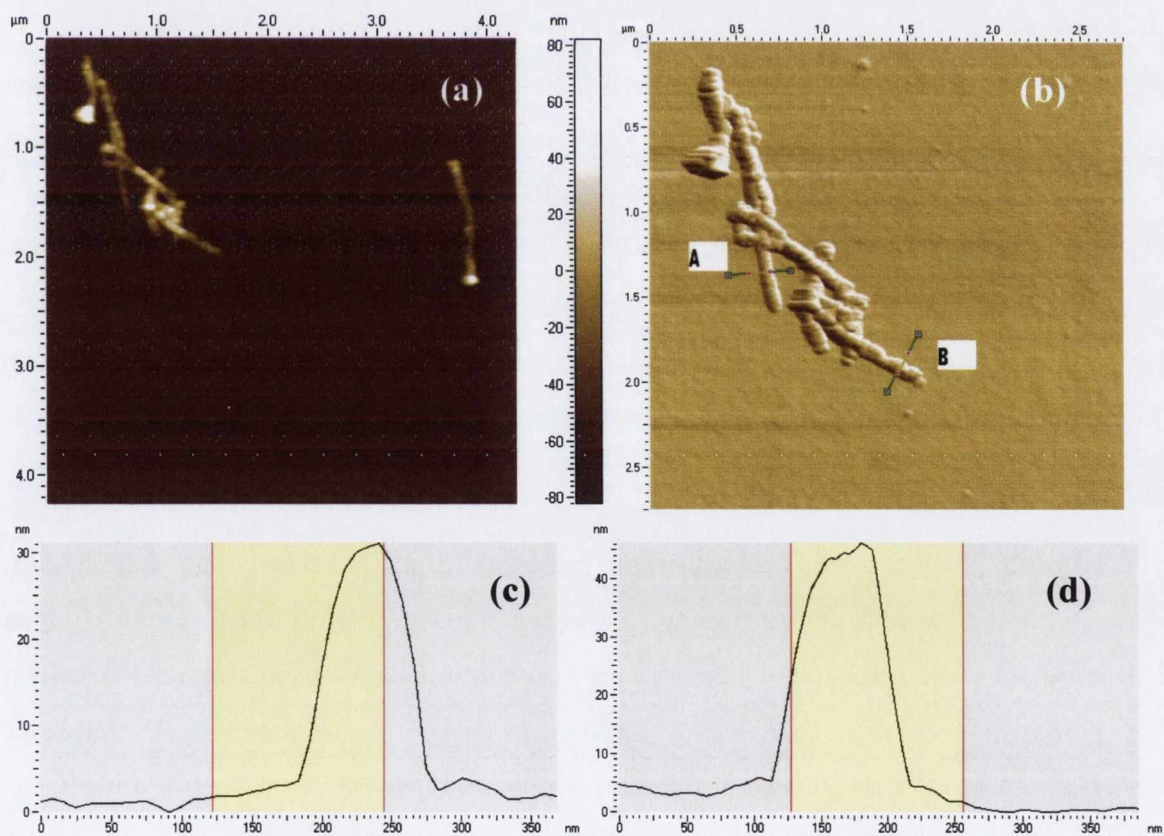


**Figure 3.21: AFM images (a) normal and (b) filtered of Ag nanowires extracted from a PAM made at 30 V with height profiles A and B from the filtered image shown below {(c) and (d)}**

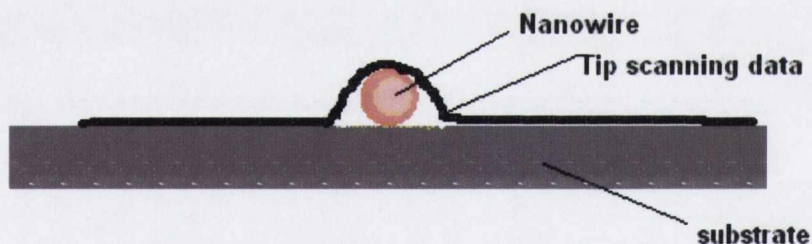


Figure 3.21 shows a group of nanowires which are aggregated and a single nanowire. The branched pore structure at the end of some of the nanowires is clearly visible. Again the diameters seem to be reasonably uniform. Height profiles and diameters were measured and are tabulated in Table 3.4.

**Table 3.4 Ag Nanowire Dimensions from AFM Measurements**

Type of PAM (and filling time)	Theoretical Diameter of pores (nm)	Height Range (AFM) (nm)	Average Height (AFM)(nm)	Width Range (AFM)(nm)	Average Width (AFM)(nm)
Oxalic, 60 V (2 hr)	60 -80	57.43 – 69.00	67.69 ± 9.68	96.39 – 145.00	115 ± 26.04
Oxalic, 30 V (6 hr)	30 - 45	31.47 – 52.15	41.33 ± 9.81	84.32 – 106.40	105.33±16.59

The height measurement of the sample gives a more accurate value of the diameter than the width measurements due to tip convolution. This is illustrated in Figure 3.22 below.



**Figure 3.22 Schematic of AFM probe tip scanning over a flat surface which has a nanowire adsorbed on it adapted from <http://chemistry.jcu.edu/mwaner/research/AFM/tipconv.htm>.**

### 3.2.1.2.5 EDX

EDX was performed to confirm the presence of metals in the pores of the PAMs. The measurements were done from the base of the pores after removal of Al and Al<sub>2</sub>O<sub>3</sub> as described in section 3.2.1.2.1. The spectra also showed peaks from sulphur (S), which was probably due to the acidic plating solution, carbon (C), which was from the thin layer of C used to coat the sample and aluminium (Al) and oxygen (O) from the PAM itself.

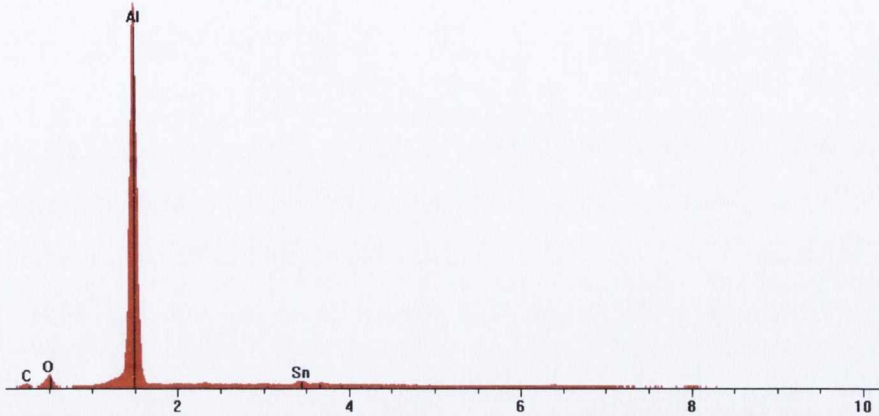


Figure 3.23: EDX Spectrum of PAM made at 40 V and filled with Sn by AC deposition

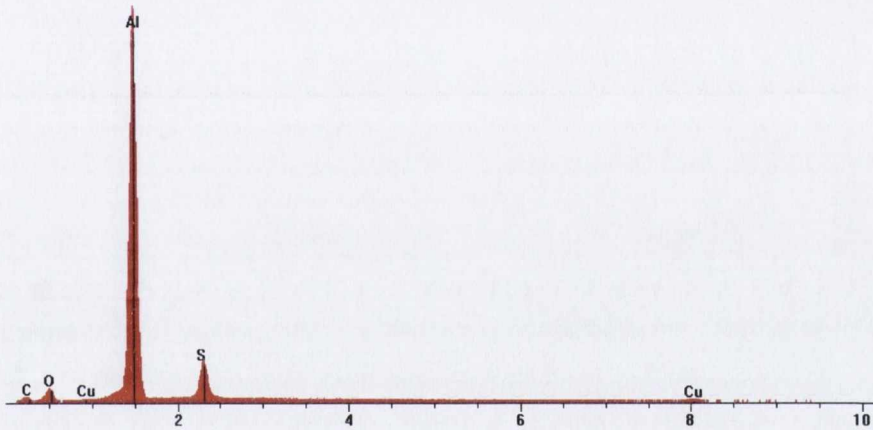


Figure 3.24: EDX Spectrum of PAM made at 20 V and filled with Cu by AC deposition

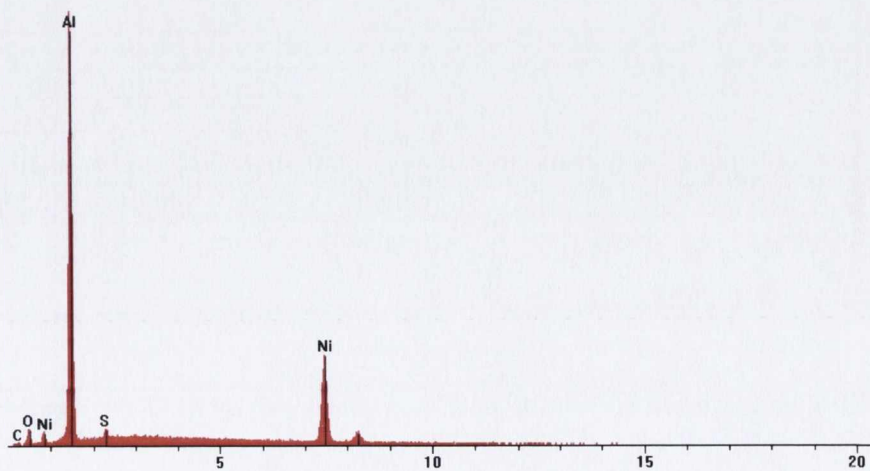


Figure 3.25: EDX Spectrum of PAM made at 40 V and filled with Ni by PED



A semi-quantitative analysis was done on PAMs containing Ag which was deposited by AC (Figure 3.26) and PED (Figure 3.27). The analysis was done on the same volume of material and the data normalised with respect to the total amount (weight percent and atomic proportion) of elements in the sample. The results are shown in the tables in the figure insets. The K-Ratio is obtained after subtraction of the background. This is the ratio of the net intensity of the sample relative to the net intensity of a standard for each element. This is then used to determine the composition of the elements [498].

■ Analysis\_9\_S001.pgt

FS: 28000

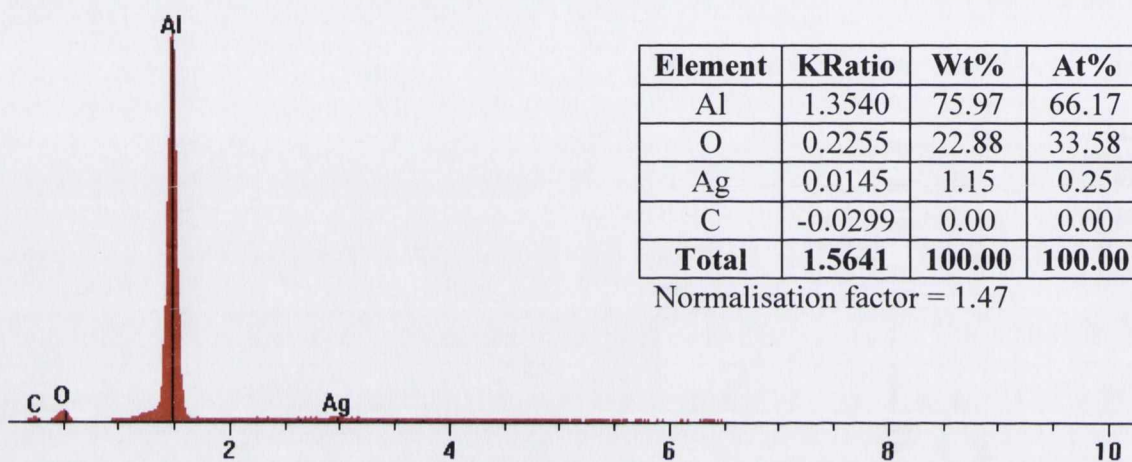


Figure 3.26: EDX Spectrum of a PAM made at 40 V and filled with Ag by AC deposition with analysis table in inset.

■ Analysis\_4\_S001.pgt

FS: 32000

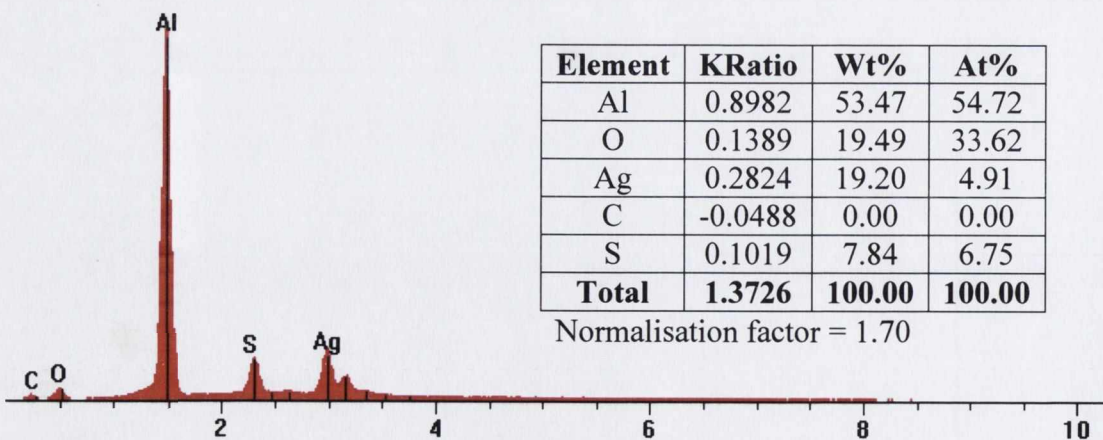


Figure 3.27: EDX Spectrum of a PAM made at 40 V and filled with Ag by PED with analysis table in inset.

This confirms that better filling is obtained by using PED (19.20 Wt % Ag for PED compared to 1.15 Wt% Ag for AC deposition or 1 Ag atom per 11 atoms Al for PED compared to 1 Ag atom for 265 atoms Al for AC deposition). The S peak is due to the  $\text{AgSO}_4$  electrolyte used in the Watts bath.

### **3.2.1.2.6 Summary**

Metal nanowires were fabricated by AC and by pulsed electrodeposition into freshly prepared PAMs. The surface morphology of the PAMs was observed by SEM and AFM to be ridged as in an egg box. EDX confirmed that the PAMs were filled with metals and that more metal was obtained when plating was done by PED. SEM and TEM characterisation also confirmed that better pore filling can be achieved by PED. The dimensions of the nanowires were also investigated by SEM and TEM. There were large variations in diameters but the average diameters for each type of nanowire were in agreement with results obtained by other authors. AFM confirmed that the surface of the nanowires was ridged but the diameters were reasonably homogeneous.

## **3.2.2 Polymer Nanowires**

### **3.2.2.1 Preparation of PANI Nanowires**

Deposition of PANI into PAMs by AC was unsuccessful. This could be because Ag acts as a catalyst for the polymerisation of aniline, which results in simultaneous electrodeposition of Ag and PANI into the nanopores of the PAM. An alternative method for the preparation of PANI using DC was used. The PAMs were prepared at 10 V in  $\text{H}_2\text{SO}_4$  as described in section 3.1.2. The aluminum foil and barrier layer at the back of the sample were removed by a solution of 0.2 M  $\text{CuCl}_2$  in 3 M HCl (for Al) followed by 10% phosphoric acid (for the barrier layer). A gold layer (~ 50 nm) was then thermally evaporated onto the sample back (by an Edwards AUTO 306 E beam evaporator) to act as the working electrode. The apparatus used was the same as for AC deposition (Figure 3.14) except the voltage was applied using a Princeton Applied Research Model 263A Scanning Potentiostat and platinum (Pt) was used as the counter electrode. Electropolymerisation was carried out at constant potential by potentiostatic deposition at 1.0 V for 10 min. The aqueous electrolytic solution contained 25.6 g / L aniline (1 mL aniline in 40 mL  $\text{H}_2\text{O}$ ) to which concentrated  $\text{H}_2\text{SO}_4$  was added until the pH of the solution was 2. The aniline (99.5% Sigma-Aldrich Ltd.) was purified by distillation in vacuum before use. The acid ( $\text{H}_2\text{SO}_4$ ) acts both as an electrolyte and dopant so that the PANI is



produced in the conducting emeraldine salt form. The polymerisation proceeds via a radical cation intermediate form (see chapter 2, section 2.1.2.2.1). The oligomers and polymers formed either dissolve in the electrolyte or are deposited in the PAM; small oligomers (3 monomer units or less) remain in solution and larger oligomers and polymers are deposited [499].

### 3.2.2.2 Characterisation of PANI nanowires

Nanowire morphology was investigated by SEM. The PAM was first treated with NaOH to expose the nanowires. Figure 3.28(a) is a SEM image of PANI nanowires which were prepared as described in section 3.2.2.1. The template was soaked in 1 M NaOH for 15 min to dissolve the alumina. Figure 3.28(b) is a TEM image of PANI nanowires which were extracted from the template as described in section 3.2.1.2.1.

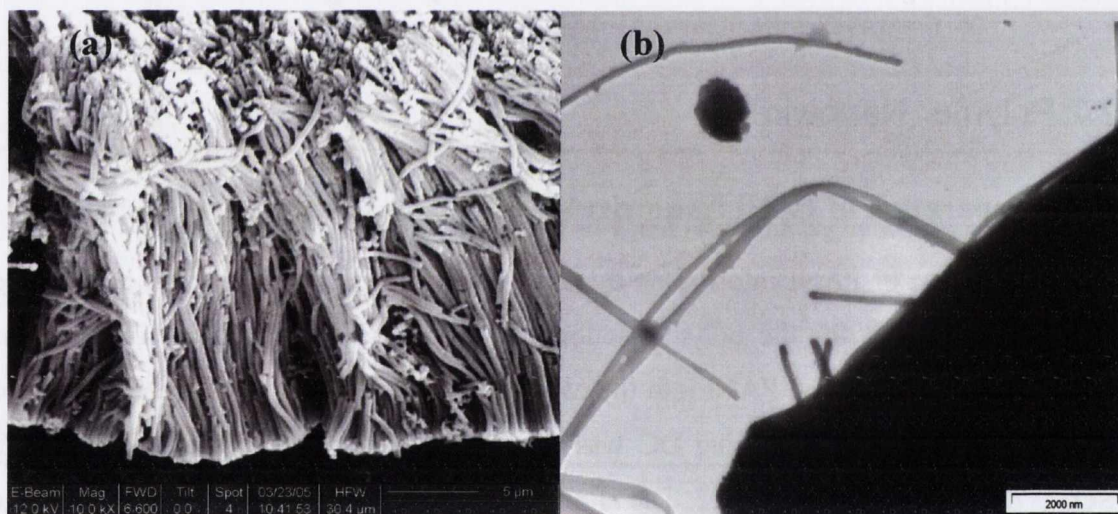


**Figure 3.28: (a) SEM image of PANI nanowires in a PAM made at 10 V and etched with NaOH, (b) TEM image of PANI nanowires extracted from PAM.**

Both SEM and TEM images show that the nanowires are smooth and have a homogeneous diameter. They are not as straight as metallic nanowires and tend to bend when exposed from the PAM.

Raman spectroscopy was used to confirm the presence of PANI. High resolution Raman microprobe spectroscopy has the advantage that a spectrum of the nanowires can be taken without removing them from the alumina matrix. The nanowires show all the characteristic peaks for PANI (see Figure 3.29 and Table 3.5).

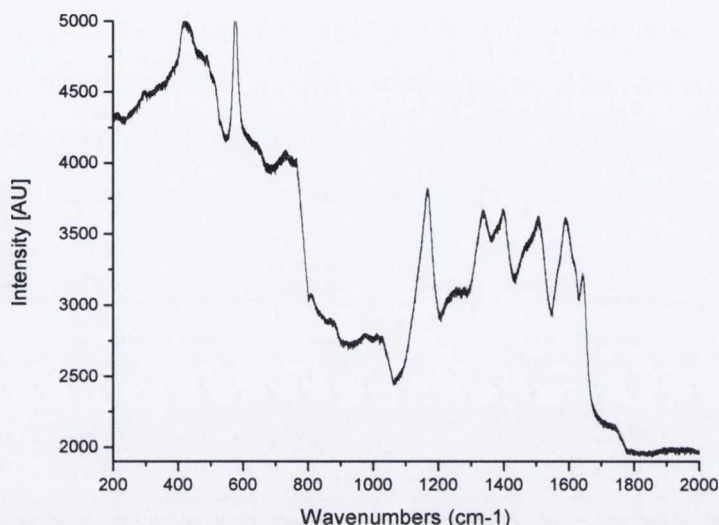


**Figure 3.29: Raman spectrum of a PANI nanowire array in a PAM (excitation  $\lambda = 633$  nm)**

**Table 3.5 Assignments for Raman bands in a PANI sample deposited in a PAM which was made at 10 V.**

Region [ $\text{cm}^{-1}$ ]	Vibration
425	C-N-C torsion and out of plane deformation of benzenoid ring
485, 585	CH out of plane and aniline deformation mode
523, 806	Deformation of benzenoid or quinoid rings
1170	CH bending of benzenoid rings
1335	C-N: stretching of modes of quinoid rings
1480 (sh)	-C=N stretching modes of quinoid rings
1405, 1595	-C-C stretching of benzenoid rings

Slight shifts and broadening occur in the CH out of plane and aniline deformation modes in the  $900 - 500 \text{ cm}^{-1}$  region. This could possibly be due to the weakening of interchain interactions. There is evidence that the nanowires are in the doped state as there is a band due to the C-N: stretching mode at  $1335 \text{ cm}^{-1}$ . The bands for the stretching modes of quinoid rings ( $1484 \text{ cm}^{-1}$ ) are not as strong as those for the benzenoid rings ( $1405 \text{ cm}^{-1}$ ,  $1595 \text{ cm}^{-1}$ ) which suggests the PANI is not fully oxidised.



The UV-vis absorption spectrum of the PANI nanowires array shows a shoulder peak at about 450 nm and a broad band at around 800 nm with a large tail (Figure 3.30). This is typical for doped PANI nanowires [410, 500] and similar to PANI salts which show three transitions 350 nm ( $\pi-\pi^*$  transition of benzenoid rings), 400-420 nm (polaron- $\pi^*$  transition), 750-800 nm ( $\pi$ -polaron transition) (Figure 3.31) [501]. However, in the spectrum for the PANI nanowires the 330 nm peak is absent, which suggests that the nanowires are not fully oxidized but are in the half-oxidised emeraldine base form. The characteristic absorption bands for the pristine undoped EB form of PANI are 320 nm and 600 nm (Figure 3.32) which are absent in this case.

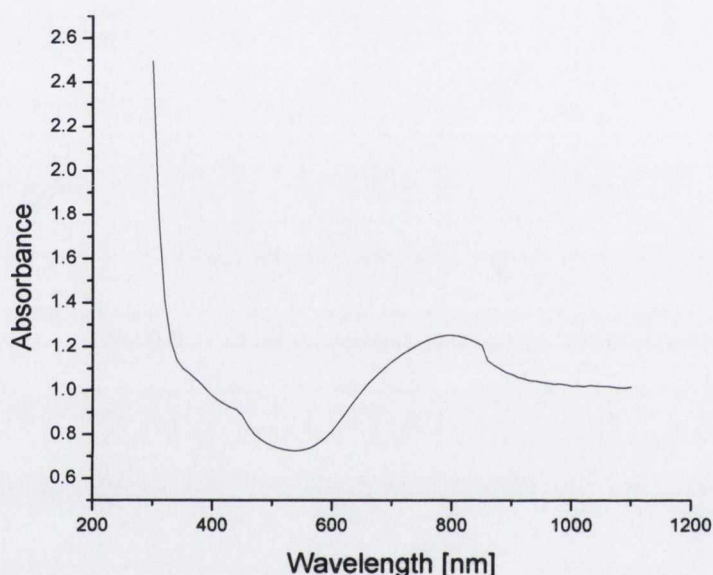


Figure 3.30 UV-vis spectrum of a PANI nanowires array in a PAM made at 10 V.

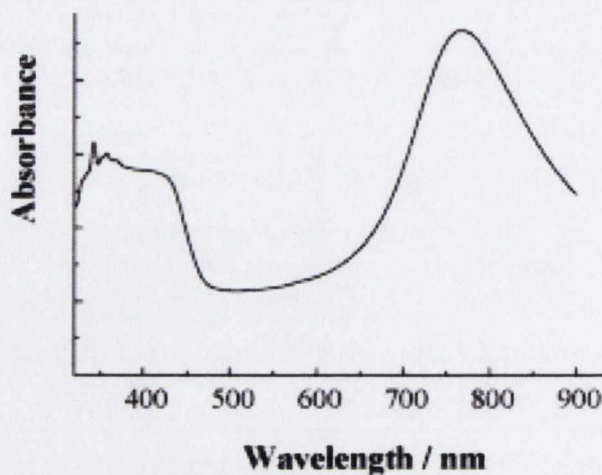


Figure 3.31 UV-vis spectrum of a dispersion of PANI / DBSA salts diluted by deionized water taken from [500].

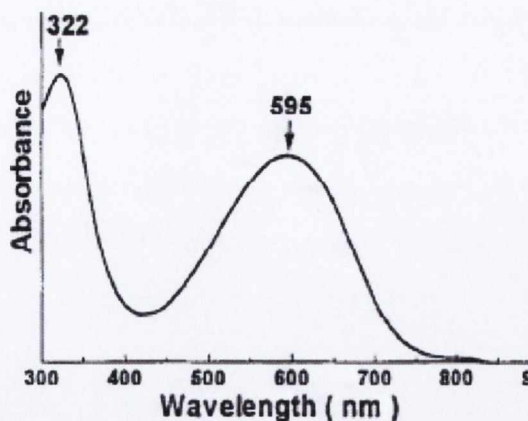


Figure 3.32 UV-vis spectrum of EB prepared PANI in THF taken from [502].

### 3.2.2.3 Summary

PANI nanowires were made by oxidative electropolymerisation of aniline into the nanopores of a PAM which was made at 10 V in  $H_2SO_4$ . This was carried out by potentiostatic deposition at 1.0 V for 10 min. The nanowires were characterized by SEM, TEM, and Raman and UV-vis spectroscopy. They were found to have a similar morphology to metallic nanowires but were less rigid and more homogeneous in diameter. Raman and UV-vis spectroscopy suggests that the nanowires are in the doped half-oxidised emeraldine base form of PANI.

## 3.2.3 Metal / Polymer Nanowires

Ag / PANI and Cu / PANI nanowires were made by simultaneous oxidative polymerization of aniline and reduction of metal from an ionic precursor.

### 3.2.3.1 Preparation of Composite Nanowires

PAMs of several different pore sizes were prepared as described in section 3.1.

Ag / PANI nanowires were deposited into the PAMs (made at 10 V, 15 V, 20 V, 30 V, 40 V, 60 V, 80 V and 140 V) at 9 V AC using an aqueous solution containing 25.6 g / L aniline, 1 g / L  $AgNO_3$ , 41 g / L  $MgSO_4 \cdot 7H_2O$  and enough  $H_2SO_4$  added until the pH of the solution was 2.



Cu / PANI nanowires were deposited into the PAMs (made at 10 V, 15 V, 20 V, 40 V, 60 V and 80 V) at 9 V AC using an aqueous solution containing 25.6 g / L aniline, 35 g / L CuSO<sub>4</sub>, 20 g / L MgSO<sub>4</sub>·7H<sub>2</sub>O and enough H<sub>2</sub>SO<sub>4</sub> added until the pH of the solution was 1.3.

Electrochemical deposition was performed in a cell with the PAM and a graphite rod as the working and counter electrodes respectively in an AC set-up as shown in Figure 3.14.

The lengths of the nanowires can be varied from a few nanometers to tens of microns by changing the deposition time. Here deposition was carried out for 10 minutes in each case.

In order to postulate the mechanism involved in the synthesis of the nanowires it was necessary to characterise the nanowires first.

### 3.2.3.2 Characterisation of Composite nanowires

#### 3.2.3.2.1 SEM, TEM and HRTEM

Nanowire morphology was investigated by SEM. The surfaces of the samples were previously etched with 0.2 M NaOH to expose the nanowires.

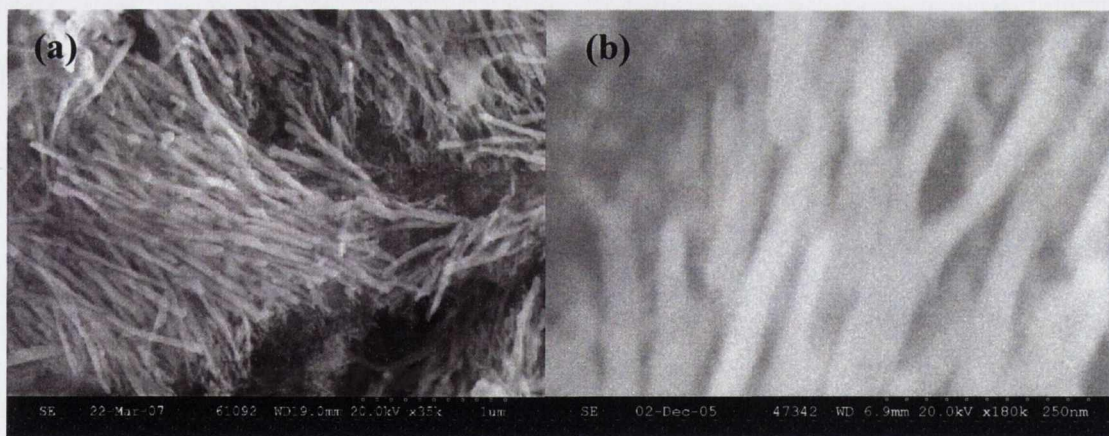
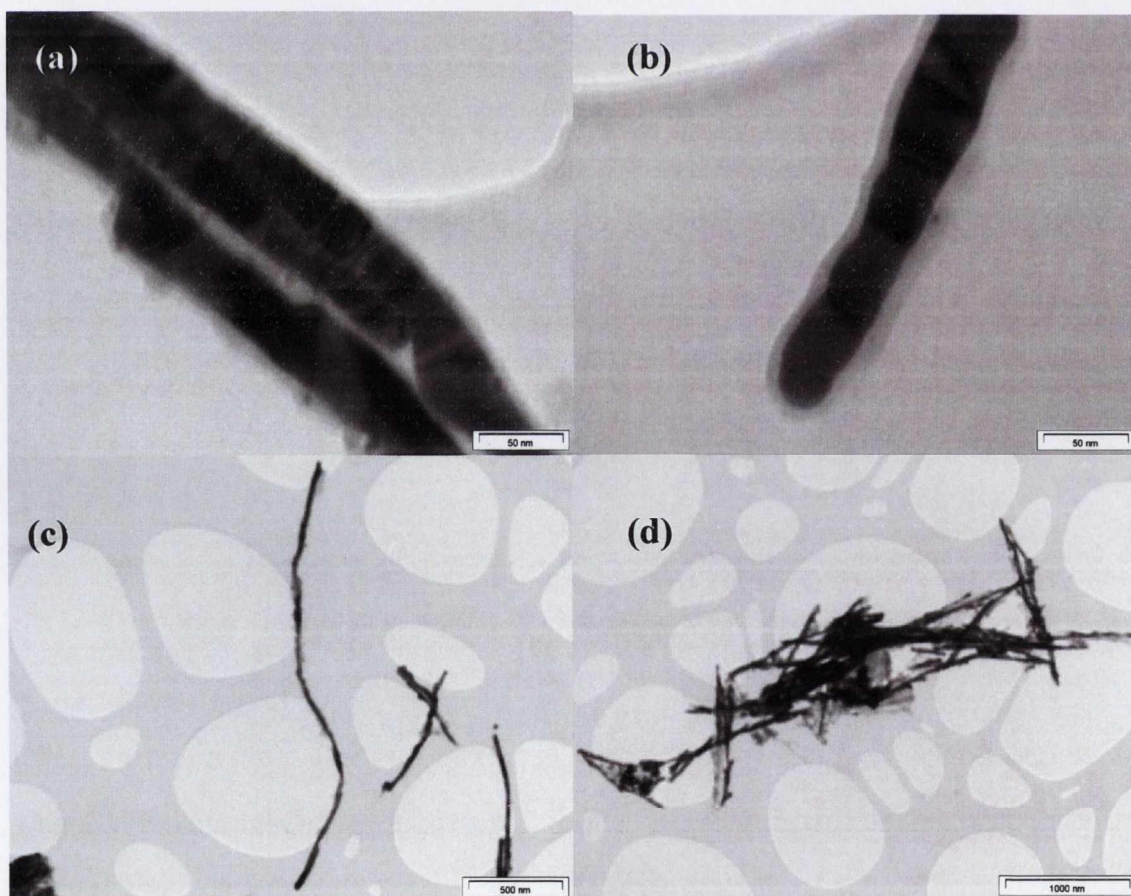


Figure 3.33: SEM images of Ag / PANI nanowires in a PAM made at 60 V (etched with NaOH)

The SEM image {Figure 3.33(a)} shows that the nanowires are fibers, which closely resemble PANI nanowires {Figure 3.28(a)} except they are more rigid and remain parallel to each other even when they are removed from the PAM. Their lengths varied between 1 and 2  $\mu\text{m}$  and the pore filling was approx 80%. Figure 3.33(b) is a magnified

view of some of the nanowires. It shows the branched pores at the end of the wires where the barrier layer of the PAM has been reduced.

TEM images {Figure 3.34(a) and (b)} give a better insight into the structure of the nanowires. They appear to consist of a polycrystalline core (light and dark bands) surrounded by a layer of amorphous material (lighter shading). The different bands are due to the different domains of the nanowire crystals which give rise to different contrasts in the TEM. Figure 3.19(c) and (d) shows a TEM image of pure Ag nanowires. They have a similar structure to the interior of the composite wires with no external shading. Thus the exterior shading in the composite wires is probably due to a coating of PANI and suggests that as the Ag nanowires are formed along the pores of the AAO template they take a coating of polymer with them. It is also apparent that the nanowires remain parallel to each other when they are removed from the PAM. Figure 3.34(c) shows that they can be dispersed as single nanowires but Figure 3.34 (d) illustrates that they tend to aggregate in the same way as Ag nanowires when extracted from the template {compare to Figure 3.19(c) of Ag nanowires}.



**Figure 3.34: TEM images of Ag / PANI nanowires extracted from a PAM which was made at 30 V**



HRTEM supports these findings {Figure 3.35(a) and (b)}. In these images the shading is seen as a white halo of amorphous carbon around the Ag core, whereas in Figure 3.35 (c) and (d) (Ag nanowires) there is no halo. For the composite nanowires the halo was always present on going through a set of 20 images in a focal series (1nm step), thus showing that it is not an artifact due to focal inconsistencies.

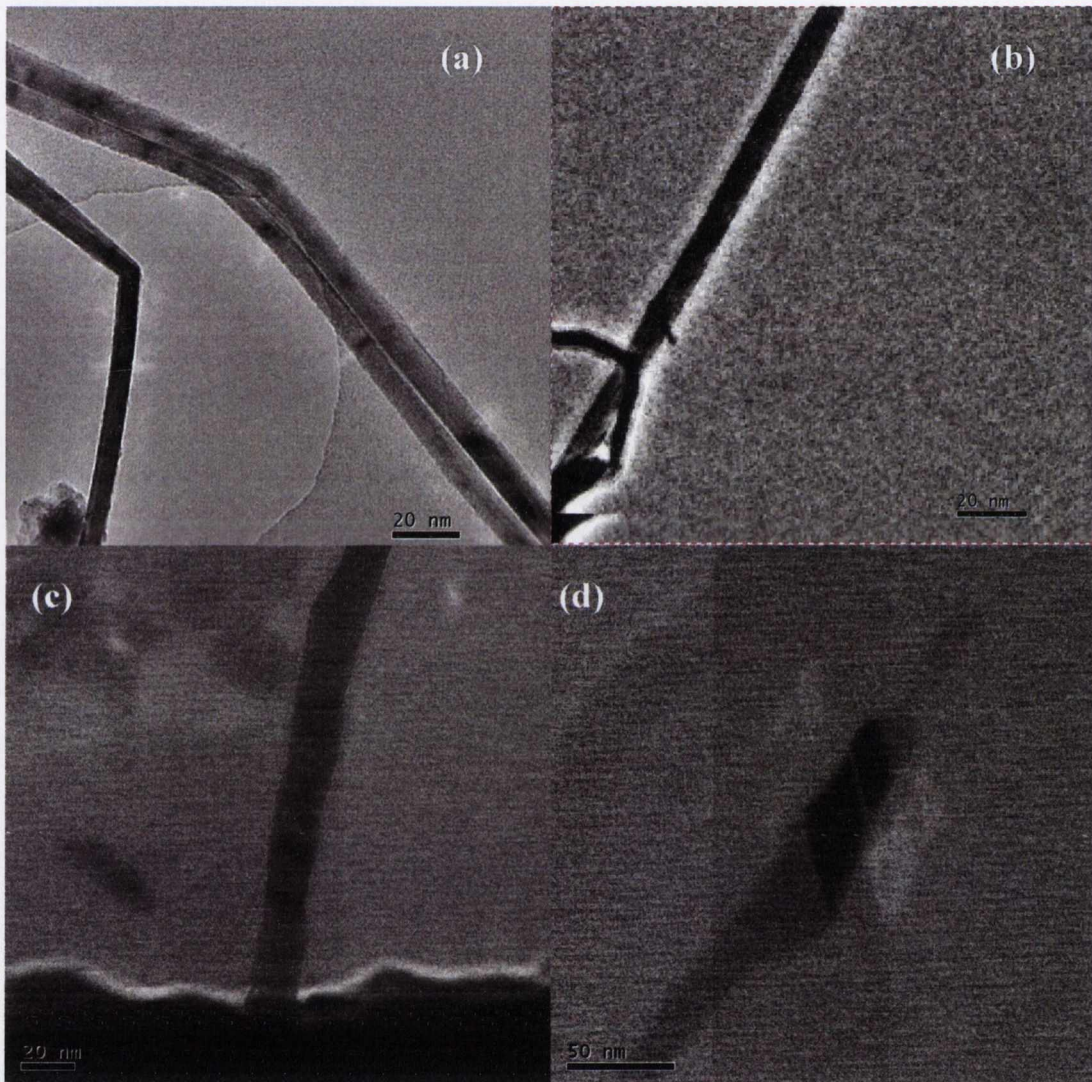


**Figure 3.35: HRTEM images of Ag nanowires from a PAM made at 20 V**

Figure 3.36 and Figure 3.37 show single composite nanowires of different sizes. The corresponding diffraction patterns are shown in the insets. Figure 3.36(b) is a selected area diffraction pattern made on the 15 nm diameter nanowire. This shows the highly crystalline nature of the core where all the Ag crystal planes are allocated. Figure 3.37 is of a 40 nm diameter nanowire which is taken at a lower magnification so the entire nanowire and halo is included in the diffraction pattern {Figure 3.37(b)}. As well as the



diffraction spots due to silver it also shows a bright ring which is indicative of amorphous carbon due to the PANI coating.

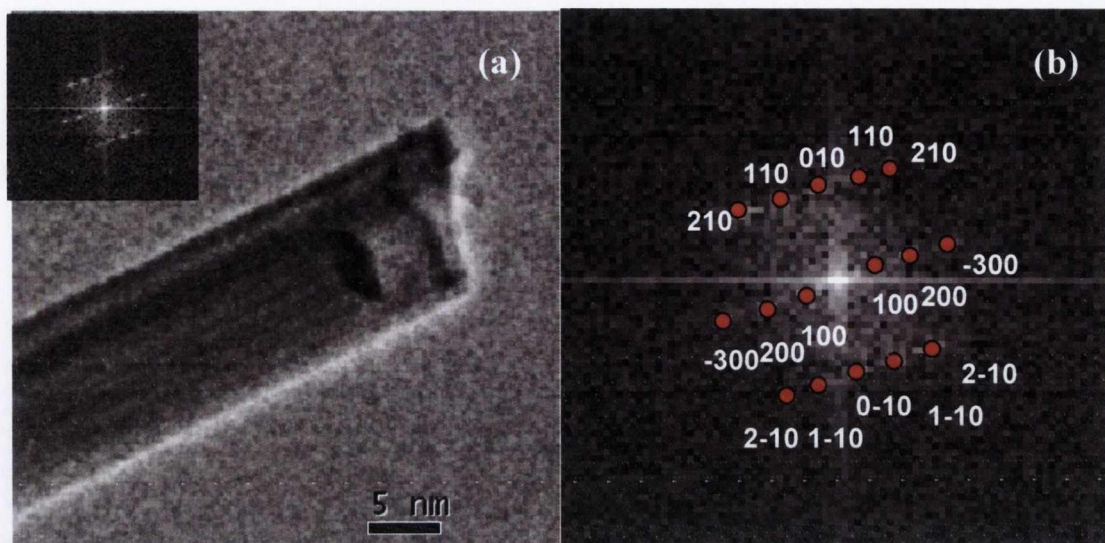


**Figure 3.36: HRTEM image of Ag / PANI nanowires from a PAM made at 20 V, with corresponding diffraction pattern in inset and (b)**

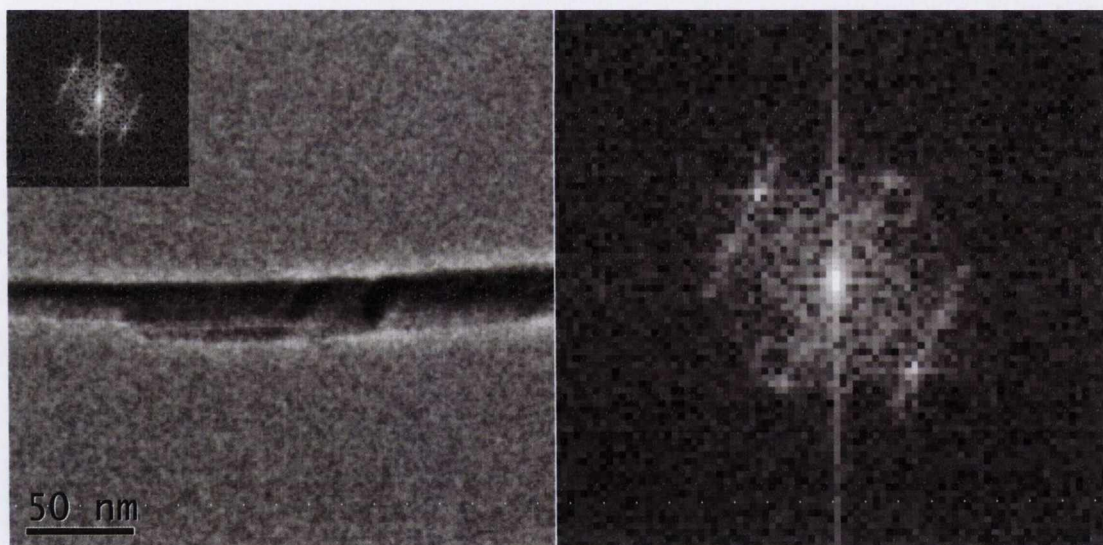


**Figure 3.37: HRTEM image of Ag / PANI nanowires from a PAM made at 40 V, with corresponding diffraction pattern (b)**

### 3.2.3.2.2 EDX and XRD

The presence of metal was confirmed by EDX.



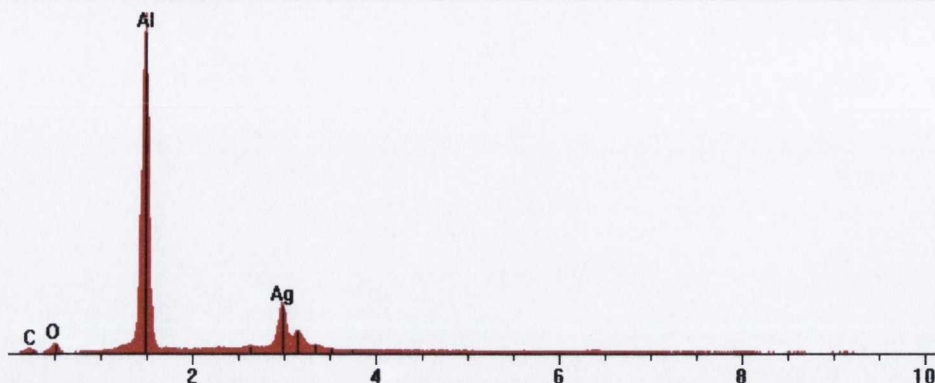


Figure 3.38: EDX of composite sample (PAM made at 40V with Ag / PANI deposited at 9V for 20 min)

The crystalline nature of the nanowires was confirmed by XRD analysis. An X-ray diffraction pattern of an Ag / PANI composite nanowire array is shown in Figure 3.39(a). A broad peak centred at  $2\theta = 25^\circ$  is observed and can be ascribed to weak ordering parallel to the polymer chain. Sharp peaks centred at  $2\theta = 38^\circ$ ,  $45^\circ$ ,  $66^\circ$  and  $77^\circ$  are also observed corresponding to (111), (200), (220) and (311) silver planes respectively. All the peaks can be indexed to face centered cubic silver belonging to space group  $Fm\bar{3}m \{225\}$ . The silver is preferentially oriented along the (111) plane. Crystallite sizes can be calculated from Scherrer's equation:

$$D = k\lambda / \beta \cos \theta \quad (3.1)$$

- where  $\lambda$  is the X-ray wavelength (0.1540nm)
- $k$  is the shape factor = 0.89
- $D$  is the average diameter of the crystals (in angstrom units)
- $\theta$  is the Bragg angle (in degrees)
- $\beta$  is the broadening measured at half height and expressed in units of  $2\theta$ .

Substituting the value for  $2\theta = 77^\circ$  gives  $D = 10$  nm, which agrees well with the TEM results.

Figure 3.39(b) shows the X-ray diffraction pattern of pure silver nanowires in AAO where the same peaks corresponding to (111), (200), (220) and (311) silver planes are clearly seen. This pattern is very close to the reported data for metallic silver (JCPDS File no. 04-0783) from the International Centre for Diffraction Data.

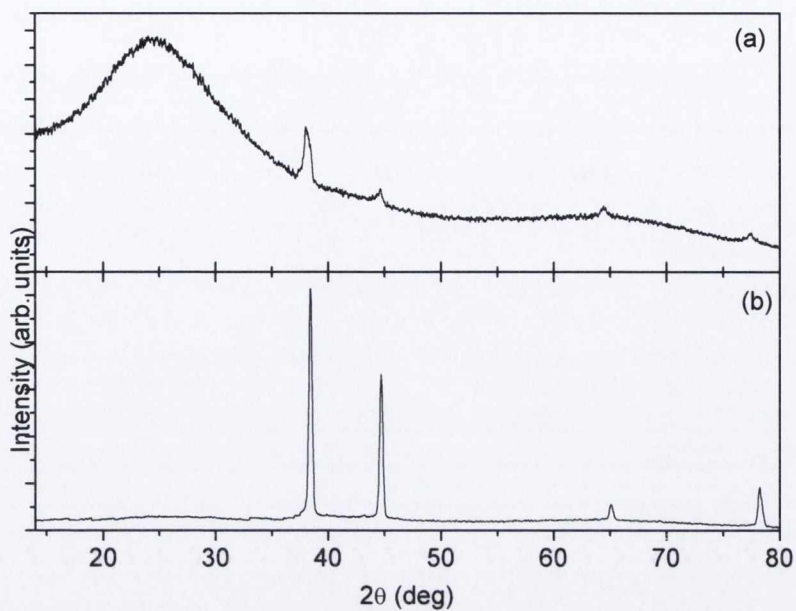


Figure 3.39: XRD of the Ag / PANI composite array (a) compared to Ag nanowire array (b)

XRD also confirms the presence of Cu in the CU / PANI nanowire array, shown in Figure 3.40(a). The PANI peak is not as broad in this case indicating that less polymer is present.

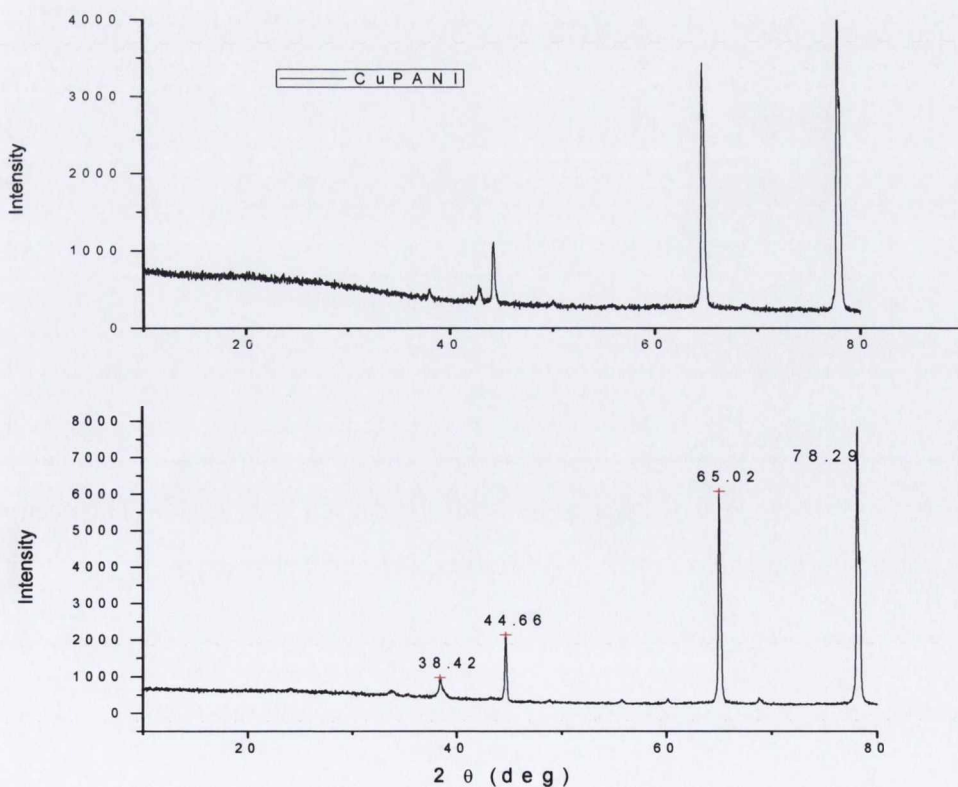
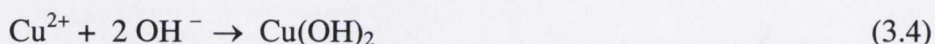


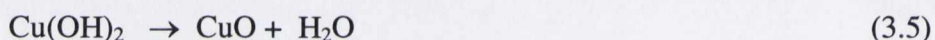
Figure 3.40: XRD of the Cu / PANI composite array (a) compared to a Cu nanowire array (b)



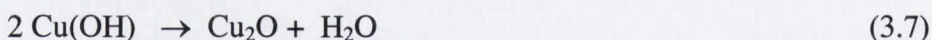
Sharp peaks centred at  $2\theta = 44.60^\circ$ ,  $65.02^\circ$  and  $78.29^\circ$  are observed corresponding to the (111) Cu plane (JCPDS File no. 04-0386), the (310) CuO plane (JCPDS File no. 05-0661) and the (400) Cu<sub>2</sub>O plane (JCPDS File no. 05-0667). There is also a small peak at  $2\theta = 38.42^\circ$  which can be attributed to the (111) CuO plane. Thus some copper oxides are formed in the copper nanowires. This is due to the reaction of Cu<sup>2+</sup> ions with OH<sup>-</sup> (reactions 3.4 – 3.7) ions which are produced during electrodeposition due to the evolution of hydrogen (3.2) at the cathode and subsequent decomposition of water (3.3) [321].



The copper hydroxide is dehydrated to produce the more stable copper oxide:



Cu<sub>2</sub>O can also be generated at the cathode surface by the following reactions [321]:



### 3.2.3.2.3 Raman Spectroscopy

Raman spectroscopy was used to confirm the presence of PANI. The composites show all the characteristic peaks for PANI (Figure 3.41 and Table 3.6).

**Table 3.6 Assignments for Raman bands in a Ag / PANI composite sample in a PAM made at 20 V**

Region [ $\text{cm}^{-1}$ ]	Vibration
415	C-N-C torsion and out of plane deformation of benzenoid ring
480, 580	CH out of plane and aniline deformation mode
523, 615, 806	Deformation of benzenoid or quinoid rings
1165	CH bending of benzenoid rings
1340	C-N: stretching of modes of quinoid rings
1475	-C=N stretching modes of quinoid ring
1410, 1595	-C-C stretching of benzenoid rings

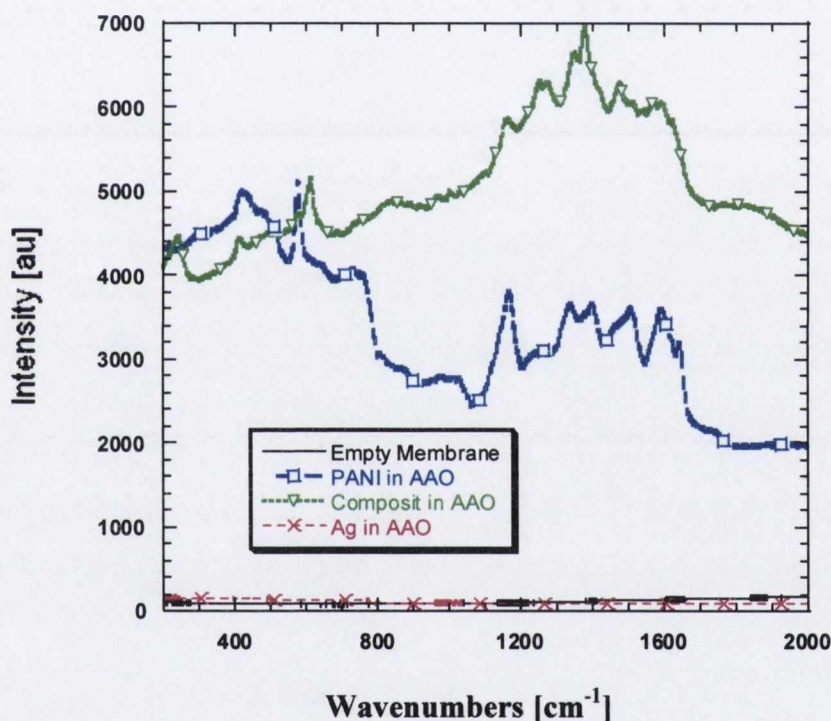


**Figure 3.41: Raman spectra of a composite nanowire array in a PAM made at 15 V, a PANI array in a PAM made at 10 V, a silver nanowire array in a PAM made at 20 V and an empty PAM (excitation  $\lambda = 633 \text{ nm}$ )**

However there are some subtle differences between these spectra and those of electrochemically-produced PANI nanowires, which give us an insight into the oxidation state of PANI in the composite. For example the intensity of the bands at  $415 \text{ cm}^{-1}$ ,  $480 \text{ cm}^{-1}$  and  $580 \text{ cm}^{-1}$  is reduced in the composite sample and the bands between  $415 \text{ cm}^{-1}$  and  $806 \text{ cm}^{-1}$  also show slight shifts and broadening in the composite. This is indicative of



the weakening of inter-chain interactions [503]. Spectral changes between  $1100\text{ cm}^{-1}$  and  $1700\text{ cm}^{-1}$  are characteristic for changes in oxidation state. The band due to the C-H bending of benzenoid-like aromatic rings in PANI is decreased to  $1165\text{ cm}^{-1}$  in the composites due to progressive oxidation of the polymer and the formation of quinoid like rings [504]. This band is also present in the PANI sample at  $1170\text{ cm}^{-1}$  and has a strong intensity, probably due to the presence of the sulphate group [505]. Bands in the region  $1250\text{-}1300\text{ cm}^{-1}$  are stronger in the composite and can be assigned to C-N stretching of the secondary aromatic amine indicative of the emeraldine salt phase of PANI [503]. Bands in the  $1300\text{-}1400\text{ cm}^{-1}$  region are due to stretching vibrations of C-N+ fragments having an intermediate single-to-double bond order and coupled to an aromatic ring [506]. The appearance of one or two bands in this range depends on whether the polymer is in the fully reduced, oxidised or the half-oxidised emeraldine form. These results show that the PANI sample has two bands at  $1335\text{ cm}^{-1}$  and  $1405\text{ cm}^{-1}$  typical of the emeraldine salt form, these two bands are also present in the composites (at  $1350\text{ cm}^{-1}$  and  $1380\text{ cm}^{-1}$ ) indicating that although it is also in the emeraldine salt state it is not identical to the PANI sample. Ring sulphonation also affects the polaronic C-N+ vibration bands in this region [505, 507]. There are also some slight differences in the higher frequency regions. These bands are due to the stretching modes of the benzenoid and quinoid rings. The band located at  $1475\text{ cm}^{-1}$  in the composite wires corresponds to the stretch vibrations of the C=N double bond, highly coupled to the quinoid ring [508]. This appears as a shoulder in the PANI sample and the band at  $1595\text{ cm}^{-1}$  due to C-C stretching of the benzenoid like rings is stronger in the PANI sample indicating that it is less oxidised than the composite. Finally the Raman scattering signal is enhanced in the composite samples due to surface-enhanced Raman scattering (SERS) of the Ag particles, which also confirms the presence of Ag in the composites.

Figure 3.42 shows Raman spectra for a range of nanowires diameters (the diameter is approximately equal to the voltage used to make the PAMs in which they are deposited). It is clear that there is no relationship between the intensity of the spectra and the nanowires' diameter. There also appears to be no shift in peak position with diameter.

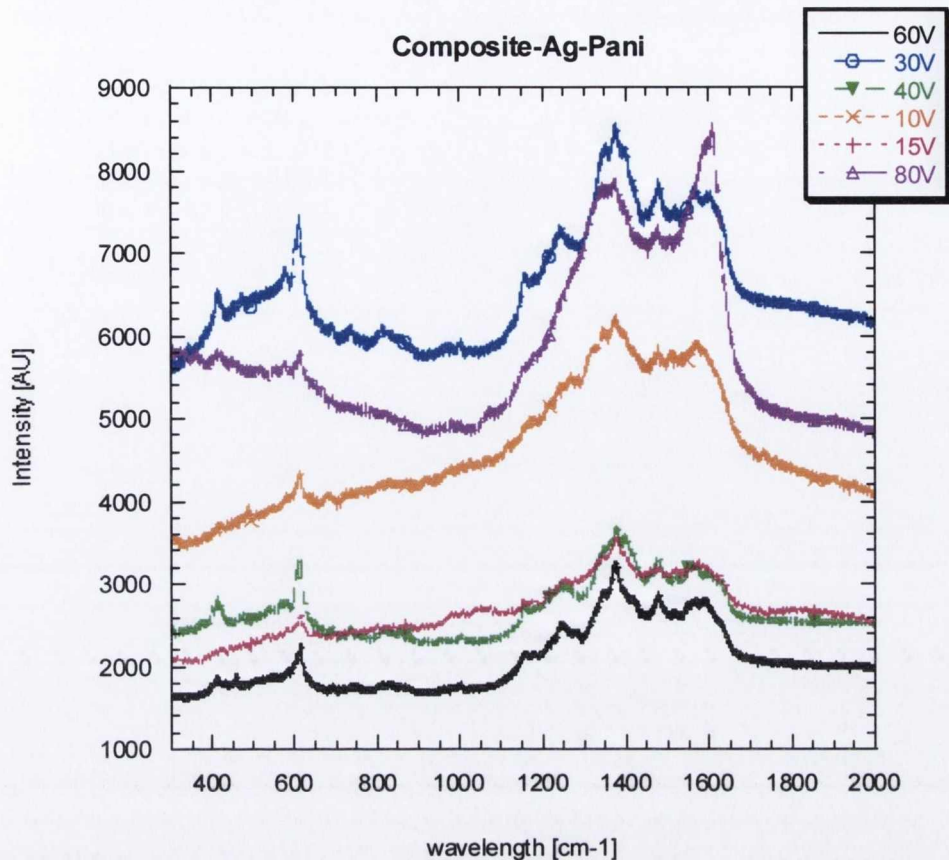


**Figure 3.42: Raman spectra of Ag/PANI composite nanowire arrays in PAMs made at 10 V, 15 V, 30 V, 40 V, 60 V and 80 V (excitation  $\lambda = 633$  nm)**

The results for Cu / PANI composites were similar. Figure 3.43 shows Raman spectra for Cu / PANI composites in a range of PAMs and Table 3.7 gives the assignments for the Raman bands in a Cu / PANI composite deposited in a PAM made at 7 V.

**Table 3.7 Assignments for Raman bands in a Cu/PANI composite in a 7V PAM**

Region [cm <sup>-1</sup> ]	Vibration
420	C-N-C torsion and out of plane deformation of benzenoid rings
525, 605, 820	Deformation of benzenoid or quinoid rings
1165	CH bending of benzenoid rings
1375	C-N: stretching of modes of quinoid rings
1470	-C=N stretching modes of quinoid rings
1590	-C-C stretching of benzenoid rings



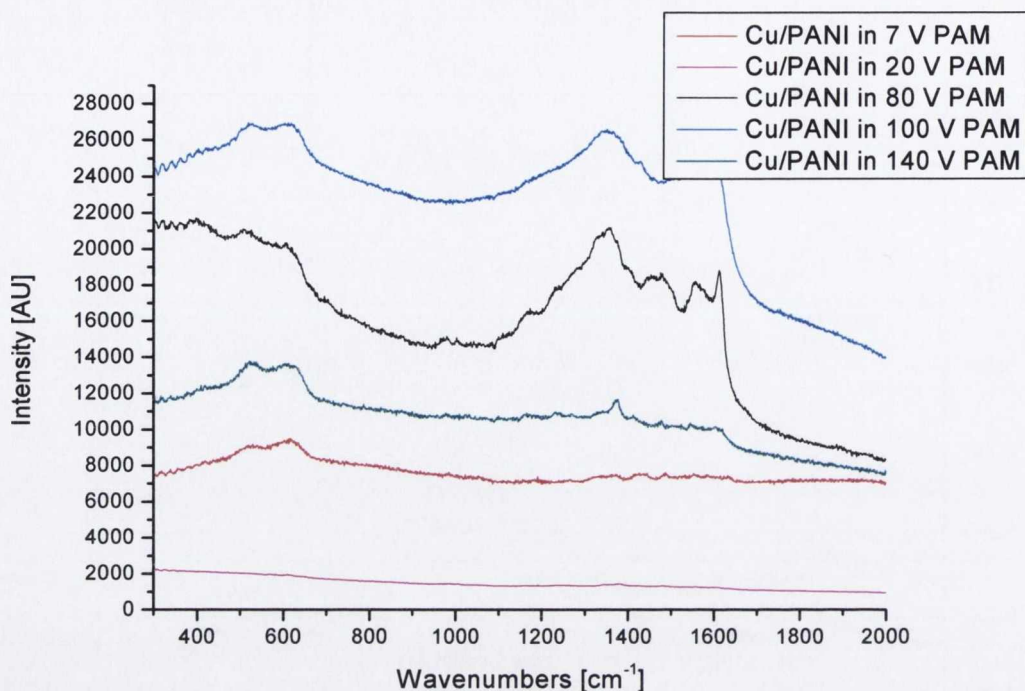


**Figure 3.43: Raman spectra of Cu / PANI composite nanowire arrays in PAMs made at 7 V, 20 V, 80 V, 100 V and 140 V (excitation  $\lambda = 633$  nm)**

From these spectra it is clear that the Raman intensity does not depend on the diameter of the nanowires (which is directly related to the voltage the PAM is made at) as the composite was deposited for the same amount of time (3 min) in each case.

### 3.2.3.2.4 FTIR Spectroscopy

Infrared spectroscopy can be used to study the oxidation state of PANI. Composite nanowires were extracted from the alumina template for FTIR analysis. As this involves treatment with sodium hydroxide (NaOH) the sulphuric acid ( $H_2SO_4$ ) doped PANI will be changed to its undoped form. This is reflected in the IR spectrum. A comparison of the spectra of these composite wires and that of a film of PANI made with  $H_2SO_4$  in the electrolyte can give us some insight into the doping effect of the  $H_2SO_4$  and the interaction of Ag with PANI.

The nanowire composites showed all the characteristic peaks for PANI {Figure 3.44(a) and Table 3.8}. The FTIR of a PANI film (the synthesis is described in chapter 4, section 4.1.1) was taken for comparison {Figure 3.44(b) below}.

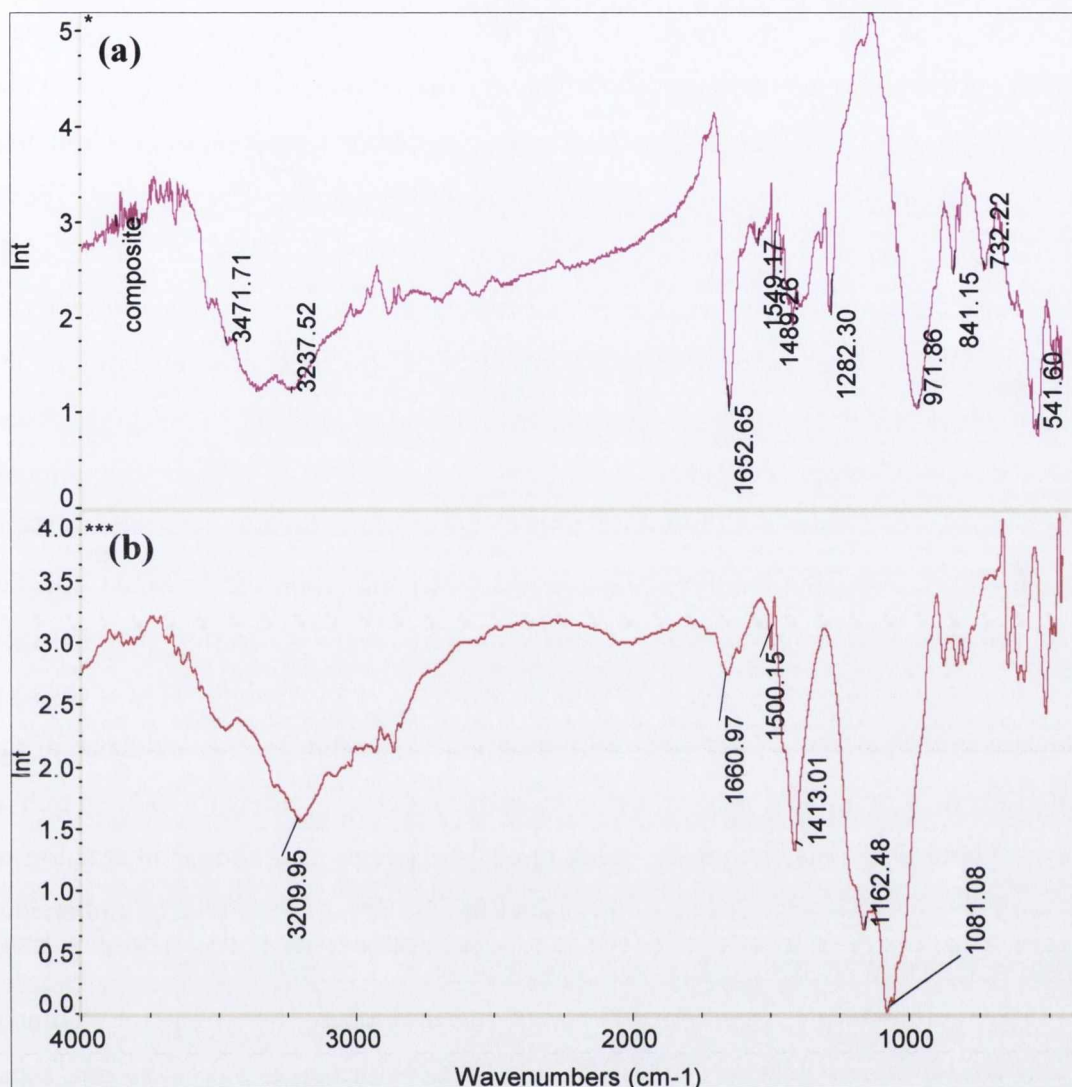


Figure 3.44: FTIR of composite wires extracted from PAM made at 40 V (a) and PANI film (b)

Table 3.8 Assignments for FTIR bands in a composite sample extracted from a PAM made at 40 V

Region [cm <sup>-1</sup> ]	Assignment
3471	Non-hydrogen-bonded N-H stretching vibration
3237	Hydrogen-bonded N-H stretching vibration
1653	C=N vibrational modes
1549	C=N and C=C stretching deformation from quinoid rings
1489	C=C stretching deformation from benzenoid rings
1282	C-N stretching of secondary aromatic amine



The intensity of the free N-H bond stretching ( $3357\text{ cm}^{-1}$ ) increases while that of the hydrogen bonded N-H stretching ( $3237\text{ cm}^{-1}$ ) decreases in the composite indicating a weakening of the hydrogen bonding between amine and imine groups. This could be due to the protonation of PANI due to the acid dopant followed by formation of co-ordination bonds between the silver metal ions and polymer nitrogen atoms. The spectrum shows many vibrational modes due to C-N (e.g.  $1653\text{ cm}^{-1}$ ,  $1549\text{ cm}^{-1}$ ,  $1489\text{ cm}^{-1}$ ,  $1282\text{ cm}^{-1}$ ) this is because the polymer contains both amine and imine units so each ring will give rise to a different vibrational mode [508]. The absence of the band at  $1189\text{ cm}^{-1}$  in the composite wires, which is due to protonated chain vibrations, is notable [509]. This band is characteristic of protonated chain vibrations  $Q=\text{NH}^+-\text{B}$  or  $\text{B}-\text{NH}^+-\text{B}$  (Q=quinoid, B=benzenoid units of polymer) [509, 510, 511] which can hydrogen bond to the -NH- or =N- groups in PANI. This bonding is weakened when the Ag is incorporated into the polymer matrix (as  $\text{Ag}^+$  is reduced to  $\text{Ag}^0$  and the -NH- groups of the polymer chain are oxidised to =N=). FTIR analysis of PANI fibrils made by Wang et al. [181] also shows a stretching vibration mode at  $1124\text{ cm}^{-1}$  similar to the PANI film. Further evidence of the two different C-N bond link ways in the composites is the presence of a C-N stretch at  $1285\text{ cm}^{-1}$  [181]. Previous studies by Hasik et al. [417] show that similar interaction of PANI with Pd compounds leads to the reduction of  $\text{Pd}^+$  to  $\text{Pd}^0$  with simultaneous oxidation of the polymer chain.

Doping transforms a certain amount of the aminobenzene group into quinoid moiety in the polymer. Characteristic bands associated with benzenoid ( $1489\text{ cm}^{-1}$ ) and quinoid ( $1549\text{ cm}^{-1}$ ) phenyl rings can be used to estimate the oxidation state of the polymer by integrating these IR bands [512]. However in the composite wires the quinoid bands are very small and masked by the large C=N vibrational modes at  $1653\text{ cm}^{-1}$ . It has been reported that in doped PANI many of the key bands corresponding to the aromatic rings are shifted to lower frequencies [513]. In fact many of the bands in the PANI sample are red shifted compared to the composite wires because of the acid dopant (e.g.  $3237\text{ cm}^{-1} > 3187\text{ cm}^{-1}$ ,  $2873\text{ cm}^{-1} > 2857\text{ cm}^{-1}$ ,  $1653\text{ cm}^{-1} > 1641\text{ cm}^{-1}$ ,  $1488\text{ cm}^{-1} > 1487\text{ cm}^{-1}$ ,  $1418\text{ cm}^{-1} > 1414\text{ cm}^{-1}$ ). There are also some extra bands due to the absorption of  $-\text{SO}_3\text{H}$  groups (e.g.  $1162\text{ cm}^{-1}$  and  $1081\text{ cm}^{-1}$ ) [500, 501, 514, 515].

There is a difference in the position of the CH out-of-plane bands. These occur at  $837\text{ cm}^{-1}$ ,  $724\text{ cm}^{-1}$ ,  $609\text{ cm}^{-1}$ ,  $536\text{ cm}^{-1}$  in the composite and  $862\text{ cm}^{-1}$ ,  $790\text{ cm}^{-1}$ ,  $728\text{ cm}^{-1}$ ,  $647\text{ cm}^{-1}$ ,  $572\text{ cm}^{-1}$ ,  $543\text{ cm}^{-1}$  in PANI.

### 3.2.3.2.5 UV-Vis Absorption Spectroscopy

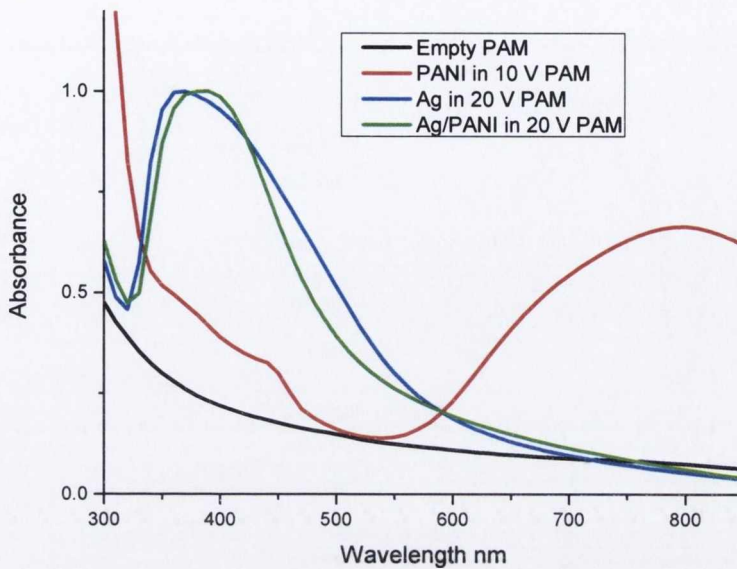


**Figure 3.45:** UV vis of a composite nanowire array in a PAM made at 20 V compared to an Ag nanowire array in a PAM made at 20 V and a PANI nanowire array in a 10 V PAM.

A UV-vis spectrum of the composite nanowires array was taken and compared to that of a PANI array and an Ag nanowire array in PAMs. Ag nanowires show a maximum absorption peak at 382 nm corresponding to a surface plasmon resonance due to the transverse oscillation of electrons along the nanowires [516]. This overlaps with the absorption band of polyaniline so it is difficult to differentiate them [410]. Khanna et al. observed that the bands at 400-420 nm due to the benzenoid rings of the PANI are overlapped and red shifted due to the presence of nanosilver [430]. These results for the composite nanowires are similar. Figure 3.45 shows that the absorption of the composite wires in AAO matches that of the Ag wires but the position of the absorption maximum is red-shifted indicating that the wires have a different electronic environment than the non-coated wires. The absorption band at 630 nm corresponding to the EB form of PANI is absent in the composite indicating that it is in the conducting ES form. The broad band centered at 835 nm is also missing because of the delocalization of electrons in the polaron band as the compact coil structure of the polymer transforms into an expanded coil structure [517]. In these composites the absorption is almost totally dominated by silver; this is supported by the TEM images which show a large Ag core and a thin PANI coating.

The  $\lambda_{\max}$  of the composite wires was found to be dependant on their diameter.



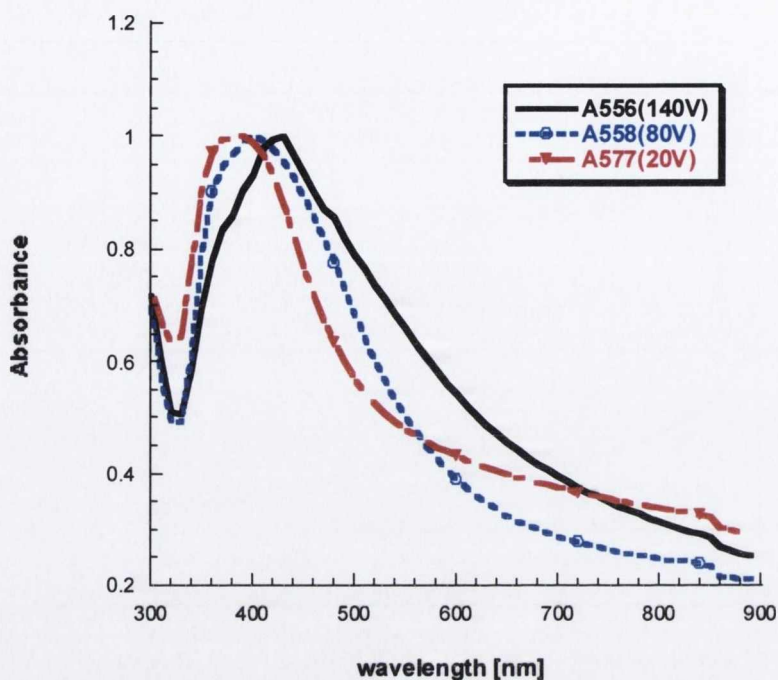


Figure 3.46: UV-vis of composite samples in PAMs made at 20V, 80V and 140V

Figure 3.46 illustrates that  $\lambda_{\text{max}}$  is shifted to higher wavelengths and the width of the absorption peak increases with increasing wire diameters. This is similar to studies done on Ag nanowires [518] and is probably due to the broad plasmon resonance that is red shifted with increasing wire diameter due to the increasing importance of multipole excitations.

### 3.2.3.3 Summary and Proposed Formation Mechanism of Composite Nanowire Synthesis

The synthesis of Ag/PANI nanowires was achieved by simultaneous electrodeposition of Ag and PANI into the nanopores of an alumina template. This was done by oxidative polymerisation of aniline and reduction of silver nitrate to silver nanowires. Deposition of PANI without Ag into these templates by the same method was unsuccessful which implies that Ag is acting as a catalyst for the polymerisation of aniline in such cases. SEM shows the fibrous nature of the composite nanowires and TEM shows they resemble Ag nanowires. HRTEM indicates that they consist of a metal core surrounded by polymer coating i.e. a nanocable. Such structures are usually made by

template processing or layer deposition [425 and references therein]. The formation mechanism of these Ag / PANI nanocables is probably similar to that of Huang et al. [419] for the synthesis of Au / Ppy nanowires and Kinyanjui et al. [420] for the electrochemical synthesis of Pt / PANI composites. Sulfuric acid acts as a dopant and Ag as a catalyst in the polymerization process. The aniline is first protonated by H<sub>2</sub>SO<sub>4</sub> to form a protonated anilinium cation. The Ag anion then acts as an electron acceptor and is reduced to Ag<sup>0</sup> while oxidative polymerization of aniline occurs. In acidic media the PNB form of PANI is reduced back to ES thus enabling further reduction of Ag<sup>+</sup> to Ag<sup>0</sup> [519]. The Ag particles act as nucleation sites for the oxidative formation of PANI which surrounds the metal core. Diffusion of the composite into the membrane then occurs as the neutrality of the system is restored. Thus the growth process of the silver nanowires and the polymerization of the polymer sheath continue simultaneously. This is similar to the process which occurs during the photochemical synthesis of PANI [430, 520].

XRD, Raman and FTIR spectroscopy were used to characterise the structure and chemical composition of the wires. Raman evidence indicated a change in the oxidation state of the PANI in the composite (formation of quinoid rings and increased C-N stretching). The evidence from FTIR indicates that there is some interaction between Ag and the nitrogen head groups of the PANI (differences in the N-H bands due to hydrogen bonding, weakening of the protonated chain vibrations and a shift in the semi-quinoid C-N stretch in the composite). UV-vis spectroscopy also supports the proposed formation mechanism of the nanocables. If the Ag was dispersed as clusters within the PANI, the surface plasmon resonance of Ag would be missing [521, 522]. The peak at 400 nm indicates that elemental silver is formed at the same time as PANI. As the aniline polymerizes it is trapped by the Ag nucleus which forms at the base of the pore. The Ag / PANI nanowires then grow along the pores of the AAO template to the surface because of the trapping effect of the template [523]. TEM shows that the composite consists of a metal core and polymer coating. Many studies give evidence of the directional aggregation of clusters of particles leading to the directional growth of nanowires [523, 524, 525, 526, 527, 528]. This is the first time composite nanowires were fabricated in a one pot method inside an alumina template. This has many advantages as the nanocables can be used as an array inside the template or extracted and used in other systems.



### 3.2.4 Semiconductor Nanowires

CdS nanowires were deposited into PAMS by AC electrodeposition (see chapter 2, section 2.1.2.4) following the methods of Routkevitch et al. [187, 251] and Suh and Lee [529]. The mechanism involves two steps; electrodeposition of solvated  $\text{Cd}^{2+}$  ions followed by sulphidation with dissolved sulphur.

$\text{Cd}^{2+}$  ions enter the pores as an electric field is applied between the Al and graphite electrodes to form elemental cadmium:



This combines with elemental sulphur which has entered the pores by diffusion to form CdS:



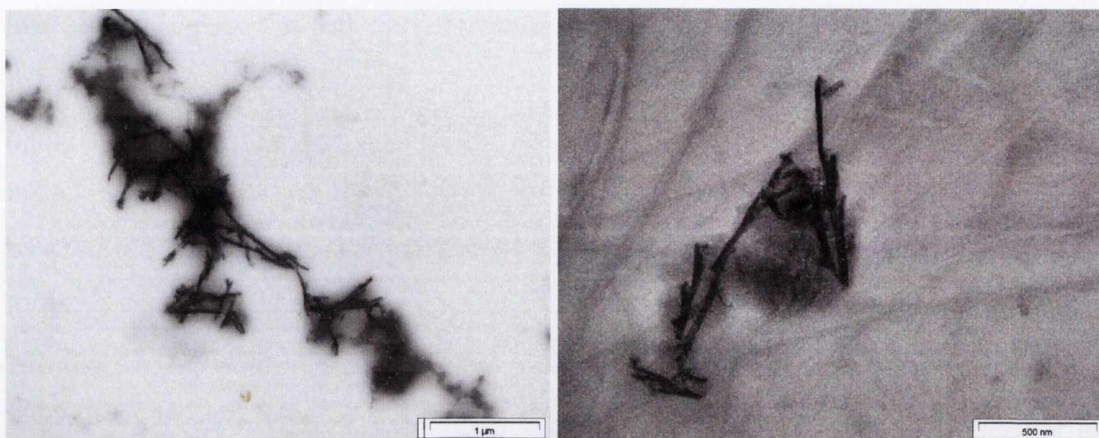
#### 3.2.4.1 Preparation of CdS nanowires

PAMs of several different pore sizes were prepared as described in section 3.1. CdS nanowires were deposited into the PAMs (made at 10 V, 20 V, 40 V, 60 V, 80 V, 100 V and 140 V) using an electrolyte containing 0.055 M  $\text{CdCl}_2$  and 0.19 M elemental sulphur (S) in dimethyl sulfoxide (DMSO), at 100 – 130°C and 25 - 30 V (60 Hz) for 5-60 min. The electrochemical cell was placed in an oil bath and the temperature was maintained by means of a Heidolph temperature controller. Immediately after fabrication the samples were washed in warm DMSO, acetone and deionised water and dried in air. Many of the surfaces of the samples were pitted due to side reactions such as re-anodisation, dissolution and corrosion of aluminium [530]. This problem was solved by making sure the empty PAMs were thoroughly washed in deionised water (to ensure no trace of acid was left) and dried in a vacuum oven before deposition. It was found that the best deposition occurred at 110°C and 30 V. The deposition time depended on the pore diameter and barrier layer thickness. For PAMS made at voltages greater than 20 V the voltage was reduced to 18 V.

#### 3.2.4.2 Characterisation of CdS nanowires

Figure 3.47 shows TEM images of the CdS nanowires which were electrodeposited (30 V, 100°C, 60 min) into a PAM made at 40 V. It can be seen that the

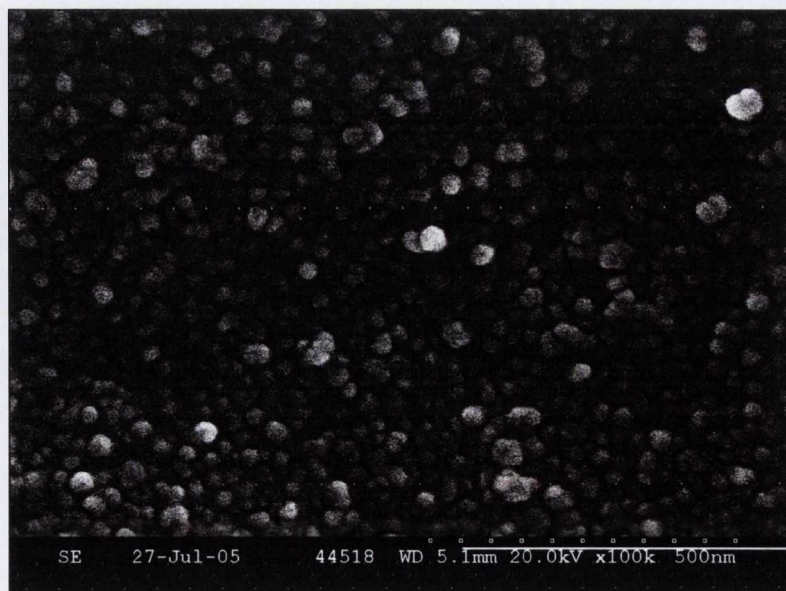
lengths of the nanowires are not uniform and that the structure contains many small branches. This could be due to inhomogeneous filling of the PAM or to the attachment of some small CdS nanoparticles as seen by Wu et al. [455].



**Figure 3.47: TEM images of CdS nanowires liberated from a PAM made at 40 V**

Using the UTHSCSA image tool program the diameters of the nanowires were found to range between 23 and 34 nm with an average diameter of  $29 \pm 4$  nm.

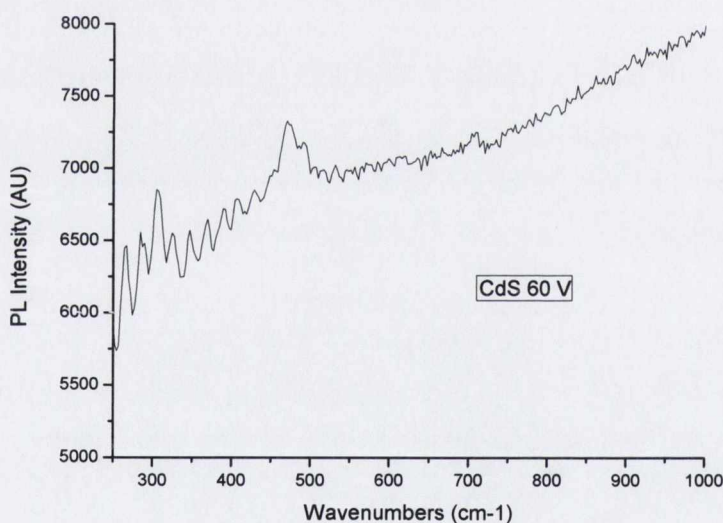
A SEM image of the top of a similar PAM filled with CdS which was etched with NaOH for 15 min is shown in Figure 3.48. It shows the tips of the nanowires, some of which are larger due to overfilling of the PAM. However there are very few empty pores so the filling factor was high.



**Figure 3.48: SEM image of a CdS filled PAM (made at 40 V), which was etched with NaOH to expose the nanowires**



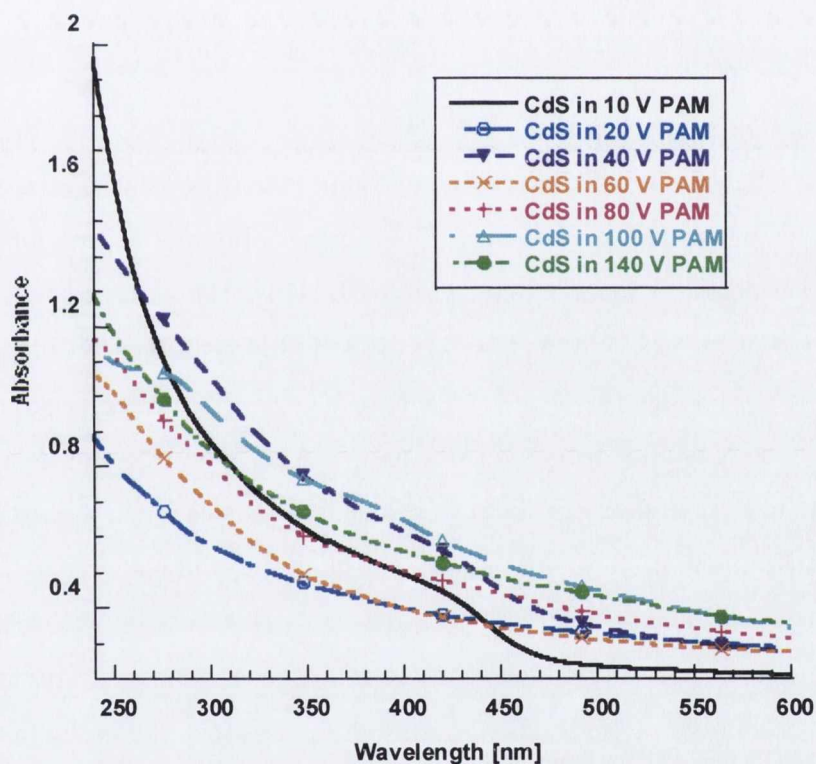
Raman was done to confirm the presence of CdS in the PAMs. An example spectrum is shown in Figure 3.49. The spectrum is quite weak and has a strong background luminescence from the PAM. The Raman peaks correspond to the first order transitional optical phonon mode (TO), the second transverse optical phonon mode (2TO) and the third order transverse optical phonon mode (3TO) of CdS at approximately 300, 500 and 700  $\text{cm}^{-1}$ . These are slightly different from those reported in the literature, for example Mondal et al. [463] observed peaks at 302, 600 and 878  $\text{cm}^{-1}$  for Raman excitation at 514 nm with an Ar-ion laser and Sue and Lee [436] observed two modes at 305 and 604  $\text{cm}^{-1}$  for excitation with 488 and 515 nm lasers. However they also observed a peak at 500 nm and noted that the spectrum obtained by excitation with the 524.5 nm laser was weaker than that obtained by the 488 nm laser. In this work the 632.8 nm line from a HeNe laser was used for excitation which is even further from the band gap edge for CdS than 514.5 nm, so it is not surprising that the spectra obtained (Figure 3.49) are quite weak. Suh and Lee [436] used SERS to get better spectra by depositing a small amount of Ag into the pores before CdS deposition.



**Figure 3.49: Raman spectrum of CdS deposited into a 60 V PAM (excitation  $\lambda = 633$  nm)**

The optical properties of CdS membranes were investigated by UV-Vis and fluorescent spectroscopy (Figure 3.50 and 3.51). The absorption onset for bulk CdS is approximately 513 nm, [462]. Figure 3.50 showed a blue shift of this to 430 nm for the nanowire array in a PAM made at 10 V, i.e. for nanowires of approximately 10 nm diameter. This is in agreement with other authors and has been ascribed to quantum confinement [531, 532, 533]. Some of the other nanowire arrays also show a blue shift in absorption onset (e.g. to 440 nm for nanowires of diameters between 40 – 120 nm and to

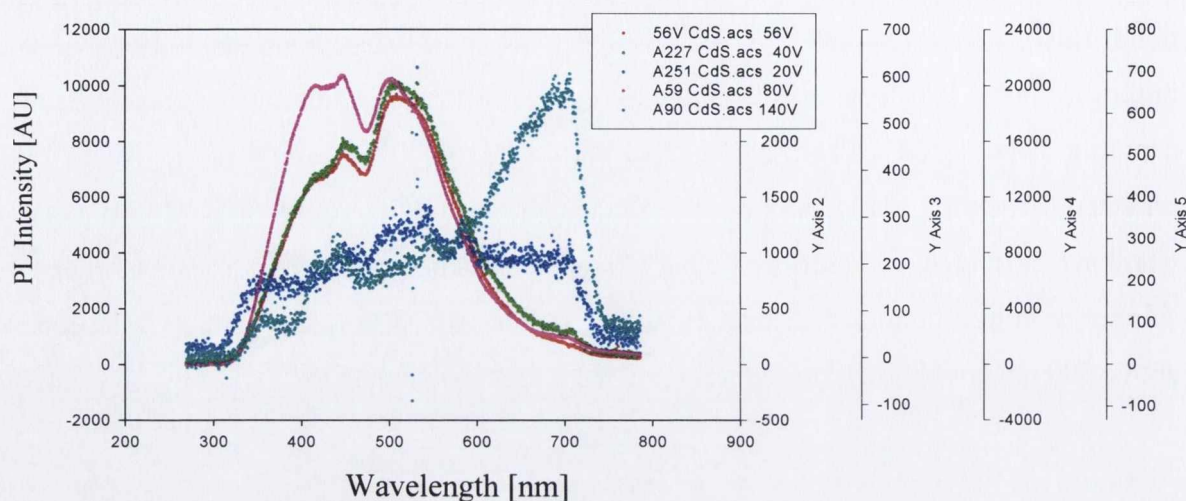
380 nm for nanowires of diameters between 100 - 150 nm). In this case quantum confinement cannot be used to explain the blue shift as the nanowire diameters (40 - 150 nm) are much larger than the exciton Bohr radius of CdS (~ 4 nm). In addition no trend was noticed for different nanowire diameters. These effects may be due to impurities in the PAMs or defects on the nanowires surfaces such as sulphur vacancies or dangling bonds [534]. Each sample has different amounts of impurities which are reflected in the different values obtained for  $\lambda_{\text{max}}$ . These findings agree with Mondal et al. who have attributed the absence of a band to band transition at 513 nm to the presence of sulphur/cadmium vacancies or interstitials [463]. The long absorption tails in the spectra above 500 nm could be due to scattering by the CdS nanowires [535].



**Figure 3.50: UV/vis of CdS samples in PAMs made at 20 V, 40 V, 60 V, 80 V, 100 V and 140 V compared to an empty PAM made at 20 V**

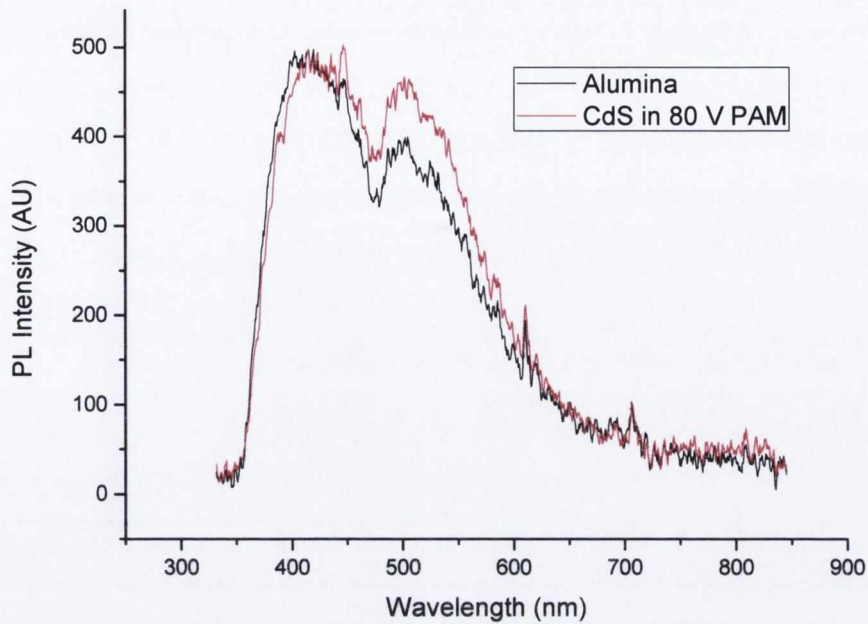


The luminescent properties were investigated by excitation at 266 nm with a Yag laser. Emission between 300 and 750 nm was obtained for all the samples (Figure 3.51).



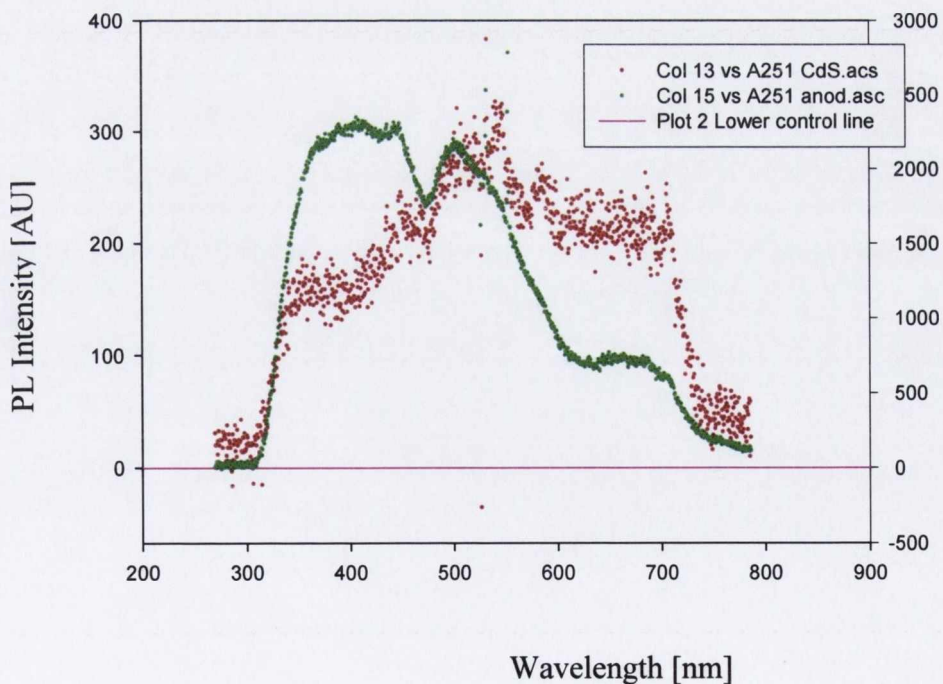
**Figure 3.51: PL spectrum of CdS samples in PAMs made at 20 V, 40 V, 60 V, 80 V and 100V**

The band at approximately 400 nm is from the PAM, the broad band at approximately 500 nm is due to band edge emission of the CdS nanowires and the band at around 700 nm is a surface luminescence which is probably due to structural defects on the nanowires surfaces or excess sulphur [450, 458, 463]. The emission was found to be very dependent on the type of PAM which was used for deposition. The samples in PAMs made at 20 V in  $H_2SO_4$  and 140 V in  $H_3PO_4$  have a very different emission and their PL intensity is also much smaller (y axis 5 is for the 20 V PAM and y axis 3 is for the 140 V PAM in Figure 3.51) than those made in oxalic acid (y axis 1, 2 and 4 correspond to the samples in PAMS made at 56 V, 40 V and 80 V in oxalic acid respectively). This is not surprising as it is well known that empty PAMs are themselves luminescent [464, 465, 466, 536]. Tajima et al. found that photoluminescence appears only on the films anodically formed in organic acids [537]. In this study the most intense luminescence was observed in the samples which were deposited in PAMs which were made in oxalic acid. It is interesting to note that the PL intensity of samples made in oxalic acid was also dependant on the pore size of the membrane (and thus on the diameter of the nanowires); for example the PL intensity for the sample in the PAM made at 80 V (corresponding to a diameter of approx 80 nm) was about twice that of the 56 V sample, which was in turn approximately 4 times greater than the 40 V sample. Figure 3.52 shows the normalized emission spectra of a sample in a PAM made at 80 V compared to an empty 80 V PAM. It can be seen that the spectra have very similar shapes.



**Figure 3.52: Normalized emission spectra of CdS nanowires in a PAM made at 80 V**

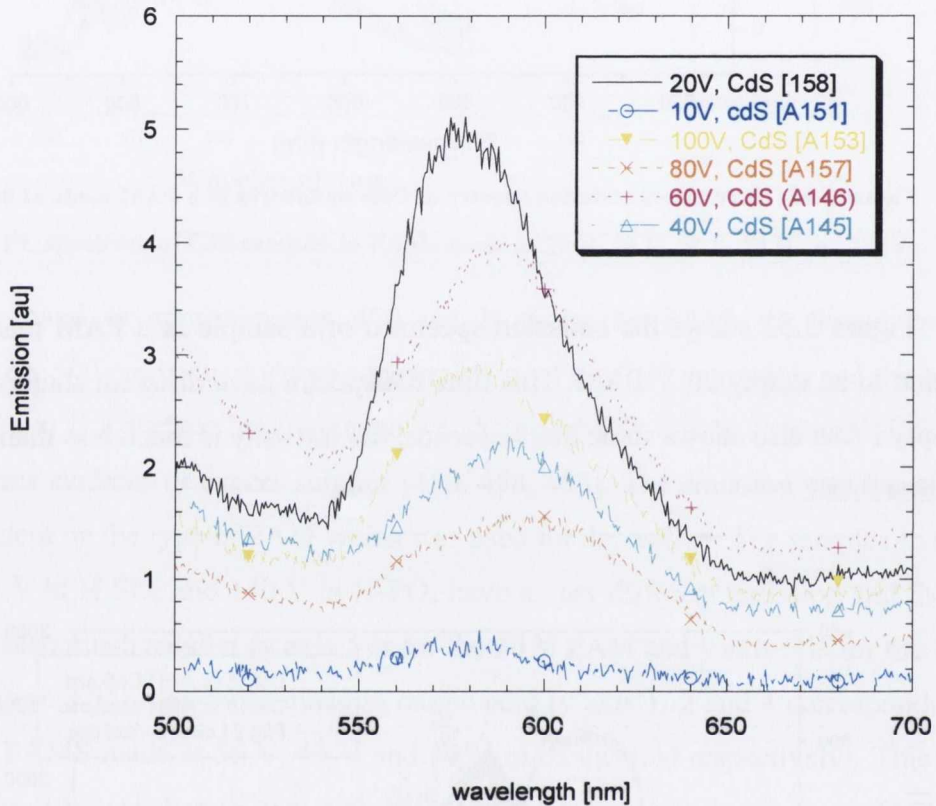
Figure 3.53 shows the emission spectrum of a sample in a PAM made at 20 V compared to an empty 20 V PAM. This time the spectra have different shapes. Although the empty PAM also shows some luminescence, the intensity is much less than that of the CdS filled PAM.



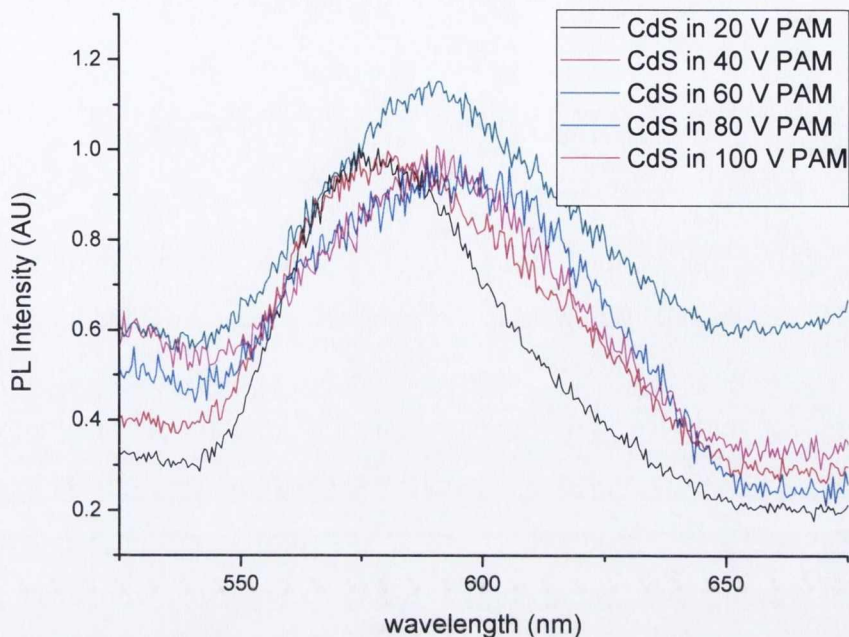
**Figure 3.53: Emission spectrum of a sample in a PAM made at 20 V compared to an empty 20 V PAM**



Figure 3.54 shows the PL of another set of CdS nanowire arrays which were excited at 400 nm. The spectra show a clear blue shift of  $\lambda_{\text{max}}$  with increasing nanowire diameter for the samples which were made in PAMs fabricated at 10 V, 20 V, 40 V, 60 V and 80 V. However the sample in the 100 V PAM is different. It has a similar  $\lambda_{\text{max}}$  to the sample made in the 20 V PAM but has a broader emission. Figure 3.55 shows the same spectra with the contributions due to the empty PAMs subtracted. Here the shift in  $\lambda_{\text{max}}$  appears to be due to the different type of PAM rather than a size effect.



**Figure 3.54: PL spectra of CdS nanowire arrays which were deposited into PAMs made at 10 V, 20 V, 40 V, 60 V, 80 V and 100 V.**



**Fig 3.55: PL of CdS samples in PAMs made at 20 V, 40 V, 60 V, 80 V and 100 V corrected for PL contribution due to the empty PAMs**

### 3.2.4.3 Summary

CdS nanowires were made by AC electrodeposition into PAMs which were made at 10 V, 20 V, 40 V, 60 V, 80 V, 100 V and 140 V. The nanowires were characterized by SEM, TEM, and UV-vis and PL spectroscopy. They were found to have a similar morphology to metallic nanowires but were less homogeneous. UV-vis showed a blue shift of this absorption onset from 513 for bulk CdS to 430 nm for the nanowire array in a PAM made at 10 V, i.e. for nanowires of approximately 10 nm diameter. PL spectroscopy shows that the nanowires exhibit a band gap emission the intensity of which depended on the type of PAM in which the nanowires were deposited; the nanowires which were fabricated in the oxalic acid PAMs emitted at a higher wavelength. Subtraction of the contribution due to the PL of the PAMs showed that the PL of the nanowires is blue shifted for all sizes; thus the alumina template made a contribution to the PL in all cases.



## Chapter 4 Results: 2-Dimensional Nanostructures

### 4.1 Silver / Polyaniline (Ag/PANI) Thin Films

The potential applications of Ag/PANI composites has been outlined in chapter 2, section 2.1.2.3. Chapter 3, section 3.2.3 describes the preparation and characterisation of an Ag/PANI nanocable. Such structures could be used in-situ in the PAMs, which are transparent in the ultraviolet, visible and infrared spectral range. They could easily be integrated into devices or chips, for example a nanoelectrode in a LED as described in chapter 5, section 5.1 or a photovoltaic cell as described in section 5.3. The nanocables can also be easily extracted from the PAM and incorporated into other polymers or coatings. However homogeneous dispersion of nanoparticles into solvents or polymers for thin film fabrication is hampered by aggregation [427] which could decrease the efficiency of the material or device. Uniform size distribution can be achieved by in-situ reduction of Ag salts in aniline [430] and stable films of polymers containing Ag nanoparticles have been formed by chemical reduction of silver salts in aqueous PVA [538]. It should thus be possible to adapt the method described in chapter 3, section 3.2.3.1 for the production of composite nanowires, which involves simultaneous oxidative polymerization of aniline and reduction of Ag from  $\text{AgNO}_3$ , to make thin films of PANI containing Ag nanoparticles. Since the formation mechanism of the Ag/PANI nanowires involves interaction between the nitrogen head groups of PANI (see section 3.2.3.3) and the Ag particles rather than formation of Ag clusters it is assumed that films formed by the same method would contain homogeneous dispersions of Ag in PANI. Similar films prepared electrochemically by an unsymmetrical square wave current method have shown that the films consist of nanofibrous PANI with homogeneously dispersed Ag microparticles [539]. Other advantages of using electrodeposition to synthesize these materials is the low cost, high deposition rates, near room temperature operation, and the possibility of tailoring their properties by adjusting deposition conditions [540]. This is explored in this chapter by varying the deposition process (applied potential and deposition time) and measuring the effect on the conductivity of the resulting films. PANI thin films were made by the same method for comparison.

### 4.1.1 Electrochemical Preparation of Thin Films

Ag / PANI thin films were prepared by electropolymerisation of PANI onto ITO from an acidic electrolyte containing silver metal ions and aniline. The method for this procedure is similar to that for the Ag/PANI nanocables (chapter 3, section 3.2.3.1) except ITO is used as a substrate and anode instead of porous alumina. Electrodeposition was carried out in a two-electrode cell with graphite electrodes using a potentiostat at constant voltage (see Figure 4.1). The graphite electrodes were polished with silicon carbide emery paper then rinsed in acetone and distilled water.

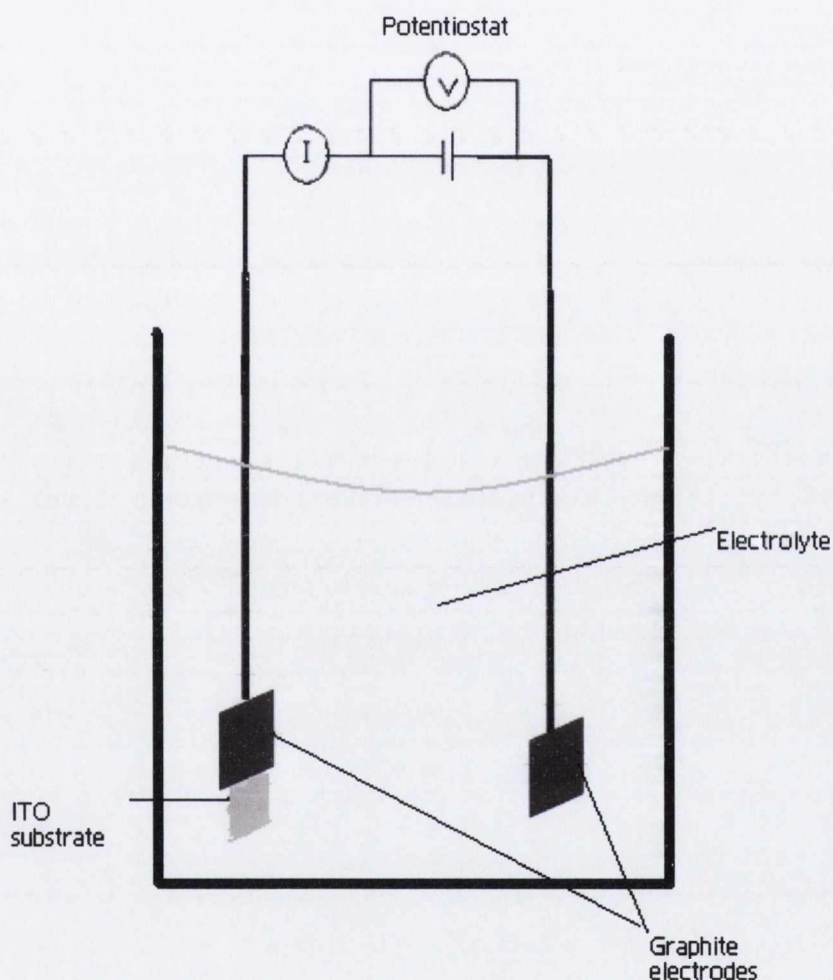


**Figure 4.1:** Schematic of apparatus used for potentiostatic electrodeposition onto ITO

The electrolyte was an aqueous solution containing 2.5 mL /L aniline, 1 g / L  $\text{AgNO}_3$ , 41 g / L  $\text{MgSO}_4 \cdot 7\text{H}_2\text{O}$  with enough  $\text{H}_2\text{SO}_4$  added until the pH of the solution was 2. The ITO was attached to the working electrode. It was first cleaned in hot acetone,



deionised water and iso-propanol. Deposition was carried out at voltages ranging from 0.8 V to 2.5 V for several different time intervals (ranging from 100 s to 4000 s).

PANI thin films were made by the same method for comparative purposes. The electrolyte was an aqueous solution containing 2.5 mL / L aniline, with enough H<sub>2</sub>SO<sub>4</sub> added until the pH of the solution was 2.

#### 4.1.2 Characterisation of Thin Films

The films were characterised by Raman, XRD and UV-vis spectroscopy. Their electrical characteristics were also measured.

##### 4.1.2.1 Raman Spectroscopy

Raman spectra were taken on the thin films to confirm the presence of PANI. All the spectra showed the characteristic peaks for PANI listed in the Table 4.1. Figure 4.2 shows a typical Raman spectrum.

**Table 4.1 Assignments for Raman bands in films on ITO samples**

Region [cm <sup>-1</sup> ]	Vibration
390-416	C-N-C torsion and out of plane deformation of benzenoid rings
574-587	CH out of plane and aniline deformation modes
523, 810	Deformation of benzenoid or quinoid rings
1166	CH bending of benzenoid rings
1320-1340	C-N: stretching of modes of quinoid rings
1478-1484	-C=N stretching modes of quinoid rings
1580 1588	-C-C stretching of benzenoid rings

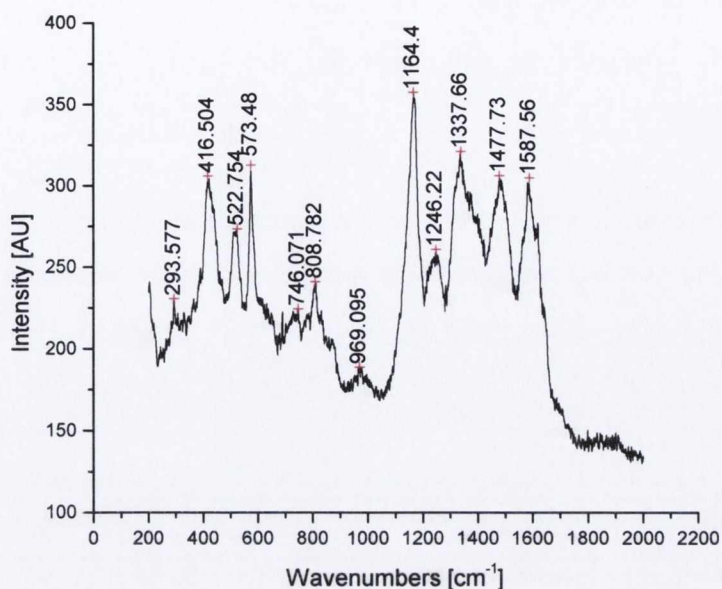


**Figure 4.2: Raman spectrum of a film of Ag / PANI on ITO prepared at 1.0 V for 1000s (Excitation  $\lambda = 633\text{nm}$ )**

The spectra were compared to spectra of PANI on ITO which were prepared under the same conditions. The intensities of the Ag / PANI spectra were greater than those of the PANI spectra due to surface-enhanced Raman scattering by Ag. This is illustrated in Figure 4.3.

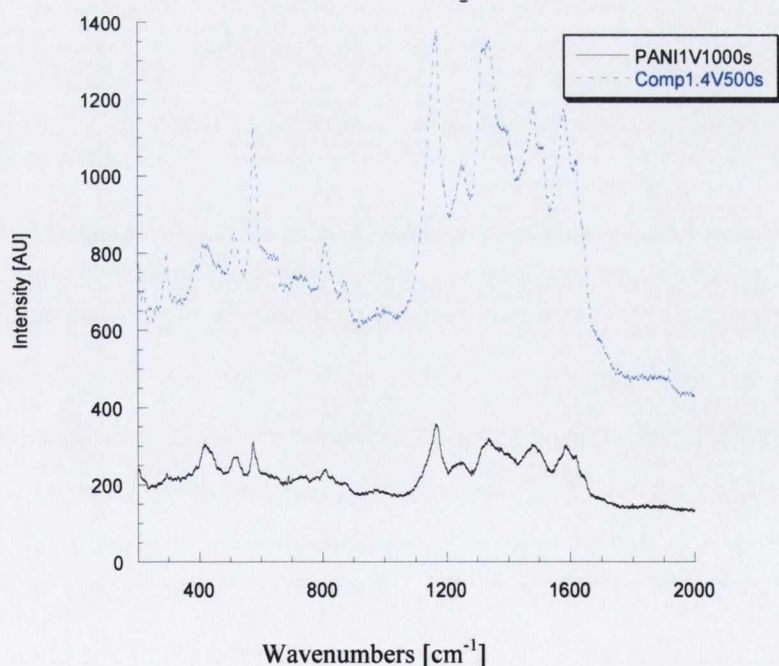


**Figure 4.3: Raman spectrum of a film of PANI on ITO prepared at 1.0 V for 1000 s compared to a film of Ag / PANI (1.4 V, 500 s) {excitation  $\lambda = 633\text{nm}$ }**



There were some differences in the bands between  $293\text{ cm}^{-1}$  and  $900\text{ cm}^{-1}$  for composite and PANI samples as illustrated in Figure 4.4. For example the relative intensities of the bands at  $415\text{ cm}^{-1}$ ,  $480\text{ cm}^{-1}$  and  $580\text{ cm}^{-1}$  were reduced in the composite sample (C-N-C torsion and out of plane deformation of benzenoid rings and CH out of plane and aniline deformation modes respectively) and all these bands also showed slight shifts and broadening in the composite. This is indicative of the weakening of inter-chain interactions probably as a result of the incorporation of Ag [503]. The C-N: stretching modes of quinoid rings at  $1340\text{ cm}^{-1}$  were also stronger in the composite indicating that it was more oxidized than the PANI.

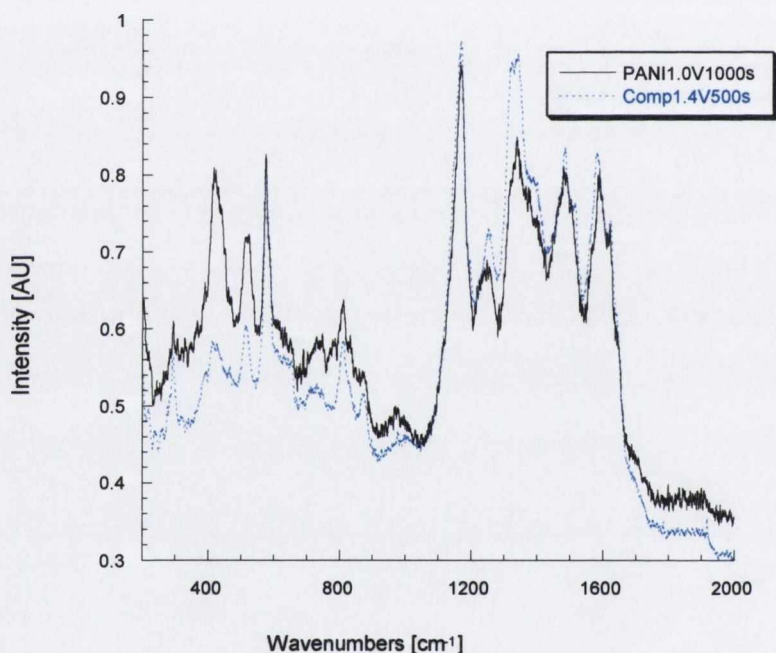


**Figure 4.4:** Normalised Raman spectrum of a film of Ag / PANI on ITO prepared at 1.4 V for 500 s compared to a film of PANI (1.0 V, 1000 s) {excitation  $\lambda = 633\text{nm}$ }

#### 4.1.2.2 XRD

The presence of Ag in the Ag / PANI films was confirmed by XRD. A typical XRD pattern of an Ag / PANI film is shown in Figure 4.5. A broad peak centred at  $2\theta = 22^\circ$  was observed and can be ascribed to PANI due to partial ordering along the polymer chain. The peak centred at  $2\theta = 38.58^\circ$ , corresponds to the (111) Ag plane. However, the peaks at  $30.56^\circ$ ,  $35.58^\circ$ ,  $50.9^\circ$  and  $60.46^\circ$  are due to the (222), (400), (440) and (622) planes of ITO respectively [541].

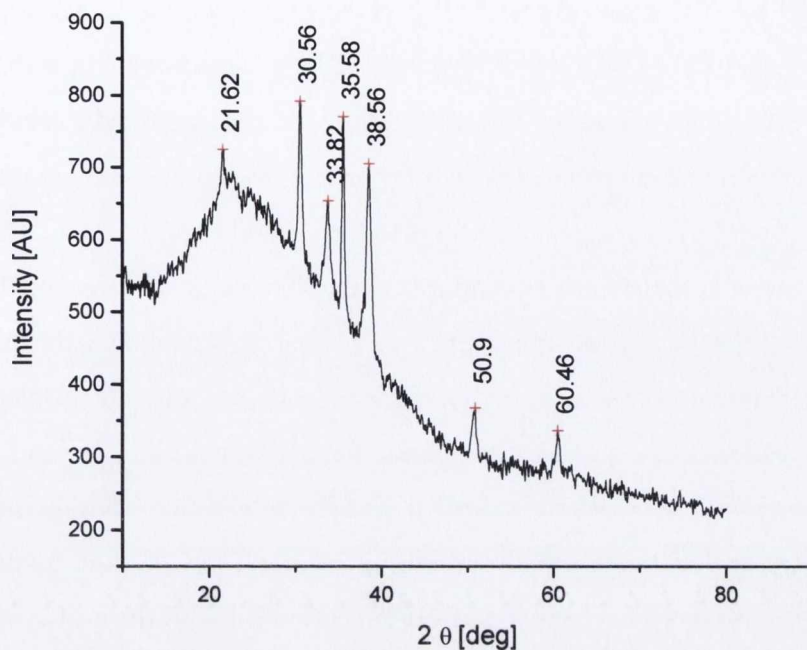


Figure 4.5: XRD pattern of the Ag/PANI film made at 0.8V for 500s

#### 4.1.2.3 UV-Vis Absorption Spectroscopy

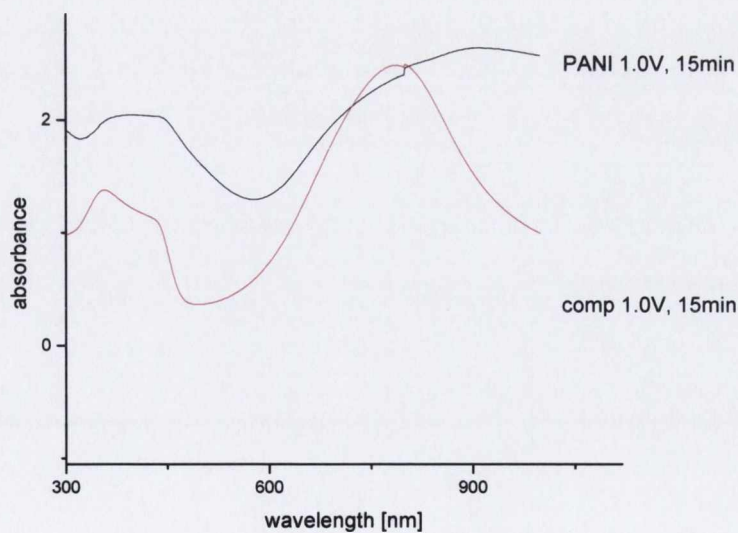


Figure 4.6: UV-Vis of an Ag / PANI film on ITO prepared at 1.0V for 1000s compared to a film of PANI on ITO prepared under the same conditions



Figure 4.6 shows typical spectra for the PANI and composite films. The spectrum for a film of PANI on ITO shows three characteristic absorption bands for doped PANI; one at 350 nm due to the  $\pi - \pi^*$  transition within the benzenoid segment; a shoulder-like absorption at 430 nm due to polaron -  $\pi^*$  transition and a polaron band transition around 900 nm [503]. The absorption at 630 nm, corresponding to the pristine emeraldine base form of PANI, is absent indicating that PANI is in the emeraldine salt form. The shape of the spectrum for the composite film is similar but there are some differences. Firstly, the bands at 354 nm and 421 nm are overlapped and red- shifted due to the presence of nanosilver [430]. Silver shows a strong band at  $\sim 400$  nm due to surface plasmon resonance of the electrons in the conduction band. Secondly, the polaron band absorption is reduced indicating an improvement in doping [511] which results from the introduction of Ag into the polymer backbone. This is similar to the effect of CdS nanoparticles on the absorption of PANI observed by Khiew et al. [542]. In bulk PANI the coil conformation of the polymer is dominant due to interchain interactions. This leads to stronger polaron interaction and the transformation of the absorption peak into a “free-carrier tail” [543] as observed for the PANI films in this study.

#### 4.1.2.4 Electrical Measurements

The conductivities of the samples were determined by monitoring changes in the current when increasing voltages were applied across the sample. A Keithly IV program was used to measure direct (DC) voltage-current characteristics and calculate resistivities as described in chapter 2, section 2.2.3. A typical DC voltage versus current curve is shown in Figure 4.7.

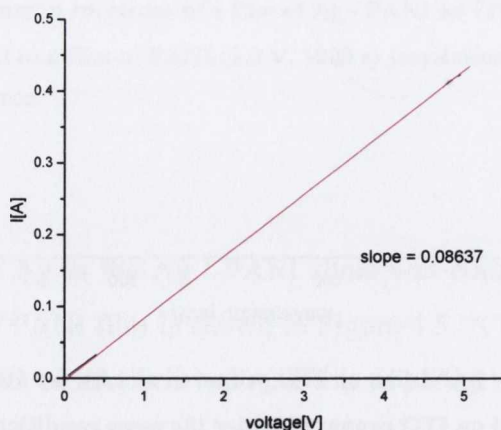


Figure 4.7: Voltage-Current characteristics for a film of Ag / PANI on ITO (1 V, 2000 s)

All the films displayed ohmic behaviour. Their conductance was obtained from the slope of the graphs and the sheet resistivities of the samples were calculated from equation 2.25 (chapter 2, section 2.2.3). Sheet conductivities were calculated from these values and all results are listed in Table 4.2.

**Table 4.2: Conductivities of Ag / PANI composite and PANI films on ITO**

Sample	Deposition Voltage (V)	Deposition Time (s)	Conductance (slope) G = Sheet Conductivity ( $\Omega^{-1} \cdot \square$ )	Resistance $G^{-1}(\Omega)$ = Sheet Resistivity ( $\Omega/\square$ )
Composite 1	1.0	500	0.0509	19.6425
Composite 2	1.2	500	0.0537	18.6150
Composite 3	1.6	500	0.0687	14.5518
Composite 4	2.5	500	0.0724	13.8217
Composite 5	1.0	1000	0.0863	11.5942
Composite 6	1.5	1000	0.0746	13.4012
Composite 7	2.5	1000	0.0743	13.4644
Composite 8	1.0	2000	0.0864	11.5781
Composite 9	1.5	2000	0.1008	9.9216
Composite 10	2.5	2000	0.1654	6.0459
PANI 1	1.5	500	0.0902	11.0828
PANI 2	2.5	500	0.0422	23.6742
PANI 3	1.0	1000	0.0798	12.5345
PANI 4	1.5	1000	0.1085	9.2132
PANI 5	1.0	2000	0.0794	12.6024
PANI 6	2.5	2000	0.0423	23.6574

From Table 4.2 it can be seen that the conductivities of the composite and PANI films are similar. One would expect the presence of Ag to increase the conductivity of the composite, however, due to the loss in symmetry in the PANI backbone when the metal ion is co-ordinated to the nitrogen atoms of the polymer backbone in place of a proton from the acid dopant, there is a corresponding loss in conductivity. This effect was observed by Kinyanjui et al. in the synthesis of Platinum PANI (Pt / PANI) composites [544, 420]. They noticed a loss in conductivity of approximately  $10^7$  of the Pt / PANI composites compared to PANI without Pt and attributed it to the segregation of charge within the polymer as Pt was included. This leads to a corresponding loss in free charge carriers compared to the acid doped PANI. The same effect is seen when  $AuCl_4^-$  is used in the electrochemical polymerisation of aniline. The conductivity of the composite in 1 M acid is reduced by  $10^7$  compared to the pristine polymer [416, 545]. Again the inclusion



of Au resulted in a polymer with a higher oxidation state and reduced proton doping. Angelopoulos et al. [546] also attributed the reduced proton doping to the steric hindrance of Au which blocks the imine nitrogen sites. One way to overcome this would be to synthesise the composites by chemical means rather than electrochemical means [544, 545] or to incorporate Ag nanoparticles into a solution of PANI by dispersion followed by spin casting. This method is described in 4.2.1.

The sheet conductivities of all films were plotted against anodising voltage (Figure 4.8) and anodising time (Figure 4.9).

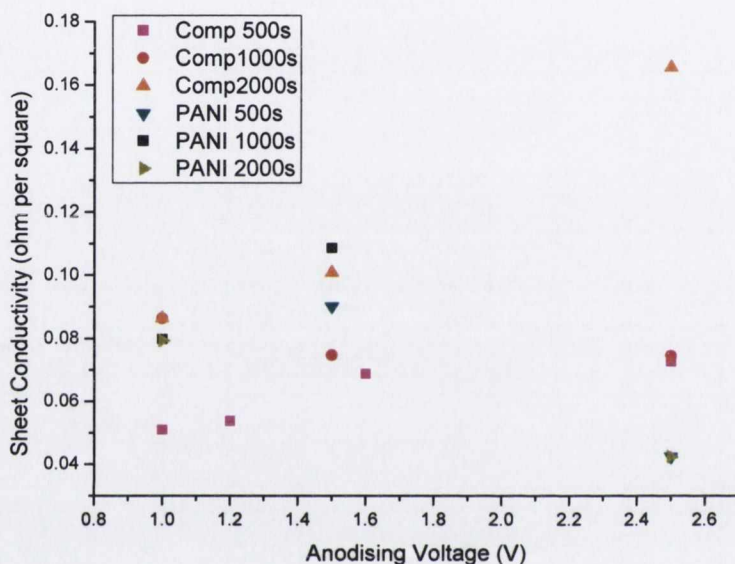


Figure 4.8: Plot of sheet conductivity against anodising voltage for composite and PANI films

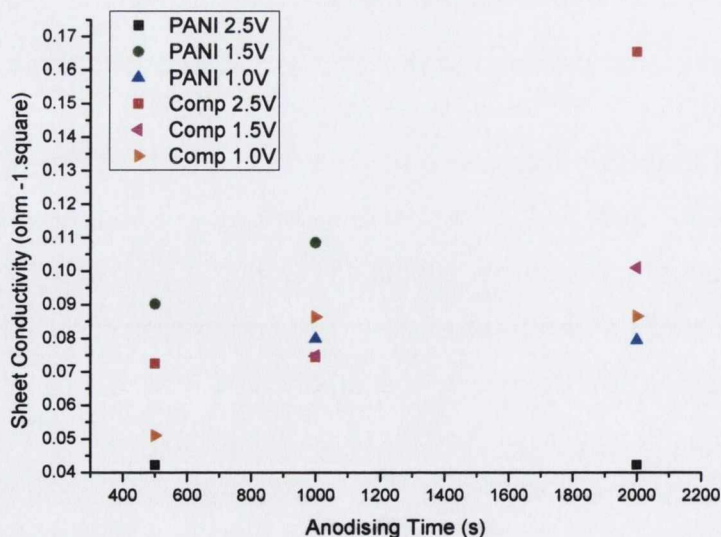
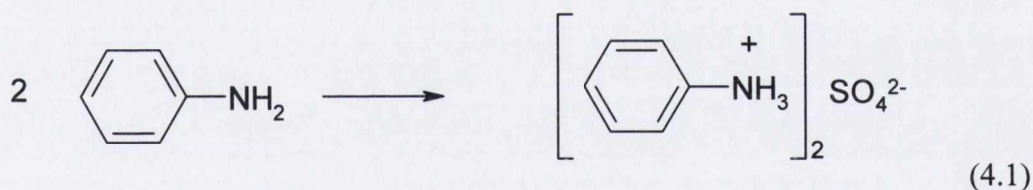


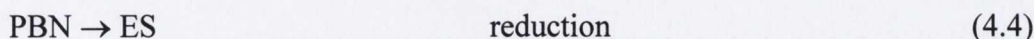
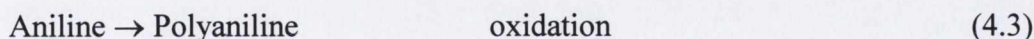
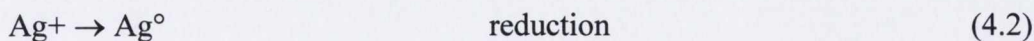
Figure 4.9: Plot of sheet conductivity against anodising time for composite and PANI films

From Figures 4.8 and 4.9 it can be seen that in all cases except PANI made at 2.5 V the conductivity increases with increasing anodising voltage and anodising time. This is not surprising as more benzenoid units are converted into quinoid units so the polymer becomes more electron deficient [546]. According to MacDiarmid and Epstein [383] the polymerisation of aniline starts off by adsorption of an oligomeric cation radical of aniline on the substrate [547]. Film thickness then increases as the polymerisation proceeds, so one would expect the conductivity of the film to increase with time anodised. However after 2000 s the film becomes unstable as PANI precipitates out of solution onto the film surface [547]; thus the PANI film has a lower conductivity than the composite films which are stabilised by the incorporation of Ag. Stejskal and co-workers have found that film growth proceeds exponentially after a short induction period [548]. This agrees with the results presented here for composite films prepared at 1.0 V and 2.5 V (Figure 4.9). The change in conductivity with voltage shows a similar trend for composite films prepared at 500 s and 2000 s (Figure 4.8) and agrees with results from Okamoto et al. [549]. However the conductivity of the PANI films decreased with increasing voltage as the PANI becomes more oxidised for the reasons stated above [546, 549].

The mechanism for polymerisation of the composite films involves a multi-step reduction / oxidation process. The aniline is protonated by  $\text{H}_2\text{SO}_4$  to form a protonated anilinium cation.



The  $\text{Ag}^-$  anion acts as an electron acceptor i.e.



Then the above procedure is repeated, thus the Ag particles act as nucleation sites for the polymerisation of aniline. This is similar to the effect of Pt on the polymerisation of PANI [545].

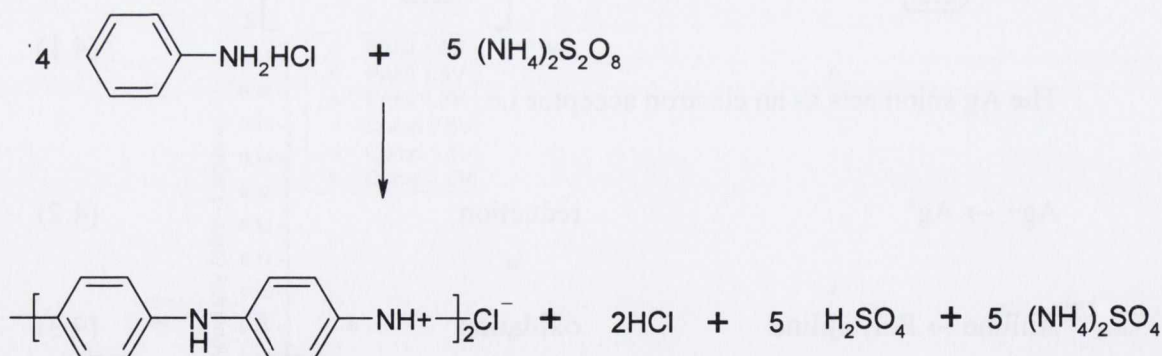


## 4.2 Polyaniline films containing Ag nanowires

### 4.2.1 Film Preparation

Films of PANI containing Ag nanowires were prepared from a mixture of emeraldine salt (ES) and Ag nanowires in N-Methylpyrrolidone (NMP). A solution of 0.1g ES was sonicated in 1 mL NMP for 10 min. This was added to a solution of 2.7 mg Ag nanowires in 1 mL NMP. A few drops of this was drop cast onto a 10 mm by 10 mm glass slide and dried in a vacuum oven at 40°C for 2 hours. Films of ES, emeraldine base (EB) {Aldrich Chemical Company} and EB doped with H<sub>2</sub>SO<sub>4</sub> were made for comparison.

The ES was prepared by chemical oxidative polymerisation of aniline. 4.3 g aniline (0.05 M), which was purified by vacuum distillation, was added to 400 mL deionised water and cooled to 0°C. The pH of the solution was adjusted to approximately 2.5 with 1 M hydrochloric acid (HCl). 13.7 g (0.06 M) oxidant initiator ammonium persulphate {(NH<sub>4</sub>)<sub>2</sub>S<sub>2</sub>O<sub>8</sub>} was dissolved in 100 mL deionised water and added to the aniline solution drop wise. The mixture was stirred for 6 hrs, and then enough methanol was added to precipitate out the dark green product. This was then collected by filtration, washed with deionised water and dried at 60°C in a vacuum oven. The mechanism is the same as that described by Sapurina et al. [548].



Scheme 4.1: Polymerisation of aniline with ammonium peroxydisulfate in water

The Ag nanowires were prepared by electrodeposition of Ag in PAMs at 9 V AC as described in chapter 3, section 3.2.1.1. The nanowires were extracted by shaking the template in a solution of 0.1 M NaOH and 30g/L PVP for 12-24 hrs, followed by washing in Millipore filtered deionised water.

## 4.2.2 Film Characterisation

### 4.2.2.1 Raman Spectroscopy

Raman was used to confirm the presence of PANI in the films. They were then compared to films made with PANI emeraldine base and salt (PANI EB and PANI ES), and doped emeraldine base (PANI EB doped).

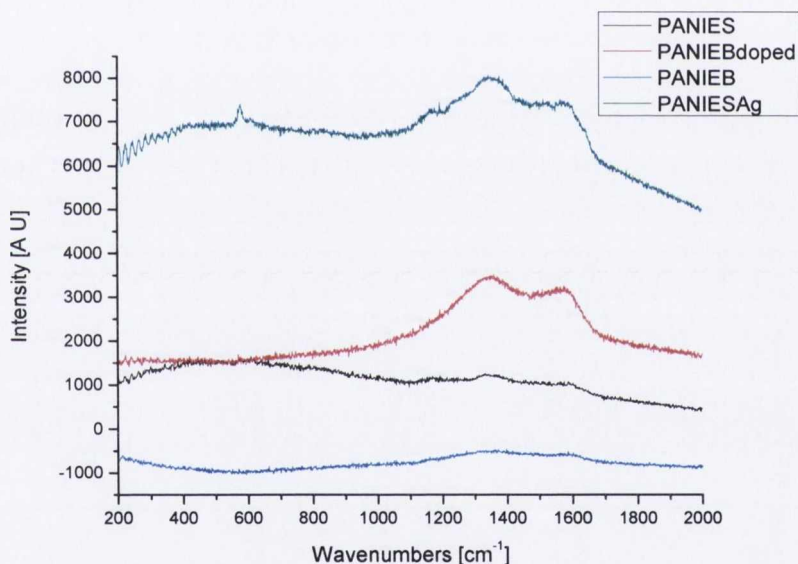


**Figure 4.10: A PANI ES film containing Ag nanowires drop-cast on glass compared to PANI EB, PANI ES and doped PANIEB films on glass (excitation  $\lambda = 633$  nm).**

Figure 4.10 shows that doping with acid increases the intensity of the Raman and doping with Ag has an even greater effect (due to SERS).

Magnification of the spectra shows that they contain the Raman bands due to PANI. This is illustrated in Figure 4.11 for PANI ES which shows the Raman bands between 390 - 416 cm<sup>-1</sup> due to C-N-C torsion and out of plane deformation of benzenoid



rings, deformation of benzenoid or quinoid rings at around 600 and 800  $\text{cm}^{-1}$  and CH bending of benzenoid rings at around 1100  $\text{cm}^{-1}$ (see Table 3.5).

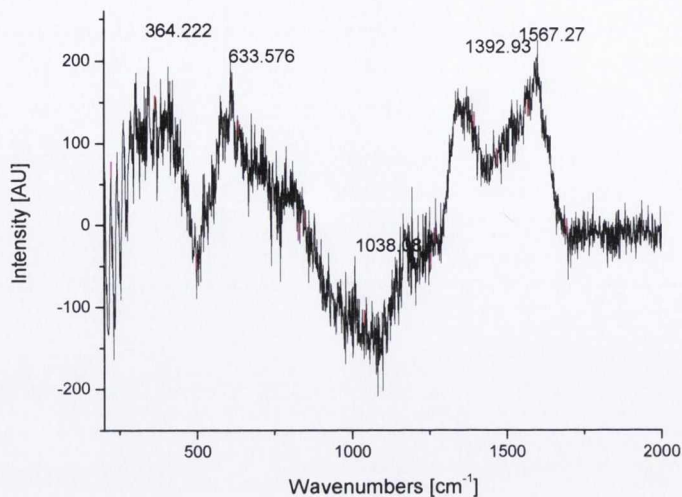


Figure 4.11: Raman spectrum for PANIES (baseline corrected, excitation  $\lambda = 633 \text{ nm}$ )

#### 4.2.2.2 XRD

XRD was performed to confirm the presence of Ag. Figure 4.12 shows the XRD diffraction pattern of a film of PANI ES containing Ag nanowires cast onto a glass slide.

The spectrum contains PANI peaks between  $18.9^\circ$  and  $33.8^\circ$  [550] and a contribution from the glass substrate at  $\sim 25^\circ$  [551]. The other peaks are due to Ag { $38.56^\circ$  is from the (110) Ag plane and  $43.00^\circ$  is from the (200) plane}.

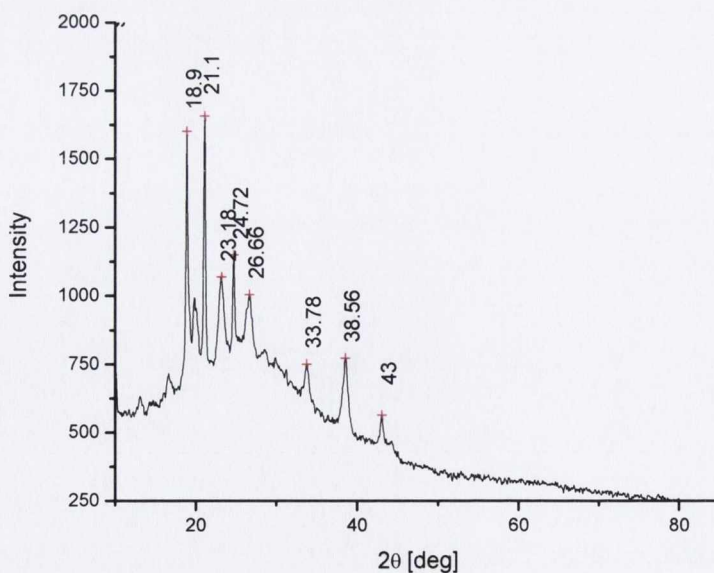


Figure 4.12: XRD Diffraction pattern of a film of PANI ES containing Ag nanowires cast onto a glass slide.

## 4.3 PANI and Ag / PANI Films on Carbon Nanotube Electrodes

### 4.3.1. PANI on Multi Wall Carbon Nanotube Electrodes (MWCNT)

The MWCNTs (Nanocyl 3100) were purified by refluxing in  $\text{HNO}_3$  for 24 hr followed by drying in an oven at  $100^\circ\text{C}$  for 24hr. 10 mg MWCNTs were dispersed in 200 mL NMP (using 5 x 2 mg MWCNTs in 20 mL NMP in vials which were sonicated with a 120 W sonic tip at 20 % amplitude for 5 min each). The vials were combined into a 500 mL round bottomed flask and 100mL NMP was added to this. The mixture was then sonicated in a sonic bath for 30 min followed by centrifugation to remove the larger particles and amorphous impurities. The suspension was filtered through a commercial PAM (Whatman Anodisc 47,  $0.02\ \mu\text{m}$  Catalogue No 6809-5002) with the aid of a vacuum and the nanotubes collected on the surface to form a mesh or mat (commonly known as a “Bucky paper”). This was first dried in air (still attached to the filter apparatus to make sure it didn’t curl) and finally in an oven at  $60^\circ\text{C}$  for 12 hr (to ensure all the NMP had evaporated). This process is illustrated in Figure 4.13.

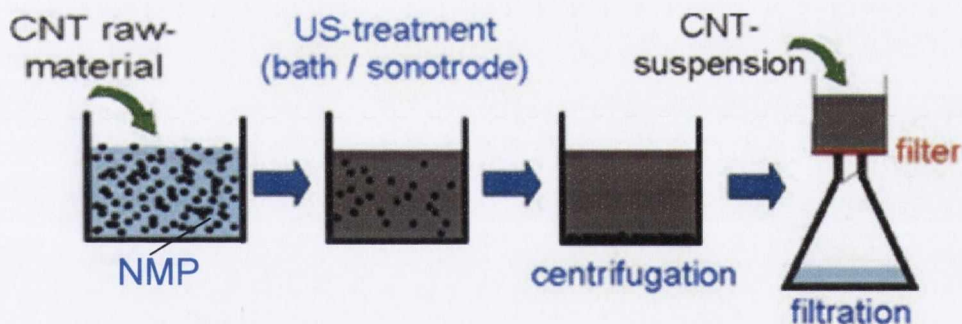
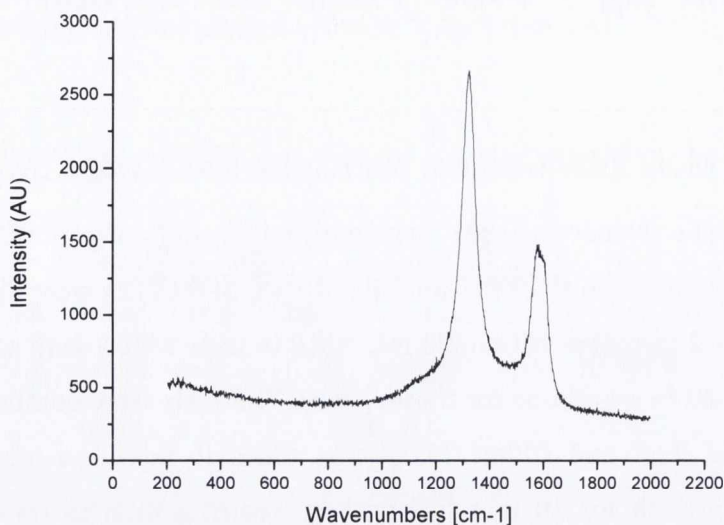


Figure 4.13: Schematic of the different steps involved in the production of a “Bucky” paper (adapted from Fraunhofer Institute for Interfacial Engineering and Biotechnology IGB web-site [552]).

PANI was deposited by potentiostatic deposition at 1.0 V for 10 min on the reverse side of the PAM (see chapter 3, section 3.2.2.1), using the MWCNT on top of the PAM as a backing electrode.

Deposition was unsuccessful and the Bucky paper peeled off the PAM. Raman showed the peaks for CNTs on the underside of the CNT (next to PAM) as shown in Figure 4.14. The characteristic G band appears at  $1600\ \text{cm}^{-1}$  and the D band at  $1300\ \text{cm}^{-1}$ .





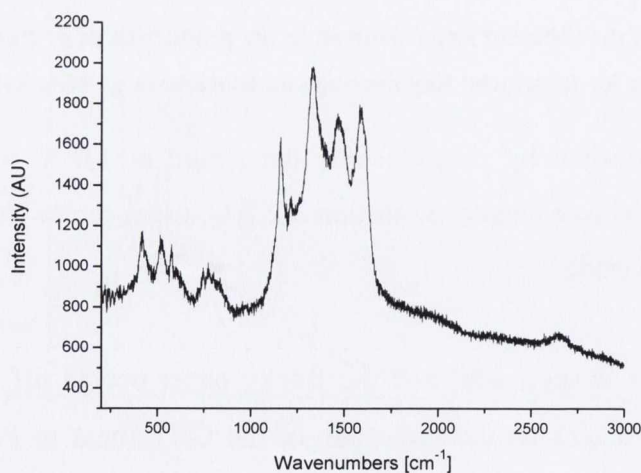
**Figure 4.14: Raman spectrum of underside of MWCNT electrode (excitation  $\lambda = 633$  nm)**

### 4.3.2. Ag / PANI on MWCNT

A Bucky paper was made on top of a commercial PAM as described in section 4.3.1 but using 5 mg MWCNT (Nanocyl) in 5 vials (0.001 g MWCNT in 10 mL NMP in each) and making the solution up to 200 mL in a round bottomed flask. When dry the PAM with attached Bucky paper was turned up-side down as before and placed on a substrate for deposition.

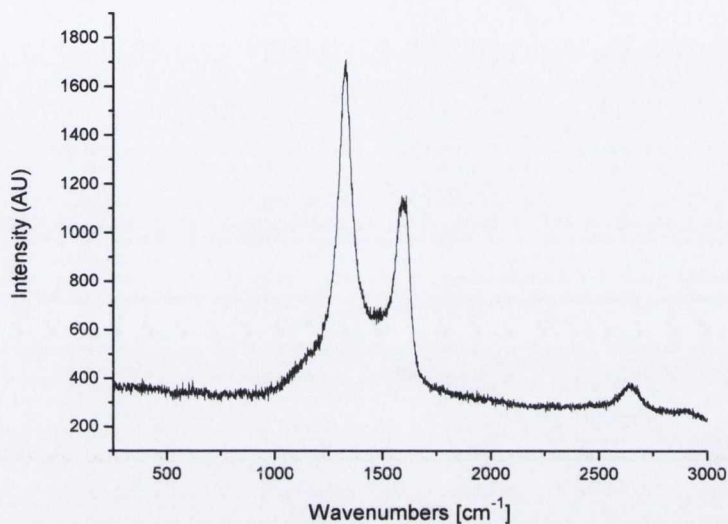
Ag / PANI were electrodeposited by AC at 9 V for 18 min as described in chapter 3 section 3.2.3.1. The Bucky paper peeled away from the PAM as before.

Raman analysis (Figure 4.15) showed that PANI was deposited on the CNT electrode under the PAM.



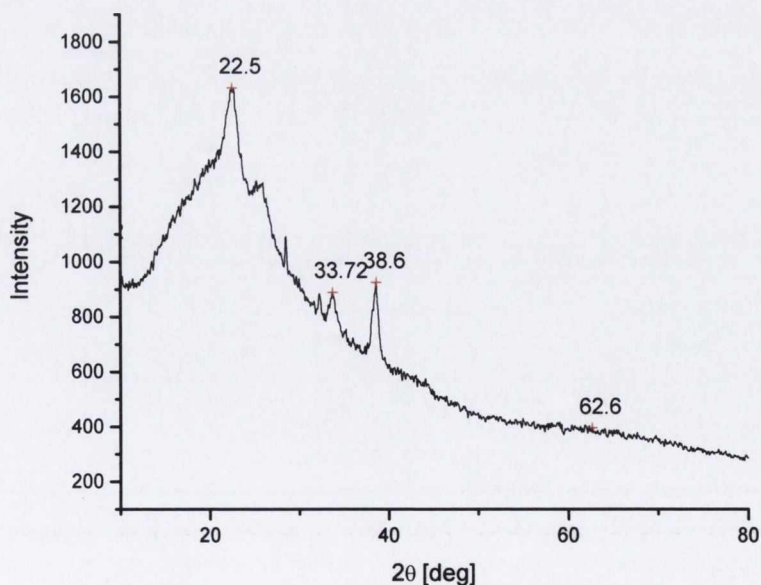
**Figure 4.15: Raman spectrum of underside of MWCNT electrode (excitation  $\lambda = 633$  nm)**

Figure 4.15 shows that the characteristic PANI peaks are present (see Table 4.1). The CNT D and G bands coincide with some of these peaks but the D\* band due to CNTs is visible at  $2600\text{ cm}^{-1}$ . Figure 4.16 shows the other side of the CNT electrode showing D, G and D\* bands.



**Figure 4.16: Raman spectrum of top of MWCNT electrode (excitation  $\lambda = 633\text{ nm}$ )**

XRD was done to confirm the presence of Ag in the film (Figure 4.17).



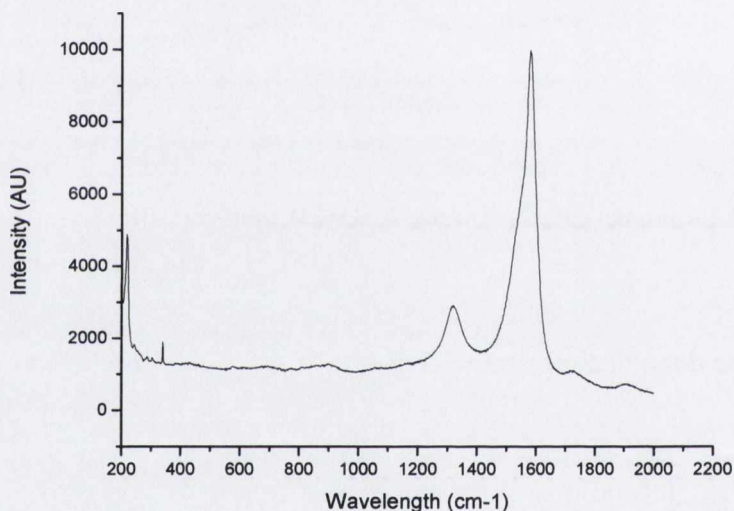
**Figure 4.17: XRD Diffraction pattern of Ag / PANI electrodeposited onto a MWCNT electrode through a commercial PAM.**



The characteristic peaks for PANI ES are  $22^\circ$  from (020) plane,  $25^\circ$  from (200) plane and  $32^\circ$  from (022) plane [544]. The Ag (111) peak is present at  $38.6^\circ$  and the peak at  $33.7^\circ$  is due to the glass substrate.

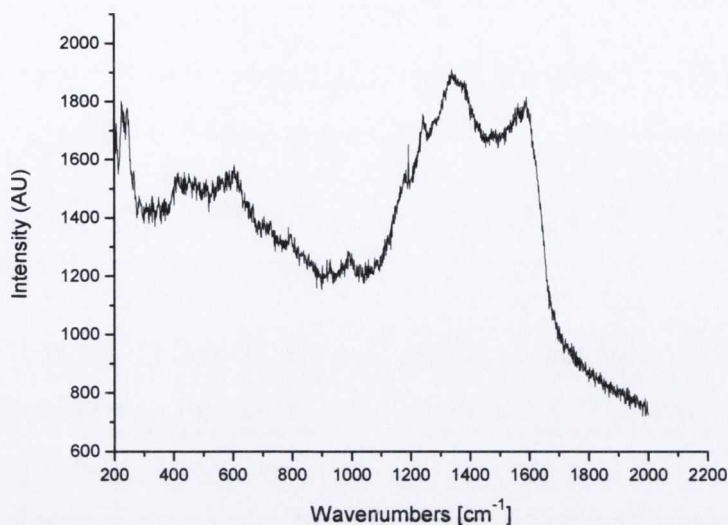
### 4.3.3 Ag / PANI on Single Wall Carbon Nanotube Electrodes (SWCNT)

The synthesis was repeated with 0.002 g SWCNT (Hipco) in 200 mL NMP and deposition of Ag / PANI at 9 V AC for 10 min. Raman showed deposition of PANI occurred on top of the Bucky paper but not in the PAM i.e. it went through the membrane. XRD showed that Ag was also deposited. The results are shown in Figures 4.18, 4.19 (Raman) and 4.20 (XRD).



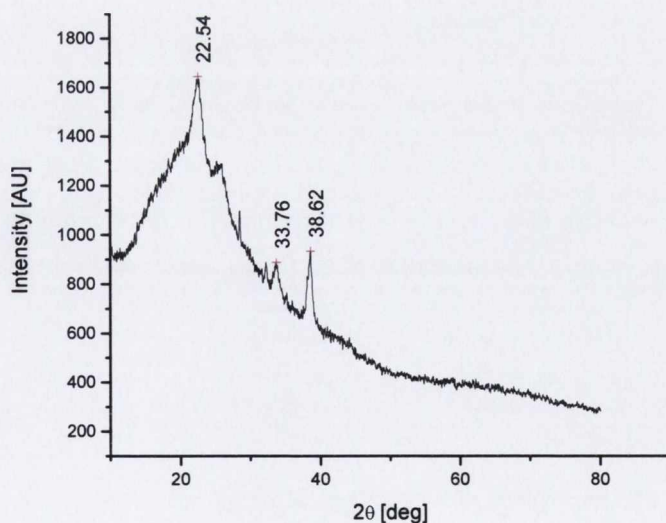
**Figure 4.18: Raman spectrum of bottom of SWCNT electrode (excitation  $\lambda = 633$  nm)**

Figure 4.18 shows the characteristic D band at  $1300\text{ cm}^{-1}$ , G band at  $1600\text{ cm}^{-1}$  as well as a radial breathing mode (RBM) at  $260\text{ cm}^{-1}$ .



**Figure 4.19: Raman spectrum of top of SWCNT electrode (excitation  $\lambda = 633$  nm)**

Some of the Raman peaks in Figure 4.19 are overshadowed by the bands due to CNTs at  $1300\text{cm}^{-1}$  and  $1600\text{cm}^{-1}$ , but the peaks due to C-N-C torsion and out of plane deformation of benzenoid rings ( $\sim 400\text{ cm}^{-1}$ ), C-H out of plane and deformation modes of aniline ( $\sim 600\text{ cm}^{-1}$ ), -C-N stretching ( $\sim 1200\text{ cm}^{-1}$ ) and C-C quinoid stretching ( $\sim 1400\text{ cm}^{-1}$ ) are visible.



**Figure 4.20: XRD Diffraction pattern of Ag / PANI ES electrodeposited onto a SWCNT electrode through a commercial PAM.**



The XRD (Figure 4.20) shows a broad peak centred at  $2\theta=22.54^\circ$  and can be ascribed to weak ordering parallel to the PANI polymer chain. Sharp peaks centred at  $2\theta=38.62^\circ$  and  $33.76^\circ$  correspond to the Ag (111) plane and glass respectively.

#### 4.3.4 PANI on SWCNT Electrode by Filtration through a Commercial PAM

A Bucky paper was made as in section 4.3.2 with 0.01 g SWCNT in 200 mL NMP but left on top of the PAM in the Buchner funnel (i.e. not reversed as before). A solution of ES was made (0.1 g ES in 100 mL NMP) and added to the Buchner funnel. The membrane was then dried as before.

Analysis (Raman, Figure 4.21) showed that PANI was found on the bottom of the PAM under the Bucky paper only i.e. it went through the Bucky paper.

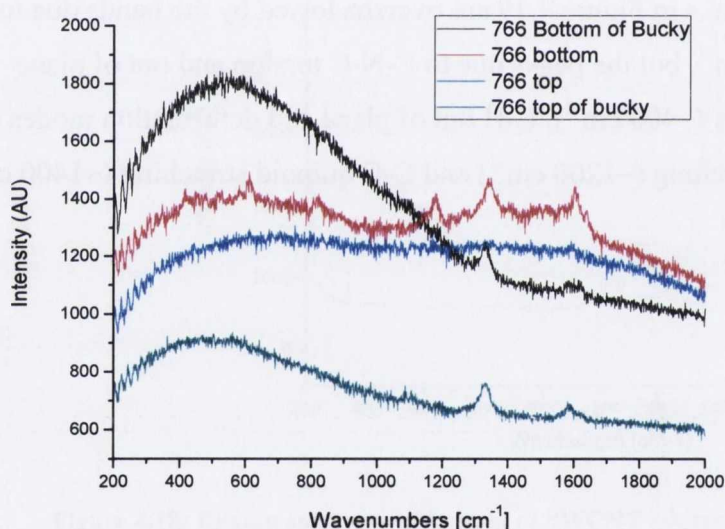


**Figure 4.21: Raman spectra of top and bottom of commercial PAM and top and bottom of Bucky paper after filtration of ES (excitation  $\lambda = 633$  nm)**

#### 4.3.5 PANI on Commercial PAM by Filtration

0.113 g ES (see section 4.2.1 for preparation) was dissolved in 100 mL NMP and filtered through a commercial PAM (Whatman Anodisc 47mm, 0.02  $\mu\text{m}$ ). A film was formed on top of the PAM but Raman confirmed the presence of PANI on both the top and bottom of the PAM so PANI had successfully gone through the pores.

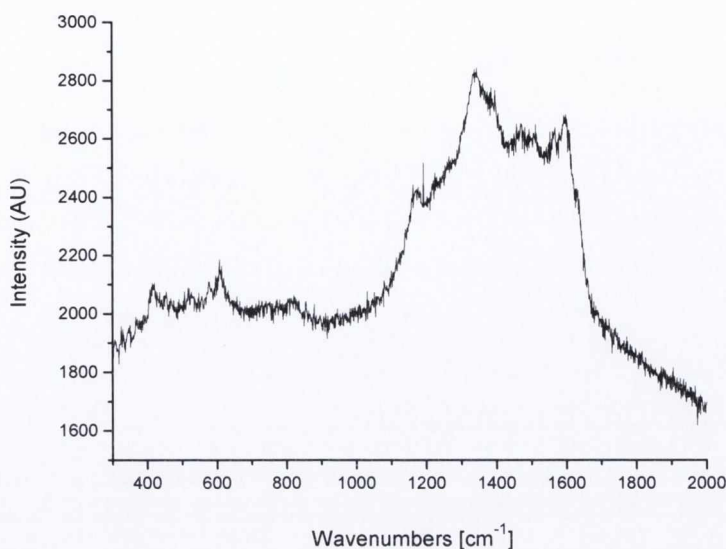


**Figure 4.22: Raman spectrum of bottom of commercial PAM after filtration of ES (excitation  $\lambda = 633$  nm)**

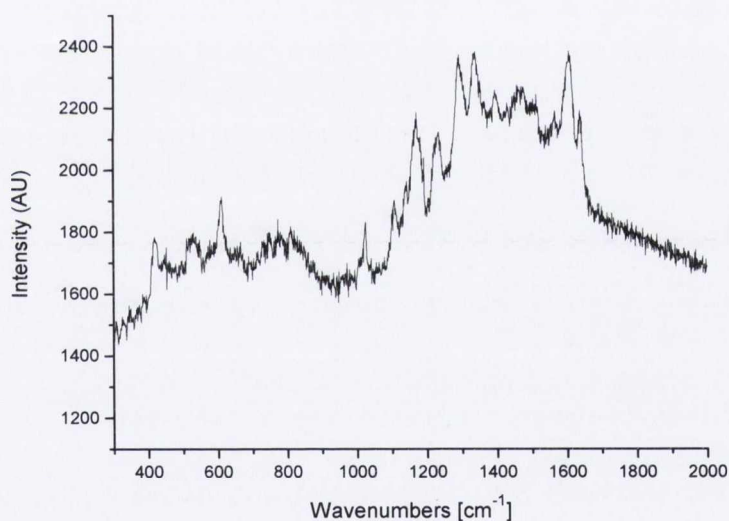


**Figure 4.23: Raman spectrum of top of commercial PAM after filtration of ES (excitation  $\lambda = 633$  nm)**

Characteristic PANI peaks {C-N-C torsion and out of plane deformation of benzenoid rings ( $\sim 400$   $\text{cm}^{-1}$ ), C-H out of plane and deformation modes of aniline ( $\sim 600$   $\text{cm}^{-1}$ ), amine deformation ( $\sim 800$   $\text{cm}^{-1}$ ), -C-N stretching ( $\sim 1200$   $\text{cm}^{-1}$ ), C-C quinoid stretching ( $\sim 1400$   $\text{cm}^{-1}$ ) and -C=N stretching ( $\sim 1500$   $\text{cm}^{-1}$ )} are present in both spectra (Figures 4.22 and 4.23). However the peaks are more defined in the top of the membrane (Figure 4.23) which contains more product. Extra peaks due to ring deformation ( $640$   $\text{cm}^{-1}$ ) and C-H bending of quinoid ( $1160$   $\text{cm}^{-1}$ ) are also visible. The strong peak at



1170  $\text{cm}^{-1}$ , due to the presence of the sulphate group, and the two bands at 1335  $\text{cm}^{-1}$  and 1405  $\text{cm}^{-1}$ , typical of the emeraldine salt form, are visible in both cases.

#### 4.3.6 PANI on Gold Electrode by Electrodeposition through a Commercial PAM

50 nm of gold was sputtered onto the back of a commercial Pam. PANI was deposited by AC at 9 V for 10 min as described in chapter 3 section 3.2.3.1.. Raman showed deposition was successful (Figure 4.24).

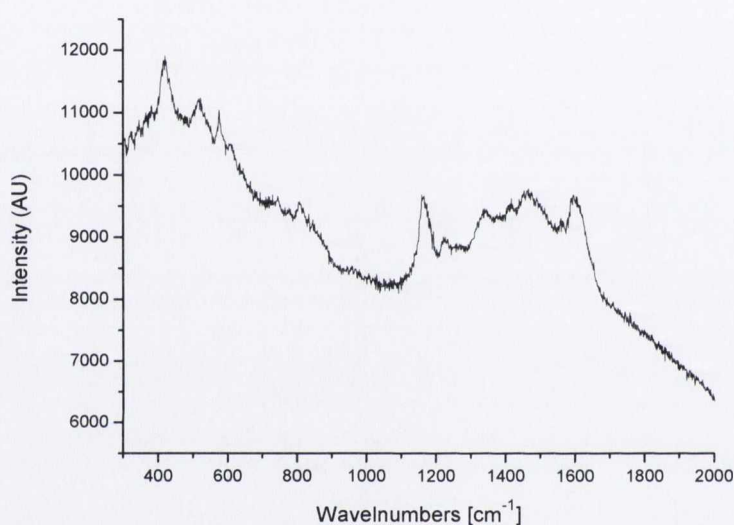


**Figure 4.24: Raman spectra of top of commercial PAM after deposition of PANI**

**(excitation  $\lambda = 633 \text{ nm}$ )**

#### 4.3.7 Summary

Ag / PANI composite films were successfully deposited on top of MWCNT and SWCNT electrodes. Deposition was facilitated by using a PAM as it added stability to the system and the Bucky paper peeled off easily after deposition. Thus it is possible to modify the Bucky paper. Deposition of PANI through a commercial PAM on a MWCNT electrode failed, although it was possible to deposit PANI into one of these PAMS using a sputtered gold electrode on the back. It was also not possible to deposit PANI on the SWCNT by filtration although filtration of ES through the PAM worked. This is probably due to the high porosity of CNTs.

## **4.4 Conclusions and Potential Applications**

PANI and Ag / PANI composite films were successfully deposited on ITO and Bucky paper electrodes. Dispersions of PANI and Ag nanowires were also cast onto glass substrates.

The applications of such structures / potential devices are enormous. PANI is already well known as a sensor for chemical vapours and biomaterials [385, 363, 364, 389, 553, 554]. The conductivity of PANI changes from  $\sigma = 10^{-10} \text{ Scm}^{-1}$  for the undoped insulating EB form to  $\sigma = 1 \text{ S cm}^{-1}$  for the conducting ES form [555]. This change is highly sensitive to chemical vapours and could be used in a sensor such as a chemical resistor [555]. The sensitivity of the sensor would be improved by using nanomaterials because of their greater exposed surface area which leads to greater penetration depth for the gas molecules. Wallace and co-workers describe the fabrication of an amperometric sensor from PANI nanoparticles [556]. There is also evidence that PANI / metal nanoparticles composites are better sensors than PANI alone [391, 392, 410, 448]. Other applications of PANI thin films include their use as a pH sensor [557] and anti-corrosion covering [371, 372, 373, 558]. PANI / nanoparticles composite materials have been used in ink jet printers [559, 560], in the fabrication of a non-volatile plastic digital memory device [561] and as catalysts [562, 563, 564]. Ag nanoparticles also have applications in catalysis and photonics [202, 329] and as antibacterial agents [90]. The possibility of using the Ag / PANI composite nanostructures fabricated in this thesis as antimicrobial agents and antibacterial coatings on surfaces is explored in chapter 5, section 5.4.



## Chapter 5: Device Applications

### 5.1 Nanowire array electrodes for light emitting diodes

Organic light emitting diodes (OLEDs) were fabricated by Adam Strevens using electrodes made from metallic nanowires arrays. The devices were compared to those which had been fabricated with conventional planar anode structures.

#### 5.1.1 Background

LEDs based on conjugated polymers have been fabricated since Burroughs et al. demonstrated the possibility of using electroluminescent polymers such as poly (para-phenylene vinylene) as the active element in a large-area LED in 1990 [353]. By 2000 this was a widely researched area and electroluminescent or semiconducting polymers were designed for applications such as LEDs, displays and photovoltaics [565]. Currently the emphasis is on increasing the efficiency and brightness of devices such as OLEDs [566, 567]. This would involve using high currents while limiting joule heating which would potentially affect the performance and life time of such a device [568]. Wilkinson et al. have shown that as the active area of the device cathode is reduced the device is less susceptible to joule heating, and by reducing the pixel size of the electrode the thermal management of the device is improved and the current density can be increased [567]. Thus a device which has a nanowire array electrode should have the same effect.

#### 5.1.2 Device Fabrication

An OLED was fabricated using an organic light emitting material sandwiched between a metal- filled PAM and a planar metal electrode as shown in Figure 5.1.

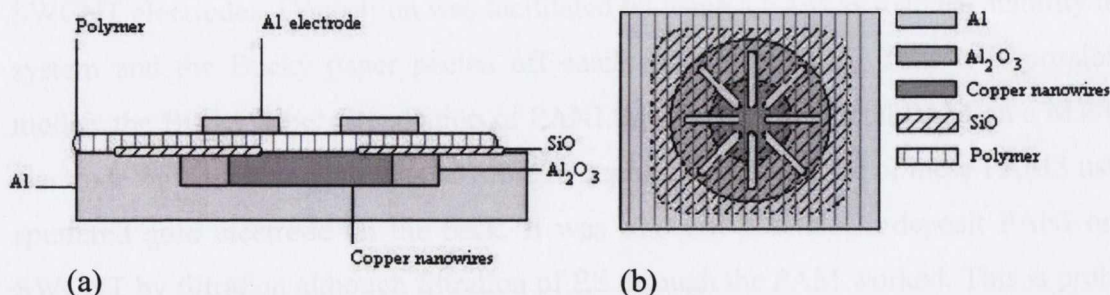


Figure 5.1: (a) Profile of the nanowire array device structure showing the multiple layers of the structure and (b) a top view showing the build up of layers on top of the sheet of aluminium foil [324].

The nanowires arrays were produced as described in chapter 3, section 3.2.1. Two types of PAM electrodes were produced, a Cu filled electrode which was plated by AC deposition and a Ni filled electrode which was plated by PED. All PAMs were produced by double anodisation (9 hr + 4 hr) of 99.999% purity, 0.25mm thick, 50 mm x 50 mm square sheets of Al foil in oxalic acid at 40 V for consistency. SEM imaging and UTHSCSA image analysis revealed the PAMs to have pores of average diameter  $50 \text{ nm} \pm 10 \text{ nm}$  and centre to centre pore spacing of  $123 \text{ nm} \pm 21 \text{ nm}$  (see Appendix 1). Cross sectional analysis by Alcové GmbH measured the PAM height as approx  $8 \text{ }\mu\text{m}$  {see chapter 3, figure 3.16 (b)}. The circular anodic alumina area (diameter 30 nm) was centred on the Al square foil and the filled metal array (diameter 20 nm) was concentric with this area.

Overfilling of the Cu PAMs was avoided by taking cross-sectional images of different filling times, and plating for just enough time to insure that the wires were almost at the top of the PAM, so that any polymer deposited on top would be in contact with them and that no Cu islands, which could lead to electrical shorts, would be on the surface of the PAM (see Figure 3.16 (b), section 3.2.1.2.2, chapter 3). It was found that 8 min was sufficient to fill a PAM which was fabricated in oxalic acid as described above. However devices made with an unfilled PAM and PAMs which had been filled for 4, 6 7 and 8 min were also fabricated for testing purposes. The Ni nanowires arrays were filled by PED, which results in 80-95% pore filling, so overfilling would lead to many more islands on top of the PAM. It was thus decided to mechanically polish the PAMs as described in 3.2.1.2.1. After polishing SEM images {Figure 3.15 (b) and (c)} showed that the surface of the PAM consisted of a well dispersed Ni nanodot array with close to 90% filling of the pores. This has the advantage that the contact area of the Ni can be more readily determined and the current density of the resulting array electrode can thus be more accurately estimated [296]. The surface roughness of the PAM is also improved after polishing. AFM cross-sectional images revealed that an unpolished membrane had, at best, a surface roughness of 30 nm over a  $2 \text{ }\mu\text{m}^2$  area whereas the polished membrane had a surface roughness of less than 5 nm over a similar area [296].

The remaining OLED layers were deposited on top of the nanowire arrays. The first layer was a 200 nm thick layer of silicon monoxide (SiO) which was thermally evaporated from a resistively heated tungsten boat at a vacuum of  $2 \times 10^{-6}$  mbar and a rate of 0.5-1.5 nm / s. A mask was used so that the SiO layer did not cover the central disk shaped area (diameter 15 mm), where the nanowire array was, and the outside edge



so that an electrical contact could be attached to the aluminium. Thus the active region of 6 mm<sup>2</sup> area was separated from the boundary of the unfilled and metal-filled PAM which is prone to overfilling. This area was then spin-coated with the polymer ethenylene-2-methoxy-5-(2-ethylhexyloxy)-1,4-phenylene-ethenylene-1,4-phenylene)] (TPD-MEH-PPV) (see Figure 5.2) at 1500 rpm from a 15 g / L chlorobenzene solution. The thickness of the polymer layer was measured to be 100 nm ± 10 nm using white light interferometry.

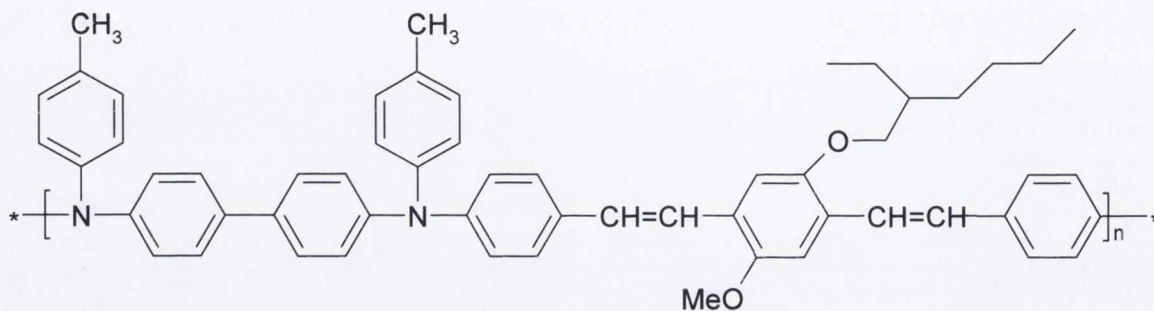


Figure 5.2: Chemical structure of TPD-MEH-PPV, the emissive polymer used in the OLED devices

Al contacts {(as shown in Figure 5.1 (b))} were thermally evaporated onto the polymer layer at a rate of 0.2 nm / s using an Edwards Autovac 306 evaporator fitted with a calibrated quartz crystal thickness monitor. An alternative device which had a solid layer of Al evaporated on top to form a 100 nm thick cathode as shown in Figure 5.3 was also made.

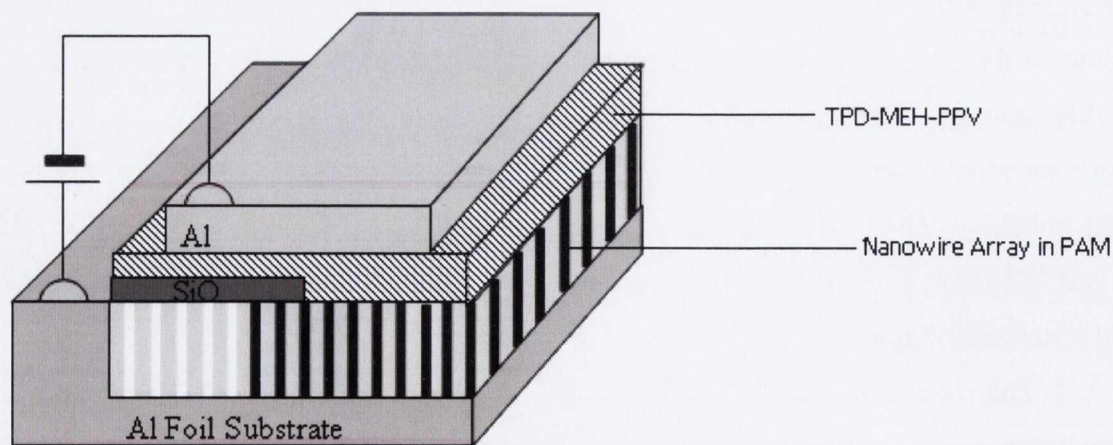


Figure 5.3: Chemical structure of TPD-MEH-PPV, the emissive polymer used in the OLED devices

[325].

The Al foil substrate forms the other electrode which has contact to the metal nanowires through metal filaments which were formed between the nanowire array and Al foil during the electrodeposition process [242].

For comparison devices with planar Cu and Ni electrodes were made by evaporating a 120 nm thick layer of Cu or Ni onto an unanodised Al foil to cover exactly the same area as the nanowire array in the other devices. SiO<sub>2</sub>, TDP-MEH-PPV and aluminium were deposited on top as before to give the same pixel area of 6 mm<sup>2</sup>.

### 5.1.3 Device Characterisation

#### 5.1.3.1 Current voltage characteristics

The DC current voltage characteristics of all the devices were measured at room temperature using a Keithley 2400 source meter interfaced to a PC. The results for the devices made with Cu nanowire arrays, a conventional Cu planar electrode and an electrode made from an empty PAM are shown in Figure 5.4. The current density (J) flowing in the Cu filled PAM electrodes was calculated by multiplying the cross-section of the active area by the pore density of the PAM. The pore density was calculated to be  $10.9 \times 10^{-13} \text{ m}^{-2}$  by the method of Gösele and co-workers [158].

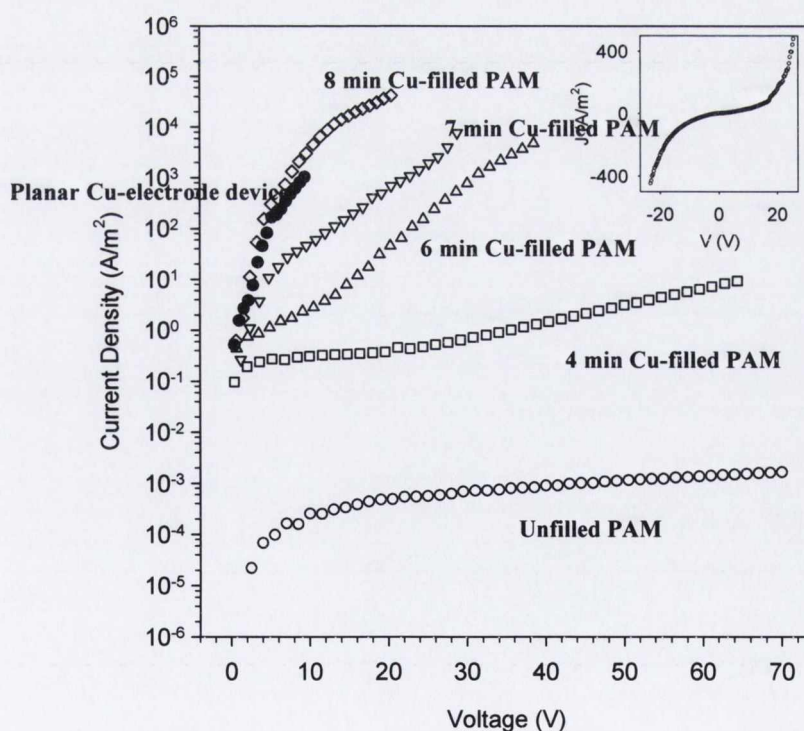


**Figure 5.4: Current Density vs. Voltage for the device made with an unfilled PAM, Cu filled PAMs and a planar electrode. The inset shows the positive and negative bias characteristic for the 7 min Cu-filled PAM device [325].**



Figure 5.4 shows that there is current flow in all the devices except the empty PAM. There is even some current flow in the under-filled 4 and 6 min PAMs due to impregnation of the pores by polymer. The highest values were obtained for the device made with the 8 min filled PAM, but it was found to be unstable (probably due to electrical shorting caused by overfilling of the pores). The devices made with 6, 7 and 8 min filled PAM electrodes attained a higher current density before failure than the device made with the planar electrode. This is attributed to improved thermal management of the devices as only the polymer film directly above the nanowires is excited. Because of the many individual active volumes in the PAM device heat stability is improved which allows an increase in current density before breakdown occurs. The inset in Figure 5.3 shows J-V data for the best device (7 min filled PAM) in forward and reverse bias. Unfortunately there is no rectification probably because the work function of Al and Cu are similar (4.28 and 4.65 eV respectively) [569].

Better rectification was obtained in the Ni nanowire electrode devices, probably due to the increased work function of Ni (5.15 eV), which is a better match for the HOMO of the polymer and should therefore improve hole injection [296]. They also achieved a higher maximum current density than the Cu nanowire electrode devices, which is not surprising, as the PAMs were filled by PED. This leads to increased filling and a much smaller barrier layer due to the longer voltage reduction after anodisation.

The ideality factor for devices can be calculated from the ideal diode law which can be expressed as:

$$I = I_0 (e^{qV/nkT} - 1) \quad (5.1)$$

where:

$I$  = the net current flowing through the diode;

$I_0$  = the diode leakage current density in the absence of light;

$V$  = applied voltage across the terminals of the diode;

$q$  = absolute value of electron charge;

$n$  = ideality factor

$k$  = Boltzmann's constant; and

$T$  = absolute temperature (K) [570].

for  $V > 50 - 100$  mV the -1 term can be ignored and so the above equation becomes:

$$I = I_0 (e^{qV/nkT}) \quad (5.2)$$

Therefore:  $\ln(I) = \ln(I_0) + (q/nkT)V$  (5.3)

Thus the slope of  $\ln(I)$  versus  $V$  gives  $q / nkT$  and at 300K  $kT/q = 28.85$  mV (thermal voltage) [565] so the ideality factor  $n$  can be calculated from:

$$n = 1 / \text{slope} \times 1 / 28.85 \text{ mV} \quad (5.4)$$

for the 7 min device the slope of  $\ln(I)$  versus  $V$  is  $30 \times 10^{-4}$  so  $n = 1.04$  for voltages between 0 and 30 V. For an ideal diode  $n = 1$  and recombination occurs via band to band or via traps in the bulk areas from the device (i.e. not in the junction) [565].

### 5.1.3.2 Electroluminescence (EL)

PAMs with semi-transparent Al electrodes (deposited to a thickness of 20 nm) were used for EL studies. A thin film of TDP-MEH-PPV was made for comparison. PL and EL measurements were made using an Oriel Multispec CCD spectrometer coupled to a liquid light guide. The thin film was excited by a 370 nm UV diode

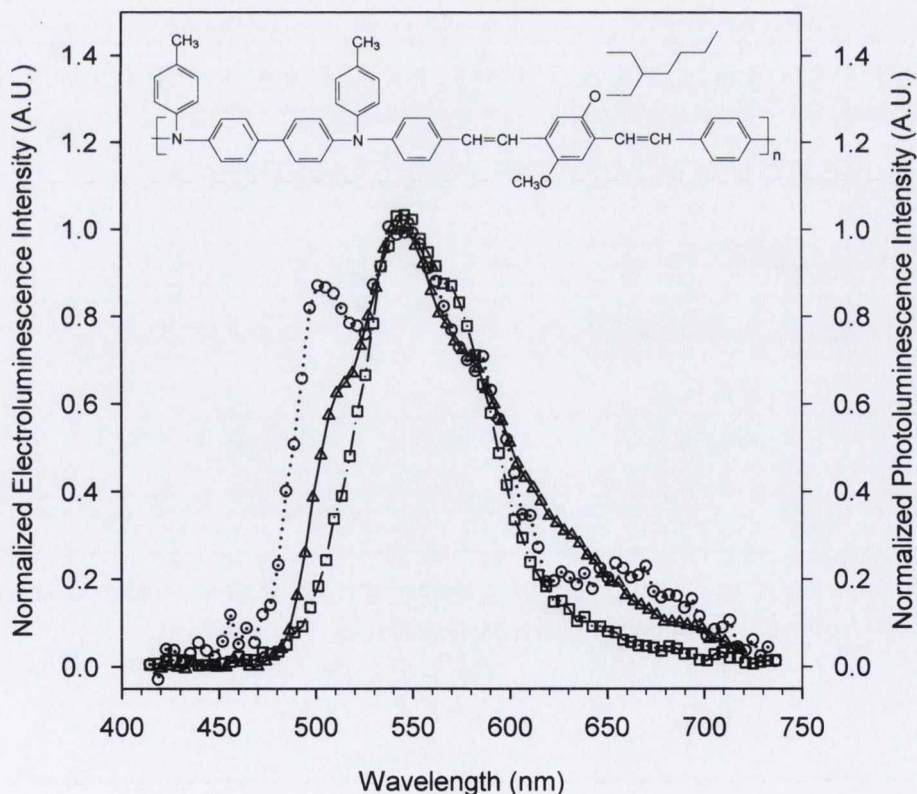
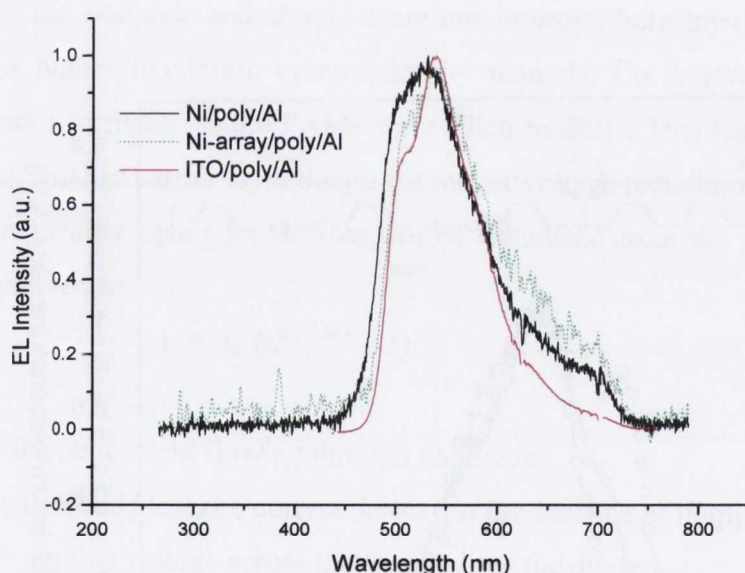


Figure 5.5: EL spectra for the 7 minute Cu-filled PAM (open circle and dotted line) and the Cu planar electrode device (open square and dash dot line) compared to the PL spectrum for the emissive material (open triangle and solid line). The inset shows the chemical structure of the emissive polymer [296].



Figure 5.5 shows normalised EL from the devices with planar and nanowire Cu electrodes compared to the PL from a neat film of TDP-MEH-PPV. The maximum emission of the polymer at 544 nm remains unchanged in all spectra indicating that the emission is from the light emitting polymer layer in all cases. There is a high energy shoulder peak at 505 nm in the film PL and nanowire EL device which is suppressed in the Cu planar device. The very noisy hump centred around 640 nm in the nanowire EL is due to shorting across the polymer layer [296]. The non-normalised spectra (not shown here) indicate that the brightness of the array devices is much larger than that of the planar devices [296]. The EL spectra of the Ni devices are similar except emission from the planar devices is broader as shown in Figure 5.6.

The un-normalised spectra indicate that the brightness of the array device is much better than the planar devices [296].



**Figure 5.6: EL spectra of Ni nanowire array device compared to the Ni planar electrode device and an ITO electrode device [296].**

### 5.1.4 Summary

Electrodes made from metallic nanowire arrays were incorporated into single layer organic light emitting diodes which used the light emitting polymer Poly[(4-methylphenyl) imino-4,4'-diphenylene-(4-methylphenyl)imino-1,4-phenylene-ethenylene-

2 – methoxy –5 - (2 -ethylhexyloxy) - 1,4-phenylene-ethenylene - 1,4 - phenylene)] as the emissive material. The DC current-voltage characteristics of both devices were measured and compared to equivalent devices with a planar metal electrode. Due to the reduction in active area in the nanowire device from that of the planar device the current density reached in the nanowire array anode device exceeded that in the planar anode device by a factor of eight. The Ni array devices had better rectification than the Cu ones and afforded a higher maximum current density. The electroluminescence spectra were also measured and a relative increase in the electroluminescence intensity was observed for the nanowire electrode devices. It is thus possible to use an array of nanowires as an electrode to inject charge into a polymer film. The individual nanowires in these arrays are comparable to the smaller individual emissive or “active” areas than have previously been published in the literature.

## **5.2 Metallic nanowires as catalysts for carbon nanotubes (CNT) growth**

### **5.2.1 Background**

Since their discovery by Iijima in 1991 [571], and the realisation of their potential due to their novel mechanical and electrical properties as outlined by Baughman et al. in 2002 [406] the production of CNTs has escalated.

The first large scale production of CNTs was done by Ebbesen and Ajayan in 1992 by plasma arcing [572]. It involves applying an electric current across two graphite electrodes in an inert gas atmosphere. In this process cations are evaporated from one electrode and deposited on the other electrode [573]. Analogous to this is the arc discharge method which was used by our group to produce CNTs from 1994 to 2004 [149-156, 405, 574]. CNTs are created through arc vaporisation of two carbon rods placed end to end with a small gap of ~ 1 mm between them. However a mixture of CNTs and soot; which contains impurities, catalytic residues and amorphous carbon is obtained, so further purification is necessary. Greater purity is achieved by laser vaporisation of graphite rods, which was invented by the Smalley group [575]; however the CNT thus grown are highly tangled and still contain impurities of catalysts and amorphous carbon. One of the most versatile methods is chemical vapour deposition (CVD) which is used by our group today [576, 577, 578]. By this method aligned



MWCNTs and SWCNTs can be made on catalysts such as Fe, Co, Ni and Mo on Si substrates or within the pores of a PAM [297, 579].

Aligned CNTs have been successively grown in PAMs which have been partially filled with metal nanowires by various groups for example Hornyak et al. [580], Zhang et al. [581], Wang et al. [582] and Krishnan et al. [583]. PAMs have also been used as templates for the growth of Y-junction CNT structures [584, 585]. Carbon nanotubes with Y branches were also grown in PAMs without catalysts by Sui et al. [586]. They attribute this to the presence of metal anions incorporated during the preparation of the PAM.

## 5.2.2 Growth of MWCNTs on PAMs

Co and Fe nanowires were electrodeposited into PAMs to act as catalysts for CNT growth. MWCNTs were successfully grown on the PAMs filled with Fe.

### 5.2.2.1 Preparation of PAMs

The PAMs were prepared by anodising aluminium foil (99 %, Goodfellows) as described in chapter 3, section 3.1. Several different size PAMs were made, e.g. 10%  $\text{H}_2\text{SO}_4$  was used at 0 °C at 20 V for the smaller pore diameters, 1%  $\text{H}_2\text{C}_2\text{O}_4$  was used at 40 V and 80 V at 0 °C for pore diameters of approximately 40 nm and 120 nm and 2%  $\text{H}_3\text{PO}_4$  was used at 100 V and 140 V at 10 °C for pore diameters up to 200 nm. The foils were anodized for the times shown in Table 3.1 so that the height of the PAM was approximately 8  $\mu\text{m}$ . They were filled with either Fe or Co by an AC electro-plating procedure at a voltage of 16V as described in chapter 3, section 3.2.1, using the electrolytes listed in Table 3.2. The filling time was chosen so that the PAMs were under-filled; however very little CNT growth was obtained for under-filled PAMs so the filling time was increased. The best result for CNT growth was obtained on PAMs prepared at 80 V in oxalic acid and plated with Fe at 16 V for 8 min. This is because growth tended to occur on flat sections of PAM where metal catalyst had agglomerated on the surface and not actually inside the pores [297]. The Al and barrier layer were removed from the PAM as described in chapter 3, section 3.2.1.2.1. The membranes were then carefully removed from the remaining Al frame using a scalpel. The freed membrane was sectioned into smaller pieces of <1 cm dimensions which were placed in a ceramic boat and loaded into the furnace tube. It is important to use the PAMs immediately after fabrication to avoid

oxidation of the catalyst metal; if this was not possible then they were stored in desiccators.

### **5.2.2.2 Chemical vapour deposition procedure**

The CVD system was built in house by Rory Leahy and described in his PhD thesis [297]. The procedure for growth of MWCNT on PAMs is as follows: the samples were introduced into the CVD chamber which was sealed and pumped down to  $10^{-3}$  mbar for approximately 20 minutes using a mechanical rotary vein pump. The chamber was then flooded with argon to remove remaining oxygen from the system. After 5 minutes the furnace set-point was adjusted to a working temperature of either 700 or 800°C and system was allowed to heat directly to this temperature. The system was purged with argon throughout the run, at rates between 800 and 5000 standard cubic centimetres per minute (sccm). When the working temperature was reached the system was allowed to sit for five minutes before the acetylene flow was started to ensure that the temperature had equilibrated. The acetylene was set at values ranging from 50 sccm to 300 sccm for approximately 60 min but the system was not cooled down for 5 min afterwards to ensure that all remaining acetylene was removed from the system. The set-point was re-set to room temperature, and the furnace was opened so that the heated section of the furnace-tube was exposed to room temperature. Once the system had reached room temperature, the argon flow was stopped, the pump was switched off and the system was gently vented to atmospheric pressure. Then the chamber was opened and the furnace boats were carefully removed.

### **5.2.2.3 Characterisation of Carbon nanotubes grown in the custom-built CVD system**

On removal from the CVD furnace it was noticed that the samples had changed from a translucent white to a shiny black [297]. SEM studies revealed that three types of MWCNTs were grown on iron-filled porous alumina membranes, long tubes and X and Y junction tubes. SEM images of some of the long tubes are shown in Figures 5.7. Tubes grown on a silicon dioxide substrate are also shown for comparison.



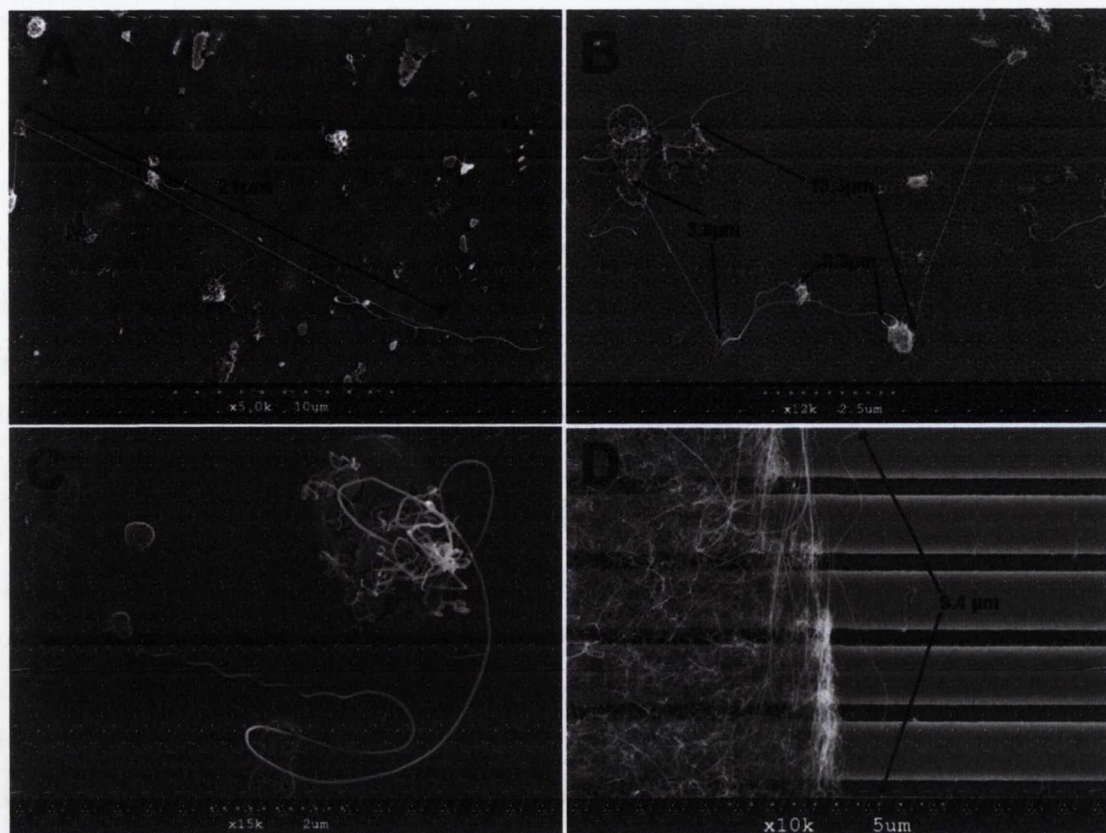


**Figure 5.7: SEM images showing long tubes grown on porous alumina membranes (A-C) and silicon dioxide substrate (D) [297]**

Figure 5.7 shows images of a selection of long tubes with high aspect ratios. Figure 5.7 (A) shows a single long tube grown on the surface of a Fe filled PAM. The growth conditions were set to a temperature of  $800^{\circ}\text{C}$ , an acetylene flow rate of 100 sccm mixed with an Argon flow of 800 sccm for 49 min. Using UTHSCSA the length of the tube was measured as  $21 \pm 2 \mu\text{m}$  with a straight part of  $17 \mu\text{m}$ . The diameter of the tube was measured as  $30 \pm 10 \text{ nm}$ , which gives an aspect ratio of around 800 for this tube. Figure 5.7 (B) shows a network of long tubes also grown on an Fe filled PAM substrate but at a temperature of  $700^{\circ}\text{C}$  under an acetylene flow rate of 100 sccm mixed with an Argon flow of 800 sccm for 56 minutes. Analysis revealed that the lengths of the tubes ranged from  $3.8 - 13.3 \mu\text{m}$  each (standard deviation  $\pm 0.3 \mu\text{m}$ ). The average diameter of the tubes was  $20 \pm 10 \text{ nm}$ , giving aspect ratio of  $1000 \pm 400$ . Figure 5.7 (C) shows another tube grown on the same substrate and under the same conditions as Figure 5.6 (B). It has a length of  $18.0 \pm 0.3 \mu\text{m}$  and a diameter of  $30 \pm 10 \text{ nm}$  giving it an aspect ratio of  $700 \pm 300$ . Figure 5.6 (D) shows long tubes which were grown on an etched Si substrate at a temperature of  $800^{\circ}\text{C}$  under an acetylene flow rate of 50 sccm mixed with

an Argon flow of 500 sccm for 40 minutes. A dense carpet of long entangled CNTs was produced; probably due to the high concentration of catalyst (1%) used which allowed more carbon to be absorbed and longer tubes to be grown.

Junction-structure MWNTs were also observed within large defects (holes or pits) on the surface of Fe filled PAMs (Figure 5.8).

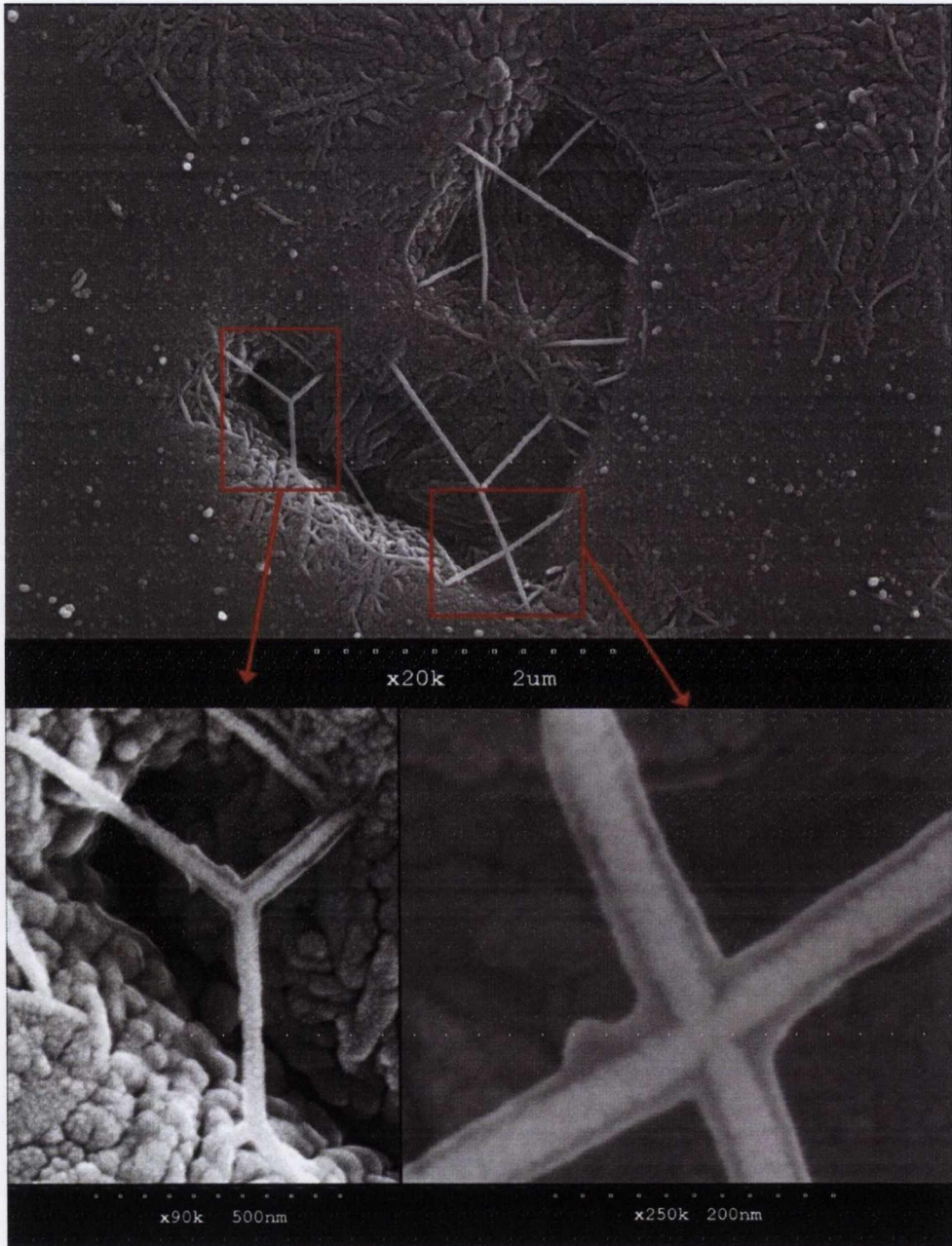


**Figure 5.8: SEM images of CNT junctions grown on PAM substrates [297]**

The CNTs shown in Figure 5.7 were grown at 800°C under a 50 sccm flow of  $C_2H_2$  for 60 minutes. The tubes measured several microns long and had diameters between 30 – 40 nm. It can be seen that the tubes span from one side of the defect to the



other and form Y or X junctions as well as straight tubes. Junction-structure CNTs were also observed from regions raised above the substrate surface. Figure 5.9 shows two separate MWNT junctions suspended above the PAM surface which grew from detritus containing Fe; probably broken shards of PAM scattered on the surface during cutting [297].

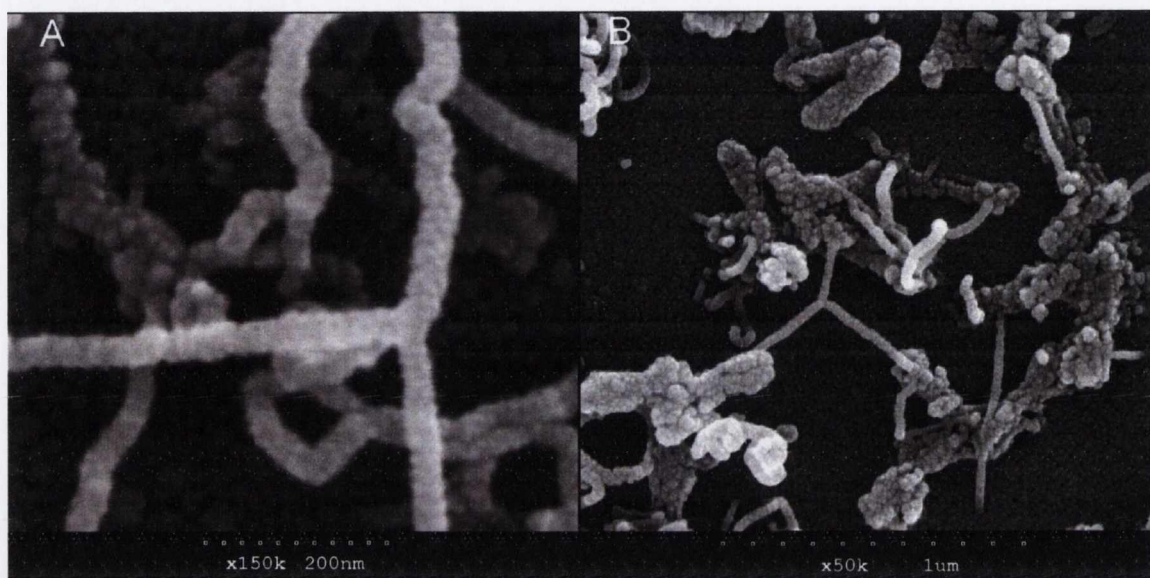


Figure 5.9: SEM images showing two separate Y-junctions grown from raised areas of PAM surface [297].

The nanotubes were analysed by Raman spectroscopy (Figure 5.10).

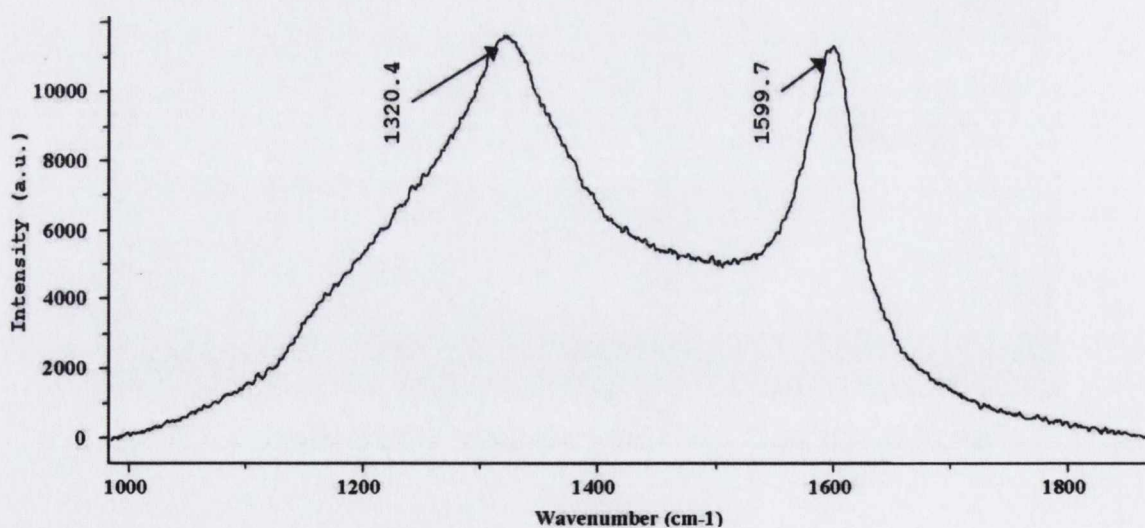


Figure 5.10: Typical Raman spectrum for MWCNTs grown on Fe-filled PAMs. The spectrum was taken using 632 nm laser light [297].

Figure 5.10 shows the Raman spectrum of a long MWCNT on top of a Fe filled PAM. This spectrum has a larger than normal D-band. The D-band can be used as a rough measure of the amount of impurities and defects in a carbon nanotube sample [587]. Ultralong CNT growth is usually achieved when “carbon poisoning” of the catalyst particles is prevented, for example Hata et al. have used water vapour in their gas mix to grow ordered arrays of CNTs 2.5mm high [588]. This is because water acts as a weak oxidiser and selectively removes amorphous carbon from around the catalyst particles without damaging the growing tubes [297]. Our custom-built CVD system contains no inlet for oxidising species so carbon poisoning of the catalyst particles is quite likely and would explain why the D-band is large relative to the G-band in this sample.

Raman spectroscopy on the junction samples showed that samples containing high proportions of junction-structure CNTs displayed a significantly larger D-band than samples containing a lower proportion of junction-structures [297]. This suggests that junction-structure CNTs tend to occur when there is a high degree of defects present in the tubes. These samples also showed a slight up-shift in the position of the G-band which could mean that these CNTs are less well graphitised [587].

The CNTs produced by this custom built CVD should exhibit ohmic behaviour as although some of the walls may be semi-conducting the overall tube would be metallic because there are a large number of concentric walls. Two-probe measurements made on the stem of a single MWNT Y-junction confirmed this. I-V plots were made and a resistance of  $6.0 \pm 0.6 \text{ M}\Omega$  was obtained from the slope of the graph. However, this value is very high compared to theoretical and experimental values measured for individual other SWNTs and MWNTs [589, 590, 591]. The discrepancy for this resistance measurement could be due to contact resistance between the MWNT and the deposited contacts [297]. E-beam lithography was used to deposit gold wires (with a Ti sticking layer) to connect individual Y-junction CNTs. The devices fabricated by this method displayed purely ohmic behaviour.

### 5.2.3 Summary

Three types of MWCNTs were grown on iron-filled porous alumina membranes, long tubes and X and Y junction tubes. Raman spectroscopy revealed that the long MWCNTs had larger D-bands relative to G-bands, which is indicative of carbon poisoning of the catalyst particles. The Raman spectra for the samples containing large amounts of junction tubes also showed increased D-bands relative to G-bands indicating a



high degree of defects present in the tubes. The G-band was also slightly up-shifted in energy suggesting that these CNTs are less well graphitised. I-V plots on single MWCNT Y-junctions showed ohmic behaviour with resistances considerably higher than those quoted in the literature. However this ohmic behaviour combined with successful aligned growth of such devices opens up the possibility of their integration into a larger nano-electronic device as “interconnects” between nano-electronic logic devices.

### **5.3 CdS Nanowire arrays in photovoltaic – organic solar cells**

Solar cells consisting of a CdS nanowire array combined with a light emitting polymer poly[2-methoxy-5-(2'-ethylhexyloxy)-*p*-phenylene vinylene] (MEH-PPV) and solar cells from blended films of nanocrystalline CdS and MEH-PPV were fabricated by Alex Rakovich. Devices fabricated from blended films of bulk CdS and MEH-PPV were fabricated for comparison.

#### **5.3.1 Background**

Solar photovoltaic (PV) energy is one of the most promising renewable energy resources for the provision of clean, efficient and sustainable power [592]. PV cells use semiconductor panels to directly convert the sun's energy into electricity. Silicon is the traditional material for solar cells, but organic semi-conducting polymers are attractive alternatives because of their low cost and versatility (e.g. flexibility, low weight). However they still have low efficiency compared to silicon solar cells [593] because the high binding energies of polymers makes dissociation of electron-hole pairs more difficult and recombination can occur readily because of their low carrier mobilities. Quantum dot semiconductor nanocrystals have become an attractive material for optoelectronic devices because of their narrow size distributions and high luminescent efficiencies [594, 595]. CdS is currently used as a large band gap n-type window material in thin film photovoltaic structures [596]

Recent research has concentrated on hybrid organic- inorganic solar cells. Device efficiency can be improved by adding a material such as inorganic nanoparticles to the polymer, which provides a potential junction for dissociation of the exciton. The nanoparticles act as electron acceptors thus facilitating charge separation electron transport [597, 598]. For example Drees and co-workers investigated the use of fullerenes

and polymers for solar cells [599] and how thermally controlled inter-diffusion could improve the polymer-fullerene interface [600]. Doping polymers such as poly[2-methoxy-5-(2'-ethylhexyloxy)-*p*-phenylene vinylene] with carbon nanotubes has been found to improve EL and PV response [601]. The combination of polymers and semiconductor quantum dots has been investigated by the MIT Institute for Soldier Technologies for fabrication of quantum dot light emitting diodes (QD-LEDs) [602]. They sandwiched the QD monolayer in between organic electron and hole transport layers on top of a transparent inorganic anode deposited on a glass substrate [603]. Alivisatos and co-workers have demonstrated that semiconductor nanorods such as CdSe can be used to fabricate hybrid solar cells with the polymer poly(3-hexylthiophene) [604] and they have recently fabricated hybrid organic-inorganic solar cells based on hyper-branched colloidal semiconductor nanocrystals [605]. Nelson and co-workers have also made hybrid solar cells from poly(3-hexylthiophene) and TiO<sub>2</sub> nanorods [606]. They found that annealing the blend films greatly improved the polymer- metal oxide interaction, resulting in much improved PV device performance [607]. CdS nanoparticles have been found to improve the electrical properties of steric acid / elcosyamine alternate layer Langmuir Blodgett films [608]

Ginger and Greenhamn used photoluminescence efficiency measurements and photoinduced absorption experiments to study the electron transfer between conjugated polymers and semiconductor nanocrystals. They also performed electrical measurements on thin films of nanocrystals in order to study the electron transport processes which are important in photovoltaic devices based on polymer/nanocrystal composites [609]. Conduction and optical studies were performed on nanocrystalline CdS thin films which were fabricated by chemical bath deposition [596, 610, 611, 612].

Similar measurements were performed on the devices made in this work [613].

### 5.3.2 Device Fabrication

Two types of devices were fabricated. The first type is made by one using a blend of a conducting polymer and inorganic semiconductor as shown in Figure 4.10 (a). The second type involves using an array of semiconductor nanorods in a PAM, the tips of which were exposed and covered with the polymer as in Figure 5.11 (b).



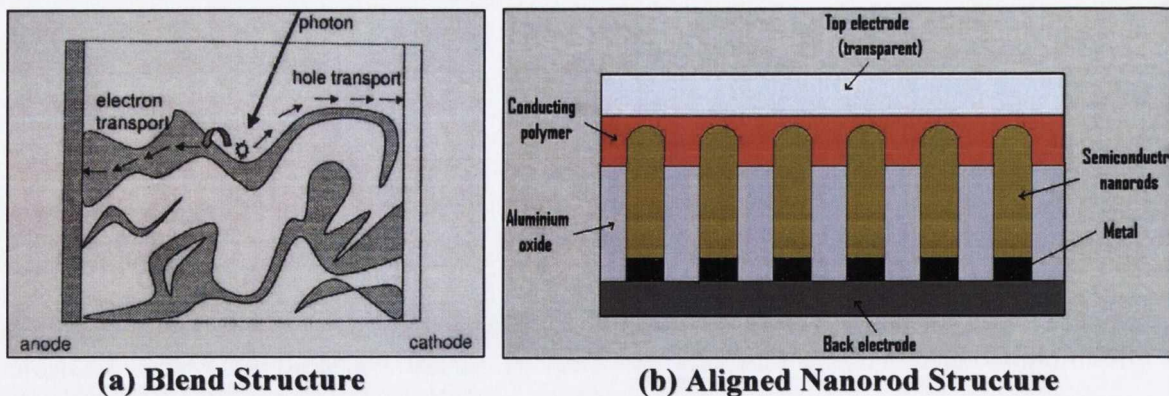


**Figure 5.11: Schematic of device structures for (a) blend and (b) nanorod / conducting polymer composites [613].**

The active materials used in the devices were poly [2-methoxy-5-(2'-ethylhexyloxy)-*p*-phenylene vinylene] (MEH-PPV) (structure shown below in Figure 5.12) and CdS. The CdS acts as an electron transporting material and provides an interface for exciton splitting as shown in Figure 5.11 (a). Chemicals were purchased from Sigma-Aldrich and used without further purification. The nanocrystalline CdS thin films were deposited by a wet chemical technique involving the reaction of thiourea and cadmium chloride (CdCl<sub>2</sub>) [612]. The nanowire array was made in a PAM which was anodised at 20V for 2.5 hours and filled with CdS using an electrolyte containing 0.055 M CdCl<sub>2</sub> and 0.19 M S in DMSO at 120°C and 30 V AC for 3 hours as described in chapter 3, section 3.2.3.1.

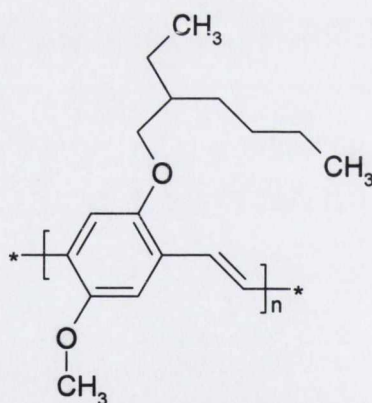


**Figure 5.12: Chemical structure of MEH-PPV, the emissive polymer used in the solar cell devices**

### 5.3.2.1 Blend Devices

In these devices ITO on glass was used as the anode. The active layer was a blend of MEH-PPV and CdS made by dissolving 1mg pure MEH-PPV in 1ml toluene and slowly adding different percentage weights of nanocrystalline CdS. This was made by

deposition of CdS from an electrolyte containing 0.02 M CdCl<sub>2</sub>, 0.13 M ammonium chloride (NH<sub>4</sub>Cl) and thiourea in deionised water onto ITO coated glass substrates using a constant DC potential of - 1.4 V. The air-dried thin film was scraped off the ITO and sonicated with the MEH-PPV in a sonic bath (Model Ney Ultrasonic) for 10 min then cast onto an etched ITO/glass substrate by spin-coating at 600 rpm using a Convac 2000 spin coater. The blend is sonicated to insure that the nanocrystalites are well dispersed in the polymer solution to insure maximum solubilisation and PL efficiency [597]. Al contacts {(as shown in Figure 5.13 (a))} were thermally evaporated onto the blend layer at a rate of 0.2 nm / s using an Edwards Autovac 306 evaporator fitted with a calibrated quartz crystal thickness monitor. Figure 5.13 (b) shows a schematic of the device [613]. A device with bulk CdS (Sigma-Aldrich) was made for comparison

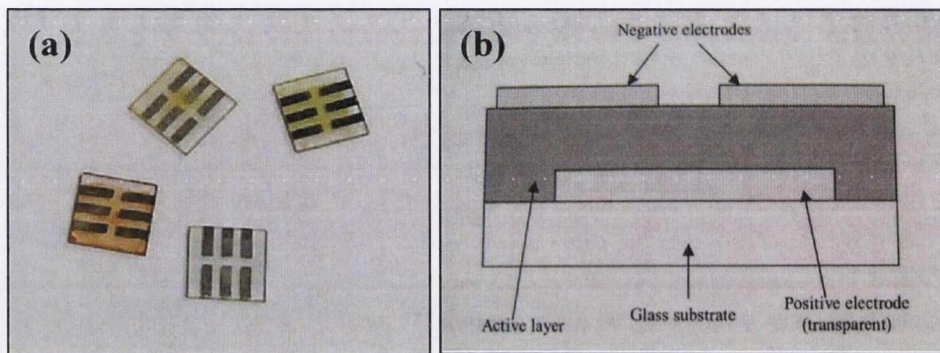


**Figure 5.13: Blend solar cells on ITO, (a) shows the actual devices with Al electrodes on top, (b) is a schematic which shows the device architecture [613].**

### 5.3.2.2 Nanorod Devices

The Al base of the CdS nanowire array was used as the anode in these devices. The top of the anodised and filled Al foil was mechanically polished as described in chapter 3, section 3.2.1.2 to make sure any over-plated material and surface debris were removed. The tips of the nanowires were then exposed by etching the surface with 0.2 M NaOH for 2 min. A film of MEH-PPV was then cast onto these by spin coating. Finally ITO was sputtered on top to act as the transparent electrode. Pictures of this process are shown below (Figure 5.14).



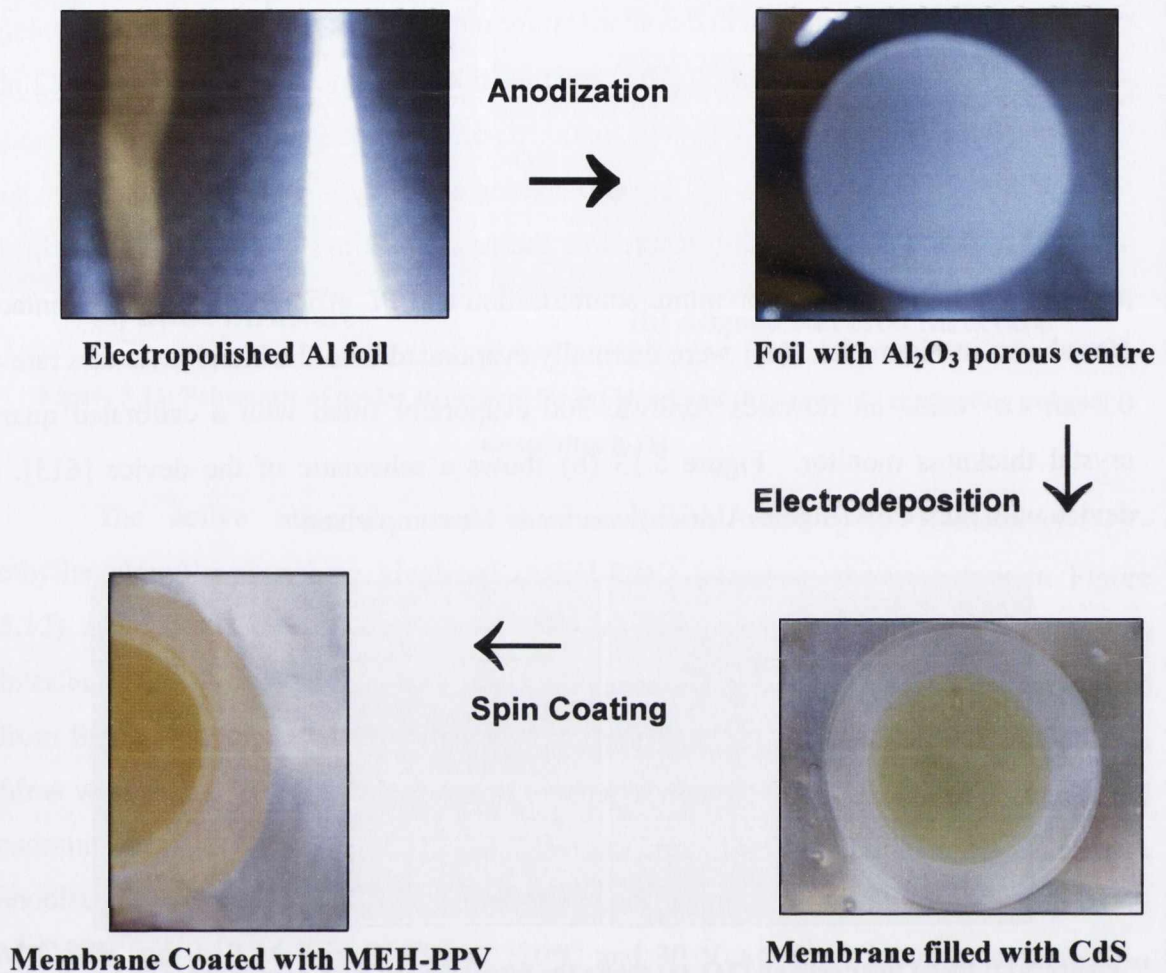


Figure 5.14: Processes used in fabrication of CdS nanorod solar cell device

### 5.3.3 Device characterisation

The devices were characterised for their efficiency as photovoltaic devices by photoluminescence emission spectroscopy and DC electrical conductivity measurements.

#### 5.3.3.1 PL Studies

PL measurements were made using an Oriel Multispec CCD spectrometer coupled to a liquid light guide. The thin films were excited by a 370 nm UV diode. Figure 5.15 shows the PL of the devices made with blended nanocrystallites of CdS and the aligned CdS nanorod array, compared to the PL of a film of MEH-PPV on ITO.

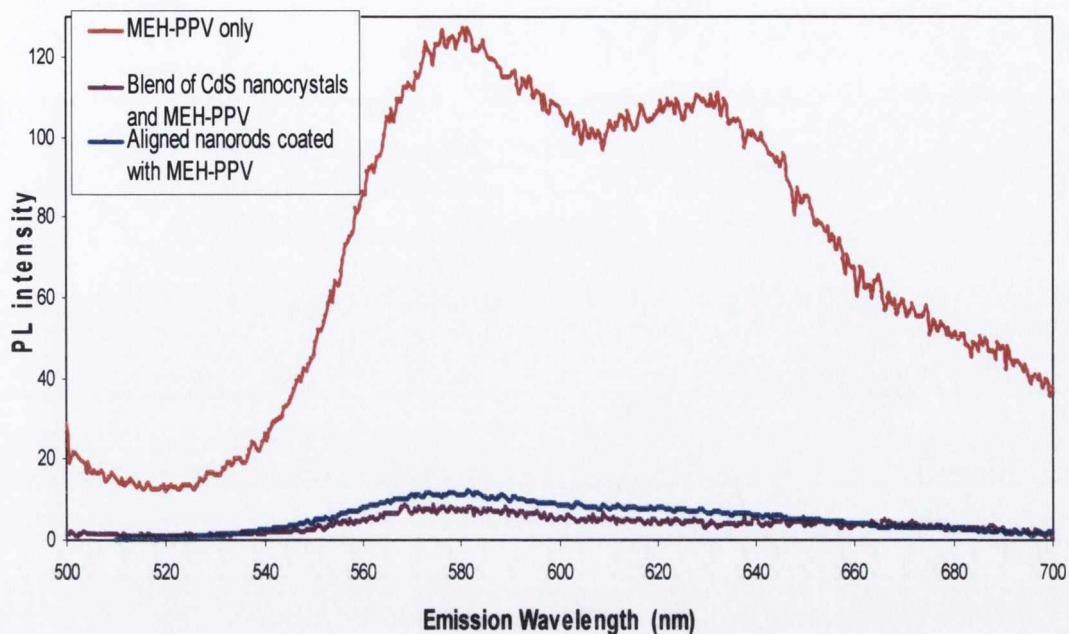


**Figure 5.15:** PL of a film made with a blend of 91% w/w CdS nanocrystals and MEH-PPV, a CdS nanorod array coated with MEH-PPV and MEH-PPV on its own [613]

The PL spectrum of MEH-PPV shows a dominant peak at about 580 nm due to maximum emission of the polymer which arises from single chain excitons and a secondary peak at about 635 nm which is due to dimeric aggregation of polymer chains. There is also a shoulder at around 700 nm which is due to interchain interactive eximers due to aggregation of the polymer chains [614]. However this PL emission is quenched for the devices made with blends of CdS nanocrystals and MEH-PPV, and CdS nanorods and MEH-PPV. This is due to charge transfer from MEH-PPV to CdS, which is an electron acceptor. Both PL spectra are quenched to about 8% of the pure emissive layer indicating that about 92% of the excitons are dissociated and that the quenching probably took place at the MEH-PPV / nanoparticles interface [615]. This implies that the efficiency of the PV device is good, because if the excitons are efficiently dissociated, direct exciton recombination is suppressed and the PL emission is quenched [616].

To investigate the amount of CdS need for efficient quenching different amounts of CdS (bulk) were added to MEH-PPV and the PL spectra taken as before.



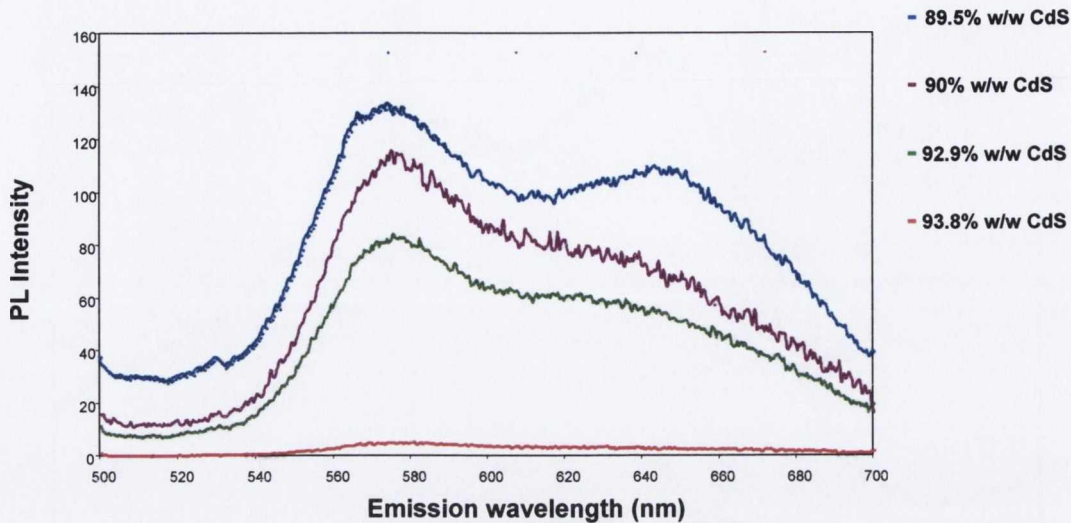


**Figure 5.16: Photoluminescence (PL) of blends of bulk CdS and MEH-PPV [605]**

As can be seen from Figure 5.16 quite a high percentage of CdS is necessary to quench the fluorescence of MEH-PPV, however almost total quenching is achieved at 93.8% w/w CdS. It is also noticeable that the intensity of the peak at 650 nm, which is attributed to the inter-chain exciton emission, increases with decreasing concentration of CdS (or increasing concentration of MEH-PPV) which is probably due to a reduction in inter-chain MEH-PPV chain segment aggregation [617].

The PL of the CdS samples did not contribute to the total PL of the devices but it was also measured for completeness sake. The results are shown in Figure 5.17.

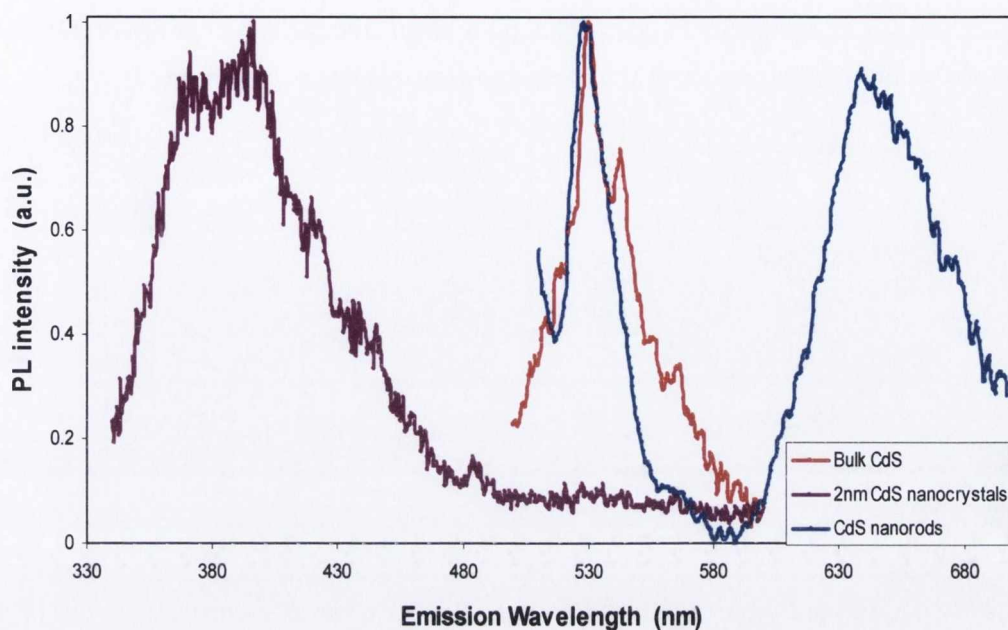


**Figure 5.17: PL of CdS nanocrystals and nanorods compared to bulk CdS [613]**

Figure 5.17 shows that the CdS samples have different emission properties which is due to their different morphology and crystal size. Optical properties are affected as the electronic band structure is transformed into discrete states due to quantum confinement [450]. The observed PL peak for the nanocrystals at 400 nm is blue shifted from bulk CdS (500 – 700 nm) because quantum confinement has occurred. The grain sizes of the crystals have been estimated from a previous study to be approximately 2 nm [612] which is smaller than the diameter of the Wannier exciton for CdS (5 nm). The photoluminescence is due to band edge recombination of surface states energy levels [618]. The CdS nanorods have the same band edge emission as bulk CdS (530 nm) as they are too large for quantum size effects (20 nm). However they show an extra peak at 650 nm which is due to structural defects on the nanowires' surface [201, 450, 458].

### 5.3.3.2 Current Voltage characteristics

It is expected that the energy transfer between CdS and MEH-PPV will improve the performance of the device. To test this current –voltage (I-V) characteristics were measured with a Keithley 2400 source meter at room temperature by applying a voltage across the contacts and measuring the response. The Al is considered to be positively biased with respect to the ITO. Measurements were done in the dark and under a light



intensity of  $100 \text{ m W / cm}^2$  using a solar simulator. The results are shown in Figure 5.18. This shows a rectified behaviour with a rectification ratio of 1.1 at 0.07 V. An open circuit voltage of 67 mV was obtained and the fill factor (ratio of maximum obtainable power to theoretical obtainable power) was estimated to be approximately 1/3.

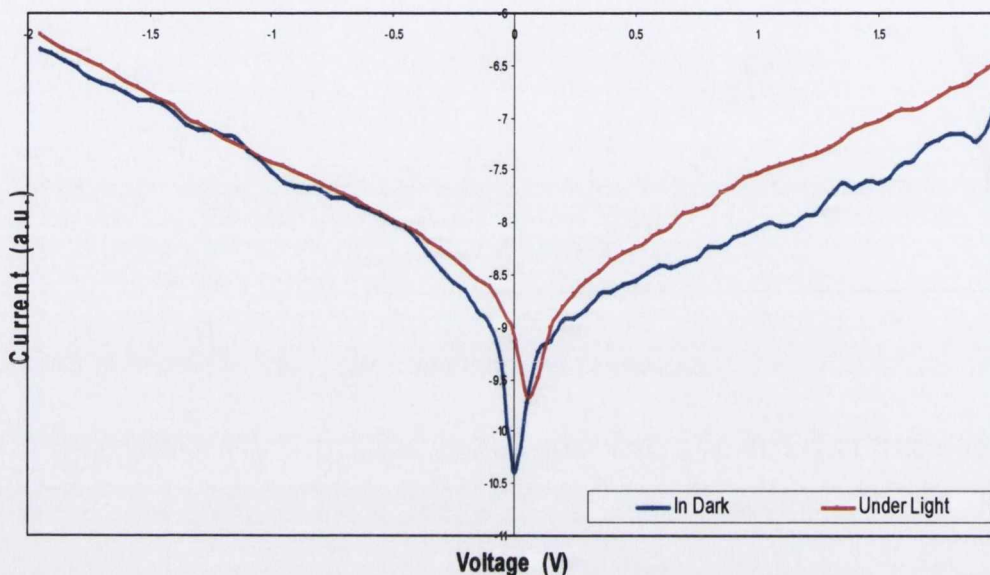


Figure 5.18: I-V curve for a blend of 93.8% w/w bulk CdS and MEH-PPV [605]

### 5.3.4 Summary

Solar cells were made with MEH-PPV as the electron donor and CdS as the electron acceptor. Two types of devices were fabricated with either a blend of CdS and MEH-PPV or MEH-PPV deposited on top of a CdS nanowire array. It is hoped that this will reduce the grain boundaries in the devices which limits the performance of the cells [612]. Quantum efficiency can also be affected by surface defects on nanowires because of their high aspect ratio [618]. The efficiency of solar cells made with MEH-PPV has been found to improve by doping with carbon nanotubes [601] and inorganic nanorods [619] due to photogenerated pair dissociation. This causes quenching of PL emission. In this work quenching in photoluminescence was observed with increased quenching with increasing concentration of CdS. An open circuit voltage of 0.05V measured for the blend which showed strongest quenching. Significant quenching was observed for both nanostructure devices which indicated that efficient exciton splitting and charge separation had taken place [613].

## 5.4 Antibacterial studies of Polyaniline Composites

The antibacterial properties of the Ag / PANI films and nanowires fabricated in this thesis were investigated by monitoring their response to exposure to bacteria. The ultimate goal would be the development of a conductive polymer surface which is antimicrobial.

### 5.4.1 Background

Silver is well known for its antimicrobial properties. It can be added to other materials to prevent bacterial growth or used as an antiseptic to prevent infection. Silver ions and silver compounds such as silver nitrate and silver sulfadiazine are used as disinfectants to destroy micro-organisms found on surfaces. They can be used to destroy bacteria, viruses, algae and fungi without causing harm to humans. In fact silver has been used since 400 BC to store water and prevent the spread of diseases [620].

Recent research has concentrated on the use of silver in coatings to prevent infection. For example antibacterial glass which is covered with a thin layer of silver is now being manufactured for use in hospitals [621], toilet seats with silver ions embedded which kill germs are manufactured by Kohler [622], anti-microbial treatments for textiles and polymers are being developed by Thompson Research Associates [623] and washing machines manufactured by Samsung now contain “Advanced Silvercase™ Technology” by using silver ions in the final rinse cycle [624]. Many antibacterial clothes are now made with silver ions impregnated into the synthetic material (usually a polymer) which is used in the manufacture of the clothes, or by physically weaving silver into the yarn [620].

The combination of a conducting polymer such as polyaniline with silver (Ag / PANI composites) could thus possibly be used to develop new surfaces with antimicrobial properties which could prevent biofilm growth. In fact polyaniline is already used for anticorrosion coatings [371, 372, 373]. Biofilms are formed by colonies of bacteria on surfaces. The outer protective slimy layer is formed as they grow and is very difficult to remove. It also causes damage to equipment and infections in people. Figure 5.19 (a) shows an SEM image of a biofilm growth of *Pseudomonas aeruginosa*, a



gram-negative, aerobic, rod-shaped bacteria, on a plastic surface. Figure 5.19 (b) shows a surface with lower bacterial growth for comparison.

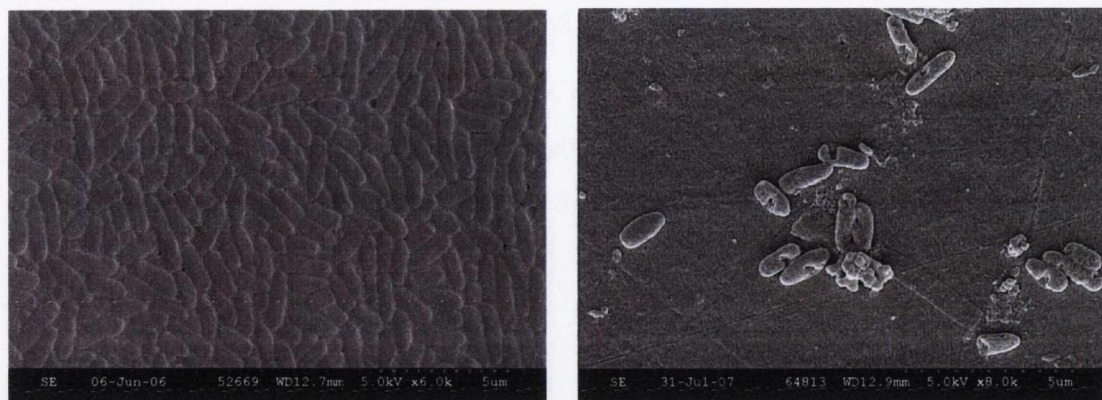


**Figure 5.19: (a) Biofilm growth of pseudomonas aeruginosa bacteria, (b) individual pseudomonas aeruginosa.**

#### 5.4.2 Antimicrobial testing using Agar plates

The antimicrobial properties of the films and nanowires were investigated by exposing them to pseudomonas aeruginosa bacteria which were incubated at 37°C overnight. Bacterial cultures were obtained from Dr Ronnie Russell from the Moyne Institute of Preventative Medicine, TCD. The samples were placed in Agar plates which had been treated with the pseudomonas and were left under atmospheric conditions for 11 days. The area where no bacterial growth took place, called the ‘zone of inhibition’, was compared for each sample.

Figure 5.20 shows an image of an Agar plate containing an Ag / PANI thin film, prepared by electrodeposition of Ag / PANI onto ITO at 1 V for 1000 s, which was exposed to the bacteria for 11 days. It is clear that bacterial growth had been inhibited in a 5 mm area around the thin film (the long side of the glass slide is 10mm).



**Figure 5.20: Ag / PANI thin film, which was prepared by electrodeposition onto ITO at 1 V for 1000 s, after exposure to pseudomonas aeruginosa bacteria for 11 days**

Figure 5.21 shows an image of an Agar plate containing an Ag / PANI thin film, prepared by electrodeposition of Ag / PANI onto ITO at 2.5 V for 2000 s, which was exposed to the bacteria for 11 days.



**Figure 5.21: Ag / PANI thin film, which was prepared by electrodeposition onto ITO at 1 V for 2000 s, after exposure to pseudomonas aeruginosa bacteria for 11 days**



This time there is a much smaller “zone of inhibition”, but in this case the composite film was much thicker as it was made at 2.5 V for 2000 s. As stated in chapter 4, section 4.1.2.4 after 2000 s the film becomes unstable as PANI precipitates out of solution onto the film surface [547] which may lead to a decrease in its antibacterial effect.

Figure 5.22 shows an image of an Agar plate where several drops of Ag / PANI nanowires which were dispersed in water were deposited onto the centre of the Agar. It is clear from this image that a large zone of inhibition exists around the deposited nanowires. This can be attributed to the migration of the silver from the nanowires into the Agar leading to a large area of inhibition. The migration of the nanowires into the Agar may also be a factor due to their small dimensions, however further investigations into the exact mechanism of interaction between the bacteria and the nanowires will have to be carried out before this can be confirmed.

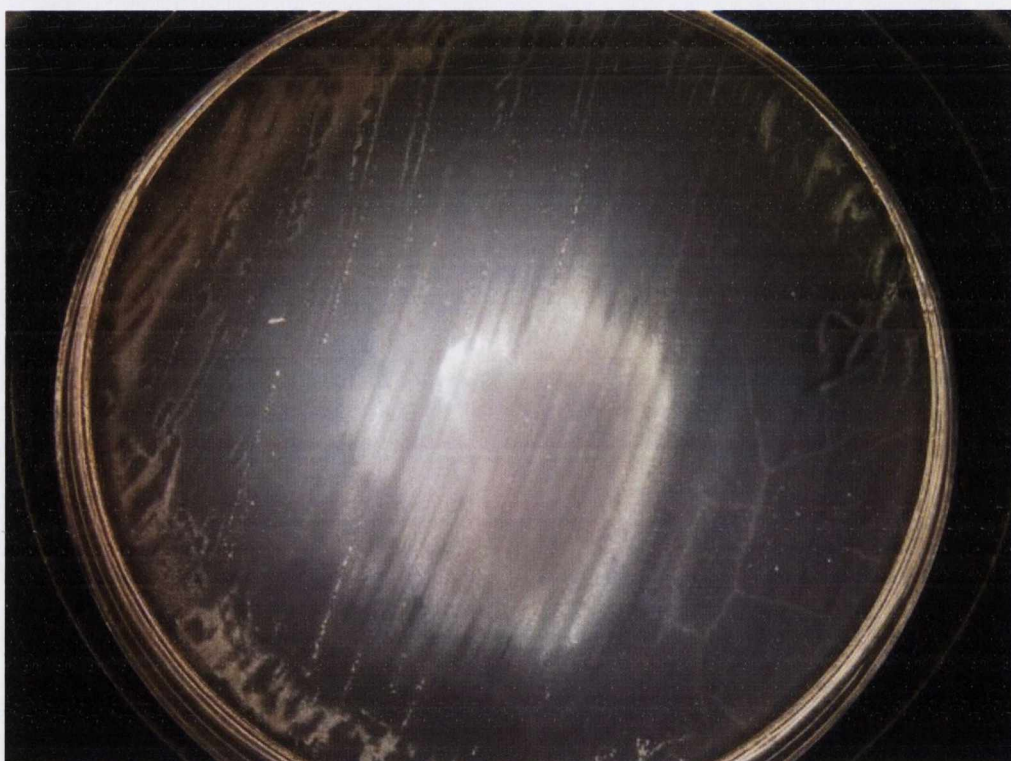


**Figure 5.22: Ag / PANI nanowires, which was prepared by electropolymerisation into a PAM, after exposure to pseudomonas aeruginosa bacteria for 11 days**

To further analyse the bacterial growth the antimicrobial activity of the PANI and PANI/Ag composites was tested by placing 1 cm<sup>2</sup> glass slide sized samples in contact with lawns of *S. Aureus* (Gram positive) and *E. Coli* (Gram negative) microbes. Both samples showed some activity against Gram negative bacteria but not to Gram positive bacteria [625].

## Chapter 6 Conclusions

### 6.1 Conclusions

Porous alumina templates were used for the successful fabrication of one-dimensional nanostructures of metals, polymers, semi-conductors and hybrid materials. This “bottom-up” approach to produce nanomaterials has the advantage that the fabrication of new materials such as organic-inorganic hybrid structures is achievable by careful selection and mixing of starting materials. In addition it is possible to control the size (diameter and length) of these materials [164] and their production is economical and relatively simple. Recent advances in the production techniques of PAMs [160], which improve the arrangement of pores in the hexagonal lattice even further, have ensured that this method to produce 1-D nanostructures remains one of the most popular and successful. Another major advantage is that although it is very easy to remove the nanowires from the PAMs, it is also possible to make devices using the nanowire array in the template because of the inert nature of alumina. This is demonstrated in this thesis, which describes the applications of nanoelectrode arrays in OLEDs and solar cells. It also means that many nanowires, which may otherwise be damaged or oxidised by exposure to the atmosphere, can be characterised in the PAMs as they are transparent in the ultraviolet, visible and infrared spectral range.

Cu and Ni nanowire arrays were fabricated as described in chapter 3 and integrated into OLEDs as described in chapter 5. The advantage of using such an array instead of a planar electrode is the improvement achieved in thermal management of the device due to a decrease in pixel size of the electrode [567]. In a planar electrode the metal is deposited onto the substrate by sputtering or evaporation and the feature sizes are limited by the dimensions of the shadow mask used ( $\geq 100\mu\text{m}$ ) and or by photolithographic methods with a limit of  $0.5\mu\text{m}$ . The alternative electrode structure consists of an array of nanowires which is effectively an array of nano-sized OLEDs. This was the first time such a structure was used in a polymer light emitting diode. The DC current-voltage characteristics of both devices were measured and compared to equivalent devices with a planar metal electrode. The nano-array devices achieved higher DC current densities prior to device failure, with the nickel array devices in particular performing best. This is attributed to the lower work function of Ni, better pore filling of



the PAM due to PED and the fact that the electrical contact between the metal nanowire array and polymer was better than that in the unpolished copper devices. The EL spectrum was found to be unaffected by using a nanostructured electrode. This work has been published in two refereed journals [324, 325].

Metal nanowires in PAMs were also used as catalysts for the growth of carbon nanotubes. Most methods used for the production of CNTs result in tangled or bent tubes; however for many applications it is important to grow aligned nanotubes, e.g. for the measurement of transport properties or in the manufacture of field effect transistors and electronic devices [626]. This has been achieved by CVD using metal catalysts in PAMs for straight [580, 581, 582, 583] and branched [584, 585, 587] CNTs. However aligned growth of CNTs inside the PAMs was not achieved in this work. This could be due to a number of factors; for example the height of the porous layer in the alumina may have been too long to allow the gas flow in the CVD reach the bottom of the pores. Dai and co-workers noted that the SWCNTs they produced on the top of Si pillars did not stick to the floor of the substrate where the gas flow was lower [627]. In this work the catalyst was grown only in the bottom of the pores in the template, however, due to the presence of impurities such as metal anions in the alumina template, it can also act as a catalyst itself so growth of CNTs can occur anywhere [586]. In our case the tubes appeared to grow from defects and impurities on the surface of the alumina and on regions raised above the surface. Other authors have noticed growth from “seed” points, e.g. CNTs have been successfully grown from scratches on Si surfaces [628]. CNT growth also took place above “holes” or “pits” on the alumina surface. Again this is not surprising; horizontally orientated nanotubes have recently been grown across trenches on Si substrates by Huang et al. [629], Lin et al. [630], Leahy et al. [578] and Angelucci et al. [631]. The long tubes grown on these PAM substrates were typically in the order of tens of microns in length; however branched CNT structures such as Y and X junctions were also successfully grown. As before they did not fill the pores of the PAM, but were grown on top or across holes or pits, spanning from one side of the defect to the other. Their growth has been attributed to the presence of defects in the nanotubes such as pentagon and heptagon carbon rings instead of the usual hexagonal carbon rings [584]. This synthesis of branched junctions is important as it is often difficult to achieve using conventional methods [572]. The CNT fabricated here showed metallic behaviour and have dimensions and aspect ratios similar to Si used in IC circuits. Such structures have a number of possible applications e.g. for the separation of ions in aqueous solution [632], as micro-electric motors and as a nanoconducting cable for wiring micro-electronic devices [633],



in electronic devices and circuits [585, 634] and in the development of digital nano-circuits [635, 636, 637].

CdS nanowires were successfully fabricated into PAMs of different pore sizes. Their photoluminescent properties were measured and found to be dependent on the type of PAM used. It was found that both the emission and wavelength of the emission was affected. The intensity of the PL was greater for the nanowires which had been fabricated in PAMs which were made in oxalic acid; and a red-shift in band emission was also noticed for these samples compared to the samples which were fabricated in the PAMs made in sulphuric or phosphoric acid. Semi-conducting nanowires have many potential applications in the photonics industry due to their novel opto-electric properties [187, 435, 437, 437]. CdS, in particular, has been used for solar cells since 1954 [445, 446, 447]. In this work a CdS nanowire array was used in a solar cell with MEH-PPV as the emissive layer. The CdS was acting as the electron transporting material or electron acceptor. Many researchers have investigated the combination of hybrid organic-inorganic solar cells, but to the best of my knowledge this is the first use of a PAM nanowire array in such a structure. It was found that the PL of the device was quenched by 92% which implied that effective charge separation had taken place so it would be suitable as a PV device [616]. Current voltage characteristics of the device showed that a difference in open circuit voltage between the measurements taken in the dark and under an intensity of  $100 \text{ mW/cm}^2$  of 0.05 V was obtained.

Polyaniline nanowires were prepared by electropolymerisation of aniline into the nanopores of an alumina template. The fabrication of composite nanowires containing silver and Polyaniline (Ag / PANI) and copper and Polyaniline (Cu / PANI) was also achieved by simultaneous oxidative polymerisation of aniline and reduction of metal salts to metal silver nanowires. Although similar metal / PANI nanowires have previously been made, this was the first reported synthesis of a composite nanowire which was made in a single step inside an alumina template. HRSEM studies showed that these nanostructures consisted of a polycrystalline metal core surrounded by a polymer coating i.e. they are nanocables. Metal/polymer composites are particularly useful, as they combine the electrical characteristics of metals and the mechanical and processing properties of polymers. Many of these composites show enhanced electrocatalytic activity and increased gas sensing properties [329, 410, 499]. A polymer coating on a metal nanowire would have the further advantage of protecting the nanowire from oxidation and corrosion. The nanocables can be used as an array inside the template or integrated into



devices or chips. The nanocables can also be easily extracted from the PAM and incorporated into other polymers or coatings. This work has also been published [638].

The same method was used to fabricate metal / PANI thin films. This should reduce the problem of aggregation associated with dispersion of nanoparticles into polymer solutions to make thin films [427] which could decrease the efficiency of the material or device. Khanna et al. have shown that uniform size distribution can be achieved by in-situ reduction of Ag salts in aniline [430] and Zhou et al. have prepared similar films by an unsymmetrical square wave current method and demonstrated that they consist of nanofibrous PANI with homogeneously dispersed Ag microparticles [539]. This method is also low cost, deposition rates are high, it can be done at near room temperature, and the properties of the materials can be tailored by adjusting deposition conditions [540].

Silver is well known for its antibacterial properties. The incorporation of Ag into polymers should add antimicrobial functionality to the polymer. The Ag / PANI composites fabricated here could thus possibly be used to develop new surfaces with antimicrobial properties which could prevent biofilm growth. The antibacterial properties of the Ag / PANI films and nanowires fabricated in this thesis were investigated by monitoring their response to exposure to bacteria. They were found to inhibit the growth of *Pseudomonas aeruginosa* bacteria and showed some activity against *E. Coli* (Gram negative) microbes but not to *S. Aureus* (Gram positive) bacteria. The ease of fabrication, anti-corrosive properties and antimicrobial properties of these films makes them ideal candidates for use in protective films and coatings.

## **6.2 Future Work**

The versatility of the template method using PAMs to prepare 1-D nanostructures has been demonstrated in this thesis. This method is universally used by many researchers in the nanotechnology field. However, to keep up to date with the present state of the art it would be necessary to up-grade our set-up. Many of these changes have already been implemented; for example new cells with better temperature control have been fabricated and we are in the process of using an automated computer program to control the anodisation and voltage reduction process. This should improve the homogeneity and ordering of the pores to the grade achieved by Kornelius Nielsch and co-workers [224]. They have also developed a new anodisation process, which is an adaptation of the so-

particular II-IV semiconductors are suitable because they have energy gaps in the visible spectrum. For example the electrical conductivity of CdSe nanowires increases by a factor of 15 when illuminated by visible light so it would be a good candidate for solar cells [641].

Attempts at growing carbon nanotubes inside PAMs were unsuccessful; SEMs showed that the majority of growth took place on the surface of the membrane. An alternative technique was tried by Daren Lee; he used thermal evaporation to deposit catalyst (Ni) at the base of the pores instead of electrodeposition and had some success [642]. SEM indicated that although there was sparser growth than for samples grown with electrodeposited catalyst, growth did take place from the pores of the membrane and not from the surface. The diameters of the tubes are also comparable to the size of the pores. Raman spectroscopy indicated that these samples were of higher purity than the samples grown with electrodeposited catalysts. Future work could involve the growth of CNTs from a nanodots array which could be made from polished samples of overfilled PAMs [285].

The bulk of this thesis was concerned with the fabrication of Ag and Ag / PANI composite nanowires and films. The antibacterial properties of Ag and the anti-corrosive properties of PANI make them ideal candidates for the application of antibacterial coatings and surfaces, which has been studied in this thesis. However these materials have many other possible applications. In particular Ag is well known for its optical properties and PANI is well known as a chemical and biological sensor.

It was already demonstrated (in chapter 3, section 3.2.3.2.4) that the optical properties of the composite nanowires depended on their diameter and this was attributed to the broad plasmon resonance that is red shifted with increasing wire diameter due to the increasing importance of multipole excitations. A study of the linear and non linear optical properties of Ag nanowires in PAMs [518] was done in this group; this could be repeated for Ag / PANI and Cu / PANI nanowires. The change in refractive index of the Ag nanowires in different solutions is presently being studied by Denise Charles with a view to developing a bio-sensor. This could also be developed to include the composite nanowires. Silver nanowires are also suitable for use as an amine vapor sensor. Murray et al. have shown that silver mesowires show a large resistance increase on exposure to ammonia [643]. Because of the increased surface area of nanomaterials they have enhanced sensing capabilities, thus PANI nanowires are more responsive to external stimuli than bulk PANI. The sensitivity of a sensor made from nanostructured PANI would be improved as the gas molecules have a greater penetration depth [391, 392]. In



called called “hard anodisation (HA)”, for long-range ordered alumina membranes. This process is carried out at voltages between 100 – 150 V and produces highly ordered porous templates with aspect ratios (pore depth to pore diameter) larger than 1,000. The PAMs are thicker and can be produced 25-35 times faster than previous membranes [160]. Tsuchiya et al. have recently used new route for the formation of PAMs in neutral electrolytes [639]. They added fluoride ions to the electrolyte which increased the ordering of the oxide layer and influenced the thickness and growth rate of the porous layers. This should lead to greater homogeneity in diameters of the nanowires produced. The nanowires and templates are also influenced by the processing history of the PAMs, for example the outer layer of alumina contains anions from the electrolyte and the nanowires may contain ions from the cathode. To avoid this as much as possible it is advisable to use inert electrodes such as platinum. It is also important to use freshly prepared electrolytes to eliminate the possibility of impurities entering the system and to make sure the anodised foils are well-rinsed to avoid the occurrence of “pitting” as in the CdS samples. The use of a laminar flow hood or clean room would be advantageous. All these features could be easily applied to our system.

As far as device fabrication goes further improvements could be implemented in the fabrication of OLEDs with nanoelectrodes arrays. An increase by a factor of 8.2 was obtained for DC driven nanowire devices which could possibly be improved if the devices were pulse driven. A range of nanoelectrodes with different nanowire diameters could be tested and compared. As well as using other metals it would also be interesting to try some organic materials in the arrays. Further development of the array device structure will include the replacement of semitransparent aluminium electrodes with vacuum sublimed copper phthalocyanine and conductive ITO deposited by plasma sputtering [640].

The CdS solar cell devices also warrant more investigation. Future work for the blend devices should involve the determination of optimum film thickness, CdS concentration and improvement of the blend morphology by varying the solvent, concentration and deposition speed. For the aligned nanorod structures optimisation of nanorods’ diameter (pore diameter) and length (etching time) could be achieved as well as determination of optimum MEH-PPV thickness. An alternative CdS electrode could be made using an over- plated CdS array which had been polished so that only the top surface of the nanowires were exposed, thus creating an array of quantum dots which could have a narrow size distribution. This could also be used to fabricate a quantum dot light emitting diode (QD-LED) [594, 602]. Of course there is also the possibility to investigate nano arrays of other semi-conductor materials for use in these devices; in

fact PANI nanofibre gas sensors have been fabricated by Kaner and co-workers and found to perform better than conventional thin films [387, 400, 555]. PANI / metal nanoparticle composites have also exhibited enhanced sensing and catalytic properties compared to pure PANI [410, 554]. The Ag / PANI and Cu / PANI composites fabricated in this thesis should thus be perfect candidates for chemical and biological sensors. It would also be interesting to compare the electrical properties of the different composite films fabricated in chapter 4 and compare these to conductivity measurements from single wires. The thermal characteristics of the composite nanostructures could also be measured and compared to the bulk materials. Finally other metal / polymer composites could be synthesized e.g. Ag, Au, Ni, Co and Fe with PANI, polypyrrole and polythiophene



## References

---

- [1] The Royal Society and Royal Academy of Engineering (RS/RAEng) report (2004) "Nanoscience and Nanotechnology: Opportunities and Uncertainties" London, The Royal Society website: <http://www.nanotech.org.uk/finalreport.html>
- [2] The Health and Safety Executive (HSE) research report (2004) Nanoparticles: An Occupational Hygiene Review, and HSC/E Health and Safety Commission Paper, HSC/04/42, John Davis "Managing the Risks from Nanotechnology", HSE website: [www.hse.gov.uk](http://www.hse.gov.uk)
- [3] The National Institute for Occupational Safety and Health (NIOSH), John Howard, Director, National Institute for Occupational Safety and Health, Centers for Disease Control and Prevention, "Approaches to Safe nanotechnology" (2005) and "Strategic Plan for NIOSH Nanotechnology research and guidance: Filling the Knowledge gaps" (2008) [http://www.cdc.gov/niosh/topics/nanotech/pdfs/NIOSH\\_nanotechStrategic\\_plan.pdf](http://www.cdc.gov/niosh/topics/nanotech/pdfs/NIOSH_nanotechStrategic_plan.pdf)
- [4] US Patent Office Class Definition, <http://www.uspto.gov/go/classification/uspc977/defs977.htm>
- [5] Buzea, C., I. I. Pacheco, et al. (2007). "Nanomaterials and nanoparticles: Sources and toxicity." *Biointerphases*. 2(4): MR17-MR71.
- [6] Feynman, R. (1960). There's Plenty of Room at the Bottom. *Engineering and Science*. 23/5/1960. California, USA, California Institute of Technology. <http://calteches.library.caltech.edu/47/03/ES.23.5.1960.0.pdf>
- [7] Lieber, C. M. (1998). "One-Dimensional Nanostructures: Chemistry, Physics and Applications." *Solid State Communications* 107(11): 607-616.
- [8] Roduner, E. (2006). "Size matters: why nanomaterials are different." *Chem. Soc. Rev.* 35: 583 - 592.
- [9] Sriraman, K. R., S. Ganesh Sundara Raman, et al. (2006). "Synthesis and evaluation of hardness and sliding wear resistance of electrodeposited nanocrystalline Ni-W alloys" *Materials Science and Engineering: A* 418(1-2): 303-311.
- [10] Khanna, S. N. (1997) "Effect on Properties of Reduced Size and Dimensions" In: Goldstein, J. A. (Ed.) *Handbook of Nanophase Materials*. New York, Marcel Dekker, pp 1-13
- [11] Switzer, J. A. (1996) "Electrodeposition of Nanoscale Architectures". In: Goldstein, J. A. (Ed.) Chapter 4, *Handbook of Nanophase Materials*. New York, Marcel Dekker, New York pp. 63-82

- 
- [12] Whetten, R. L., D. M. Cox, et al. (1985). "Correspondence between Electron Binding Energy and Chemisorption Reactivity of Iron Clusters." *Phys. Rev. Lett.* 54: 1494 – 1497
- [13] Park, B. (2007). "Current and Future Applications of Nanotechnology." *Issues in Environmental Science and Technology* 24(Nanotechnology: Consequences for Human Health and the Environment): 1-18.
- [14] Li, Y., P. Leung, et al. (2006). "Antimicrobial effect of surgical masks coated with nanoparticles." *Journal of Hospital Infection* 62(1): 58-63.
- [15] Jirage, K. B., J. C. Hulteen, et al. (1997). "Nanotubule-Based Molecular-Filtration Membranes " *Science* 278(5338): 655 - 658.
- [16] Vlasiouk, I., A. Krasnoslobodtsev, et al. (2004). ""Direct" Detection and Separation of DNA Using Nanoporous Alumina Filters" *Langmuir* 20(23): 9913 -9915.
- [17] Meller, A., L. Nivon, et al. (2001). "Voltage-Driven DNA Translocations through a Nanopore." *Phys. Rev. Lett.* 86: 3435 - 3438.
- [18] Vlasiouk, I.; Takmakov, P.; Smirnov, S. (2005) "Sensing DNA Hybridization via Ionic Conductance Through a Nanoporous Electrode". *Langmuir* 21, 4776-4778.
- [19] Rabin, Y. and M. Tanaka (2005). "DNA in Nanopores: Counterion Condensation and Coion Depletion." *Phys. Rev. Lett.* 94: 148103.
- [20] Uhrich, K. E., S. M. Cannizzaro, et al. (1999). "Polymeric Systems for Controlled Drug Release." *Chem. Rev* 99: 3181-3198.
- [21] Panchapakesan, B. and E. Wickstrom (2007). "Nanotechnology for Sensing, Imaging, and Treating Cancer" *Surgical Oncology Clinics of North America* 16(2): 293-305.
- [22] Matsusaki, M., K. Larsson, et al. (2005). "Nanosphere Induced Gene Expression in Human Dendritic Cells." *Nano Lett.* 5(11): 2168 - 2173.
- [23] Silva, G. A., C. Czeisler, et al. (2004). "Selective Differentiation of Neural Progenitor Cells by High-Epitose Density Nanofibres." *Science* 303: 1352-1355.
- [24] Chan, W.-S. (2001). "Lab on a Chip"- The Development of a Nanoporous Membrane for Bioanalytical Chemistry". SURI 2003, Purdue University, Lafayette, 47906 USA. <http://www.nanohub.org/resources/808/>.
- [25] Smith, C. H. and M. Tondra (2004). "Magnetoresistive Detection of Flowing and Immobilized Assay Labels Nanomaterials" 2004 Nanobiotechnology and Nanomedicine Conference, Stamford, Conn. USA
- [26] Thompson, S. E. and S. Parthasarathy (2006). "Moore's law: the future of Si microelectronics." *Materials Today* 9(6):20-25.  
[http://www.azom.com/details.asp?ArticleID=1066#\\_Phosphors\\_for\\_High Definition](http://www.azom.com/details.asp?ArticleID=1066#_Phosphors_for_High Definition)



- 
- [27] Ross, C. A., H. I. Smith, et al. (2000). "Fabrication of Patterned Media for High Density Magnetic Storage " *Microelectronic Engineering* 53(1): 67-67(1)
- [28] Sun, S., D. Weller, et al., (2001). "Self-Assembled Magnetic Nanoparticle Arrays" In Plummer et al. (Eds) *The Physics of High Density Magnetic Recording*, Springer Verlag , Chapter 9
- [29] Marinero, E. E. S., CA), T. M. M. H. Reith, CA), et al. (1999). "Thin film disk with acicular magnetic grains" United States, International Business Machines Corporation (Armonk, NY) 5989674.
- [30] Dubin, V. M. (2006). "Method to assemble structures from nano-materials". USA, Intel Corporation. US Patent 7122461.
- [31] Dubin, V. M. and T. S. Dory (2008). "Packaging of Integrated Circuits with Carbon Nanotube Arrays to Enhance Heat Disipation through a Thermal Interface". USA, Intel Coporation. 7316061.
- [32] Na, P. S., N. Park , et al. (2006). "A Field Effect Transistor Fabricated with Metallic Single-Walled Carbon Nanotubes" *Fullerenes, Nanotubes and Carbon Nanostructures* 14(2 & 3 December): 141 - 149.
- [33] Xu, Z.-X., V. A. L. Roy, et al. (2007). "Nanocomposite field effect transistors based on zinc oxide/polymer blends" *Applied Physics Letters* 90(22): 223509 (1-3).
- [34] Cholewa, M., S. P. Lau, et al. (2008). "Radiation detector having coated nanostructure and method", National University of Singapore, Agency for Science, Technology and Research, Pohang University of Science and Technology, Nanyang Technological University. 7388201
- [35] Star, A., J.-C. P. Gabriel, et al. (2003). "Electronic Detection of Specific Protein Binding Using Nanotube FET Devices." *Nano Lett.; (Letter)*; 3(4): 459-463.
- [36] Novak, J. P., E. S. Snow, E. J. Houser, D. Park, J. L. Stepnowski, and R. A. McGill. "Nerve agent detection using networks of single-walled carbon nanotubes" *Applied Physics Letters* 83:4026 (2003).
- [37] Tondra, M. (2007). "Microchip-Based Sensors for Detection of Magnetic Microbead Labels". IVD Technology, Diagnostic Biosensors LLC.  
<http://www.devicelink.com/ivat/archive/07/05/009.html>
- [38] Gao, X., W. Yang, et al. (2007). "A Wireless, Magnetoelastic Biosensor for Rapid Detection of Glucose Concentrations in Urine Samples." *Sensors and Actuators B* 128: 161-167.
- [39] Varghese, O. K., G. K. Mor, et al. (2004). "A Titania Nanotube-Array Room-Temperature Sensor for Selective Detection of Hydrogen at Low Concentrations " *Journal of Nanoscience and Nanotechnology* 4(7): 733-737
- [40] Kang, B. S., F. Ren , et al. (2005). "PH measurements with single ZnO nanorods integrated with a microchannel." *Applied Physics Letters* 86: 112105 [1-3].

- 
- [41] Rout, C. S., S. H. Krishna, et al. (2006). "Hydrogen and ethanol sensors based on ZnO nanorods, nanowires and nanotubes" *Chemical Physics Letters* 418: 586-590.
- [42] Wang, J., J. Chen, et al. (2006). "Sulphur-polypyrrole composite positive electrode materials for rechargeable lithium batteries." *Electrochimica Acta* 51(22): 4634-4638.
- [43] Xu, J., C. Jia, et al. (2007). "Electrochemical properties of anatase TiO<sub>2</sub> nanotubes as an anode material for lithium-ion batteries" *Electrochimica Acta* 52(28): 8044-8047.
- [44] Dubin, V. M., S. Swalumar, et al. (2007). "Forming Self Aligned Nano Electrodes". USA, Intel Coporation. 7312155.
- [45] Li, N., C. R. Martin, et al. (2000). "High-rate, high-capacity, nanostructured tin oxide electrode." *Electrochemical and Solid-State Letters* 3(7): 316-318
- [46] Campbell, D. J., K. E. Korte, et al. (2007). "Fabrication and analysis of photonic crystals." *Journal of Chemical Education* 84: 1824-1826.
- [47] Jiang, P., C.-H. Sun, et al. "Self-Assembled Photonic Crystals and Templated Nanomaterials" *Current Nanoscience* 4: 296-305(10).
- [48] Gupta, R., M. J. Dyer, et al. (2002). "Preparation and characterization of surface plasmon resonance tunable gold and silver films" *J. Appl. Phys.* 92: 5264.
- [49] Song, D., N. Tokranova, et al. (2008). "New approaches for chip-to-chip interconnects: integrating porous silicon with MOEMS." *J. Micro/Nanolith. MEMS MOEMS* 7: 021013 [1-8].
- [50] Baumberg, J. (2007). "Tailoring NanoMaterials for light-matter interactions" *Lasers and Electro-Optics, 2007 and the International Quantum Electronics Conference. CLEOE-IQEC 2007*
- [51] Anh, T. K., L. Quoc Minh, et al. (2003). "Nanomaterials containing rare-earth ions Tb, Eu, Er and Yb: preparation, optical properties and application potential." *Journal of Luminescence* 102-103: 391-394
- [52] Ruoxue, Y., P. Pausauskie, et al. (2007). "Nanowires for Subwavelength Waveguides" *Nano-Optoelectronics Workshop, 2007. NOW '07. International.*
- [53] Lee, H. W. H., A. H. Chin, et al. (2005). "Optical devices with engineered nonlinear nanocomposite materials". UK, MEDER electronic UK Ltd. US 6961499
- [54] Star, A., Y. Lu, et al. (2004). "Nanotube Optoelectronic Memory Devices " *Nano Lett.; (Letter);* 4(9): 1587-1591
- [55] Mor, G. K., K. Shankar, et al. (2006). "Use of Highly-Ordered TiO<sub>2</sub> Nanotube-Arrays in Dye-Sensitized Solar Cells." *Nano Letters* 6: 215-218.



- 
- [56] Difei, Q., M. Fischbein, et al. (2005). "Efficient polymer-nanocrystal quantum-dot photodetectors" *Applied Physics Letters* 86(9 Nanoscale Science and Design): 093103 [1-3].
- [57] Bach, U., D. Corr, et al. (2002). "Nanomaterials-Based Electrochromics for Paper-Quality Displays." *Advanced Materials* 14(11): 845-848.U.
- [58] Kymakis, E., I. Alexandrou, et al. (2003). "High open-circuit voltage photovoltaic devices from carbon-nanotube-polymer composites." *Progress in Photovoltaics: Research and Applications* 93(3): 1764-1768.
- [59] Ago, H., K. Petritsch, et al. (1999). "Composites of carbon nanotubes and conjugated polymers for photovoltaic devices." *Advanced Materials* 11 (15): 1281-1285.
- [60] Lampert, C. M. (1994). "Towards large-area photovoltaic nanocells: experiences learned from smart window technology." *Solar Energy Materials and Solar Cells* 32(3): 307-321
- [61] Pradhan, B., S. K. Batabyal, et al. (2006). "Functionalized carbon nanotubes in donor/acceptor-type photovoltaic devices." *Applied Physics Letters* 88 (9): 093106.
- [62] Hasobe, T., H. Imatori, et al. (2005). "Photovoltaic Cells Using Composite Nanoclusters of Porphyrins and Fullerenes with Gold Nanoparticles" *J. Am. Chem. Soc* 127(4): 1216 -1228.
- [63] Maria, A., P. W. Cyr, et al. (2005). "Solution-processed infrared photovoltaic devices with >10% monochromatic internal quantum efficiency." *Applied Physics Letters* 87(NANOSCALE SCIENCE AND DESIGN 21): 213112 [1-3].
- [64] Raffaella, R. P., B. J. Landi, et al. (2005). "CdSe quantum dot-single wall carbon nanotube complexes for polymeric solar cells." *Solar Energy Materials and Solar Cells* 87(1-4): 733-746.
- [65] Shi, J., Y. Zhu, et al. (2004). "Recent developments in nanomaterial optical sensors " *TrAC Trends in Analytical Chemistry* 23(5): 351-360
- [66] Zhou, D. and D.-J. Kang (2005). "Creating functional nanostructured materials at the crossroad of physics, chemistry and materials science " *International Journal of Nanotechnology* 2(4): 440-468(29)
- [67] Antonietti, M. (2003). "Nanostructured materials: Self-organization of functional polymers." *Nat Mater* 2(1): 9-10.
- [68] Hu, J. (2007). "Shape memory polymers and textiles". Hong Kong Polytechnic University, Hong Kong, Woodhead Publishing Limited, Abington Hall, Abington, Cambridge, CB21 6AH, England.
- [69] Guillorn, M. A., B. Ilic, et al. (2006). "Vertically aligned nanostructure scanning probe microscope tips", UT-Battelle, LLC (Oak Ridge, TN, US) United States Patent 7151256

- 
- [70] Lieber, C. M., J. H. H. Hafner, TX), et al. (2004). "Direct growth of nanotubes, and their use in nanotweezers" USA, And, President. Fellows of Harvard College (Cambridge, MA) United States Patent 6743408.
- [71] Ozin, G. A. (1992). "Nanochemistry: Synthesis in Diminishing Dimensions." *Advanced Materials* 4(10): 612-649.
- [72] Wang, N. (2008). "Growth of nanowires." *Materials Science & Engineering R-Reports* 60(1-6): 1-51.
- [73] Spanier, J. E., Ed. (2006). "One-Dimensional Semiconductor and Oxide Nanostructures." *Nanomaterials Handbook*, CRC Press
- [74] Wagner, R. S. and W. C. Ellis (1964). "Vapor-liquid-solid mechanism of single crystal growth." *Applied Physics Letters* 4: 89-90.
- [75] Wagner, R. S. (1965). " Vapor-Liquid-Solid Mechanism OF Crystal Growth and its Application to Silicon " *Transactions of the Metallurgical Society of Aime*
- [76] Wang, Y., V. Schmidt, et al. (2006). "Epitaxial growth of silicon nanowires using an aluminium catalyst." *Nature Nanotechnology* 1(3): 186-189
- [77] Hiruma, K., T. Katsuyama, et al. (1991). "Quantum size microcrystals grown using organometallic vapor phase epitaxy." *Applied Physics Letters* 59(4): 431-433.
- [78] Hiruma, K., M. Yazawa, et al. (1993). "GaAs free-standing quantum-size wires." *Journal of Applied Physics* 74(5): 3162-3171
- [79] Hiruma, K., M. Yazawa, et al. (1995). "Growth and optical properties of nanometer-scale GaAs and InAs whiskers." *Journal of Applied Physics* 77(2): 447-462.
- [80] Gibart, P. (2004). "Metal organic vapour phase epitaxy of GaN and lateral overgrowth." *Reports on Progress in Physics* 5: 667-715
- [81] Ikejiri, K., T. Sato, et al. (2008). "Growth characteristics of GaAs nanowires obtained by selective area metal-organic vapour-phase epitaxy." *Nanotechnology* 26: 265604.
- [82] [http://en.wikipedia.org/wiki/Chemical\\_vapor\\_deposition](http://en.wikipedia.org/wiki/Chemical_vapor_deposition)
- [83] Dietz, T. G., M. A. Duncan, et al. (1981). "Laser production of supersonic metal cluster beams." *J. Chem. Phys.* 74/11:6511-6512.
- [84] Morales, A. M. and C. M. Lieber (1998). "A Laser Ablation Method for the Synthesis of Crystalline Semiconductor Nanowires." *Science* 279(5348): 208-211.
- [85] Yu, D. P., C. S. Lee, et al. (1998). "Synthesis of nano-scale silicon wires by excimer laser ablation at high temperature." *Solid State Communications* 105(6): 403-407.
- [86] Pan, Z. W., Z. R. Dai, et al. (2001). "Nanobelts of Semiconducting Oxides." *Science* 291(5510): 1947-1949.



- 
- [87] Heath, J. R. and F. K. LeGoues (1993). "A liquid solution synthesis of single crystal germanium quantum wires " *Chemical Physics Letters* 208(3-4): 263-8
- [88] Kasuga, T., M. Hiramatsu, et al. (1998). "Formation of Titanium Oxide Nanotube." *Langmuir* 14(12): 3160-3163.
- [89] Wang, X. and Y. Li (2002). "Selected-Control Hydrothermal Synthesis of  $\alpha$ - and  $\beta$ -MnO<sub>2</sub> Single Crystal Nanowires." *J. Am. Chem. Soc.* 124(12): 2880-2881.
- [90] Xia, Y., P. Yang , et al. (2003). "One-Dimensional Nanostructures: Synthesis, Characterization, and Applications." *Advanced Materials* 15(5): 353-389.
- [91] Peng, X., U. Manna, et al. (2000). "Shape control of CdSe nanocrystals " *Nature* 404(6773): 59-61.
- [92] Sun, Y., B. Gates, et al. (2002). "Crystalline Silver Nanowires by Soft Solution Processing." *Nano Lett.* 2(2): 165-168.
- [93] Taylor, G. F. (1924). "A method of drawing metallic filaments and a discussion of their properties and uses." *Physical Review* 23(5): 655-660
- [94] Penner, R. M., M. J. Heben, et al. (1990). "Fabrication and use of nanometry-sized electrodes in electrochemistry." *Science* 250(4984): 1118-1121.
- [95] Bean, K. E. (1978). "Anisotropic etching of silicon." *Electron Devices, IEEE Transactions on* 25(10): 1185-1193.
- [96] Cheng, S. L., S. L. Wong, et al. "Large-area Co-silicide nanodot arrays produced by colloidal nanosphere lithography and thermal annealing." *Ultramicroscopy*. In Press, Corrected Proof.
- [97] Tseng, A. A., K. Chen, et al. (2003). "Electron Beam Lithography in Nanoscale Fabrication: Recent Development." *IEEE Transactions on Electronics Packaging Manufacturing* 26(2): 141-149.
- [98] Kretz, J., H. Roeper, et al. (2008). "Integration of EBDW of one entire metal layer as substitution for optical lithography in 220 nm node microcontrollers." *Microelectronic Engineering* 85(5-6): 792-795.
- [99] Broers, A. N. (1995). "Fabrication Limits of Electron Beam Lithography and of UV, X-Ray and Ion-Beam Lithographies." *Philosophical Transactions: Physical Sciences and Engineering* 353(1703): 291-311.
- [100] Broers, A. N. (1964). "Micromachining by Sputtering Through a Mask of Contamination Laid Down by an Electron Beam." 1st International Conference on Electron and Ion Beam Science and Technology, New York, John Wiley & Sons, Inc.
- [101] Juhasz, R., N. Elfstrom, et al. (2005). "Controlled Fabrication of Silicon Nanowires by Electron Beam Lithography and Electrochemical Size Reduction." *Nano Lett.* 5(2): 275-280.

- 
- [102] Gotschy, W., K. Vonmetz, et al. (1996). "Thin films by regular patterns of metal nanoparticles: Tailoring the optical properties by nanodesign." *Applied Physics B: Lasers and Optics* 63(4): 381-384.
- [103] Bhuvana, T. and G. U. Kulkarni (2008). "Highly Conducting Patterned Pd Nanowires by Direct-Write Electron Beam Lithography." *ACS Nano* 2(3): 457-462.
- [104] Chou, S. Y., P. R. Krauss, et al. (1996). "Nanoimprint lithography." *J. Vac. Sci. Technol. B* 14(6): 4129-4133.
- [105] Piner, R. D., J. Zhu, et al. (1999). "Dip-pen nanolithography." *Science* 283(5402): 661-663
- [106] Haaheim, J. and O. A. Nafday (2008). "Dip Pen Nanolithography: A 'Desktop Nanofab' Approach Using High-Throughput Flexible Nanopatterning." *Scanning* 30: 137-150.
- [107] Kim, K. S., L. Kyoung Nam, et al. (2008). "Formation of nanometer-scale structures using conventional optical lithography." *Thin Solid Films* 516(7): 1489-1492.
- [108] Prabhakaran, K., S. Gotzinger, et al. (2006). "Ultrafine luminescent structures through nanoparticle self-assembly." *Nanotechnology* 17 3802-3805.
- [109] Korgel, B. A. and D. Fitzmaurice (1998). "Self-Assembly of Silver Nanocrystals into Two-Dimensional Nanowire Arrays." *Advanced Materials* 10(9): 661-665.
- [110] Hassenkam, T., K. Nørgaard, et al. (2002). "Fabrication of 2D Gold Nanowires by Self-Assembly of Gold Nanoparticles on Water Surfaces in the Presence of Surfactants." *Advanced Materials* 14(16): 1126-1130.
- [111] Tang, Z., N. A. Kotov, et al. (2002). "Spontaneous Organization of Single CdTe Nanoparticles into Luminescent Nanowires." *Science* 297(5579): 237-240.
- [112] Hanaoka, T.-A., H.-P. Kormann, et al. (1998). "Three-Dimensional Assemblies of Gold Colloids in Nanoporous Alumina Membranes." *European Journal of Inorganic Chemistry* 1998(6): 807-812.
- [113] Hornyak, G., M. Kröll, et al. (1997). "Gold Clusters and Colloids in Alumina Nanotubes." *Chemistry - A European Journal* 3(12): 1951-1956.
- [114] Santoso, S., W. Hwang, et al. (2002). "Self-assembly of Surfactant-like Peptides with Variable Glycine Tails to Form Nanotubes and Nanovesicles." *Nano Lett.* 2(7): 687-691.
- [115] Alivisatos, A. P., K. P. Johnsson, et al. (1996). "Organization of 'nanocrystal molecules' using DNA." *Nature* 382(6592): 609-611
- [116] Mirkin, C. A., R. L. Letsinger, et al. (1996). "A DNA-based method for rationally assembling nanoparticles into macroscopic materials." *Nature* 382(6592): 607-609.



- 
- [117] Martin, C. R., L. S. Van Dyke, et al. (1990). "Template Synthesis of Organic Microtubules." *J. Am. Chem. Soc* 112: 8976-8977.
- [118] Martin, C. R., R. Parthasarathy, et al. (1993). "Template synthesis of electronically conductive polymers - A new route for achieving higher electronic conductivities" *Synthetic Metals* 55(2-3): 1165-1170.
- [119] Martin, C. R. (1994). "Nanomaterials: A Membrane-Based Synthetic Approach." *Science* 266(5193): 1961-1966.
- [120] Menon, V. P. and C. R. Martin (1995). "Fabrication and Evaluation of Nanoelectrode Ensembles." *Analytical Chemistry* 67/13: 1920-1928.
- [121] Martin, C. R. (1996). "Membrane-Based Synthesis of Nanomaterials " *Chem. Mater.* 8(8): 1739 -1746.
- [122] Hulteen, J. C. and C. R. Martin (1997). "A General Template-Based Method for the Preparation of Nanomaterials." *J. Mater. Chem.* 7(7): 1075-1087.
- [123] Masuda, H. and K. Fukuda (1995). "Ordered Metal Nanohole Arrays Made by a Two-Step Replication of Honeycomb Structures of Anodic Alumina." *Science* 268(5216): 1466-1468.
- [124] Tonucci, R. J., B. L. Justus, et al. (1992). "Nanochannel Array Glass." *Science* 258(5083): 783-785.
- [125] Beck, J. S., J. C. Vartuli, et al. (1992). "A new family of mesoporous molecular sieves prepared with liquid crystal templates." *J. Am. Chem. Soc* 114: 10834 - 10843.
- [126] Pearson, D. H. and R. J. Tonucci (1995). "Nanochannel Glass Replica Membranes." *Science* 270(5233): 68-70.
- [127] Wu, C.-G. and T. Bein (1994). "Conducting carbon wires in ordered, nanometer-sized channels" *Science* 266(5187): 1013-101
- [128] Wulff, G., Ed. (1990). "Biomimetic reactions using organized polymeric supports." *Biomimetic Polymers*. New York, Plenum.
- [129] Sankaran, V., C. C. Cummins, et al. (1990). "Small lead sulfide (PbS) clusters prepared via ROMP block copolymer technology." *J. Am. Chem. Soc.* 112(19): 6858-6859.
- [130] Dauginet-De Pra, L. and S. Demoustier-Champagne (2005). "Investigation of the electronic structure and spectroelectrochemical properties of conductive polymer nanotube arrays." *Polymer* 46(5): 1583-1594.
- [131] Mann, S. and F. C. Meldrum (1991). "Controlled synthesis of inorganic materials using supramolecular assemblies." *Advanced Materials* 3(6): 316-318.

---

[132] Bai, H., K. Xu, et al. (2007). "Fabrication of Au nanowire of uniform length and diameter using a new monodisperse and rigid biomolecular template, collagen-like triple helix" *Angew. Chem. Intl. Ed.* 46: in print

[133] Clark, T. D. and M. R. Ghadiri (1995). "Supramolecular Design by Covalent Capture. Design of a Peptide Cylinder via Hydrogen-Bond- Promoted Intermolecular Olefin Metathesis." *J. Am. Chem. Soc.* 117(49): 12364-12365.

[134] Mo, X., M. P. Krebs, et al. (2006). "Directed Synthesis and Assembly of Gold Nanoparticles Using Purple Membrane" *Small* 2(4): 526-529.

[135] Monson, C. F. and A. T. Woolley (2003). "DNA-Templated Construction of Copper Nanowires." *Nano Lett.* 3(3): 359-363.

[136] Aldaye, F. A. and H. F. Sleiman (2007). "Dynamic DNA Templates for Discrete Gold Nanoparticle Assemblies: Control of Geometry, Modularity, Write/Erase and Structural Switching." *J. Am. Chem. Soc.* 129(14): 4130-4131.

[137] Whaley, S. R., D. S. English, et al. (2000). "Selection of peptides with semiconductor binding specificity for directed nanocrystal assembly." *Nature* 405(6787): 665-668.

[138] Mao, C., D. J. Solis, et al. (2004). "Virus-Based Toolkit for the Directed Synthesis of Magnetic and Semiconducting Nanowires." *Science* 303(5655): 213-217.

[139] Douglas, T. and M. Young (2006). "Viruses: Making Friends with Old Foes." *Science* 312(5775): 873-875.

[140] Jorritsma, J., M. A. M. Gijs, et al. (1996). "General technique for fabricating large arrays of nanowires" *Nanotechnology* 7: 263-265.

[141] Locharenrat, K., A. Sugawara, et al. (2007). "Shadow deposition of copper nanowires on the faceted NaCl(1 1 0) template." *Surface Science* 601(18): 4449-4453.

[142] O'Mahony, J. D., J. F. McGilp, et al. (1994). "Nucleation and evolution of the Au-induced 5 x 2 structure on vicinal Si(111)." *Physical Review B* 49(4): 2527.

[143] Fasol, G. and K. Runge (1997). "Selective electrodeposition of nanometer scale magnetic wires." *Applied Physics Letters* 70(18): 2467-2468.

[144] Fasol, G. (1998). "Applied Physics: Nanowires: Small Is Beautiful." *Science* 280(5363): 545-546.

[145] Ramanathan, K., M. Bangar, et al. (2004). "Individually Addressable Conducting Polymer Nanowires Array." *Nano Letters* 4(7): 1237-1239.

[146] Ajayan, P. M. and S. Iijima (1993). "Capillarity-induced filling of carbon nanotubes." *Nature* 361(6410): 333-334.

[147] Tsang, S. C., Y. K. Chen, et al. (1994). "A simple chemical method of opening and filling carbon nanotubes " *Nature* 372(6502): 159-162



- 
- [148] Guerret-Piecourt, C., Y. L. Bouar, et al. (1994). "Relation between metal electronic structure and morphology of metal compounds inside carbon nanotubes." *Nature* 372(6508): 761-765.
- [149] Coleman, J. N. (1999). *Physical Properties of a Polymer Nanotube Composite*. School of Physics. Dublin, Trinity College. PhD
- [150] Lahr, B. (2001). *Mechanical Properties of Carbon Nanotube Polymer Composites*. School of Physics. Dublin, Trinity College. PhD
- [151] Kilbride, B. (2001). *AC and DC Conductivity of Polymer-Nanotube Composite Thin Films* School of Physics. Dublin, Trinity College. MSc.
- [152] Fournet, P. (2003). *Organic Light-Emitting Diodes and Photovoltaic Devices : Incorporation of Carbon Nanotubes as Charge Transport Media*. School of Physics. Dublin, Trinity College. PhD.
- [153] Cadek, M. (2003). *Mechanical Reinforcement Effects of Carbon Nanotube Polymer Composites*. School of Physics. Dublin, Trinity College. PhD.
- [154] O'Flaherty, S. (2003). *Nonlinear Optical Extinction in Polymer-Carbon Nanotube and Phthalocyanine Systems* School of Physics. Dublin, Trinity College. PhD.
- [155] Ryan, K. (2005). *Polymer Crystallisation as a Reinforcement Mechanism for Polymer-Carbon Nanotube Composites* School of Physics. Dublin, Trinity College. PhD
- [156] Lahiff, E (2006) "Synthesis and Properties of a Novel Carbon Nanotube-Polymer Thin Film Composite." School of Physics. Dublin, Trinity College. PhD
- [157] Li, A.-P., F. Mueller, et al. (1999). "Fabrication and Microstructuring of Hexagonally Ordered Two-Dimensional Nanopore Arrays in Anodic Alumina." *Adv. Mater.* 11(6): 483-487; Li, A.-P., F. Mueller, et al. (1999). "Polycrystalline and Monocrystalline Nanopore Arrays with Hexagonal Ordering on Alumina." *J. Vac. Sci. Technol. A.* 17(4): 1428-1431; Li, A.-P., F. Mueller, et al. (2000). "Polycrystalline and Monocrystalline Pore Arrays with Large Interpore Distance in Anodic Alumina." *Electrochemical and Solid-State Letters* 3(3): 131-134.
- [158] Choi, J., K. Nielsch, et al. (2003). "Fabrication of Monodomain Alumina Pore Arrays with an Interpore Distance Smaller than the Lattice Constant of the Imprint Stamp." *J. Vac. Sci. Technol. B.* 21(2): 763-766.
- [159] Asoh, H., S. Ono, et al. (2003). "Growth of Anodic Porous Alumina with Square Cells." *Electrochem. Acta* 48: 3171-3174.
- [160] Lee, W., R. Ji, et al. (2006). "Fast Fabrication of Long Range Ordered Porous Alumina Membranes by Hard Anodisation." *Nature Materials* 5(9): 741-747; Lee, W., K. Schwirm, et al. (2008). "Structural Engineering of Nanoporous Anodic Aluminum Oxide Formed by Pulse Anodisation of Aluminum." *Nature Nanotechnology* 3: 234-239; Schwirm, K., W. Lee, et al. (2008). "Self-Ordered Anodic Aluminium Oxide Formed by H<sub>2</sub>SO<sub>4</sub> Hard Anodization." *ACS Nano* 2(2): 302-310.

- 
- [161] Shawaqfeh, A. T. and R. E. Baltus (1999). "Fabrication and characterization of single layer and multi-layer anodic alumina membranes" *Journal of Membrane Science* 157(2): 147-158.
- [162] Gu , P., H. Miao, et al. (2004). "Investigation of elastic modulus of nanoporous alumina membrane" *J. Mater. Sci* 39(10): 3369-3373.
- [163] Xia, Z., L. Riester, et al. (2004). "Mechanical Properties of Highly Ordered Nanoporous Anodic Alumina." *Rev. Adv. Mater. Sci.* 6: 131-139.
- [164] Inguanta, R., M. Butera, et al. (2007). "Fabrication of metal nano-structures using anodic alumina membranes grown in phosphoric acid solution: Tailoring template morphology." *Applied Surface Science* 253: 5447-5456.
- [165] Masuda, H., K. Nishio, et al (1993). "Preparation of Microporous Metal Membranes by Two-Step Replication of the Microstructure of Anodic Alumina." *Thin Solid Films* 223: 1-3.
- [166] Riveros, G., S. Green, et al. (2006). "Silver nanowire arrays electrochemically grown into nanoporous anodic alumina templates." *Nanotechnology* 17: 561-570.
- [167] Cao, H. Q., Z. Xu, et al. (2001). "Template Synthesis and Magnetic Behaviour of an Array of Cobalt Nanowires." *Adv. Mater.* 13(2): 121-123
- [168] Garcia, J. M., A. Asenjo, et al. (1999). "Magnetic behavior of an array of cobalt nanowires." *J. Appl. Phys.* 85: 5480-5482.
- [169] Nielsch , K., F. Müller, et al. (2000). "Uniform Nickel Deposition into Ordered Alumina Pores by Pulsed Electrodeposition." *Adv. Mater.* 12(8): 582-586.
- [170] Sellmyer, A. D. J., A. M. Zheng, et al. (2001). "Magnetism of Fe, Co and Ni nanowires in self-assembled arrays." *Journal of Physics: Condensed Matter* 13: R433-R460
- [171] Paulus, P. M., F. Luis, et al. (2001). "Low-temperature study of the Magnetization Reversal and Magnetic Anisotropy of Fe, Ni and Co Nanowires." *J. Magn. Magn. Mater.* 224: 180-196.
- [172] Sauer, G., G. Brehm and S. Schneider "Highly Ordered Monocrystalline Silver Nanowire Arrays." *J. Appl. Phys.* 2001, 91(5): 3243-3247
- [173] Vojkuvka, L., L. F. Marsal, et al. (2007). Study of Porous Alumina Porosity after Pore Widening Process. 2007 Spanish Conference on Electron Devices.
- [174] Nielsch, K., J. Choi, et al. (2002). "Self-ordering regimes of porous alumina: the 10% porosity-rule." *Nanoletters* 2(7): 677-680.
- [175] Bao, J., Z. Xu, et al. (2004). "Fabrication of cobalt nanostructures with different shapes in alumina template." *Scripta Materialia* 50(1): 19-23.



- 
- [176] Zhang, J., Y. Yan, et al. (2006). "Microarrays of silver nanowires embedded in anodic alumina membrane templates: size dependence of polarization characteristics." *Appl. Opt.* 45: 297-304
- [177] Kim, K., M. Kim, et al. (2006). "Pulsed electrodeposition of palladium nanowire arrays using AAO template" *Materials Chemistry and Physics* 96(2-3): 278-282.
- [178] Xu, J. and X. Huang (2008). "Pulsed electrodeposition of monocrystalline Ni nanowire array by intermittent symmetric square wave." *Materials Letters* 62(10-11): 1491-1494.
- [179] Martin, C. R. (1995). "Template Synthesis of Electrically Conductive Polymer Nanostructures." *Accounts of chemical research* 28(2): 61-68.
- [180] Huczko, A. (2000). "Template-based synthesis of nanomaterials " *Journal Applied Physics A: Materials Science & Processes* 70(4): 365-376
- [181] Wang, C., Z. wang, et al. (2000). "Well-Aligned polyaniline Nano-fibril Array membrane and its field Emission Property." *Chemical Physics Letters* 341: 431-434.
- [182] Joo, J., K. T. Park, et al. (2003). "Conducting Polymer Nanotube and Nanowire Synthesis by using Nanoporous Template: Synthesis, Characteristics and Applications." *Synthetic Metals* 135-136: 7-9.
- [183] Lee, W., M.-K. Jin, et al. (2003). "Nanostructuring of a Polymeric Substrate with Well Defined Nanometer Scale Topography and Tailored Surface Wettability." *Langmuir* 20: 7665-7669.
- [184] Steinhart, M., J. H. Wendorf, et al. (2002). "Polymer Nanotubes by Wetting of Ordered Porous Templated." *Science* 296(14.06.2002): 1997; Steinhart, M., J. H. Wendorf, et al. (2003). "Nanotubes a la Carte: Wetting of Porous Templates." *Chem. Phys. Chem* 4: 1171-1176; Steinhart, M., R. B. Wehrspohn, et al. (2004). "Nanotubes by Template Wetting: A Modular Assembly System." *Angew. Chem. Int. ed.* 43: 1334-1344.
- [185] Klein, J. D., R. D. Herrick, et al. (1993). "Electrochemical Fabrication of Cadmium Chalcogenide Microdiode Arrays." *Chem. Mater.* 5(7): 902-904
- [186] Hoyer, P. (1996). "Semiconductor Nanotube Formation by a Two-Step Template Process." *Adv. Mater.* 8(10): 857-859.
- [187] Routkevitch, D., T. Bigioni, et al. (1996). "Electrochemical Fabrication of CdS Nanowire Arrays in Porous Anodic Aluminium Oxide Templates." *J. Phys. Chem.* 100: 14037-14047.
- [188] Xu, D., Y. Xu, et al. (2000). "Preparation and Characterisation of CdS Nanowire Arrays by Electrodeposition in Porous Anodic Aluminium Oxide Templates." *Chem. Phys. Lett.* 325: 340-344.

- 
- [189] Shi, G., C. M. Mo, et al. (2000). "Photoluminescence of ZnO Nanoparticles in Alumina Membrane with Ordered Pore Arrays." *Solid State Communications* 115: 253-256.
- [190] Cheng, G. S., S. H. Chen, et al. (2000). "Highly Ordered Nanostructures of Single Crystalline GaN Nanowires in Anodic Alumina." *Materials Science & Engineering A286*: 165-168.
- [191] Peng, X. S., J. Zhang, et al. (2001). "Synthesis of Highly Ordered CdSe Nanowire Array Embedded in Anodic Alumina Membranes by Deposition in Ammonia Alkaline Solution." *Chem. Phys. Lett.* 343: 470-474.
- [192] Zheng, M. J., L. D. Zhang, et al. (2002). "Fabrication and Optical Properties of Large Scale Uniform Zinc Oxide Nanowire Arrays by One-Step Electrochemical Deposition Techniques." *Chem. Phys. Lett.* 363: 123-128.
- [193] Peng, X. S., G. W. Meng, et al. (2002). "Electrochemical Fabrication of Ordered Ag<sub>2</sub>S Nanowire Arrays." *Materials Research Bulletin* 37: 1369-1375.
- [194] Fan, Z., D. Dutta, et al. (2006). "Electrical and photoconductive properties of vertical ZnO nanowires in high density arrays." *Applied Physics Letters* 89(21): 213110.
- [195] Che, G., B. B. Lakshmi, et al. (1998). "Chemical Vapor Deposition Based Synthesis of Carbon Nanotubes and Nanofibers Using a Template Method." *Chem. Mater.* 10(1): 260-267.
- [196] Suh, J. S. and J. S. Lee (1999). "Highly ordered two-dimensional carbon nanotube arrays." *Applied Physics Letters* 75(14): 2047-2049.
- [197] Jeong, S.-H. and K.-H. Lee (2003). "Fabrication of the aligned and patterned carbon nanotube field emitters using the anodic aluminum oxide nano-template on a Si wafer." *Synthetic Metals* 139 (2): 385-390
- [198] Sklar, G. P., K. Paramguru, et al. (2005). "Pulsed electrodeposition into AAO templates for CVD growth of carbon nanotube arrays." *Nanotechnology* 8: 1265-1271.
- [199] Cepak, V. M., J. C. Hulteen, et al. (1998). "Fabrication and characterization of concentric-tubular composite micro and nanostructures using the template-synthesis method." *J. Mater. Res.* 13: 3070-3080
- [200] Kawai, S. and R. Ueda (1975). "Magnetic Properties of Anodic Oxide Coatings on Aluminum Containing Electrodeposited Co and Co-Ni." *Journal of the Electrochemical Society* 122(1): 32-36.
- [201] Yoon, C. and J. S. Suh (2002). "Electrochemical Fabrication of CdS/Co Nanowire Arrays in Porous Aluminum Oxide Templates." *Bulletin of the Korean Society* 23(11): 1519-1523.
- [202] Nicewarner-Pena, S. R., R. G. Freeman, et al. (2001). "Submicrometer Metallic Barcodes." *Science* 294(5540): 137-141.



- 
- [203] Piraux, L., J. M. George, et al. (1994). "Giant magnetoresistance in magnetic multilayered nanowires." *Applied Physics Letters* 65(19): 2484-2486.
- [204] Doudin, B. and J.-P. Ansermet (1995). "A New Method to Construct Nanostructured Materials of Controlled Morphology." *Nanostructured Materials* 6(1-4): 521-524.
- [205] Pirota, K. R., D. Navas, et al. (2004). "Novel Magnetic Materials Prepared by Electrodeposition Techniques: arrays of Nanowires and Multi-Layered Nanowires." *Journal of Alloys and Compounds* 369: 18-26.
- [206] Li, A.-P., F. Mueller, et al. (1998). "Hexagonal Pore Arrays with a 50-420nm Interpore Distance Formed by Self Organisation in Anodic Alumina." *Journal of Applied Physics* 84(11): 6023-6025.
- [207] Hanaoka, T.-A., A. Heilmann, et al. (1998). "Alumina Membranes Templates for Novel Nanocomposites." *Applied Organometallic Chemistry* 12(5): 367-373.
- [208] Jessensky, O., F. Mueller, et al. (1998). "Self Organised Formation of Hexagonal Pore Arrays in Anodic Alumina." *Applied Physics Letters* 72(10): 1173-1175.
- [209] Parkhutik, V. P. and V. I. Shershulsky (1992). "Theoretical Modeling of Porous Oxide Growth on Aluminum." *Journal of Physics D: Applied Physics* 25:1258-1263.
- [210] Diggle, J. W., T. C. Downie, et al. (1968). "Anodic Oxide Films on Aluminium." *Chemical Review* 69: 365-405.
- [211] O'Sullivan, J. P. and G. C. Wood (1970). "The Morphology and Mechanism of Formation of Porous Anodic Films on Aluminium." *Proceedings of the Royal Society of London* 317: 511-543.
- [212] Furneaux, R. C., W. R. Rigby, et al. (1989). "The Formation of Controlled-Porosity Membranes from Anodically Oxidised Aluminium." *Nature* 337: 147-149.
- [213] Lohrengel, M. M. (1993). "Thin anodic Oxide Layers on aluminium and Other Valve Metals: High-Field Regime." *Materials Science and Engineering R11* (6): 243-294.
- [214] Thompson, G. E. and G. C. Wood (1981). "Porous anodic film formation on aluminium." *Nature* 290(5803): 230-232.
- [215] Thompson, G. E. and G. C. Wood, Eds. (1983). *Anodic Films on Aluminium. Treatise on materials science and technology*, Academic Press, New York; London. Vol 23, pp 205-329.
- [216] Thompson, G. E., R. C. Furneaux, et al. (1978). "Nucleation and growth of porous anodic films on aluminum." *Nature* 272: 433-435.
- [217] Paulus, P. M. (2000). *Nanometer-sized Metal Particles studied by Moessbauer Effect Spectroscopy and Magnetic Probes*. Sociale Wetenschappen. Leiden, Universiteit Leiden. PhD: 150.

- 
- [218] Wehrspohn, R. B., A.-P. Li, et al., In: Oxide films, Herbert, K. R., Lillard, R. S. et al., (Eds) The Electrochemical Society Proceedings Series, PV 2000-4, Pennington, NJ, 2000, p. 271.
- [219] Kröll, M. (2000). Herstellung und Charakterisierung Metallischer Nanodraethe in Nanoporesen Aluminiumoxidmembranen. Chemie. Essen, Universitaet-GH. Dr rer. nat. (PhD): 161.
- [220] Gerein, N. J. and J. A. Haber (2005). "Effect of ac Electrodeposition Conditions on the Growth of High Aspect Ratio Copper Nanowires in Porous Aluminum Oxide Templates." *J. Phys. Chem. B* 109(37): 17372-17385.
- [221] Ono, S. and N. Masuko (2003). "Evaluation of pore diameter of anodic porous films formed on aluminum." *Surface and Coatings Technology* 169-170: 139-142.
- [222] Bai, A., C.-C. Hu, et al. (2008). "Pore diameter control of anodic aluminum oxide with ordered array of nanopores." *Electrochimica Acta* 53(5): 2258-2264.
- [223] Wehrspohn, R. B., K. Nielsch, et al. (2001). "Electrochemically prepared high-aspect-ratio highly ordered pore arrays and applications". 198th Meeting of the Electrochemical Society Phoenix, USA.
- [224] Nielsch, K. (2002). "Hochgeordnete Ferromagnetische Nano-stabensembles." *Matematischen-naturwissenschaftlichen Technischen Fakultät der Martin-Luther-Universitaet-Halle-Wittenberg. Dr rer. nat. (PhD): 109*
- [225] Masuda, H., H. Yamada, et al. (1997). "Highly Ordered Nanochannel-Array Architecture in Anodic Alumina." *Applied Physics Letters* 71(19): 2770-2772.
- [226] Pang, S. W., T. Tamamura, et al. (1998). "Direct nano-printing on Al substrate using a SiC mold." *Journal of Vacuum Science & Technology B: Microelectronics and Nanometer Structures* 16(3): 1145-1149
- [227] Asoh, H., K. Nishio, et al. (2001). "Conditions for Fabrication of Ideally Ordered Anodic Porous Alumina Using Pretextured Al." *Journal of The Electrochemical Society* 148(4): B152-B156.
- [228] Masuda, H., H. Asoh, et al. (2001). "Square and Triangular Nanohole Array Architectures in Anodic Alumina." *Advanced Materials* 13(3): 189-192.
- [229] Mikulskas, I., S. Juodkazis, et al. (2001). "Aluminum Oxide Photonic Crystals Grown by a New Hybrid Method." *Advanced Materials* 13(20): 1574-1577.
- [230] Choi, J., R. B. Wehrspohn, et al. (2003). "Moiré Pattern Formation on Porous Alumina Arrays Using Nanoimprint Lithography." *Advanced Materials* 15(18): 1531-1534.
- [231] Fan, H. J., W. Lee, et al. (2005). "Arrays of vertically aligned and hexagonally arranged ZnO nanowires: a new template-directed approach." *Nanotechnology* 16(6): 913-917.



- 
- [232] Lee, W., M. Alexe, et al. (2005). "Metal Membranes with Hierarchically Organized Nanotube Arrays." *Chem. Mater.* 17(13): 3325-3327
- [233] Lee, P. S., O. J. Lee, et al. (2005). "Vertically Aligned Nanopillar Arrays with Hard Skins Using Anodic Aluminum Oxide for Nano Imprint Lithography." *Chem. Mater.* 17(24): 6181-6185.
- [234] Lee, W., R. Ji, et al. (2006). "Wafer-Scale Ni Imprint Stamps for Porous Alumina Membranes Based on Interference Lithography." *Small* 2(8-9): 978-982.
- [235] Tsuchiya, H., S. Berger, et al. (2007). "A new route for the formation of self-organized anodic porous alumina in neutral electrolytes." *Electrochemistry Communications* 9(4): 545-550.
- [236] Furneaux, R. C., G. E. Thompson, et al. (1978). "The application of ultramicrotomy to the electronoptical study of the surface films on aluminium." *Corros. Sci.* 18:853-881
- [237] Imran, M. M. A. (2008). "Structural and Magnetic Properties of Electrodeposited Ni Nanowires." *Journal of Alloys and Compounds* 455: 17-20.
- [238] Lakshmi, B. B., P. K. Dorhout, et al. (1997). "Sol-Gel Template Synthesis of Semiconductor Nanostructures." *Chem. Mater.* 9(3): 857-862
- [239] Bean, C. P. (12/09/1969). PROCESS FOR FILLING PORES U. S. P. 3483095. United States, GEN ELECTRIC 3483095
- [240] Possin, G. E. (1970). "A method for Forming Very Small Diameter Wires." *Review of Scientific Instruments* 41: 772-774.
- [241] Williams, W. D. and N. Giordano (1984). "Fabrication of 80 [A-ring] metal wires." *Review of Scientific Instruments* 55(3): 410-412; and Williams, W. D. and N. Giordano (1986). "Experimental study of localization and electron-electron interaction effects in thin Au wires." *Physical Review B* 33(12): 8146-8154.
- [242] Gruberger, J. and E. Gileadi (1986). "Plating on Anodized Aluminium - 1. The Mechanism of Charge Transfer Across the Barrier-Layer Oxide Film on 1100 Aluminium." *Electrochem. Acta* 31(12): 1531-1540.
- [243] Zhao, Y., M. Chen, et al. (2005). "A Facile Approach to Formation of Through-Hole Porous Anodic Aluminium oxide Film." *Materials Letters* 5911: 40-44.
- [244] Hamnn, C. H. and W. Vielstich (1981). *Electrochemie (Electrochemistry) II* Weinheim, pocket text Verlag
- [245] Ebling, D. and J. W. Schultze (1990). "Galvanische Behandlung von Aluminiumoberflaechen fur Photoelektrische Anwendungen." *Metalloberflaeche* 44: 491.
- [246] Caboni, V. (1936). I. Patent. Italy. 339232

---

[247] Langbein-Pfandhauser GmbH. Elssner, G. (1940). Verfahren zur Elektrolytischen Färbung von Gegenständen aus Aluminium mit Oxydischer Oberflächenschicht. Deutsches Patent (Germany) 741753.

[248] Sautter, W., G. Ibe, et al. (1974). "Investigations of the Process of Electrolytic Coloring of Anodized Aluminum and the Structure of the Color Producing Particles. [Untersuchungen Über die Elektrolytische Färbung von Anodisch oxidiertem Aluminium und die Structure der Farbgebenden Teilchen.]" *Aluminium* 50 (2): 143-149.

[249] Routkevitch, D., A. A. Tader, et al. (1996). "Nonlithographic Nanowire Arrays." *IEEE Trans. Electron Devices* 43(10): 1646-1658.

[250] Routkevitch, D., J. Chan, et al. (1997). "Porous Anodic Alumina Templates for Advanced Nanofabrication" *Electrochemical Society Proceedings* 97(7): 350-357.

[251] Routkevitch, D., T. L. Hasletta, et al. (1996). "Synthesis and resonance Raman spectroscopy of CdS nano-wire arrays" *Chemical Physics* 210(1-2): 343-352.

[252] Jaminas, A., G. Niaura, et al. (2004). "Spectroscopic Evidence of a Novel Array AC Fabrication within the Alumina Template Pores from Acidic Cu (II)-Thiourea Solution." *Applied Surface Science* 239: 72-78.

[253] Gao, J.-H., Q.-F. Zhan, et al. (2006). "Thermally activated magnetization reversal process of self-assembled Fe<sub>55</sub>Co<sub>45</sub> nanowire arrays" *Journal of Magnetism and Magnetic Materials* 305(2): 365-371.

[254] Zhang, L.-Y., X. De-Sheng, et al. (2006). "Magnetic Properties of Amorphous  $\beta$ -FeOOH Nanowire Arrays" *Journal of Magnetism and Magnetic Materials* 305(1): 228-232.

[255] Xu, J. M. and Y. Xu (2006). "Fabrication of Amorphous Co and Co-P Nanometer Array with Different Shapes in Alumina Template by AC Deposition." *Materials Letters* 60: 2069-2072.

[256] Mueller, F., A.-D. Mueller, et al. (2001). "Highly Resolved Electric Force Microscopy of Metal-Filled Anodic Alumina." *Applied Surface Science* 171: 125-129.

[257] Puipe, J.-C. and F. Leaman, Eds. (1986). "Theory and Practice of Pulse Plating". Orlando, USA, American Electroplaters and Surface Finishers Society.

[258] Erb, U., A. M. El-sherik, et al. (1993). "Nanocrystalline Metals". Canada, Integran Technologies Inc. (1 Meridian Road, Toronto, Ontario, M9W 4Z6, CA). EP0670916.

[259] Nielsch, K., R. B. Wehrspohn, et al. (2002). "High density hexagonal nickel nanowire array." *Journal of Magnetism and Magnetic Materials* 249(1-2): 234-240.

[260] Zhang, Y., G. Li, et al. (2002). "Antimony Nanowire Arrays Fabricated by Pulsed Electrodeposition in Anodic Alumina Membranes" *Advanced Materials* 14(17): 1227 - 1230.



---

[261] Lainer, V.I. In: F.A. Lowenheim, Editor, *Modern electroplating*, Wiley, New York (1963), pp. 138–178

[262] International Union of Pure and Applied Chemistry. "transition element". *Compendium of Chemical Terminology* Internet edition.

[263] <http://www.webelements.com/iron/physics.html>

[264] Baik, J. M., M. Schierhorn, et al. (2008). "Fe Nanowires in Nanoporous Alumina: Geometric Effect versus Influence of Pore Walls." *J. Phys. Chem. C* 112(7): 2252-2255.

[265] Peng, Y., H.-L. Zhang, et al. (2000). "Magnetic properties and magnetization reversal of alpha-Fe nanowires deposited in alumina film." *Journal of Applied Physics* 87(10): 7405-7408.

[266] Lee, K. H., H. Y. Lee, et al. (2002). "Magnetic properties and crystal structures of self-ordered ferromagnetic nanowires by ac electroforming." *Journal of Applied Physics* 91(10): 8513-8515.

[267] Yang, S., H. Zhu, et al. (2000). "Preparation and magnetic property of Fe nanowire array." *Journal of Magnetism and Magnetic Materials* 222(1-2): 97-100.

[268] Napolsky, K. S., A. A. Eliseev, et al. (2003). "Preparation of ordered magnetic iron nanowires in the mesoporous silica matrix." *Materials Science and Engineering: C* 23(1-2): 151-154.

[269] Chernysheva, M. V., A. A. Eliseev, et al. (2006). "Ordered nanowire arrays in the mesoporous silica thin films." *Thin Solid Films* 495(1-2): 73-77.

[270] Lin, J.-L., D. Y. Petrovykh, et al. (2001). "Self-assembled Fe nanowires using organometallic chemical vapor deposition and CaF<sub>2</sub> masks on stepped Si(111)." *Applied Physics Letters* 78 829-831. .

[271] Chu, S. Z., S. Inoue, et al. (2005). "Fabrication of integrated arrays of ultrahigh density magnetic nanowires on glass by anodization and electrodeposition." *Electrochimica Acta* 51(5): 820-826.

[272] Kishi, T., H. Nakanishi, et al. (2003). "Stable Structures of Fe Nanowires on Cu(111) " *Japanese Journal of Applied Physics* 42 4633-4635.

[273] Kato, S., H. Shinagawa, et al. (2005). "Application of ferromagnetic nano-wires in porous alumina arrays for magnetic force generator." *Science and Technology of Advanced Materials* 6(3-4): 341-343.

[274] Geng, F. and H. Cong (2006). "Fe-filled carbon nanotube array with high coercivity." *Physica B: Condensed Matter* 382(1-2): 300-304.

[275] Kishi, T., M. David, et al. (2007). "Adsorption of Fe and Co Nanowires to (3,3) Single-Walled Carbon Nanotubes." *Jpn. J. Appl. Phys* 46: 1788-1791

---

[276] Yen, J. H., I. C. Leu, et al. (2005). "Effect of nanowire catalyst for carbon nanotubes growth by ICP-CVD." *Diamond and Related Materials* 14(3-7): 841-845.

[277] <http://www.webelements.com/cobalt/physics.html>

[278] Zeng, H., M. Zheng, et al. (2000). "Magnetic properties of self-assembled Co nanowires of varying length and diameter." *Journal of Applied Physics* 87(9 II): 4718-4720.

[279] Qin, D. H., M. Lu, et al. (2001). "Magnetic force microscopy of magnetic domain structure in highly ordered Co nanowire arrays." *Chemical Physics Letters* 350(1-2): 51-56.

[280] Rivas, J., A. Kazadi Mukenga Bantu, et al. (2002). "Preparation and magnetic behavior of arrays of electrodeposited Co nanowires." *Journal of Magnetism and Magnetic Materials* 249(1-2): 220-227.

[281] Vila, L., P. Vincent, et al. (2004). "Growth and field-emission properties of vertically aligned cobalt nanowire arrays." *Nano Letters* 4(3): 521-524.

[282] Hoshino, K. and Y. Hitsuoka (2005). "One-step template-free electrosynthesis of cobalt nanowires from aqueous  $[\text{Co}(\text{NH}_3)_6]\text{Cl}_3$  solution." *Electrochemistry Communications* 7(8): 821-828.

[283] Hu, H. N., H. Y. Chen, et al. (2005). "Textured Co nanowire arrays with controlled magnetization direction." *Journal of Magnetism and Magnetic Materials* 295(3): 257-262.

[284] Cho, J. U., J.-H. Wu, et al. (2006). "Control of magnetic anisotropy of Co nanowires." *Journal of Magnetism and Magnetic Materials* 303(2): e281-e285.

[285] Lee, J. S., G. H. Gu, et al. (2001). "Well-ordered Co nanowire arrays for aligned carbon nanotube arrays." *Synthetic Metals* 124(2-3): 307-310.

[286] Sinha, A. K., D. W. Hwang, et al. (2000). "A novel approach to bulk synthesis of carbon nanotubes filled with metal by a catalytic chemical vapor deposition method." *Chemical Physics Letters* 332(5-6): 455-460

[287] Katok, K. V., V. A. Tertykh, et al. (2006). "Pyrolytic synthesis of carbon nanostructures on Ni, Co, Fe/MCM-41 catalysts." *Materials Chemistry and Physics* 96(2-3): 396-401.

[288] Knez, M., A. M. Bittner, et al. (2003). "Biotemplate synthesis of 3-nm nickel and cobalt nanowires." *Nano Letters* 3(8): 1079-1082.

[289] <http://en.wikipedia.org/wiki/Nickel>

[290] AlMawlawi, D., N. Coombs, et al. (1991). "Magnetic properties of Fe deposited into anodic aluminum oxide pores as a function of particle size." *Journal of Applied Physics* 70(8): 4421-4425.



- 
- [291] Rahman, I. Z., K. M. Razeed, et al. (2003). "Fabrication and characterization of nickel nanowires deposited on metal substrate." *Journal of Magnetism and Magnetic Materials* 262(1): 166-169.
- [292] Wackelgard, E. (1996). "A study of the optical properties of nickel-pigmented anodic alumina in the infrared region." *Journal of Physics: Condensed Matter* 8(27): 5125-5138.
- [293] Bentley, A. K., A. B. Ellis, et al. (2005). "Suspensions of nickel nanowires as magneto-optical switches." *Nanotechnology* 16(10): 2193-2196.
- [294] Yoo, B., Y. Rheem, et al. (2006). "Magnetically assembled 30 nm diameter nickel nanowire with ferromagnetic electrodes." *Nanotechnology* 17: 2512-2517.
- [295] Jeong, J.-H., S.-H. Kim, et al. (2007). "High-frequency noise absorbing properties of nickel nanowire arrays prepared by DC electrodeposition." *physica status solidi (a)* 204(12): 4025-4028.
- [296] Strevens, A. (2006). *Organic Light-Emitting Diodes – New Emissive Materials and Device Architecture*. School of Physics. Dublin, Trinity College. PhD
- [297] Leahy, R. (2007). *Fabrication and characterisation of arrays of straight and branched carbon nanotubes*. School of Physics. Dublin, Trinity College. PhD.
- [298] Lei, Y., J.T.L. Thong, K.S. Yeong, L.W. Teo, W.K. Chim and W.K. Choi., *Proceedings of The International Conference on Carbon in 2002, Sept 15-20, Beijing, P. R. China*.
- [299] Lei, Y., L.W. Teo, et al. "Fabrication of Highly Ordered Nanoparticle Arrays Using Thin Porous Alumina Masks "Advanced Materials for Micro- and Nano-Systems (AMMNS); <http://hdl.handle.net/1721.1/3662>
- [300] Davydov, D. N., J. Haruyama, et al. (1998). "Nonlithographic nanowire-array tunnel device: Fabrication, zero-bias anomalies, and Coulomb blockade." *Physical Review B* 57(21): 13550.
- [301] Bentley, A. K., v. Farhoud, et al. (2005). "Template Synthesis and Magnetic Manipulation of Nickel Nanowires." *Journal of Chemical Education* 82: 765-768.
- [302] Park, B. H. and I. Kim (2007). "Electrodeposited Nickel nanowire Array." *Adv. Mater. Res.* 26-28: 585-588.
- [303] Nielsch, K., R. Hertel, et al. (2002). "Switching behavior of single nanowires inside dense nickel nanowire arrays." *Magnetics, IEEE Transactions on* 38(5): 2571-2573.
- [304] Pradhan, B. K., T. Kyotani, et al. (1999). "Nickel nanowires of 4 nm diameter in the cavity of carbon nanotubes." *Chem. Commun.:* 1317 - 1318.
- [305] Wang, D.-P., D.-B. Sun, et al. "Preparation of one-dimensional nickel nanowires by self-assembly process." *Materials Chemistry and Physics In Press, Corrected Proof*.

---

[306] <http://en.wikipedia.org/wiki/Copper>

[307] Riveros, G., H. Gómez, et al. (2005). "Crystallographically-oriented single-crystalline copper nanowire arrays electrochemically grown into nanoporous anodic alumina templates." *Applied Physics A: Materials Science & Processing* 81(1): 17-24.

[308] Theis, T. N. (2000). "The future of interconnection technology." *IBM Journal of Research and Development* 44(3): 379-390.

[309] Noyce, J. O., H. Michels, et al. (2006). "Use of Copper Cast Alloys To Control *Escherichia coli* O157 Cross-Contamination during Food Processing." *Appl. Environ. Microbiol.* 72(6): 4239-4244.

[310] Gant, V. A., M. W. D. Wren, et al. (2007). "Three Novel Highly Charged Copper-Based Biocides: Safety and Efficacy Against Healthcare-Associated Organisms." *J. Antimicrob. Chemother.* 60(2): 294-299.

[311] University of Illinois at Urbana-Champaign. (2008). "Copper Nanowires Grown By New Process Create Long-lasting Displays." *Science Daily* 30 April <<http://www.sciencedaily.com/releases/2008/04/080428142028.htm>>.

[312] Brötz, J., F. Maurer, et al. (2005). Controlled Deposition of Copper Nanowires for Field Emission Investigations. *Microstructure Analysis in Materials Science*. Freiberg, 15-17 June, 2005

[313] Krongelb, S., L. T. Romankiw, et al. (1998). "Electrochemical process for advanced package fabrication" *IBM Journal of Research and Development* 42(5 Electrochemical Microfabrication): 575-586.

[314] Toimil Molares, M. E., E. M. Hohberger, et al. (2003). "Electrical characterization of electrochemically grown single copper nanowires." *Applied Physics Letters* 82(13): 2139-2141.

[315] Cao, H. Q., L. Wang, et al. (2006). "Synthesis and IV Properties of Aligned Copper Nanowires." *Nanotechnology* 17: 1736-1739.

[316] Zhou, Y., A. S. Sreekala, et al. (2008). "Resistance of copper nanowires and comparison with carbon nanotube bundles for interconnect applications using first principles calculations." *Journal of Physics: Condensed Matter* 9: 095209.

[317] Bansal, S., E. Toimil-Molares, et al. (2005). Nanoindentation of single crystal and polycrystalline copper nanowires. *Electronic Components and Technology Conference, 2005. Proceedings. 55th.*

[318] Zong, R.-L., J. Zhou, et al. (2005). "Optical properties of transparent copper nanorod and nanowire arrays embedded in anodic alumina oxide." *The Journal of Chemical Physics* 123(9): 094710.

[319] Zhang, J., L. Zhang, et al. (2004). "Polarization properties of ordered copper nanowire microarrays embedded in anodic alumina membrane." *Chemical Physics Letters* 400(1-3): 158-162.



- 
- [320] Pang, Y. T., G. W. Meng, et al. (2003). "Copper nanowire arrays for infrared polarizer." *Applied Physics A: Materials Science & Processing* 76(4): 533-536.
- [321] Gao, T., G. Meng, et al. (2002). "Electrochemical synthesis of copper nanowires." *Journal of Physics: Condensed Matter* 14(3): 355-363.
- [322] Chang, Y., M. L. Lye, et al. (2005). "Large-Scale Synthesis of High-Quality Ultralong Copper Nanowires." *Langmuir* 21(9): 3746-3748.
- [323] Wang, Z. and M. Brust (2007). "Fabrication of nanostructure via self-assembly of nanowires within the AAO template." *Nanoscale Research Letters* 2(1): 34-39.
- [324] Strevens, Adam E., Lipson, Stephen M., Drury, Anna et al. (2003) "Nanowire array electrode structure for organic light-emitting diodes". *Proc. SPIE* 4876:168-175
- [325] Strevens Adam. E., Drury Anna, Lipson Stephen. M., et al. (2005) "Hybrid light-emitting polymer device fabricated on a metallic nanowire array" *Applied Physics Letters* 86 (14): Art. 143503 (1-3)
- [326] <http://en.wikipedia.org/wiki/Silver>
- [327] Doering, W. E. and S. Nie (2002). "Single-Molecule and Single-Nanoparticle SERS: Examining the Roles of Surface Active Sites and Chemical Enhancement." *J. Phys. Chem. B* 106(2): 311-317.
- [328] Nie, S. and S. R. Emory (1997). "Probing Single Molecules and Single Nanoparticles by Surface-Enhanced Raman Scattering." *Science* 275(5303): 1102-1106.
- [329] He, H. and N.J. Tao (2003) "Electrochemical fabrication of metal nanowires" in: "Encyclopedia of nanoscience and nanotechnology", H.S. Nalwa (Ed) American Scientific Publishers, New York, 2003, Vol 10, pp1-18.
- [330] Kreibig, U. and M. Vollmer (1995) "Optical properties of metal clusters", Springer series in materials science, Springer Verlag Berlin, vol 25, pp187-201
- [331] Schider, G., J. R. Krenn, et al. (2001). "Optical properties of Ag and Au nanowire gratings." *Journal of Applied Physics* 90(8): 3825-3830.
- [332] Choi, J., G. Sauer et al. (2003) "Hexagonally Arranged Monodisperse Silver Nanowires with Adjustable Diameter and high Aspect Ratio" *Chem. Mater.* 15, 776-779
- [333] Zhang, X. Y., L. D. Zhang, et al. (2001). "Fabrication and characterization of highly ordered Au nanowire arrays." *Journal of Materials Chemistry* 11(6): 1732-1734.
- [334] Pang, Y. T., G. W. Meng, et al. (2003). "Silver nanowire array infrared polarizers" *Nanotechnology* 14(1): 20-24(5).
- [335] Wu, X., H. Li, et al. (2002). "Agglomeration and the surface passivating film of Ag nano-brush electrode in lithium batteries." *Solid State Ionics* 149(3-4): 185-192.

---

[336] Zhang, J., X. Wang, et al. (2002). "Fabrication, Morphology and Structural Characterization of Ordered Single-Crystal Ag Nanowires." *Applied Physics A: Materials Science & Processing* 75(4): 485-488.

[337] Choi, J., G. Sauer et al. (2003) "Monodisperse Metal Nanowire Arrays on Si by Integration of Template Synthesis with Silicon Technology" *J. Mater. Chem.* 13, 1100-1103

[338] Hu, J. Q., Q. Chen et al. "A Simple and Effective Route for the Synthesis of Crystalline Silver Nanorods and Nanowires". *Advanced Functional Materials* 204, 14/2, 183-189

[339] Zhao, W.-B., J.-J. Lei et al. "Photochemical Synthesis of Au and Ag Nanowires on a Porous Aluminium Oxide Template" *J. Crystal Growth* 2002, 258, 176-180

[340] Lei, Y., L. D. Zhang, et al. (2001). "Preparation and photoluminescence of highly ordered TiO<sub>2</sub> nanowire arrays." *Applied Physics Letters* 78(8): 1125-1127.

[341] Limmer, S. J., S. Seraji, et al. (2002). "Template-Based Growth of Various Oxide Nanorods by Sol-Gel Electrophoresis." *Advanced Functional Materials* 12(1): 59-64

[342] Kim, S. H., B. S. Choi, et al. (2007). "Low temperature synthesis and growth mechanism of Ag nanowires." *Journal of Alloys and Compounds* 433(1-2): 261-264.

[343] R McNeill, R Siudak, JH Wardlaw and DE Weiss (1963) "Electronic Conduction in Polymers. I. The Chemical Structure of Polypyrrole" *Australian Journal of Chemistry* 16(663):1056-1075

[344] BA Bolto and DE Weiss (1963) "Electronic Conduction in Polymers. II. The Electrochemical Reduction of Polypyrrole at Controlled Potential" *Australian Journal of Chemistry* 16(6):1076-1089

[345] BA Bolto, R McNeill and DE Weiss (1963) "Electronic Conduction in Polymers. III. Electronic Properties of Polypyrrole" *Australian Journal of Chemistry* 16(6):1090 - 1103

[346] J. E. McGinness , P. Corry, P. Proctor (1974) "Amorphous Semiconductor Switching in Melanins" *Science* 183:853-855

[347] H. Shirakawa and S. Ikeda, (1971) "Infrared Spectra of Poly (acetylene)" *Polymer Journal* 2(2): 231-244

[348] Shirakawa, H., T. Ito, et al. (1972). "Raman Scattering and Electronic Spectra of Poly (acetylene)." *Polymer Journal* 4(4): 460-462

[349] Ito, T., H. Shirakawa, et al. (1974). "Simultaneous polymerization and formation of polyacetylene film on the surface of concentrated soluble Ziegler-type catalyst solution." *Journal of Polymer Science: Polymer Chemistry Edition* 12(1): 11-20



- 
- [350] Ito, T., H. Shirakawa, et al. (1975). "Thermal cis/trans isomerization and decomposition of polyacetylene." *Journal of Polymer Science: Polymer Chemistry Edition* 13(8): 1943-1950.
- [351] Hideki Shirakawa, Edwin J. Louis, Alan G. MacDiarmid, Chwan K. Chiang and Alan J. Heeger (1977) "Synthesis of Electrically Conducting Organic Polymers :Halogen Derivatives of Polyacetylene, (CH)<sub>x</sub> *Journal of the Chemical Society, Chemical Communications* 1977: 578 - 580
- [352] Chiang, C. K., C. R. Fincher, et al. (1977). "Electrical Conductivity in Doped Polyacetylene." *Physical Review Letters* 39(17): 1098-1101
- [353] Burroughes, J. H., D. D. C. Bradley, et al. (1990). "Light-emitting diodes based on conjugated polymers." *Nature* 347(6293): 539-541.
- [354] Halls, J. J. M., C. A. Walsh, et al. (1995). "Efficient photodiodes from interpenetrating polymer networks." *Nature* 376(6540): 498-500.
- [355] Halls, J. J. M., D. R. Baigent, et al. (1996). "Light-emitting and photoconductive diodes fabricated with conjugated polymers." *Thin Solid Films* 276(1-2): 13-20.
- [356] Burroughes, J. H., C. A. Jones, et al. (1988). "New semiconductor device physics in polymer diodes and transistors." *Nature* 335(6186): 137-141
- [357] Tessler, N., G. J. Denton, et al. (1996). "Lasing from conjugated-polymer microcavities." *Nature* 382(6593): 695-697.
- [358] Wan, M., Z. Wei, et al. (2003). "Studies on Nanostructures of Conducting Polymers via Self-assembly Method." *Synthetic Metals* 135-136: 175-176.
- [359] Yunze Long, Lijuan Zhang, Yongjun Ma, Zhaojia Chen, Nanlin Wang, Ze Zhang, Meixiang Wan (2003). "Electrical Conductivity of an Individual Polyaniline Nanotube Synthesized by a Self-Assembly Method" *Macromolecular Rapid Communications*, 24/16: 938-942 (2003)
- [360] Heeger, A. J. (2001). "Semiconducting and Metallic Polymers: The Fourth Generation of Polymeric Materials." *J. Phys. Chem. B* 105(36): 8475-8491
- [361] Letheby, H. (1862). "On the production of a blue substance by the electrolysis of sulphate of aniline." *J. Chem. Soc.* 15: 161 - 163.
- [362] MacDiarmid, G. and R.B Kaner (1986). In: "Handbook of Conducting Polymers", T.A. Skotheim (Ed) Marcel Dekker, New York, vol 1, p718.
- [363] Dixit, V., S. C. K. Misra, et al. (2005). "Carbon monoxide sensitivity of vacuum deposited polyaniline semiconducting thin films." *Sensors and Actuators B: Chemical* 104(1): 90-93.
- [364] Bartlett, P. N. and P. R. Birkin (1993). "The application of conducting polymers in biosensors." *Synthetic Metals* 61(1-2): 15-21

- 
- [365] Somasiri, N. L. D. and A. G. Macdiarmid (1988). "Polyaniline: characterization as a cathode active material in rechargeable batteries in aqueous electrolytes." *Journal of Applied Electrochemistry* 18(1): 92-95
- [366] Desilvestro, J. W. Scheifele, and O. Haas. (1992) "Insitu determination of gravimetric and volumetric charge-densities of battery electrodes—Polyaniline in aqueous and nonaqueous electrolytes." *J Electrochem Soc* 139 (10):2727–2736.
- [367] Gazard, M. and A. Skotheim, Eds. (1986). *Handbook of Conducting Polymers*. New York, Marcel Dekker, vol 1, Chap 19
- [368] Arbizzani, C., M. Mastragostino, et al., Eds. (1997). *Handbook of Organic Conductive Molecules and Polymers*. New York, Wiley, vol 4, Chap. 11
- [369] Joo, J., and A.J. Epstein. (1994) "Electromagnetic-radiation shielding by intrinsically conducting polymers." *Applied Physics Letters* 65 (18):2278–2280.
- [370] Trivedi, D.C., and S.K. Dhawan. (1993) "Shielding of electromagnetic-interference using polyaniline." *Synthetic Metals* 59 (2):267–272.
- [371] Thompson, K. G. and B. C. Benicewicz (2000). "Corrosion-Protective Coatings from Electroactive Polymers." *Polymer Preprints* 41(2): 1731-173.
- [372] Lu, W.K., R.L. Elsenbaumer, and B. Wessling. (1995) "Corrosion protection of mild-steel by coatings containing polyaniline." *Synthetic Metals* 71 (1–3):2163–2166.
- [373] Fahlman, M., S. Jasty, and A.J. Epstein. (1997) "Corrosion protection of iron=steel by emeraldine base polyaniline: An x-ray photoelectron spectroscopy study." *Synthetic Metals* 85 (1–3):1323–1326.
- [374] Skotheim, T. J., R. L. Elsenbaumer, et al., Eds. (1998). *Handbook of Conducting Polymers*, 2nd ed. New York Marcel Dekker., p 1097
- [375] Chandrasekhar, P., Ed. (1999). *Conducting Polymers, Fundamentals and Applications: A Practical Approach*. Boston, Kluwer Academic, p. 760
- [376] Rupprecht, L., Ed. (1999). *Conductive Polymers and Plastics: In Industrial Applications (SPE/ PDL Series) (Hardcover) Plastics Design Library (July 1, 1999)*
- [377] Epstein, A. J., Ed. (2001). *Conjugated Polymers and Low Molecular Weight Organic Solids*. In R. Farchioni and G. Grosso (Eds.) *Organic Electronic Materials*, Vol. 41, p. 3, Springer, Amsterdam
- [378] Nalwa, H. S., Ed. (2004). *Encyclopedia of Nanoscience and Nanotechnology*. Los Angeles American Scientific Publishers. Vol. 2
- [379] Macdiarmid, A. G., J.-C. Chiang, et al. (1985). "'Polyaniline': Interconversion of Metallic and Insulating Forms." *Molecular Crystals and Liquid Crystals* 121: 173 - 180.



- [380] Huang, W. S., B. D. Humphrey, et al. (1986). "Polyaniline, a novel conducting polymer—Morphology and chemistry of its oxidation and reduction in aqueous-electrolytes." *J Chem Soc Faraday Trans I* 82: 2385.
- [381] McManus, P. M., R. J. Cushman, et al. (1987). "Influence of oxidation and protonation on the electrical conductivity of polyaniline." *J. Phys. Chem.* 91(3): 744-747
- [382] Epstein, A. J., A. G. MacDiarmid, (1989) Proc. Int. Winter School on Electronic Polymer Properties, Kirchberg, Austria, March, 1989, Kuzmany, H (Ed) Solid State Science, Vol 91, pp282-289, Springer Verlag, Berlin.
- [383] MacDiarmid, A. G. and A. J. Epstein (1989). "Polyanilines: a novel class of conducting polymers." *Faraday Discuss. Chem. Soc.* 88: 317 - 332.
- [384] Michael J. Sailor, C. L. C. (1994). "Conducting polymer connections for molecular devices." *Advanced Materials* 6(9): 688-692.
- [385] Boyle, A., E. M. Geniès, et al. (1989). "Application of the electronic conducting polymers as sensors: Polyaniline in the solid state for detection of solvent vapours and polypyrrole for detection of biological ions in solutions." *Synthetic Metals* 28(1-2): 769-774
- [386] Geniès, E. M., A. Boyle, et al. (1990). "Polyaniline: A historical survey." *Synthetic Metals* 36(2): 139-182.
- [387] Huang, J., S. Virji, et al. (2004). "Nanostructured Polyaniline Sensors." *Chemistry - A European Journal* 10(6): 1314-1319; Huang, J. and R. B. Kaner (2007). *Polyaniline Nanofibers: Syntheses, Properties and Applications*. In: Skotheim, T. J. and Reynolds, J. R. *Handbook of Conducting Polymers*, 2nd ed. New York, Marcel Dekker
- [388] Kanungo, M., A. Kumar, et al. (2003). "Microtubule Sensors and Sensor Array Based on Polyaniline Synthesized in the Presence of Poly(styrene sulfonate)." *Anal. Chem.* 75(21): 5673-5679.
- [389] Janata, J. and M. Josowicz (2003). "Conducting polymers in electronic chemical sensors." *Nature Materials* 2: 19-24.
- [390] A. G. MacDiarmid, J. C. Chiang, A. F. Richter et al. (1987) In: L. Alcacer (Ed) *Conducting Polymers, special Applications*, Reidel Publishing Co, Dordrecht, p.105
- [391] Huang, J.X., S. Virji, B.H. Weiller, and R.B. Kaner. (2003) "Polyaniline nanofibers: Facile synthesis and chemical sensors." *J Am Chem Soc* 125 (2):314-315.
- [392] Huang, J. (2006). "Syntheses and applications of conducting polymer polyaniline nanofibers." *Pure Appl. Chem* 78(1): 15-27
- [393] Green, A. G. and A. E. Woodhead (1910). "CCXLIII. - Aniline-black and allied compounds. Part I." *Journal of the Chemical Society, Transactions* 97: 2388-2403; Green, A. G. and A. E. Woodhead (1912). "CXVII.—Aniline-black and allied compounds. Part II." *J. Chem. Soc., Trans.*, 101: 1117 - 1123

- 
- [394] Sun, Y., A. G. MacDiarmid, et al. (1990). "Polyaniline: synthesis and characterization of pernigraniline base." *J. Chem. Soc., Chem. Commun.*: 529 - 531.
- [395] Wei, X. L., Y. Z. Wang, et al. (1996). "Synthesis and Physical Properties of Highly Sulfonated Polyaniline." *J. Am. Chem. Soc.* 118(11): 2545-2555.
- [396] Campos, T. L. A., D. F. Kersting, et al. (1999). "Chemical synthesis of polyaniline using sulphanilic acid as dopant agent into the reactional medium." *Surface and Coatings Technology* 122: 3-5.
- [397] Luzny, W. and E. Banka (2000). "Relations between the Structure and Electric Conductivity of Polyaniline Protonated with Camphorsulfonic Acid." *Macromolecules* 33(2): 425-429.
- [398] Ohsawa, T., T. Kabata, et al. (1989). "Polaronic transition in electrochemical polymerized polyaniline." *Synthetic Metals* 29(1): 203-210.
- [399] Watanabe, A., K. Mori, et al. (1989). "Polyanilines prepared by electrochemical polymerization: Molecular weight of polyaniline films." *Journal of Polymer Science Part A: Polymer Chemistry* 27(13): 4431-4437.
- [400] Huang, J. and R. B. Kaner (2004). "Nanofiber Formation in the Chemical Polymerization of Aniline: A Mechanistic Study." *Angewandte Chemie International Edition* 43(43): 5817-5821.
- [401] Wu, C.G., and T. Bein. (1994) "Conducting polyaniline filaments in a mesoporous channel host." *Science* 264 (5166):1757-1759.
- [402] Gupta, V and N. Miura (2005) "Large Area Network of Polyaniline Nanowires Prepared by Potentiostatic Deposition Process" *Electrochemistry Communications* 7/10:995-999
- [403] Wei, Z. X., L. J. Zhang, et al. (2003). "Self-assembling Sub-Micro-Sized Tube Junctions and Dendrites of conducting polymers." *Adv. Mater.* 15(16): 1382-1385.
- [404] Zhang, Z. M., Z. X. Wei, et al. (2002). "Nanostructures of Polyaniline doped with Inorganic Acids." *Macromolecules* 35: 5937-5942.
- [405] Cadek, M., J. N. Coleman, et al. (2002). "Morphological and mechanical properties of carbon-nanotube-reinforced semicrystalline and amorphous polymer composites." *Applied Physics Letters* 81(27): 5123-5125.
- [406] Baughman, R. H., A. A. Zakhidov, et al. (2002). "Carbon Nanotubes--the Route toward Applications." *Science* 297(5582): 787-792.
- [407] Rawstern, R. (2004) "Nanotube Surveys." *Disruptive Technology Series, Nanotechnology Now.* November 3, 2004 Version. <http://www.nanotech-now.com/nanotube-survey-april2003.htm>
- [408] Collins, P. and J. Hagerstron "Carbon Nanotubes: a high performance Conductive Additive" *Hyperion catalysis International* <http://www.hyperioncatalysis.com/articles.htm>



- 
- [409] Gelves, G. A., B. Lin, et al. (2006). "Low Electrical Percolation Threshold of Silver and Copper Nanowires in Polystyrene Composites." *Advanced Functional Materials* 16(18): 2423-2430.
- [410] Pillalamarri, S. K., F. D. Blum, et al. (2005). "One-Pot Synthesis of Polyaniline-Metal Nanocomposites." *Chem. Mater.* 17(24): 5941-5944.
- [411] Jia, Z., Z. Wang, et al. (1999). "Study on poly(methyl methacrylate)/carbon nanotube composites" *Materials Science and Engineering: A* 271(1): 395-400.
- [412] Putz, K. W., C. A. Mitchell, et al. (2004). "Elastic modulus of single-walled carbon nanotube/poly(methyl methacrylate) nanocomposites." *Journal of Polymer Science Part B-Polymer Physics* 42(12): 2286-2293.
- [413] Velasco-Santos, C., A. L. Martinez-Hernandez, et al. (2003). "Improvement of Thermal and Mechanical Properties of Carbon Nanotube Composites through Chemical Functionalization." *Chem. Mater.* 15(23): 4470-4475.
- [414] Kumar, S., T. D. Dang, et al. (2002). "Synthesis, Structure, and Properties of PBO/SWNT Composites." *Macromolecules* 35(24): 9039-9043.
- [415] Mallick, K., M. J. Witcomb, et al. (2005). "Preparation and characterization of a conjugated polymer and copper nanoparticle composite material: A chemical synthesis route." *Materials Science and Engineering: B* 123(2): 181-186.; Mallick, K., M. J. Witcomb, et al. (2006). "In situ synthesis of copper nanoparticles and poly(o-toluidine): A metal-polymer composite material." *European Polymer Journal* 42(3): 670-675; Mallick, K., M. J. Witcomb, et al. (2006). "Self-assembly of silver nanoparticles: Formation of a thin silver film in a polymer matrix." *Materials Science and Engineering: C* 26(1): 87-91.
- [416] Kinyanjui, J. M., D. W. Hatchett, et al. (2004). "Chemical Synthesis of a Polyaniline/Gold Composite Using Tetrachloroaurate." *Chem. Mater.* 16(17): 3390-3398.
- [417] Hasik, M., A. Drelinkiewicz, et al. (1997). "Polyaniline containing palladium -- new conjugated polymer supported catalysts." *Synthetic Metals* 84(1-3): 93-94.
- [418] Hasik, M., C. Paluszkiwicz, et al. (2005). "Reactions of polyaniline with transition metal ions in nonaqueous solutions." *Journal of Molecular Structure* 744-747: 677-683.
- [419] Huang, K., Y. Zhang, et al. (2006). "Preparation of Highly Conductive, Self-Assembled Gold/Polyaniline Nanocables and Polyaniline Nanotubes." *Chemistry - A European Journal* 12(20): 5314-5319.
- [420] Kinyanjui, J. M., N. R. Wijeratne, et al. (2006). "Chemical and electrochemical synthesis of polyaniline/platinum composites." *Electrochimica Acta* 51(14): 2825-2835.
- [421] Li, Z. F., M. T. Swihart, et al. (2004). "Luminescent Silicon Nanoparticles Capped by Conductive Polyaniline through the Self-Assembly Method." *Langmuir* 20(5): 1963-1971.

- 
- [422] Quaroni, L. and G. Chumanov (1999). "Preparation of Polymer-Coated Functionalized Silver Nanoparticles." *J. Am. Chem. Soc.* 121(45): 10642-10643.
- [423] Sarma, T. K. and A. Chattopadhyay (2004). "One Pot Synthesis of Nanoparticles of Aqueous Colloidal Polyaniline and Its Au-Nanoparticle Composite from Monomer Vapor." *J. Phys. Chem. A* 108(39): 7837-7842.
- [424] Feng, X., Y. Liu, et al. (2006). "One-step synthesis of AgCl/polyaniline core & shell composites with enhanced electroactivity." *Nanotechnology* 17(14): 3578-3583.
- [425] Chen, A., H. Wang, et al. (2005). "One-step process to fabricate Ag-polypyrrole coaxial nanocables." *Chemical Communications*(14): 1863-1864.
- [426] K. Ghosh, S. N. M. (1996). "Mechanical properties of silver-powder-filled polypropylene composites." *Journal of Applied Polymer Science* 60(3): 323-331
- [427] Wang, Y., Q. Yang, et al. (2005). "Preparation of silver nanoparticles dispersed in polyacrylonitrile nanofiber film spun by electrospinning." *Materials Letters* 59(24-25): 3046-3049.
- [428] Gelves, G. A., U. Sundararaj , et al. (2005). "Electrostatically Dissipative Polystyrene Nanocomposites containing Copper Nanowires." *Macromolecular Rapid Communications* 26(21): 1677-1681.
- [429] Yang, C.-H., Y.-K. Chih, et al. (2006). "Self-doped polyaniline nanostructures for casting metal nanorods." *Electrochemical and Solid State Letters* 9(2): G49-G52.
- [430] Khanna, P. K., N. Singh, et al. (2005). "Synthesis of Ag/polyaniline nanocomposite via an in situ photo-redox mechanism " *Materials Chemistry and Physics* 92(1): 214-219
- [431] Park, S., J.-H. Lim, et al. (2004). "Self-Assembly of Mesoscopic Metal-Polymer Amphiphiles " *Science* 303(5656): 348-351; Park, S., S. W. Chung, et al. (2004). "Hybrid Organic-Inorganic, Rod-Shaped Nanoresistors and Diodes." *J. Am. Chem. Soc.* 126(38): 11772-11773.
- [432] Kumar, R. V., Y. Mastai, et al. (2001). "Sonochemical synthesis of amorphous Cu and nanocrystalline Cu<sub>2</sub>O embedded in a polyaniline matrix " *Journal of Materials Chemistry* (), (), 11(4): 1209-1213
- [433] <http://www.atp.ruhr-uni-bochum.de/rt1/semicond/node6.html>
- [434] Law, M., J. Goldberger, et al. (2004). "Semiconductor Nanowires and Nanotubes." *Annual Review of Materials Research* 34(1): 83-122.
- [435] Duan, X. and C. M. Lieber (2000). "General Synthesis of Compound Semiconductor Nanowires." *Advanced Materials* 12(4): 298-302.
- [436] Suh, J. S. and J. S. Lee (1997). "Surface enhanced Raman scattering for CdS nanowires deposited in anodic aluminum oxide nanotemplate." *Chemical Physics Letters* 281(4-6): 384-388.



- 
- [437] Gao, T., G. W. Meng, et al. (2004). "Blue Luminescence of CdS Nanowires Synthesised by Sulfurization." *Chin. Phys. Lett.* 21(5): 959-962.
- [438] Kunz, A. B., R. S. Weidmant, et al. (1981). "Pressure-induced modifications of the energy band structure of crystalline CdS." *J. Phys. C: Solid State Phys.* 14: L581-L584.
- [439] Kittel, C. (1995). *Introduction to Solid State Physics- 7th Edition*, Wiley-India
- [440] Alivisatos, A. P., T. D. Harris, et al. (1989). "Electron--vibration coupling in semiconductor clusters studied by resonance Raman spectroscopy." *The Journal of Chemical Physics* 90(7): 3463-3468.
- [441] Brus, L. E. (1984). "Electron--electron and electron-hole interactions in small semiconductor crystallites: The size dependence of the lowest excited electronic state." *The Journal of Chemical Physics* 80(9): 4403-4409.
- [442] Smith, R. W. (1957). "Low-Field Electroluminescence in Insulating Crystals of Cadmium Sulfide." *Physical Review* 105(3): 900.
- [443] Tao, G., M. Guo-Wen, et al. (2004). "Blue Luminescence of CdS Nanowires Synthesized by Sulfurization." *Chinese Physics Letters* 21(5): 959-962.
- [444] <http://www.precisionmulticontrols.com/PDFdownload/Sulfidevssilicon.pdf>
- [445] Reynolds, D. C., G. Leies, et al. (1954). "Photovoltaic Effect in Cadmium Sulfide." *Phys. Rev. Lett.* 96(2): 533 – 534
- [446] Luque, A. and S. Hegedus (2003). *Handbook of Photovoltaic Science and Engineering*, John Wiley and Sons
- [447] Kishore, R. K., V. Naseem, H.A. Brown, W.D. (2000). Vacuum-evaporated, CdCl<sub>2</sub>-doped cadmium sulfide films for solar cell applications. *Photovoltaic Specialists Conference, 09/15/2000 - 09/22/2000, Conference Record of the Twenty-Eighth IEEE*
- [448] Agarwal, R., C. Barrelet, et al. ( 2005). "Lasing in single cadmium sulfide nanowire optical cavities." *Nano Lett.* 5( 5): 917-920.
- [449] Wu, G. S., X. Y. Yuan, et al. (2004). "A simple synthesis route to CdS nanomaterials with different morphologies by sonochemical reduction." *Materials Letters* 58(5): 794-797.
- [450] Orii, T., S. Kaito, et al. (2002). "Photoluminescence of CdS Nanoparticles Suspended in Vacuum and its Temperature increase by Laser irradiation." *Journal of Physics: Condensed Matter* 14: 9743-9752.
- [451] Lade, S. J. and C. D. Lokhande (1997). "Electrodeposition of CdS from Non-Aqueous Bath." *Materials Chemistry and Physics* 49: 160-163.
- [452] Nishino, J., S. Chatani, et al. (1999). "Electrodeposition Method for Controlled Formation of CdS Films from Aqueous Solutions." *Journal of Electroanalytical Chemistry* 473: 217-222.

- 
- [453] Senthil, K., D. Mangalaraj, et al. (2001). "Structural and Optical Properties of CdS Thin Films." *Applied Surface Science* 169-170: 476-479.
- [454] Innocenti, M., S. Cattarin, et al. (2002). "Characterisation of Thin Films of CdS deposited on Ag(111) by ECALE. A Morphological and Photoelectrochemical Investigation." *Journal of Electroanalytical Chemistry* 532: 219-225.
- [455] Wu, S.-D., Z. Zhengang, et al. (2001). "Preparation of CdS Semiconductor Nanowires by a Convenient Ultraviolet Irradiation Technique." *Chemistry Letters*: 396-397.
- [456] He, J., X.-N. Zhao, et al. (2002). "preparation of cdS nanowires by the Decomposition of the Complex in the Presence of Microwave Irradiation." *Journal of Crystal Growth* 240: 389-394.
- [457] Ge, X., Y. Ni, et al. (2002). "A Novel Route to Prepare CdS nano-rods." *Radiation Physics and Chemistry* 64: 223-227.
- [458] Chen, Y.-T., J.-B. Ding, et al. (2002). "A Facile Route to Preparation of CdS Nanorods " *Materials Chemistry and Physics* 77(3): 734-737.
- [459] Rao, C. N. R., A. Govindaraj, et al. (2001). "Surfactant-assisted synthesis of semiconductor nanotubes and nanowires." *Applied Physics Letters* 78(13): 1853-1855.
- [460] Xu, D., Z. Liu, et al. (2005). "Solvothermal Synthesis of CdS Nanowires in a Mixed Solvent of Ethylenediamine and Dodecanethiol." *J. Phys. Chem. B* 109(30): 14344-14349.
- [461] Fan, J., T. Gao, et al. (2002). "Synthesis of CdS nanowires by sulfurization." *Materials Letters* 57(3): 656-659.
- [462] Xu, D., Y. Xu, et al. (2000). "Preparaton and Characterisation of CdS Nanowire Arrays by DC Electrodeposition in Porous Anodic Aluminium Oxide Templates." *Chemical Physics Letters* 325: 340-344.
- [463] Mondal, S. P., A. Dhar, et al. (2007). "Optical properties of CdS nanowires prepared by dc electrochemical deposition in porous alumina template." *Materials Science in Semiconductor Processing* 10(4-5): 185-193.
- [464] Vrublevsky, I., A. Jagminas, et al. (2008). "Effect of Heat Treatment on the Structure of Incorporated Oxalate Species and Photoluminescent Properties of Porous Alumina Films Formed in Oxalic Acid." *Applied Surface Science* 254: 7326-7330.
- [465] Yamamoto, Y., N. Baba, et al. (1981). "Coloured materials and photoluminescence centres in anodic film on aluminium." *Nature* 289(5798): 572-574.
- [466] Gao, T., G. Meng, et al. (2003). "Blue luminescence in porous anodic alumina films: the role of the oxalic impurities." *Journal of Physics: Condensed Matter* 15(12): 2071-2079.



- 
- [467] Li, Z. and K. Huang (2007). "The effect of high-temperature annealing on optical properties of porous anodic alumina formed in oxalic acid." *Luminescence* 22(4): 355-361.
- [468] Xu, J. (2008). "Fabrication and photoluminescence property of CdS nanowire array by template electrodeposition." *Journal of Wuhan University of Technology--Materials Science Edition* 23(1): 118-120.
- [469] Hornyak, G. L., S. Peschel, et al. (1998). "TEM, STM and AFM as tools to study clusters and colloids." *Micron* 29(2-3): 183-190.
- [470] [www.tcd.ie/cma](http://www.tcd.ie/cma)
- [471] <http://cime.epfl.ch/page12526.html>
- [472] <http://www.mse.iastate.edu/microscopy/whatsem.html>
- [473] <http://www.qub.ac.uk/emu/facilities.html>
- [474] <http://www.unl.edu/CMRAcfem/temoptic.htm>
- [475] <http://www.mpip-mainz.mpg.de/groups/butt/spmlab/spmequipment/multimode>
- [476] Binnig, G., C. F. Quate, et al. (1986). "Atomic Force Microscope." *Physical Review Letters* 56(9): 930-933
- [477] <http://mcff.mtu.edu/acmal/images/NanoIISchematic.jpg>
- [478] [http://imaging-imagerie.nrc-cnrc.gc.ca/nanoscope-iii\\_e.html](http://imaging-imagerie.nrc-cnrc.gc.ca/nanoscope-iii_e.html)
- [479] [http://www.scienceofspectroscopy.info/edit/index.php?title=X-ray\\_Spectroscopy](http://www.scienceofspectroscopy.info/edit/index.php?title=X-ray_Spectroscopy)
- [480] [http://www.4pi.com/teksupport/Rev10online/manual/39\\_9-mxmap16.htm](http://www.4pi.com/teksupport/Rev10online/manual/39_9-mxmap16.htm)
- [481] Woodruff D. P. and T.A. Delchar "Modern Techniques of Surface Science" Second Edition, Cambridge Solid State Science Series Cambridge University Press
- [482] [http://upload.wikimedia.org/wikipedia/commons/0/0a/Bragg\\_diffraction.png](http://upload.wikimedia.org/wikipedia/commons/0/0a/Bragg_diffraction.png)
- [483] <http://mrsec.wisc.edu/Edetc/modules/xray/X-raystm.pdf>
- [484] Williams, D. H. and I. Fleming "Spectroscopic Methods in Organic Chemistry", 5th Edition, Mc Graw Hill, International (UK) Ltd.
- [485] <http://www.spectroscopynow.com/coi/cda/detail.cda?id=18427&type=EducationFeature&chId=2&page=1>
- [486] <http://www.jobinyvon.com/SiteResources/Data/MediaArchive/files/Raman/applications/bands.pdf>
- [487] [http://en.wikipedia.org/wiki/Absorption\\_spectroscopy](http://en.wikipedia.org/wiki/Absorption_spectroscopy)

- 
- [488] <http://www.webschool.bc.ca/ubcpharm/theory/theory/index.html>
- [489] Gore, M. G., Ed. Spectrophotometry and Spectrofluorimetry - a Practical Approach, Oxford University Press
- [490] [http://en.wikipedia.org/wiki/Fluorescence\\_spectroscopy](http://en.wikipedia.org/wiki/Fluorescence_spectroscopy)
- [491] <http://teaching.shu.ac.uk/hwb/chemistry/tutorials/molspec/uvvisab1.htm>
- [492] <http://www.ece.gatech.edu/research/labs/vc/theory/sheetRes.html>; Whitaker, J. C., Ed. Electronics Handbook, Second Edition, Taylor and Francis.
- [493] [http://en.wikipedia.org/wiki/Sheet\\_resistance](http://en.wikipedia.org/wiki/Sheet_resistance)
- [494] <http://www.mpi-halle.mpg.de/department2/research-areas/ordered-porous-materials/porous-alumina/abstract/self-organization-lithography/>
- [495] Schoneberger, C., B. M. I. van der Zande, et al. (1997). "Template Synthesis of Nanowires in Porous Polycarbonate Membranes: Electrochemistry and Morphology." *J. Phys. Chem. B* 101: 5497-5505.
- [496] Goad, D. G. W. and M. Moskovits (1978). "Colloidal metal in aluminum-oxide." *Journal of Applied Physics* 49(5): 2929-2934
- [497] Kawai, S. and I. Ishiguro (1976). "Recording Characteristics of Anodic Oxide Films on Aluminum Containing Electrodeposited Ferromagnetic Metals and Alloys." *Journal of The Electrochemical Society* 23(7): 1047-1051.
- [498] [http://serc.carleton.edu/research\\_education/geochemsheets/wds.html](http://serc.carleton.edu/research_education/geochemsheets/wds.html);  
<http://www.miplaza.com/materialsanalysis/projects/technicalnotessurfaceandthinfilmanalysis/semepma.pdf>;
- [499] Malinauskas, A. (2004). "Self-doped polyanilines." *Journal of Power Sources* 126(1-2): 214-220.
- [500] Zhang, L. and M. Wan (2002). "Synthesis and characterization of self-assembled polyaniline nanotubes doped with D-10-camphorsulfonic acid." *Nanotechnology* 13(6): 750-755.; Zhang, L. and M. Wan (2005). "Chiral polyaniline nanotubes synthesized via a self-assembly process." *Thin Solid Films* 477(1-2): 24-31.
- [501] Yang, J., Y. Ding, et al. "Uniform rice-like nanostructured polyanilines with highly crystallinity prepared in dodecylbenzene sulfonic acid micelles." *Materials Chemistry and Physics* 112(2): 322-324
- [502] Ichinohe, D., T. Arai, et al. (1997). "Synthesis of Soluble Polyanilines in Reversed Micellar Systems." *Synthetic Metals* 84: 75-75.
- [503] Abdiryim, T., Z. Xiao-Gang, et al. (2005). "Comparative studies of solid-state synthesized polyaniline doped with inorganic acids." *Mater.Chem. Phys. Lett.* 90: 367-372.



---

[504] Quillard, S., K. Berrada, et al. (1995). "In situ Raman spectroscopic studies of the electrochemical behavior of polyaniline. ." *New Journal of Chemistry* 19(4): 365-374

[505] Niaura, G., R. Mazeikiene, et al. (2004). "Structural changes in conducting form of polyaniline upon ring sulfonation as deduced by near infrared resonance Raman spectroscopy." *Synthetic Metals* 145(2-3): 105-112.

[506] Boyer, M. I., S. Quillard, et al. (2000). "Vibrational Study of the FeCl<sub>3</sub>-Doped Dimer of Polyaniline; A Good Model Compound of Emeraldine Salt." *J. Phys. Chem. B* 104(38): 8952-8961.

[507] Yue, J., A. J. Epstein, et al. (1990). "Sulfonic Acid Ring-Substituted Polyaniline, A Self-Doped Conducting Polymer." *Molecular Crystals and Liquid Crystals* 189: 255 - 261.

[508] Ibrahim, M. and E. Koglin (2005). "Spectroscopic study of Polyaniline Emeraldine Base: Modelling Approach." *Acta Chim. Slov.* 52: 159-163.

[509] Hasik, M., A. Drelinkiewicz, et al. (2001). "FTIR spectroscopic investigations of polyaniline derivatives-palladium systems." *Journal of Molecular Structure* 596(1-3): 89-99.

[510] Colomban, P., A. Gruger, et al. (1994). "Infrared and Raman study of polyaniline Part I. Hydrogen bonding and electronic mobility in emeraldine salts." *Journal of Molecular Structure* 317(3): 261-271.

[511] Han, M. G., S. K. Cho, et al. (2002). "Preparation and characterization of polyaniline nanoparticles synthesized from DBSA micellar solution." *Synthetic Metals* 126(1): 53-60.

[512] Tang, J., X. Jing, et al. (1988). "Infrared spectra of soluble polyaniline." *Synthetic Metals* 24(3): 231-238.

[513] Mathai, C. J., S. Saravanan, et al. (2002). "Effect of iodine doping on the bandgap of plasma polymerized aniline thin films." *Journal of Physics D: Applied Physics* 35(17): 2206-2210.

[514] Gemeay, A. H., I. A. Mansour, et al. (2005). "Preparation and characterization of polyaniline/manganese dioxide composites via oxidative polymerization: Effect of acids." *European Polymer Journal* 41(11): 2575-2583.

[515] Xia, H. and Q. Wang (2001). "Synthesis and Characterization of Conductive Polyaniline Nanoparticles Through Ultrasonic Assisted Inverse Microemulsion Polymerization." *Journal of Nanoparticle Research* 3(5): 399-409.

[516] Caswell, K. K., C. M. Bender, et al. (2003). "Seedless, Surfactantless Wet Chemical Synthesis of Silver Nanowires." *Nano Lett.* 3(5): 667-669.

[517] Athawale, A. A., M. V. Kulkarni, et al. (2002). "Studies on chemically synthesized soluble acrylic acid doped polyaniline." *Materials Chemistry and Physics* 73(1): 106-110.

- 
- [518] Kröll, M., S. M. O'Flaherty and W. J. Blau (2002) "Optical properties of silver nanowires in nanoporous alumina membranes" Presented at SPIE conference Opto-Ireland, Galway.
- [519] O'Mullane, A. P., S. E. Dale, et al. (2004). "Fabrication and electrocatalytic properties of polyaniline/Pt nanoparticle composites." *Chem. Commun.*: 1606 - 1607.
- [520] de Barros, R. A., W. M. de Azevedo, et al. (2003). "Photo-induced polymerization of polyaniline." *Materials Characterization* 50(2-3): 131-134.
- [521] Sun, Y., Y. Yin, et al. (2002). "Uniform Silver Nanowires Synthesis by Reducing AgNO<sub>3</sub> with Ethylene Glycol in the Presence of Seeds and Poly(Vinyl Pyrrolidone)." *Chem. Mater.* 14(11): 4736-4745.
- [522] Selvan, T., J. P. Spatz, et al. (1998). "Gold-Polypyrrole Core-Shell Particles in Diblock Copolymer Micelles." *Advanced Materials* 10(2): 132-134.
- [523] Sun, X.-Y., F.-Q. Xu, et al. (2005). "Cyclic voltammetry for the fabrication of high dense silver nanowire arrays with the assistance of AAO template." *Materials Chemistry and Physics* 90(1): 69-72.
- [524] Wu, Y., G. Cheng, et al. (2004). "Composite mesostructures by nano-confinement." *Nat Mater* 3(11): 816-822.
- [525] Gu, X., C. Nie, et al. (2006). "Synthesis of silver nanorods and nanowires by tartrate-reduced route in aqueous solutions." *Materials Chemistry and Physics* 96(2-3): 217-222.
- [526] Cui, S., Y. Liu, et al. (2007). "Construction of silver nanowires on DNA template by an electrochemical technique." *Materials & Design* 28(2): 722-725.
- [527] Liu, Y., Y. Chu, et al. (2005). "A novel solution-phase route for the synthesis of crystalline silver nanowires." *Materials Research Bulletin* 40(10): 1796-1801.
- [528] Chimentão, R. J., I. Kirm, et al. (2005). "Sensitivity of styrene oxidation reaction to the catalyst structure of silver nanoparticles." *Applied Surface Science* 252(3): 793-800.
- [529] Suh, J. S. and J. S. Lee (1997). "Surface enhanced Raman scattering for CdS nanowires deposited in anodic aluminum oxide nanotemplate." *Chemical Physics Letters* 281(4-6): 384-388.
- [530] Baranski, A. S. and W. R. Fawcett (1980). "The Electrodeposition of Metal Chalcogenides." *Journal of The Electrochemical Society* 127(3): 766-767.
- [531] Zhang, H., X. Ma, et al. (2003). "Single crystalline CdS nanorods fabricated by a novel hydrothermal method." *Chem. Phys. Lett.* 377(5-6): 654-657.
- [532] Wang, Y. and N. Herron (1990). "Quantum size effects on the exciton energy of CdS clusters." *Phys. Rev. B* J1 - PRB 42(11): 7253 LP - 7255.



---

[533] Wang, H., P. Fang, et al. (2008). "Structural and optical characterization of CdS nanorods synthesized by a PVA-assisted solvothermal method." *Journal of Alloys and Compounds* **461**(1-2): 418-422.

[534] Lei, Y., W. Chim, et al. (2005). "Highly Ordered CdS Nanoparticle Arrays on Silicon Substrates and Photoluminescence Properties." *Applied Physics Letters* **86**: 103106(3).

[535] Yao, J., G. Zhao, et al. (2005). "Solvothermal synthesis and characterization of CdS nanowires/PVA composite films." *Materials Letters* **59**(28): 3652-3655.

[536] Li, Z. and K. Huang (2007). "The effect of high-temperature annealing on optical properties of porous anodic alumina formed in oxalic acid." *Luminescence* **22**(4): 355-361.

[537] Sakae Tajima, Nobuyoshi Baba, Kenichi Shimizu, and Issei Mizuki, "Photoluminescence of Anodic Oxide Films on Aluminium," *ElectroComponent Science and Technology*, vol. 3, no. 2, pp. 91-95, 1976. doi:10.1155/APEC.3.91

[538] Khanna, P. K., N. Singh, et al. (2005). "Synthesis and characterization of Ag/PVA nanocomposite by chemical reduction method." *Materials Chemistry and Physics* **93**(1): 117-121.

[539] Zhou, H. H., X. H. Ning, et al. (2006). "Synthesis of polyaniline-silver nanocomposite film by unsymmetrical square wave current method." *Thin Solid Films* **510**(1-2): 164-168. Zhou, H. H., X. H. Ning, et al. (2006). "Synthesis of polyaniline-silver nanocomposite film by unsymmetrical square wave current method." *Thin Solid Films* **510**(1-2): 164-168.

[540] Xiao, F., C. Hangarter, et al. (2008). "Recent progress in electrodeposition of thermoelectric thin films and nanostructures." *Electrochimica Acta* **53**(28): 8103-8117.

[541] Shigesato, Y., S. Takaki, et al. (1991). "Crystallinity and Electrical Properties of Tin-doped Indium Oxide Films by DC Magnetron Sputtering." *Appl. Surf. Sci.* **48/49**: 269-275

[542] Khiew, P. S., N. M. Huang, et al. (2004). "Synthesis and characterization of conducting polyaniline-coated cadmium sulphide nanocomposites in reverse microemulsion." *Materials Letters* **58**(3-4): 516-521.

[543] de Azevedo, W. M., M. O. E. Schwartz, et al. (2004). "Synthesis and characterization of polyaniline/clay nanocomposite." *physica status solidi (c)* **1**(S2): S249-S255.

[544] Kinyanjui, J. M., R. Harris-Burr, et al. (2004). "Hexachloroplatinate-initiated synthesis of polyaniline/platinum composite." *Macromolecules* **37**(23): 8745-8753.

[545] Kinyanjui, J. M., J. Hanks, et al. (2004). "Chemical and Electrochemical Synthesis of Polyaniline/Gold Composites." *J. Electrochem. Soc.* **151**(12): D113-D120.

- 
- [546] Angelopoulos, M., G. E. Asturias, et al. (1988). "Polyaniline: Solutions, Films and Oxidation State." *Molecular Crystals and Liquid Crystals* 160: 151 - 163.
- [547] Stejskal, J., I. Sapurina, et al. (1999). "In-situ polymerized polyaniline films." *Synthetic Metals* 105(3): 195-202.
- [548] Sapurina, I., A. Riede, et al. (2001). "In-situ polymerized polyaniline films - 3. Film formation." *Synthetic Metals* 123(3): 503-507.
- [549] Okamoto, H., M. Okamoto, et al. (1998). "Structure development in polyaniline films during electrochemical polymerization. II: Structure and properties of polyaniline films prepared via electrochemical polymerization." *Polymer* 39(18): 4359-4367
- [550] Irimia-Vladu, M. and J. W. Fergus (2006). "Suitability of emeraldine base polyaniline-PVA composite film for carbon dioxide sensing." *Synthetic Metals* 156(21-24): 1401-1407.
- [551] Jozefowicz, M. E., R. Laversanne, et al. (1989). "Multiple lattice phases and polaron-lattice spinless-defect competition in polyaniline." *Physical Review B* 39(17): 12958-12961.
- [552] [http://www.igb.fraunhofer.de/www/gf/GrenzflMem/nano/CNT/en/CNT\\_Bucky-Paper.en.html](http://www.igb.fraunhofer.de/www/gf/GrenzflMem/nano/CNT/en/CNT_Bucky-Paper.en.html)
- [553] Kikas, T., H. Ishida, et al. (2002). "Chemical Plume Tracking. 3. Ascorbic Acid: A Biologically Relevant Marker." *Anal. Chem.* 74(15): 3605-3610.
- [554] Wallace, G. G., M. Smyth, et al. (1999). "Conducting electroactive polymer-based biosensors." *TrAC Trends in Analytical Chemistry* 18(4): 245-251.
- [555] Virji, S., J. Huang, et al. (2004). "Polyaniline Nanofiber Gas Sensors: Examination of Response Mechanisms." *Nano Lett.* 4(3): 491-496. [old 357]
- [556] Morrin, A., O. Ngamna, et al. (2005). "An Amperometric Enzyme Biosensor Fabricated from Polyaniline Nanoparticles." *Electroanalysis* 17(5-6): 423-430.
- [557] Ayad, M. M., N. A. Salahuddin, et al. (2008). "pH sensor based on polyaniline and aniline-anthranilic acid copolymer films using quartz crystal microbalance and electronic absorption spectroscopy." *Polymers for Advanced Technologies* 19(8): 1142-1148.
- [558] Kalendová, A., D. Veselý, et al. (2008). "Anticorrosion efficiency of organic coatings depending on the pigment volume concentration of polyaniline phosphate." *Progress in Organic Coatings* 63(2): 228-237.
- [559] Small, W. R., F. Masdarolomoor, et al. (2007). "Inkjet deposition and characterization of transparent conducting electroactive polyaniline composite films with a high carbon nanotube loading fraction." *Journal of Materials Chemistry* 17(41): 4359-4361.
- [560] de Barros, R. A., C. R. Martins, et al. (2005). "Writing with conducting polymer." *Synthetic Metals* 155(1): 35-38.



---

[561] Tseng, R. J., J. Huang, et al. (2005). "Polyaniline Nanofiber/Gold Nanoparticle Nonvolatile Memory." *Nano Lett.* 5(6): 1077-1080.

[562] Qi, Z. and P. G. Pickup (1998). "High performance conducting polymer supported oxygen reduction catalysts." *Chem. Commun.*: 2299 - 2300.

[563] Qi, Z., M. C. Lefebvre, et al. (1998). "Electron and proton transport in gas diffusion electrodes containing electronically conductive proton-exchange polymers." *Journal of Electroanalytical Chemistry* 459(1): 9-14.

[564] Hable, C. T. and M. S. Wrighton (1991). "Electrocatalytic oxidation of methanol by assemblies of platinum/tin catalyst particles in a conducting polyaniline matrix." *Langmuir* 7(7): 1305-1309.

[565] Friend, R. H. "Semiconducting polymers towards device applications: LEDs, displays and photovoltaics." Conference Digest: Lasers and Electro-Optics Europe, 10-15 Sept 2000 Nice.

[566] Thompson, M. E. and S. R. Forest (2001). "Enhancing the Efficiencies, Color Purities, and Lifetimes of Organic Light Emitting Diodes." Abstracts of Papers of the American Chemical Society 221:U481.

[567] Wilkinson, C. I., D. G. Lidzey, et al. (2001). "Enhanced performance of pulse driven small area polyfluorene light emitting diodes." *Applied Physics Letters* 79(2): 171-173.

[568] Smith, L. H., J. A. E. Wasey, et al. (2004). "Light outcoupling efficiency of top-emitting organic light-emitting diodes." *Applied Physics Letters* 84(16): 2986-2988.

[569] (1991-1992). *Handbook of Chemistry and Physics*, 72 nd edition. Boston, CRC Press.

[570] <http://pvc-drom.pveducation.org/index.html>

[571] Iijima, S. (1991). "Helical Nanotubes of graphitic carbon." *Nature* 354: 56-58.

[572] Ebbesen, T. W. and P. M. Ajayan (1992). "Large-scale synthesis of carbon nanotubes." *Nature* 358(6383): 220-222.

[573] <http://www.azonano.com/Details.asp?ArticleID=1561#1>

[574] Curran, S., A. P. Davey, et al. (1999). "Evolution and evaluation of the polymer nanotube composite." *Synthetic Metals* 103(1-3): 2559-2562.

[575] Guo, T., P. Nikolaev, et al. (1995). "Self-Assembly of Tubular Fullerenes." *J. Phys. Chem.* 99(27): 10694-10697.

[576] Leahy, R., K. Vijayamohan, et al. (2003). Gas desorption in single-wall carbon nanotube mats during vacuum annealing, Galway, Ireland, SPIE-Int. Soc. Opt. Eng.

- 
- [577] Lahiff, E., R. Leahy, et al. (2004). Controlling the position and morphology of nanotubes for device fabrication, Tirol, Austria, AIP.
- [578] Leahy, R. W., E. Lahiff, et al. (2005). Controlled growth of arrays of straight and branched carbon nanotubes, Dublin, Ireland, International Society for Optical Engineering, Bellingham WA, WA 98227-0010, United States.
- [579] Terranova, M. L., V. Sessa, et al. (2006). "The World of Carbon Nanotubes: An Overview of CVD Growth Methodologies." *Chemical Vapor Deposition* 12(6): 315-325.
- [580] Hornyak, G. L., A. C. Dillon, et al. (1999). "Template synthesis of carbon nanotubes." *Nanostructured Materials* 12(1-4): 83-88.
- [581] Zhang, X. Y., L. D. Zhang, et al. (2001). "Template synthesis of high-density carbon nanotube arrays." *Journal of Crystal Growth* 223(1-2): 306-310.
- [582] Wang, C., M. Li, et al. (2000). "Well-aligned carbon nanotube array membrane synthesized in porous alumina template by chemical vapor deposition." *Chinese Science Bulletin* 45(15): 1373-1376.
- [583] Krishnan, R., H. Q. Nguyen, et al. (2005). "Wafer-level ordered arrays of aligned carbon nanotubes with controlled size and spacing on silicon." *Nanotechnology* 16(6): 841-845.
- [584] Hou, P.-X., S. Bai, et al. (2003). "Observations of novel carbon nanotubes with multiple hollow cores." *Carbon* 41(13): 2477-2480.
- [585] Li, J., C. Papadopoulos, et al. (1999). "Nanoelectronics: Growing Y-junction carbon nanotubes." *Nature* 402(6759): 253-254.
- [586] Sui, Y. C., B. Z. Cui, et al. (2002). "Growth of carbon nanotubes and nanofibres in porous anodic alumina film." *Carbon* 40(7): 1011-1016.
- [587] Doorn, S. K., L. X. Zheng, et al. (2005). "Raman spectroscopy and imaging of ultralong carbon nanotubes." *Journal of Physical Chemistry B* 109(9): 3751-3758.
- [588] Hata, K., D. N. Futaba, et al. (2004). "Water-assisted highly efficient synthesis of impurity-free single-walled carbon nanotubes." *Science* 306(5700): 1362-1364.
- [589] Tans, S. J., M. H. Devoret, et al. (1997). "Individual single-wall carbon nanotubes as quantum wires." *Nature* 386(6624): 474-477.
- [590] Langer, L., V. Bayot, et al. (1996). "Quantum transport in a multi-walled carbon nanotube." *Physics Review Letters* 76: 479.
- [591] Bandaru, P. R., C. Daraio, et al. (2005). "Novel electrical switching behaviour and logic in carbon nanotube Y-junctions." *Nature Materials* 4(9): 663-666.
- [592] Muneer, T., M. Asif, et al. (2003). "Generation and transmission prospects for solar electricity: UK and global markets." *Energy Conversion and Management* 44(1): 35-52.



---

[593] Sun, S.-S. and N. S. Sariciftci, Eds. (2005). *Organic Photovoltaics: Mechanisms, Materials, and Devices* CRC Press,

[594] Coe-Sullivan, S., W. Woo, et al. (2003). "Tuning the Performance of Hybrid Organic/Inorganic Quantum Dot Light-Emitting Devices." *Organic Electronics* 4: 123.

[595] Steckel, J. S., J. P. Zimmer, et al. (2004). "Blue Luminescence from (CdS)ZnS Core-Shell Nanocrystals." *Angewandte Chemie International Edition* 43(16): 2154-2158.

[596] Chaure, N. B., S. Bordas, et al. (2003). "Investigation of electronic quality of chemical bath deposited cadmium sulphide layers used in thin film photovoltaic solar cells." *Thin Solid Films* 437: 10-17.

[597] Nish, A., J.-Y. Hwang, et al. (2008). "Direct spectroscopic evidence of energy transfer from photo-excited semiconducting polymers to single-walled carbon nanotubes." *Nanotechnology* 19(9): 095603.

[598] Landi, B. J., R. P. Raffaele, et al. (2005). "Single-wall carbon nanotube-polymer solar cells." *Progress in Photovoltaics: Research and Applications* 13(2): 165-172.

[599] Hoppe, H., A. Drees, et al. (2005). "Nano-crystalline fullerene phases in polymer/fullerene bulk-heterojunction solar cells: A transmission electron Microscopy study." *Synthetic Metals* 152(1-3): 117-120.

[600] Drees, M., K. Premaratne, et al. (2002). "Improved polymer-fullerene interface in photovoltaic devices by thermally-controlled interdiffusion." *Abstracts of Papers of the American Chemical Society* 224: U367-U367.

[601] Xu, Z., Y. Wu, et al. (2005). "Carbon nanotube effects on electroluminescence and photovoltaic response in conjugated polymers." *Applied Physics Letters* 87(26): 263118-3.

[602] Coe-Sullivan, Seth, (2005) "Hybrid Organic/Quantum Dot Thin Film Structures and Devices," Ph. D. Thesis, Department of Electrical Engineering and Computer Science, MIT Institute for Soldier Technologies

[603] Coe-Sullivan, S., J. S. Steckel, L.-A. Kim, M. G. Bawendi, Vladimir Bulovic, Method for fabrication of saturated RGB quantum dot light emitting devices, *Proc. SPIE* 5739, pp. 108-115, 2006.

[604] Huynh, W. U., J. J. Dittmer, et al. (2002). "Hybrid nanorod-polymer solar cells." *Science* 295(5564): 2425-2427.

[605] Gur, I., N. A. Fromer, et al. (2007). "Hybrid solar cells with prescribed nanoscale morphologies based on hyperbranched semiconductor nanocrystals." *Nano Letters* 7(2): 409-414.

[606] Boucle, J., S. Chyla, et al. (2008). "Hybrid solar cells from a blend of poly(3-hexylthiophene) and ligand-capped TiO<sub>2</sub> nanorods." *Advanced Functional Materials* 18(4): 622-633.

- 
- [607] Boucle, J., S. Chyla, et al. (2008). "Hybrid bulk heterojunction solar cells based on blends of TiO<sub>2</sub> nanorods and P3HT." *Comptes Rendus Physique* 9(1): 110-118.
- [608] Çapan, R., A. K. Ray, et al. (2007). "Electrical characterisation of stearic acid/eicosylamine alternate layer Langmuir-Blodgett films incorporating CdS nanoparticles." *Thin Solid Films* 515(7-8): 3956-3961.
- [609] Ginger, D. S. and N. C. Greenham (2001). "Charge transport in semiconductor nanocrystals." *Synthetic Metals* 124(1): 117-120.
- [610] Pradhan, B., A. K. Sharma, et al. (2005). "Optical Studies on Chemical Bath Deposited Nanocrystalline CdS Thin Films." *Journal of Nanoscience and Nanotechnology* 5: 1130-1134.
- [611] Chaure, S., N. B. Chaure, et al. (2006). "Self-Organised CdSSe Quantum Dots Thin Films." *Journal of Nanoscience and Nanotechnology* 6: 731-737
- [612] Chaure, S., N. B. Chaure, et al. (2007). "Stoichiometric effects on optical properties of cadmium sulphide quantum dots." *IET Circuits, Devices & Systems* 1(3): 215-219.
- [613] Rakovich, A., S. N. Chaure, et al. (2005). Charge Carrier Dynamics in CdS/MEH-PPV Composites: Implications for the Use of Organised Nanowires in Novel Photovoltaics. SURE (Summer Undergraduate Research Experience) Dublin, Trinity College Dublin.
- [614] Choi, D. H., M. J. Cho, et al. (2006). "Luminescence properties of MEH-PPV and its crosslinked polymer: Effect of crosslink on photoluminescence and electroluminescence." *Synthetic Metals* 156(9-10): 685-689.
- [615] Salafsky, J. S., W. H. Lubberhuizen, et al. (1998). "Photoinduced charge separation and recombination in a conjugated polymer-semiconductor nanocrystal composite." *Chemical Physics Letters* 290(4-6): 297-303.
- [616] Qiao, F., A. Liu, et al. "Enhanced photovoltaic characteristics of solar cells based on n-type triphenodioxazine derivative." *Microelectronics Journal* In Press, Corrected Proof.
- [617] Zhang, S., Z. Lü, et al. (2008). "Effect of energy transfer on electroluminescent performance in blend-layer organic light-emitting devices." *Journal of Luminescence* 128(9): 1523-1527.
- [618] Sadhu, S., P. Saha Chowdhury, et al. (2008). "Synthesis and time-resolved photoluminescence spectroscopy of capped CdS nanocrystals." *Journal of Luminescence* 128(7): 1235-1240.
- [619] Liu, J., W. Wang, et al. (2008). "Surface ligand effects in MEH-PPV/TiO<sub>2</sub> hybrid solar cells." *Solar Energy Materials and Solar Cells* 92(11): 1403-1409.
- [620] [http://en.wikipedia.org/wiki/Silver#cite\\_note-10](http://en.wikipedia.org/wiki/Silver#cite_note-10)



- 
- [621 ] AGC Flat Glass Europe launches world's first antibacterial glass" (2007-09-04)
- [622] <http://www.us.kohler.com/>
- [623 ] <http://www.expresstextile.com/20050731/perspectives01.shtml>
- [624][http://web.archive.org/web/20060531115914/http://www.samsung.com/PressCenter/PressRelease/PressRelease.asp?seq=20060213\\_0000233684](http://web.archive.org/web/20060531115914/http://www.samsung.com/PressCenter/PressRelease/PressRelease.asp?seq=20060213_0000233684) or ^ "Samsung laundry featuring SilverCare Technology". Samsung. Retrieved on 2007-08-06.
- [625] Dr Ronnie Russell, Moyne Institute for Preventative Medicine, Trinity College Dublin, Dublin 2 , Ireland, personal communication
- [626] Collins, P. G. and P. Avouris (2000). "Nanotubes for Electronics." *Scientific American* 283(6): 67-69.
- [627] Franklin, N. and H. J. Dai (2000). "An enhance chemical vapor deposition method to extensive single-walled nanotube networks with directionality." *Advanced Materials* 12: 890-893.
- [628] Ting, J.-M., T.-P. Li, et al. (2004). "Carbon nanotubes with 2D and 3D multiple junctions." *Carbon* 42: 2997–3002.
- [629] Huang, L., S. J. Wind, et al. (2003). "Controlled Growth of Single-Walled Carbon Nanotubes from an Ordered Mesoporous Silica Template." *Nano Lett.* 3(3): 299-303.
- [630] Lin, C.-C., P.-L. Chen, et al. (2005). "Selective growth of horizontally-oriented carbon nanotube bridges on patterned silicon wafers by electroless plating Ni catalysts." *Diamond and Related Materials* 14(11-12): 1867-1871.
- [631] Angelucci, R., R. Rizzoli, et al. (2007). "Growth of carbon nanotubes by Fe-catalyzed chemical vapor processes on silicon-based substrates." *Physica E: Low-dimensional Systems and Nanostructures* 37(1-2): 11-15.
- [632] Park, J. H., S. B. Sinnott, et al. (2006). "Ion separation using a Y-junction carbon nanotube." *Nanotechnology* 17(3): 895-900.
- [633] Zheng, L. X., M. J. O'Connell, et al. (2004). "Ultralong single-wall carbon nanotubes." *Nature Materials* 3(10): 673-676.
- [634] Kong, L.-B. (2005). "Synthesis of Y-junction carbon nanotubes within porous anodic aluminum oxide template." *Solid State Communications* 133(8): 527-529.
- [635] Xu, H. (2005). "The logical choice for electronics?" *Nature Materials* 4(9): 649-650.
- [636] Terrones, M. (2004). "Carbon nanotubes: synthesis and properties, electronic devices and other emerging applications." *International Materials Reviews* 49(6): 325-377.

---

[637] Graham, A. P., G. S. Duesberg, et al. (2004). "Towards the integration of carbon nanotubes in microelectronics." *Diamond and Related Materials* 13(4-8): 1296-1300.

[638] Drury, A., S. Chaure, et al. (2007). "Fabrication and characterization of silver/polyaniline composite nanowires in porous anodic alumina." *Chemistry of Materials* 19(17): 4252-4258.

[639] Tsuchiya, H., S. Berger, et al. (2007). "A new route for the formation of self-organized anodic porous alumina in neutral electrolytes." *Electrochemistry Communications* 9(4): 545-550.

[640] Dr Adam Strevens, personal communication

[641] Pena, D. J., J. K. N. Mbindyo, et al. (2002). "Template Growth of Photoconductive Metal-CdSe-Metal Nanowires." *J. Phys. Chem. B* 106(30): 7458-7462.

[642] Darren Lee, personal communication

[643] Murray, B. J., E. C. Walter, et al. (2004). "Amine Vapor Sensing with Silver Mesowires." *Nano Lett.* 4(4): 665-670.



## Appendix A 1

Analysis of a typical 40V membrane (99.999% Al, doubly anodised) using UTHSCSA Image Tool Computer Program.

Diameter of pores (nm)		Inter-pore Distance (nm) from first anodisation (oxide removed)	Inter-pore distance (nm) after second anodisation
45.87	50.84	122.11	102.36
37.26	57.82	122.16	121.08
53.90	55.65	97.07	112.26
36.54	58.18	135.47	158.59
55.84	53.20	137.39	159.27
45.40	46.79	105.30	115.46
49.88	55.56	107.75	112.41
53.60	53.60	132.83	120.00
62.78	45.40	103.63	109.31
46.45	66.09	120.13	109.71
65.44	49.88	142.07	118.49
26.95	59.99	115.70	131.89
36.10	50.84	99.06	118.31
47.58	54.78	117.52	135.35
44.45	44.45	130.77	145.70
42.48	49.02	154.69	154.52
64.87	64.45	166.10	106.28
51.05	52.69	115.13	115.28
47.13	47.13	178.49	142.98
51.67	34.12	112.79	112.65
45.40	71.75	100.38	142.53
73.95	47.13	143.05	102.36
49.13	41.85	93.17	121.08
56.41	48.58	107.09	112.26
54.09	55.56	117.94	158.59
58.91	29.59	121.71	159.27
48.25	35.95	135.96	115.46
55.46	46.45		112.41
64.37	43.97		

### Summary



Mean Diameter of pores: 50.44nm (Std. Dev. 9.62nm)

Mean Interpore Distance (First Anodisation): 123.54 nm (Std. Dev. 21.03 nm)

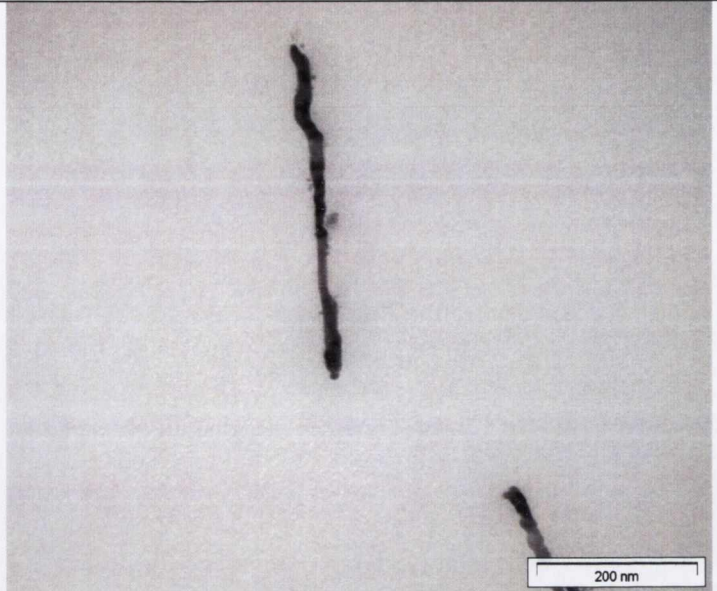
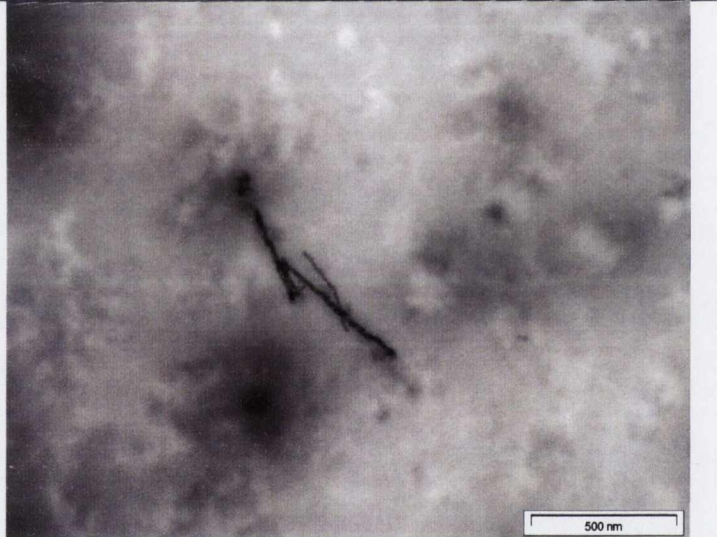
Mean Interpore Distance (Second Anodisation): 125.93nm (Std. Dev. 18.03nm)

## Appendix A 2

Analysis of single Ag nanowires made in a 20V membrane (99% Al, doubly anodised) using UTHSCSA Image Tool computer program.

TEM Image of Nanowire	Diameter (nm)		
 <p data-bbox="325 1072 685 1137">Mean Diameter = 13.42 nm Std. Dev = 2.97 nm</p>	14.17 8.70 15.83 14.52 12.04 12.22 15.04 10.24 13.41 11.81 10.27 11.05 11.14 11.02 11.02 10.50	12.82 12.04 13.59 14.17 14.26 15.04 11.02 12.60 12.70 13.48 14.19 16.53 11.92 11.05 13.41	14.17 12.62 9.49 17.34 21.27 19.93 20.47 21.96 13.45 13.75 14.09 11.63 12.99 12.45 9.74
 <p data-bbox="382 1683 635 1749">Mean = 9.89 nm Std. Dev = 3.47 nm</p>	11.61 8.91 11.10 11.05 9.94 11.61 19.41 8.91 9.41 6.72	7.20 6.10 16.29 14.41 11.93 11.61 10.63 8.91 7.37 6.10	7.40 6.10 15.39 8.30 4.42 11.05 11.53 5.00 8.30



 <p>Mean = 14.64 Std. Dev = 4.00</p>	8.00 17.88 16.00 12.65 18.82 23.53 13.40 18.36 18.82	15.76 17.54 14.20 12.55 12.65 14.12 11.09 11.09 10.98	10.98 7.84 11.42 19.08 14.12 20.45 18.82 9.54 15.69
 <p>Mean = 18.96 Std. Dev = 3.94</p>	19.19 19.19 17.34 15.16 20.55 22.21 28.77 28.12 22.36 20.55	17.34 20.96 15.71 19.54 15.81 18.20 22.44 22.14 16.95	16.95 16.95 23.90 14.36 15.81 14.36 12.87 14.84 18.20

## Summary

Mean diameter of nanowire 1 = 13.42 nm (Std. Dev = 2.97 nm)

Mean diameter of nanowire 2 = 8.89 nm (Std. Dev = 3.47 nm)

Mean diameter of nanowire 3 = 14.64 nm (Std. Dev = 4.00 nm)

Mean diameter of nanowire 4 = 18.96 nm (Std. Dev = 3.94 nm)

---

## Appendix B

### List of Publications

- [1] A. Drury, S. Chaure, M. Kroell, V. Nicolosi, N. Chaure, W. J. Blau, "Fabrication and Characterisation of Silver/Polyaniline Composite Nanowires in Porous Anodic Alumina" *Chemistry of Materials* **2007**, *19*, 4252
- [2] J. J. Doyle, V. Nicolosi, S. M. O'Flaherty, D. Vengust, A. Drury, D. Mihailovic, J. N. Coleman, W. J. Blau, "Nonlinear optical response of MoS<sub>2</sub> nanowires" *Chemical Physics Letters* **2007**, *435*, 109.
- [3] R. P. Hodson, A. E. Strevens, A. Drury, "Nanostructured metal filled porous alumina as an anode in polymer light-emitting diodes" presented at *Opto-Ireland 2005 Conference*, Dublin, Ireland, Apr 05-06, **2005**.
- [4] A. E. Strevens, A. Drury, S. M. Lipson, M. Kroll, W. J. Blau, H. H. Horhold, "Hybrid light-emitting polymer device fabricated on a metallic nanowire array" *Applied Physics Letters* **2005**, *86*.
- [5] S. Giordani, S. D. Bergin, A. Drury, T. N. Mhuirheartaigh, M. Ruther, J. N. Coleman, W. J. Blau, "Effect of solvent and dispersant on the bundle dissociation of single-walled carbon nanotube" presented at *Opto-Ireland 2005 Conference*, Dublin, IRELAND, Apr 05-06, **2005**.
- [6] S. Giordani, S. D. Bergin, A. Drury, E. Ni Mhuirheartaigh, J. N. Coleman, W. J. Blau, "Effect of solvent and dispersant on the bundle dissociation of single-walled carbon nanotubes" presented at *Conference of the NATO Advanced-Study-Institute on Carbon Nanotubes - From Basic Research to Nanotechnology*, Sozopol, BULGARIA, May 21-31, **2005**.
- [7] S. Giordani, S. D. Bergin, A. Drury, E. Ni Mhuirheartaigh, J. N. Coleman, W. J. Blau, "Effect of solvents and dispersants on the bundle dissociation of single-walled carbon nanotube" presented at *19th International Winterschool and Euroconference on Electronic Properties of Novel Materials*, Kirchberg, AUSTRIA, Mar 12-19, **2005**.
- [8] K. P. Ryan, M. Cadek, A. Drury, M. Ruether, W. J. Blau, J. N. Coleman, "Carbon nanotube nucleated polymer crystallization" presented at *Symposium on Advanced Multifunctional Nanocarbon Materials and Nanosystems held at the E-MRS Spring Meeting*, Strasbourg, France, May 24-28, **2004**.
- [9] K. P. Ryan, S. M. Lipson, A. Drury, M. Cadek, M. Ruether, S. M. O'Flaherty, V. Barron, B. McCarthy, H. J. Byrne, W. J. Blau, J. N. Coleman, "Carbon Nanotube Nucleated Crystallinity in a Conjugated Polymer Based Composite" *Chemical Physics Letters* **2004**, *391*, 329.



---

[10] Ryan K.P, Cadek M, Drury A, et al. "Carbon nanotube nucleated polymer crystallization" *Fullerenes Nanotubes and Carbon Nanostructures* 13: 431-434 Suppl. 1 **2005**

[11] S. M. Lipson, J. N. Coleman, A. Drury, D. F. O'Brien, W. J. Blau, A. J. Cadby, P. A. Lane, D. D. C. Bradley, "Alternating and direct current characterization and photoinduced absorption studies of modified conjugated polymer thin films" *Journal of Applied Physics* **2004**, 95, 6138.

[12] R. Murphy, J. N. Coleman, M. Cadek, B. McCarthy, M. Bent, A. Drury, R. C. Barklie, W. J. Blau, "High yield, non-destructive purification and quantification method for multi walled carbon nanotubes", presented at *227th National Meeting of the American-Chemical Society, Anaheim, CA, Abstracts of papers of the American Chemical Society 227: 182-IEC Part 1*, Mar 28-Apr 01, **2004**.

[13] M. E. Brennan, J. N. Coleman, A. Drury, B. Lahr, T. Kobayashi, W. J. Blau, "Nonlinear photoluminescence from van Hove singularities in multiwalled carbon nanotubes" *Optics Letters* **2003**, 28, 266.

[14] J. L. Gallani, L. Bonomme, A. Drury, W. J. Blau, "Photosensitive magnetism of radicals coupled with carbon nanotubes" *Organic Electronics* **2003**, 4, 15.

[15] H. Manaa, F. Z. Henari, A. Al-Saie, A. Drury, T. Kobayashi, W. J. Blau, "Light Amplification and Lasing in a (meta-phenylene vinylene) copolymer" *Journal of Applied Physics* **2003**, 93, 1871.

[16] S. M. O'Flaherty, R. Murphy, S. V. Hold, M. Cadek, A. Drury, J. N. Coleman, W. J. Blau, "Optical limiting properties of carbon nanostructure and polymer dispersions", presented at Conference on Organic Photonic Materials and Devices V, San Jose, Ca, Jan 27-30, 2003. *Proc. SPIE* Vol. 4991, p. 194-203.

[17] S. M. O'Flaherty, R. Murphy, S. Hold, A. Drury, M. Cadek, J. N. Coleman, W. Blau, "Polymer and carbon nanostructure dispersions for optical limiting", presented at *17th International Winterschool/Euroconference on Electronic Properties of Novel Materials*, Kirchberg, Austria, Mar 08-15, **2003**.

[18] S. M. O'Flaherty, S. V. Hold, M. E. Brennan, M. Cadek, A. Drury, J. N. Coleman, W. J. Blau, "Nonlinear Optical Resonse of Multiwalled Carbon-Nanotube Dispersions" *Journal of the Optical Society of America B-Optical Physics* **2003**, 20, 49-57. also *Virtual Journal of Nanoscale Science & Technology - Carbon Nanotubes, C60, and Related Studies* 7 (2003), 4, SM O'Flaherty, SV Hold, M Cadek, A Drury, JN Coleman, WJ Blau;

[19] A. Drury, S. Maier, M. Ruther, W. J. Blau, "Investigation of Different Synthetic Routes to and Structure-Property Relationships of Poly (m-phenylene-co-2,5-dioctyloxy-p-phenylene vinylene)" *Journal of Materials Chemistry* **2003**, 13, 485.

[20] M. Cadek, R. Murphy, B. McCarthy, A. Drury, B. Lahr, R. C. Barklie, M. Panhuis, J. N. Coleman, W. J. Blau, "Optimisation of the arc-discharge production of multi-walled carbon nanotubes". *Carbon* **2002**, 40, 923.

- 
- [21] A. Drury, S. Maier, M. Ruther, W. J. Blau, "Property-structure relationships of some derivatives of poly (m-phenylene vinylene)", presented at *Conference on Optics and Photonics Technologies and Applications*, Galway, Ireland, Sep 05-06, **2002**. *Proc. SPIE Vol. 4876*, p. 740-749.
- [22] J. N. Coleman, K. P. Ryan, S. M. Lipson, A. Drury, M. Cadek, M. I. H. Panhuis, R. P. Wool, V. Barron, W. J. Blau, "Effect of nanotube inclusions on-polymer morphology in composite systems", presented at *16th International Winterschool on Electronic Properties of Novel Materials*, Kirchberg, Austria, Mar 02-09, **2002**. *AIP Conf. Proc.* 633 (2002) 557
- [23] P. Fournet, J. N. Coleman, D. F. O'Brien, B. Lahr, A. Drury, C. R. McNeill, P. C. Dastoor, G. G. Wallace, H. H. Horhold, W. J. Blau, "Carbon nanotube composites as efficient charge transport media in organic optoelectronic devices", presented at *Conference on Optics and Photonics Technologies and Applications*, Galway, Ireland, Sep 05-06, **2002**. *Proc. SPIE Vol. 4876*, p. 338-349.
- [24] G. Kiernan, V. Barron, D. Blond, A. Drury, J. Coleman, R. Murphy, M. Cadek, W. Blau, "Characterisation of nanotube based artificial muscles materials", presented at *Conference on Optics and Photonics Technologies and Applications*, Galway, Ireland, Sept 05-06, **2002**. *Proc. SPIE Vol. 4876*, p. 775-782.
- [25] S. M. Lipson, A. J. Cadby, J. N. Coleman, P. A. Lane, A. Drury, D. F. O'Brien, D. D. C. Bradley, W. J. Blau, "Optical and electrical studies of modified conjugated polymer films", presented at *Conference on Optics and Photonics Technologies and Applications*, Galway, Ireland, Sep 05-06, **2002**. *Proc. SPIE Vol. 4876*, p. 350-360.
- [26] Lipson S. M., Coleman J. N., Drury A, O'Brien D.F., Blau W.J., Cadby A.J., Lane P.A., Bradley D.D.C. "Alternating and direct current characterization and photoinduced absorption studies of modified conjugated polymer thin films". *J. Appl. Phys.* 95 (11): 6138-6144 Part 1 June 1 2004.
- [27] A. E. Strevens, S. M. Lipson, A. Drury, M. Kroell, H. H. Horhold, W. J. Blau, "Nanowire array electrode structure for organic light emitting diodes", presented at *Conference on Optics and Photonics Technologies and Applications*, Galway, Ireland, Sep 05-06, **2002**. *Proc. SPIE 4876:168-175 (2003)*
- [28] B. E. Kilbride, J. N. Coleman, J. Fraysse, P. Fournet, M. Cadek, A. Drury, S. Hutzler, S. Roth, W. J. Blau, "Experimental observation of scaling laws for alternating current and direct current conductivity in polymer-carbon nanotube composite thin films" *Journal of Applied Physics* **2002**, 92, 4024.
- [29] B. McCarthy, J. N. Coleman, R. Czerw, A. B. Dalton, M. I. H. Panhuis, A. Maiti, A. Drury, P. Bernier, J. B. Nagy, B. Lahr, H. J. Byrne, D. L. Carroll, W. J. Blau, "A Microscopy and Spectroscopy Study of Interactions between Carbon Nanotubes and a Conjugated Polymer" *Journal of Physical Chemistry B* **2002**, 106, 2210.
- [30] R. Murphy, J. N. Coleman, M. Cadek, B. McCarthy, M. Bent, A. Drury, R. C. Barklie, W. J. Blau, "High Yield, Non-destructive Purification and Quantification Method for Carbon Nanotubes" *Journal of Physical Chemistry B* **2002**, 106, 3087.



- 
- [31] R. Murphy, J. N. Coleman, S. M. O'Flaherty, M. Cadek, B. McCarthy, A. Drury, R. C. Barklie, W. J. Blau, "Comparative study of two polymer carbon nanotube composites using electron paramagnetic resonance and transmission electron microscopy", presented at *Conference on Optics and Photonics Technologies and Applications*, Galway, Ireland, Sep 05-06, **2002**. *Proc. SPIE Vol. 4876*, p. 659-666.
- [32] S. M. O'Flaherty, S. V. Hold, M. Cadek, A. Drury, J. N. Coleman, W. J. Blau, "Nanosecond nonlinear optical extinction in dispersed multi walled carbon nanotubes excited at 532 nm", presented at *Conference on Optics and Photonics Technologies and Applications*, Galway, Ireland, Sep 05-06, **2002**. *Proc. SPIE Vol. 4876*, p. 750-757.
- [33] K. P. Ryan, S. M. Lipson, S. M. O. Flaherty, V. Barron, M. Cadek, A. Drury, H. J. Byrne, R. P. Wool, W. J. Blau, J. N. Coleman, "Photoluminescence quenching and degradation studies to determine the effect of nanotube inclusions on polymer morphology in conjugated polymer-carbon nanotube composites", presented at *Conference on Optics and Photonics Technologies and Applications*, Galway, Ireland, Sep 05-06, **2002**. *Proc. SPIE Vol. 4876*, 361-368.
- [34] M. Cadek, R. Murphy, B. McCarthy, A. Drury, B. Lahr, R.C. Barklie, M. in het Panhuis, J.N. Coleman and W.J. Blau "Optimisation of Carbon Nanotube Production by Arc Discharge" in *Electronic Properties of Molecular Nanostructures*, edited by H. Kuzmany, J. Fink, M. Mehring, S. Roth, AIP Conference Proceedings **591**, New York, **2001**, 179 – 182
- [35] A. B. Dalton, J. N. Coleman, M. I. H. Panhuis, B. McCarthy, A. Drury, W. J. Blau, B. Paci, J. M. Nunzi, H. J. Byrne, Controlling the optical properties of a conjugated copolymer through variation of backbone isomerism and the introduction of carbon nanotubes" *Journal of Photochemistry and Photobiology a-Chemistry* **2001**, *144*, 31-41.
- [36] K. G. Ryder, S. M. Lipson, A. Drury, S. M. O'Flaherty, W. J. Blau, "Model study in molecular engineering for nonlinear photonic devices: poly (arylene ethynylene) and poly (arylene vinylene) copolymers", presented at *Conference on Linear and Nonlinear Optics of Organic Materials*, San Diego, Ca, Aug 01-02, **2001**. *Proc. SPIE Volume 4461*, pp 246-259,
- [37] P. Fournet, J. N. Coleman, B. Lahr, A. Drury, W. J. Blau, D. F. O'Brien, H. H. Horhold, "Enhanced brightness in organic light-emitting diodes using a carbon nanotube composite as an electron-transport layer" *Journal of Applied Physics* **2001**, *90*, 969.
- [38] P. Fournet, J. N. Coleman, D. F. O'Brien, B. Lahr, A. Drury, H. H. Horhold, W. J. Blau, "Enhanced brightness in organic light-emitting diodes using a carbon nanotube composite as an electron-transport layer", presented at *Conference on Organic Light-Emitting Materials and Devices V*, San Diego, Ca, Jul 30-Aug 01, **2001**. *Proc. SPIE Vol. 4464*, p. 239-247
- [39] S. M. Lipson, A. J. Cadby, P. A. Lane, D. F. O'Brien, A. Drury, D. D. C. Bradley, W. J. Blau, "The photophysics of thin polymer films of poly-(meta-phenylene-co-2,5-dioctoxy-paraphenylenevinylene)" *Monatshefte Fur Chemie* **2001**, *132*, 151.



- 
- [40] S. M. Lipson, D. F. O'Brien, A. Drury, H. J. Byrne and W. J. Blau, M. in het Panhuis, R. W. Munn, W.J. Blau, "Optimal Polymer Characteristics for Nanotube Solubility" *Synthetic Metals* **2001** 121 (1-3), 1187 - 1188
- [41] S. M. Lipson, D. F. O'Brien, A. Drury, H. J. Byrne, W. J. Blau, "Increased luminescence efficiency in PmPV thin films by modified thin-film preparation techniques", presented at *16th International Conference on Science and Technology of Synthetic Metals (ICSM 2000)*, Gastein, Austria, Jul 15-21, **2000**. *Synthetic Metals*, Volume 119, Issues 1-3, 15 March 2001, Pages 569-570
- [42] S. Maier, A. Drury, A. P. Davey, H. J. Byrne, W. Blau, "Bulky sidegroup polymers - synthesis and characterisation", presented at *16th International Conference on Science and Technology of Synthetic Metals (ICSM 2000)*, Gastein, Austria, Jul 15-21, **2000**. *Synthetic Metals*, Volume 119, Issues 1-3, 15 March 2001, Pages 85-86
- [43] A. B. Dalton, B. Paci, K. Henderson, G. Chambers, B. McCarthy, J. N. Coleman, A. Drury, C. Fiorini, J. M. Nunzi, W. J. Blau, H. J. Byrne, "Isomerism and inter-chain effects in a semi-conjugated co-polymer, poly(m-phenylenevinylene-co-2,5-dioctyloxy-p-phenylenevinylene)", presented at *16th International Conference on Science and Technology of Synthetic Metals (ICSM 2000)*, Gastein, Austria, Jul 15-21, **2000**. *Synthetic Metals*, Volume 119, Issues 1-3, 15 March 2001, Pages 557-558
- [44] K. Henderson, A. B. Dalton, G. Chambers, A. Drury, S. Maier, A. G. Ryder, W. Blau, H. J. Byrne, "Solvent effects on the luminescent properties of conjugated molecules", presented at *16th International Conference on Science and Technology of Synthetic Metals (ICSM 2000)*, Gastein, Austria, Jul 15-21, **2000**. *Synthetic Metals*, Volume 119, Issues 1-3, 15 March 2001, Pages 557-558
- [45] A. Drury, S. Maier, A. P. Davey, A. B. Dalton, J. N. Coleman, H. J. Byrne, W. J. Blau, "Systematic trends in the synthesis of (meta-phenylene vinylene) copolymers", presented at *16th International Conference on Science and Technology of Synthetic Metals (ICSM 2000)*, Gastein, Austria, Jul 15-21, **2000**. *Synthetic Metals*, Volume 119, Issues 1-3, 15 March 2001, Pages 151-152
- [46] J. N. Coleman, A. B. Dalton, S. Curran, A. Rubio, A. P. Davey, A. Drury, B. McCarthy, B. Lahr, P. M. Ajayan, S. Roth, R. C. Barklie, W. J. Blau, "Phase Separation of Carbon Nanotubes and Turbostratic Graphite using a Functional Organic Polymer"; *Advanced Materials* 12 (2000) 213-216. See also *Advanced Materials* 12 (2000) 401-401
- [47] J. N. Coleman, D. F. O'Brien, A. B. Dalton, B. McCarthy, B. Lahr, A. Drury, R. C. Barklie, W. J. Blau, "Measurement of nanotube content in pyrolytically generated carbon soot" *Chemical Communications* **2000**, 2001.
- [48] K. Henderson, K. P. Kretsch, A. Drury, S. Maier, A. P. Davey, W. Blau, H. J. Byrne, "Correlation of molecular vibrational structure with luminescent quantum yields", presented at *2nd International Conference on Electroluminescence of Molecular Materials and Related Phenomena (ICEL-2)*, Sheffield, England, May 15-18, **1999**. *Synthetic Metals* 111-112 (2000) 559-561



- 
- [49] S. Maier, A. P. Davey, A. Drury, H. J. Byrne, W. Blau, "Mono- and polycyclic aromatic polymers - synthesis and properties", presented at *International Conference on Science and Technology of Synthetic Metals (ICSM 98)*, Montpellier, France, Jul 12-18, **1998**. *Synthetic Metals* 101 (1999) 31-32
- [50] S. A. Curran, P. M. Ajayan, W. J. Blau, D. L. Carroll, J. N. Coleman, A. B. Dalton, A. P. Davey, A. Drury, B. McCarthy, S. Maier, A. Strevens, "A composite from poly(m-phenylenevinylene-co-2,5-dioctoxy-p-phenylenevinylene) and carbon nanotubes: A novel material for molecular optoelectronics"; Oct 1 1998, *Advanced Materials* **1998**, 10, 1091.
- [51] S. Curran, A. P. Davey, J. Coleman, A. Dalton, B. McCarthy, S. Maier, A. Drury, D. Gray, M. Brennan, K. Ryder, M. L. de la Chapelle, C. Journet, P. Bernier, H. J. Byrne, D. Carroll, P. M. Ajayan, S. Lefrant, W. Blau, "Evolution and evaluation of the polymer nanotube composite", presented at *International Conference on Science and Technology of Synthetic Metals (ICSM 98)*, Montpellier, France, Jul 12-18, **1998**. *Synthetic Metals* 103 (1-3): 2559-2562
- [52] J. N. Coleman, A. B. Dalton, S. Curran, A. P. Davey, B. McCarthy, A. Drury, H. J. Byrne, S. Roth, W. Blau, "Optical and electrical properties of a polymer-nanotube composite", presented at *3rd International Conference on Excitonic Processes in Condensed Matter (EXCON 98) / 194th Meeting of the Electrochemical-Society*, Boston, Ma, Nov 01-05, **1998**. *Electrochemical Society Proceedings* Volume 98-25
- [53] A. P. Davey, A. Drury, S. Maier, H. J. Byrne, W. J. Blau, "Synthesis and optical properties of phenylene-vinylene copolymers", presented at *International Conference on Science and Technology of Synthetic Metals (ICSM 98)*, Montpellier, France, Jul 12-18, **1998**. *Synthetic Metals* 103 (1999) 2479-2579
- [54] A.P Davey, A. Drury, S. Maier, H.J. Byrne, W.J. Blau "Synthesis and Optical Properties of Phenylene-vinylene Copolymers" *Synthetic Met.* 103 (1999) 2479-2579
- [55] A. Drury, S. Burbridge, A. P. Davey, W. J. Blau, "Poly(5-tert-butyl)benzothiophene: a soluble form of polyisothianaphthene with a large nonlinear optical response"; *Journal of Materials Chemistry* **1998** 8 (11): 2353-2355
- [56] J. Hockemeyer, A. Castel, P. Riviere, J. Satge, K. G. Ryder, A. Drury, A. P. Davey, W. J. Blau, "Synthesis and Nonlinear Optical Studies on some new Germanium and Tin Polymers" *Applied Organometallic Chemistry* **1997**, 11, 513- 521.
- [57] S. Curran, S. Roth, A. P. Davey, A. Drury, W. Blau, "Photoconduction and photovoltaic effects from a conjugated polymer poly-tert-butyl-isothianaphthalene", presented at *Symposium G on Nonlinear Optical and Optoelectronic Organic Materials, at the 1996 E-MRS Spring Conference*, Strasbourg, France, Jun 04-07, **1996**. *Synthetic Metals*, 1996, 83, 239 *Synthetic Metals*, 1996, 83, 239
- [58] S. J. Burbridge, H. Page, A. Drury, A. P. Davey, J. Callaghan, W. Blau, "Nonlinear-Optical Properties of a Soluble Form of Polyisothianaphthene", presented at *11th National Quantum Electronics Conference*, Belfast, North Ireland, Aug 30-Sep 02, **1993**. *Non-linear Optics* 10 (1995) 139 – 146

---

[59] A. Drury, A.P. Davey and W.J. Blau "Synthesis of a Soluble Form of the Low Bandgap Polymer Poly(3-butyl)isothianaphthene" *Nonlinear Optics* 10 (1995)167 – 172

[60] Burbridge, H. Page, A. Drury, A.P. Davey, J. Callaghan and W. Blau Nonlinear Optical Properties of a Soluble Form of Polyisothionaphthene *Journal of Modern Optics* 41 (1994) 1217 – 1225

[61] A.Drury, A.P.Davey, S. Burbridge, H. Page, and W.Blau "The Synthesis of the narrow-Gap, Nonlinear, Organic Polymer Poly(terbutylisothianaphthene)" *Nonlinear Optics*, 1994 1-6

[62] S.J. Burbridge, H. Page, A. Drury, A.P.Davey, J. Callaghan, W. Blau "The third Order Nonlinear Optical Response of a Soluble Form of Polyisothionaphthene". in *Nonlinear Optics, Principles, Materials, Phenomena & Devices*, UK, 10, no.1-4, 1995, pp.139-46

[63] P. Lemoine, W. Blau, A. Drury, C. Keely, "Molecular Weight Effects on the 248 nm Photoablation of Polystyrene Spun Films" *Polymer* 1993, 34, 5020- 5028.